Blue Carbon Benefits of Seagrass Restoration

Matthew Paul Julius Oreska
Charlottesville, Virginia

Master of Philosophy, University of Cambridge, 2009
Bachelors of Science, The College of William and Mary, 2007

A Dissertation presented to the Graduate Faculty
of the University of Virginia in Candidacy for the Degree of
Doctor of Philosophy

Department of Environmental Sciences

University of Virginia
May 2018

Karen J. McGlathery (Advisor) ________________________________

John H. Porter ________________________________

Patricia Wiberg (Out of discipline representative) ________________________________

Mark White (Representative of the graduate faculty) ________________________________

Abstract

In recent years, studies have noted that seagrass meadow collapse results in a greenhouse gas (GHG) flux, because the C_{org} sequestered in plant biomass and bed sediment (SOC) is rapidly remineralized and outgassed to the atmosphere absent seagrass bed stabilization. Given the estimated size of the existing seagrass 'blue carbon' sequestered stock and the global meadow loss rate, the global CO_2 flux from seagrass habitat conversion is sufficiently large to warrant concern about climate impacts. Observers have, therefore, called for incentivizing seagrass conservation and restoration through the allocation of voluntary offset-credits. The new *Methodology for Tidal Wetland and Seagrass Restoration* provides a framework that the Verified Carbon Standard (VCS) can use to quantify and award offsets to applicant seagrass projects. However, absent a seagrass offset-credit case study, prospective projects do not have a benchmark for expectations about the offset-credit return from seagrass restoration. Despite extensive research on seagrass carbon burial, questions remain about how best to account for seagrass bed accretion, scale SOC measurements to estimate meadow-scale stocks, identify SOC sources (i.e. allochthonous C_{org}), account for possible trace gas increases, and demonstrate that restoration projects are 'additional,' especially in regions with pre-existing meadows. These questions can be addressed by studying the recent *Zostera marina* (eelgrass) restoration in the Virginia Coast Reserve (VCR). The large (>6 km^2), successfully-restored meadow in South Bay, VA, provides an ideal test case for quantifying the net GHG benefit that can be achieved through restoration.

The South Bay meadow restoration has resulted in the net removal of almost 10,000 tCO_2 from the atmosphere since 2001. This benefit derives in large part from canopy-sedimentation effects that enhance the burial of seagrass C_{org} and *in situ* benthic microalgae at mid-meadow sites. Measuring and mapping SOC concentrations, organic matter stable isotope ratios, and sediment grain size throughout this meadow revealed SOC concentration gradients resulting from hydrodynamic 'edge effects.' Sediment fractionates by size as it is advected into the meadow, resulting in more fine-grained deposition at interior meadow sites. These sites, therefore, accumulate more SOC from seagrass and from microalgae than sites closer to the meadow perimeter, irrespective of site meadow age. Measuring seasonal trace gas fluxes confirmed that seagrass presence also increases the release of both CH_4 and N_2O, but the enhanced release rates have a marginal effect on the net GHG benefit.

The continued natural expansion of the restored *Z. marina* meadows in the VCR suggests that the GHG benefit resulting from the restoration effort will continue to increase, even absent continued broadcast seeding. As a consequence, a new VCR restoration effort that applies for VCS offset-credits may not qualify as 'additional.' Species distribution models applied to natural eelgrass recruitment data suggest that total eelgrass area within the VCR will eventually increase from 25 to approximately 34 km^2. However, applying the same machine learning models to survival data from the eelgrass restoration seed plots suggests that additional restoration effort could, potentially, triple the total restored area in the VCR. If coastal managers decide to undertake this additional restoration, VCS offset-credits can partially defray the cost.

Table of Contents

Table of Figures

Table of Tables

Acknowledgements

I wish to thank my adviser, Karen McGlathery, for her guidance and for providing me with opportunities to pursue multiple academic interests at UVA. This dissertation, in its present form, would not have been possible had Dr. McGlathery not encouraged me to work directly with Restore America's Estuaries (RAE) on the Verified Carbon Standard (VCS) *Methodology for Tidal Wetland and Seagrass Restoration* shortly after I arrived at UVA and fully supported me in that endeavor. I also want to thank my other PhD committee members, Pat Wiberg, John Porter, and Mark White, for their guidance and mentorship, and our VCS *Methodology* collaborators, Pat Megonigal, Steve Emmett-Mattox, Brian Needelman, Steve Crooks, Igino Emmer, and Doug Myers, for sharing their expertise.

This dissertation would not have been possible without the help of my collaborators and a multitude of other individuals who assisted me in different ways. In addition to my committee members, I want to give special thanks to Lillian Aoki, Grace Wilkinson, Brent McKee, J. J. Orth, and Dave Wilcox. By generously sharing their research and expertise, they made different chapters in this dissertation possible. I also want to credit Pat Megonigal for his extensive, sometimes informal, collaborative support, including advice on aspects of my graduate work and for providing access to essential lab equipment at the Smithsonian Environmental Research Center.

I am indebted to too many individuals for field and/or lab support to name them all here; however, I am especially grateful to Meg Miller, Drew Peresta, Marshall Otter,

and Molly Bost, for their lab assistance, Aaron Mills, Max Castorani, Matt Reidenbach, and Joel Carr, for conceptual advice and/or technical assistance, and Art Schwarzschild, Donna Fauber, and Pat Luckenbach for material support. Multiple other individuals at our ABCRC field station also contributed in ways both large and small over the past several years. I want to specifically thank Cy Clemo and Hales Parcells for their field and lab assistance. In addition to Lillian, fellow UVA grad students and post docs provided important advice and support, especially Jill Greiner, Marie-Lise Delgard, Amélie Berger, Abby Lunstrum, Martin Volaric, Alice Besterman, and Ross Timmerman, among others.

I would be remiss if I did not mention the extensive support, both financial and non-financial, provided to me by the many individuals who comprise the Jefferson Scholars Foundation community and by Sam Lake, Troy Hartley, and everyone at Virginia Sea Grant. These academic networks greatly enriched my time at UVA. I am, likewise, very grateful to other colleagues who positively shaped my understanding of blue carbon and the Virginia Coast Reserve system, including but not limited to Barry Truitt, Ariana Sutton-Grier, Tiffany Troxler, Stefanie Simpson, Whitman Miller, Tom Arnold, Nick Meade, Hank Badger, and Royce Bridger.

Last, but definitely not least, I am indebted to my family for their support throughout this process, especially my father, Julius Oreska, for inspiring me to pursue a PhD, my mother, Marian Sayre-Oreska, and my brother, Julian Oreska. My grandparents, Robert and Elora Sayre, also provided support and inspiration, as did many other family members and friends. Your many contributions made this work possible.

Chapter 1. Introduction: Can carbon offset-credits finance seagrass restoration?

Parts of this chapter were published as:

Oreska, M. 2016. Can coastal restoration slow climate change? Gates Cambridge Blog. https://www.gatescambridge.org/multimedia/blog/can-coastal-restoration-slow-climate-change (accessed 21 Dec 2016).

1.1. Background

Two decades ago, the United Nations Framework Convention on Climate Change (UNFCCC) recognized that different land use activities, especially slash-and-burn deforestation, contributed significantly to greenhouse gas (GHG) pollution in the atmosphere (Holloway and Giandomenico 2009). In response, the UNFCCC called for incentives to slow deforestation (UNFCCC 2007) and the Intergovernmental Panel on Climate Change (IPCC) created guidelines to help countries track emissions from their 'Agriculture, Forestry and Other Land Use' (AFOLU) sectors (IPCC 2006). The UN Reducing Emissions from Deforestation and Forest Degradation Programme (REDD+) was launched in 2008, which allowed developed countries to pay developing countries to protect their remaining forests (UN-REDD 2017). Voluntary offset certification standards, including the Verified Carbon Standard (VCS), quickly proved instrumental to this effort, allocating offset-credits to individual forestry projects that limited GHG emissions relative to a business-as-usual baseline. By leveraging widespread, private sector concern about carbon footprint reduction, the VCS created a source of non-governmental finance for projects aimed at reducing deforestation. By 2012, VCS-certified credits accounted for half of the credits exchanged on voluntary offset markets, 43M of the 75.5M t CO_2-equivalent (CO_2e) GHG emissions reductions transacted that year (Forest Trends 2013). Almost one third of the voluntary credits traded in 2012 came from forestry/land use projects (Forest Trends 2013).

Efforts to protect the 'green carbon' in terrestrial forests have been modestly successful, but forests only account for part of the global carbon cycle. More than three-quarters of the carbon circulating through the Earth system passes instead through the ocean (IPCC 2001). Excess CO_2 uptake by the ocean is increasing ocean pCO_2 concentrations, resulting in ocean acidification. Coastal plant communities, therefore, play an important role by fixing some of the CO_2 diffusing across the air-water interface and transferring organic carbon (C_{org}) to coastal sediments (Zimmerman et al. 2015; Howard et al. 2017A). Many coastal plant beds are anaerobic, facilitating long-term (i.e. > decadal) sequestration of enhanced sediment C_{org} (SOC) stocks (Smith 1981; Mateo et al. 2006; Duarte et al. 2013A). Recent work indicates that seagrass meadows represent a major sink in the global carbon cycle (Fourqurean et al. 2012; Duarte 2017). However, just as deforestation contributes to increased atmospheric CO_2 loading, seagrass meadow collapse potentially represents a major source of GHG emissions back to the atmosphere (Pendleton et al. 2012). Fourqurean et al. (2012) estimate that seagrass meadow loss results in carbon emissions as high as 300 Tg C yr^{-1}, roughly equivalent to the annual energy sector emissions from Japan (DOE 2015).

1.2. Disappearing coastal habitats

A variety of anthropogenic impacts contribute to global seagrass loss, and meadow declines will likely continue to accelerate absent efforts to reverse these trends (Orth et al. 2006A; Waycott et al. 2009). More than one third of the human population lives within 100 km of the ocean (UNEP 2018), creating development pressures that impact coastlines. Urban/industrial run-off and coastal development represent the primary anthropogenic threats to seagrasses, globally, along with eutrophication, dredging, aquaculture, and other impacts (Orth et al. 2006A; Grech et al. 2012). An estimated one third of the world's seagrass meadows have disappeared since the 1800s (Waycott et al. 2009). Seagrass meadows are not as geographically extensive as terrestrial forests, but they often contain much higher concentrations of C_{org} in their soils (Duarte 2017).

In 2009, the U.N. Environment Program called for using offset-credit finance to protect the remaining CO_2 sequestered in threatened salt marshes, mangrove forests, and seagrass meadows (Nellemann et al. 2009). Several countries have taken steps to protect mangrove forests through UN-REDD, and the IPCC recently created a set of GHG accounting guidelines to assist countries that want to include marsh, mangrove, and seagrass 'blue carbon' in their national GHG inventory assessments (IPCC 2014)**;** however, a new global framework was needed to extend voluntary offset-credits to seagrass projects.

1.3. A tool in the fight against climate change

In 2012, Restore America's Estuaries (RAE) spearheaded the creation of the first generally-applicable, offset-credit accounting framework for vegetated habitats in tidal wetlands. This effort aimed to create an offset accounting protocol for mangrove forest, salt marsh, and seagrass meadow restoration projects for the VCS under their new Wetlands Restoration and Conservation category, part of the VCS AFOLU sector (cf. VCS 2017). RAE asked the University of Virginia to contribute the seagrass sections to the resulting offset protocol, *VM0033: Methodology for Tidal Wetland and Seagrass*

Restoration (Emmer et al. 2015A), which the VCS adopted for use in 2015. VCS-issued credits can now help finance seagrass restoration projects anywhere in the world. Selling VCS-awarded credits will hopefully provide a financial impetus to prospective seagrass restoration projects that are otherwise constrained by implementation costs.

The *Methodology* was designed to be rigorous and yield accurate net benefit calculations, yet flexible enough to accommodate a diverse range of coastal restoration projects (Emmer et al. 2015B). We used the best available scientific information to craft individual *Methodology* provisions. However, adapting GHG accounting methods developed for terrestrial settings for projects in intertidal and subtidal environments required addressing several sources of uncertainty. These scientific considerations are described in a forthcoming study (Needelman et al. *in review*).

In cases where we confronted persistent knowledge gaps, we either required that managers conduct direct monitoring to obtain accurate values or conservatively underestimate the offset benefit. For example, we required that projects deduct carbon from outside the project area that accumulates within a meadow—allochthonous carbon—from the total sequestered stock, because this carbon may or may not have returned to the atmosphere absent the project (CEC 2014). Another challenge involved determining whether seagrass meadows generally increase methane (CH_4) and nitrous oxide (N_2O) production, two harmful GHGs with higher global warming potential than CO_2 (Neubauer and Megonigal 2015). Absent sufficient data to provide a specific CH_4 'default value' for net benefit accounting, many seagrass projects will be required to measure CH_4, but we allowed seagrass projects to assume that any N_2O increase is negligible, based on the only available seagrass N_2O data (Shieh and Yang 1997; Emmer et al. 2015B). In other cases, we gave prospective project managers a range of approved accounting options. Rather than measuring all of the necessary accounting parameters, managers may justify using conservative default values in select cases (Emmer et al. 2015A sections 8.1.4, 9.2.4, 9.3.2, and 9.3.3). These default values include an IPCC (2014) seagrass restoration 'emission factor,' -0.43 t C ha^{-1} yr^{-1}, which purports to represent the net removal of carbon from the atmosphere by seagrass meadows, generally. The *Methodology* allows its use for estimating specific carbon pools, including SOC enhancement (e.g. Emmer et al. 2015A section 8.1.4). However, this number derives from studies in existing seagrass meadows comprised of the matte-forming species *Posidonia oceanica* (Mateo and Romero 1997; Serrano et al. 2012), so it may not be conservative for offset accounting in restored systems.

The VCS *Methodology* was circulated at the UN climate change meeting in Paris, COP21, and it has already assisted a mangrove restoration project in Indonesia (VCS 2015). More 'blue carbon' projects may follow in the near future, including seagrass projects. In 2016, California created the California Ocean Protection Trust Fund to finance seagrass restoration programs for climate mitigation (CA PRC § 35500). However, a seagrass restoration project has not yet applied for VCS credits (VCS 2018: http://vcsprojectdatabase.org/), and absent a proof-of-concept case study, prospective projects do not have a basis for expectations about the financial benefit of seagrass offset-credits from the VCS.

1.4. Seagrass restoration in Virginia

The aforementioned knowledge gaps motivate the individual studies presented in this dissertation. The following studies address specific, outstanding questions about carbon offset-crediting in restored seagrass systems by analyzing restored *Zostera marina* (eelgrass) beds in the Virginia Coast Reserve, a Long-Term Ecological Research site encompassing the marsh-lagoon-barrier island system on the Atlantic side of the southern Delmarva Peninsula (VCR-LTER). This system hosted *Z. marina* meadows until 1932 (CF 1932), when they disappeared during the North Atlantic Eelgrass Pandemic. Meadows from North America to Europe disappeared between 1931 and 1932 (Cottam 1935), likely due to an outbreak of *Labyrinthula zosterae* (Muehlstein et al. 1991). By 1935, some *Z. marina* meadows had recovered, including several in the Chesapeake Bay (Cottam 1935). The failure of the southern Delmarva seaside meadows to recover naturally may have been due to seed limitation (Orth et al. 2012).

Active *Z. marina* restoration in the VCR-LTER began in the late 1990s (Orth et al. 2006B) and achieved remarkable success by the mid-2000s, particularly in South Bay, Virginia (Orth et al. 2010). Eelgrass seeds were broadcast by hand in restoration seed plots, which coalesced into meadows that now expand naturally (Orth et al. 2006B). By 2012, restored meadows covered a total of 17 km^2 in four seaside bays, South Bay, Cobb Bay, Hog Island Bay, and Spider Crab Bay (Orth and McGlathery 2012), making the VCR-LTER eelgrass restoration, arguably, the most successful seagrass restoration project on the planet. This effort also achieved success at comparatively low cost. Seagrass restoration typically costs anywhere between $1.9K and $4M/ha (Paling et al. 2009); the

VCR-LTER restoration unit area cost was approximately $1.2K/ha (Reynolds et al. 2016). Additional information on the *Z. marina* recovery in this system can be found in a special issue of the *Marine Ecology Progress Series* (v. 448).

Recent work in the VCR-LTER has confirmed that restored meadow sites are accumulating C_{org} in both SOC and seagrass biomass (McGlathery et al. 2012; Greiner et al. 2013). This restoration, therefore, represents an ideal study system for answering the over-arching question motiving this dissertation: can carbon offset-credits finance seagrass restoration?

1.5. Specific questions motivating studies in this dissertation:

Chapter 2: How should we quantify SOC enhancement attributable to seagrass restoration? This chapter discusses methods for establishing a SOC baseline for GHG offset accounting, given challenges quantifying sedimentation rates in energetic subtidal habitats. SOC enhancement attributable to a seagrass project can be determined by subtracting baseline (i.e. bare site) SOC concentrations from observed seagrass meadow SOC concentrations. However, sediment accretion within the seagrass bed complicates comparisons between seagrass and bare site SOC profiles. I outline methods for establishing a seagrass bed marker-horizon for depth-calibrating sediment cores using the ‘layer with soil organic carbon indistinguishable from the baseline SOC concentration’ that we permitted for seagrass restoration projects in the VCS

Methodology (Emmer et al. 2015A section 9.3.7). This approach is applied in subsequent chapters to the restored *Z. marina* study system in the VCR.

Chapter 3: Can we estimate the total meadow SOC stock by scaling an average (i.e. unit area) SOC concentration by meadow area? The distribution of SOC within a seagrass meadow may vary spatially due to hydrodynamic 'edge effects,' which would complicate efforts to quantify the total, enhanced SOC stock within a given meadow. If SOC accumulates faster in one part of a meadow than another, restoration project managers must stratify (i.e. subdivide) the meadow area and track SOC enhancement in the respective areas separately to account for the discrepancy (Emmer et al. 2015A). This study provides the first documentation of seagrass SOC concentration spatial gradients attributable to hydrodynamic effects at the meadow-scale, the spatial scale relevant to blue carbon offset projects. The SOC stock calculated in this study also provides the basis for the meadow-scale C_{org} stock-change comparison presented in Chapter 5.

Chapter 4: Where does seagrass bed SOC originate, inside or outside of the meadow? An offset-credit project cannot claim credit for allochthonous C_{org}, which is fixed outside of the designated project area, because this C_{org} may or may not be associated with project activities and because its fate absent the project cannot be known with certainty (Emmer et al. 2015A). This offset accounting requirement helps ensure that certified credits correspond to a 1:1 removal of GHG from the atmosphere, but it is problematic for seagrass projects, because approximately half of the SOC in many seagrass beds appears to be non-seagrass C_{org} and may, therefore, be allochthonous (Kennedy et al. 2010). I used the spatial gradients identified in Chapter 3 and a Bayesian stable isotope mixing model approach to identify SOC by geographic origin within our study system.

Chapter 5: What is the net GHG (i.e. offset-credit) benefit of seagrass restoration? Increased CO_2 sequestration generates a positive climate benefit, but possible increases in the harmful GHGs methane (CH_4) and nitrous oxide (N_2O) may substantially negate this benefit, given their high global warming potentials. Restoring a seagrass meadow may increase the release of both GHGs relative to the business-as-usual baseline for the system, but there is currently insufficient data on the production of these GHGs in seagrass systems to estimate their net effect. The VCS *Methodology* requires that projects specifically account for CH_4, but we assumed that increased N_2O release would be negligible (i.e. *de minimis*) for offset-credit-accounting purposes, which the VCS defines as < 5% of the measured GHG benefit (Emmer et al. 2015B).

Chapter 6: Are there areas within the VCR system where regional managers can initiate additional *Z. marina* restoration, and would a new restoration effort be 'additional' under the VCS additionality criterion for offset projects (Emmer et al. 2015A)? The existing, restored meadows are not eligible for offset-credits, because the VCS only awards credits to new (i.e. additional) restoration efforts responding to the existence of an offset-credit market. Although Chapter 5 provides a retrospective proof-of-concept for seagrass carbon offset-credit finance, RAE and other blue carbon proponents are interested in initiating a new restoration project that can receive VCS credits to validate the seagrass offset concept. The VCR represents a promising test system, because of past *Z. marina* restoration success (Orth et al. 2010); however, there is uncertainty about whether other *Z. marina*-habitable areas exist within the system that are not already allocated for shellfish aquaculture. Managers are concerned about possible use conflicts that may constrain additional habitat restoration (Luckenbach and Ross 2011). Assuming new, habitable areas exist, another restoration effort would not necessarily be 'additional' for VCS offset-credit purposes if eelgrass will eventually recolonize these areas through natural seed dispersal.

VM0033: Methodology for Tidal Wetland and Seagrass Restoration was created for the VCS by Dr. Igino Emmer, Silvestrum; Dr. Brian Needelman, University of Maryland; Steve Emmett-Mattox, Restore America's Estuaries; Dr. Steve Crooks, Environmental Science Associates; Dr. Pat Megonigal, Smithsonian Environmental Research Center; Doug Myers, Chesapeake Bay Foundation; Matthew Oreska, University of Virginia; Dr. Karen McGlathery, University of Virginia; and David Shoch, Terracarbon.

The Methodology can be obtained from: http://database.v-c-s.org/methodologies/methodology-tidal-wetland-and-seagrass-restoration-v10 (accessed 11 March 2018).

Chapter 2. A method for calculating seagrass sediment organic carbon enhancement

Oreska, M.P.J., K.J. McGlathery, I.M. Emmer, B.A. Needelman, S. Emmett-Mattox, S. Crooks, J.P. Megonigal, D. Myers. 2018. Comment on 'Geoengineering with seagrasses: is credit due where credit is given?' *Environmental Research Letters* 13:038001. DOI:10.1088/1748-9326/aaae72

Abstract

In their recent review, ‘Geoengineering with seagrasses: is credit due where credit is given?,’ Johannessen and Macdonald (2016) invoke the prospect of carbon offset-credit over-allocation by the Verified Carbon Standard as a pretense for their concerns about published seagrass carbon burial rate and global stock estimates. Johannessen and Macdonald (2016) suggest that projects seeking offset-credits under the Verified Carbon Standard methodology *VM0033: Methodology for Tidal Wetland and Seagrass Restoration* will overestimate long-term (100 yr) sediment organic carbon (SOC) storage because issues affecting carbon burial rates bias storage estimates. These issues warrant serious consideration by the seagrass research community; however, VM0033 does not refer to seagrass SOC ‘burial rates’ or ‘storage.’ Projects seeking credits under VM0033 must document greenhouse gas emission reductions over time, relative to a baseline scenario, in order to receive credits. Projects must also monitor changes in carbon pools, including SOC, to confirm that observed benefits are maintained over time. However, VM0033 allows projects to conservatively underestimate project benefits by citing default values for specific accounting parameters, including CO_2 emissions reductions. We, therefore, acknowledge that carbon crediting methodologies such as VM0033 are sensitive to the quality of the seagrass literature, particularly when permitted default factors are based in part on seagrass burial rates. Literature-derived values should be evaluated based on the concerns raised by Johannessen and Macdonald (2016), but these issues should not lead

to credit over-allocation in practice, provided VM0033 is rigorously followed. These issues may, however, affect the feasibility of particular seagrass offset projects.

2.1. Introduction

In their review of the seagrass carbon literature, Johannessen and Macdonald (2016) (hereafter, J&M) discuss methodological issues that may bias published seagrass carbon burial rates upward and imply that inattention to these issues in "six published international protocols" will result in over-allocation of carbon offset-credits to seagrass projects by the Verified Carbon Standard (VCS). J&M outline six problems that potentially affect measurements of sediment organic carbon (SOC) storage, most of them related directly or indirectly to calculating seagrass SOC burial fluxes. According to J&M, seagrass studies frequently 1.) confuse sediment carbon inventories with fluxes, 2.) extrapolate carbon measurements taken in *Posidonia* spp. meadows to generate global estimates, 3.) neglect bioturbation, 4.) neglect remineralization, 5.) neglect export due to "energy of the environment," and 6.) count allochthonous SOC as a seagrass GHG benefit. These issues are fairly common in the broader seagrass literature; however, the VCS only awards offset-credits (i.e. Verified Carbon Units) for observed, enhanced GHG sequestration—not anticipated carbon 'storage' estimated from burial rates. Of the six protocols discussed by J&M, only the VCS-approved *VM0033: Methodology for Tidal Wetland and Seagrass Restoration* (Emmer et al. 2015A) can presently be used to generate seagrass offset-credits (note, however, that one of the other 'protocols,' Emmer et al. 2015B, is the VM0033 users' manual).

Given J&M's concerns about the quality of the seagrass carbon literature and apparent confusion about offset-crediting, we feel that it is important to identify the areas where their specific concerns are relevant for crediting purposes and to clarify offset-crediting concepts for the broader seagrass research community. We agree that the issues raised by J&M warrant serious consideration by seagrass researchers, especially sediment organic carbon (SOC) remineralization over short (i.e. ≤ 100-yr) timescales. We also agree that the problems J&M discuss may affect the proper application of seagrass offset-credits through VM0033 provisions that allow restoration projects to cite literature-derived values for specific GHG accounting parameters. The VCS allows projects to conservatively underestimate the net GHG benefit using default values in cases where direct measurements cannot be obtained. However, we also note that offset-credits are only issued by the VCS for net GHG emissions reductions achieved by the project, relative to a baseline (i.e. business-as-usual) scenario without the project. Projects may anticipate future GHG benefits by calculating SOC accumulation from burial fluxes or another extrapolation technique, but VCS credits are only awarded *ex post* (Emmer et al. 2015A section 9), after an independent, third-party validator confirms that projected emissions reductions have taken place.

2.2. Defining the seagrass offset-credit benefit

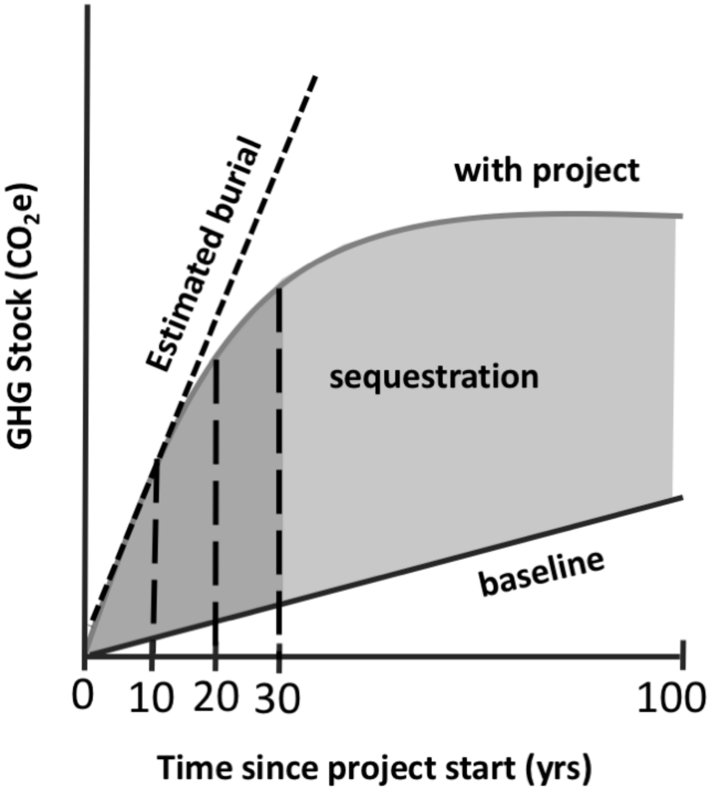

Figure 2.1. Project GHG sequestration: VM0033 only allocates credits for demonstrated, enhanced GHG sequestration (i.e. emissions reductions) in the project scenario relative to a baseline (i.e. business-as-usual) scenario [note: GHG emissions may increase, decrease, or remain static in the baseline scenario]. Projects must verify emissions reductions during the project period (30 years) and revise future benefit expectations if needed (light gray).

The GHG accounting process required by VCS to determine the creditable GHG benefit differs in important respects from methods used by recent studies to calculate seagrass 'blue carbon' benefits (e.g. Mcleod et al. 2011; Fourqurean et al 2012; Greiner et al. 2013). First, the VCS-approved, net GHG benefit must account for GHG emissions in the baseline and project scenarios, including potential CO_2 and CH_4 increases in the project scenario that reduce the overall benefit. Emission of GHGs during the construction of the project are also subtracted. Second, the VCS requires that offset projects periodically monitor changes in particular GHG pools that affect net CO_2e emissions, including SOC, over a 30-year project period (Emmer et al. 2015A sections 8.1.1 and 8.2.1). Most seagrass literature studies are based on short-duration field surveys, lack decadal-scale measurement data, and, therefore, resort to estimating long-term (i.e. ≥ 100-yr) SOC stock changes using burial rates. Third, VM0033 and other reputable methodologies are designed to underestimate the net GHG benefit unless applicant projects take thorough, rigorous, direct measurements that convince validators that the actual project benefit is higher than the conservative, estimated benefit. Projects are not required to monitor GHG benefits after the end of the project period, but they must quantify the risk that gains will be lost in this future time period (VCS 2012). VCS places a proportional number of credits into a risk 'buffer pool,' which can be released to projects over time, provided reversals do not materialize (Emmer et al. 2015A section 8.5.3).

J&M are correct that seagrass meadows are transient systems, and future SOC losses can occur due to events such as erosion and dieback. Their specific concerns provide important insights into how non-permanence risk analysis should be performed (VCS 2012). Long-term seagrass monitoring studies are clearly needed to better understand the factors that influence risk on decadal timescales. If a project cannot demonstrate that future benefit reversal risk is low, the project will likely be unfeasible, because high uncertainty will lead to a large credit withholding.

Although seagrass restoration projects may attempt to quantify CO_2 emissions in the project and baseline scenarios without direct sampling of specific carbon pools (e.g. using eddy flux), in practice, most seagrass projects will need to monitor SOC changes over decadal timescales to verify GHG emission reductions relative to the baseline scenario. We agree that a project will overestimate the net GHG benefit if they equate the project benefit with SOC burial and fail to account for remineralization (J&M problem #4) or export (J&M problem #5) of that stock over time. Some recent studies specifically equate seagrass SOC 'burial' and 'sequestration' rates (e.g. Mcleod et al. 2011), but actual sequestration will be lower than expected burial over time, because of SOC remineralization within the bed (Figure 2.1). We, therefore, advise validators and the VCS to be mindful of the issues described by J&M, especially with respect to long-term projections. Sediment cores collected at intervals over the project period—either for stock change assessment or repeated burial flux calculations—should confirm this lower sequestration over time. We also agree with J&M that projects, validators, and the VCS should consider factors that bias sedimentation rates if they calculate burial fluxes (J&M problem #3). However, we note that projects do not need to estimate SOC 'burial rates' in order to receive offset-credits, provided projects can account for bed accretion and erosion within the meadow. Taking repeated sediment cores over time (the stock change method) circumvents both bioturbation effects on sedimentation rates (J&M problem #3) and mineralization effects on SOC (J&M problem #4).

2.3. Feasibility of the stock change approach

J&M dismiss the stock change method as “difficult, if not impossible” for assessing SOC changes in sediment cores, pointing out that hummocky bed surfaces, horizontal sediment advection, slow accretion times, and near-surface mixing complicate efforts to establish a marker horizon in seagrass beds. These issues complicate stock-change accounting but do not render it scientifically invalid.

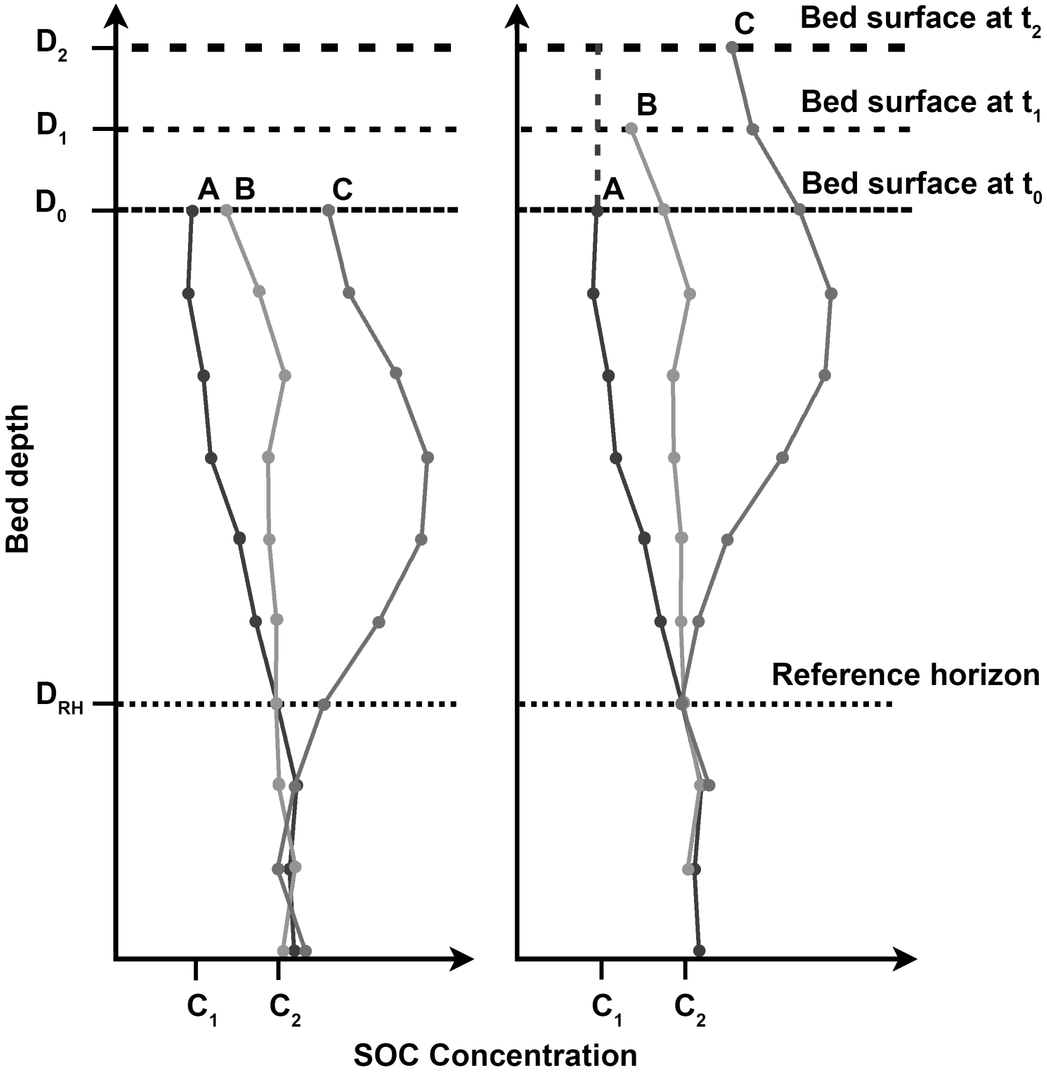

Figure 2.2. Establishing the seagrass reference horizon: VM0033 allows several methods for establishing a seagrass bed reference horizon, the bed depth (D_{RH}) where depth- and time-calibrated SOC core profiles collected prior to the meadow restoration (A) and after meadow establishment (B and C) exhibit the same SOC concentration (C_2). Note that the bed surface at t_0 in profile A calibrates to subsurface horizons in profiles B and C after accounting for accretion (right panel). The creditable GHG benefit in each time step corresponds to the difference between the meadow profile (B and C) and the bare profile (A) concentrations. Projects will not be able to claim credit for all of the SOC above D_0 in the calibrated figure, because they must discount recalcitrant SOC that could have been deposited in the baseline scenario. This fraction corresponds to the SOC between D_O and D_2 and left of C_1 in this illustration.

We acknowledge that projects cannot precisely compare changes in SOC concentrations along depth-calibrated profiles over time without a reference plane and that these and other dynamics within seagrass meadows complicate this process. VM0033 permits several options for identifying a reference plane in seagrass systems, some of which may not be feasible for a given project. In addition to installing a physical reference plane and other common techniques, projects may identify “a strongly contrasting soil layer” or compare cores down to “a layer with soil organic carbon indistinguishable from the baseline SOC concentration” (Emmer et al. 2015A section 9.3.7). These methods can potentially be used to quantify accretion at meadow sites without calculating sedimentation rates, which may be subject to variable sediment velocity (J&M problem #1) and sediment mixing due to bioturbation (J&M problem #3). For example, meadow restoration increases fine-sediment deposition (McGlathery et al. 2012), which may result in a "contrasting soil layer" attributable to bed accretion, provided the finer, accreted sediment abruptly transitions to coarser sediment in cores. Another method, the "indistinguishable" SOC concentration approach, can be employed using the following steps (Figure 2.2):

1.) Project proponents collect sediment cores prior to meadow restoration (t_0) and periodically after meadow establishment ($t_{1,2,3\ldots}$) (note: cores from a comparable bare control site can be substituted for the t_0 observation).
2.) The surface horizon of the bare core will equate to a subsurface horizon at meadow sites if there is meadow-mediated bed accretion (Bos et al. 2007). The meadow SOC concentration profile may, therefore, appear to decrease to an equivalent background concentration at a deeper core depth than would be suggested by comparing the two SOC profiles side-by-side. Projects can depth-calibrate the bare and meadow profiles by aligning the point on both profiles where the SOC concentrations first become indistinguishable.
3.) The net SOC increase attributable to the meadow above this reference plane is then determined by subtracting the bare concentration (t_0) from the meadow SOC concentration (t_1) at each time-equivalent point along the two profiles and summing the differences. Dividing the total net increase by the time that has transpired since t_0 yields an accumulation rate. Meadow SOC

profile shapes may vary considerably depending on location (cf. chapter 3), which is why projects should collect multiple, spatially-distributed cores.

4.) Projects must conduct periodic monitoring, because the amount of SOC enhancement within the meadow may increase in a non-linear fashion and fluctuate after the meadow reaches maturity. Meadow cores collected in subsequent time periods ($t_{2,3,4....}$) may show additional SOC from both surface accretion and belowground biomass accumulation (Figure 2.2). If profiles exhibit considerable variability, VM0033 requires that projects take additional samples and constrain parameter uncertainty using confidence intervals (Emmer et al. 2015A section 8.5.2).

This stock change approach will capture any SOC losses due to remineralization (J&M problem #4) or export (J&M problem #5), along with any SOC increase within the bed from belowground biomass. This latter SOC accumulation pathway further complicates the burial flux approach. The profiles in Figure 2.2 are based on seagrass restoration studies that show SOC concentration changes within the bed following revegetation (e.g. Greiner et al. 2013; Marbà et al. 2015). The carbon concentration peak observed approximately 4 cm below the sediment-water interface in a restored seagrass bed by Greiner et al. (2013) corresponds with the rhizosphere in that system.

This outlined method may not be appropriate in all cases. If a project attempts to use this method to establish the reference plane but a third-party validator concludes that it is subject to error, VCS will not certify the requested offset-credits. Projects can instead calculate bed SOC accumulation using an approved equation, for example J&M's

"direct method." However, all projects must determine the bed depth to which the meadow enhances sediment SOC. Nowhere in VM0033 or in the associated manual (Emmer et al. 2015B) are projects allowed to count all of the SOC within the top meter of a seagrass bed as a GHG benefit.

2.4. In some cases, literature issues will affect carbon crediting methodologies

In cases where measuring a specific stock change proves prohibitive, carbon credit methodologies allow projects to estimate the change in both the project and baseline scenarios using default values and approved models. We agree that the issues raised by J&M may affect the use of literature-derived values; for this reason, the use of these values in VM0033 is severely restricted. Literature values and models must derive from the "same or similar systems," as defined by the VCS (Emmer et al. 2015A section 8.1.4.1), and projects must be able to justify their use "as appropriate for project conditions" to the validator and ultimately to the VCS (Emmer et al. 2015A sections 8.1.4, 8.2.4, 9.3.2, and 9.3.3). The concerns raised by J&M are, therefore, important, because proposed projects will use the scientific literature to support their calculations, and independent validators should be aware that some sources overestimate benefits.

The concerns of J&M about the quality of data in the seagrass literature may be particularly relevant in cases where projects cite a general default factor. For example, a project may use the latest IPCC (2014) Tier 1 seagrass restoration default value, currently -0.43 t C ha^{-1} yr^{-1} (IPCC 2014: p. 4.29, Table 4.12), to estimate emissions reductions in the project scenario. This figure need not be accurate, provided it conservatively underestimates the net GHG benefit. It is essential to understand that use of this default value must be justified as conservative for project conditions to the independent validator, and the project must still deduct an allochthonous carbon fraction from this number (see below). As J&M point out, values from *Posidonia oceanica* studies are not conservative estimates for all seagrass systems, because this matte-forming species generates unusually high sediment SOC stocks (J&M problem #2). The IPCC (2014) value derives from two *P. oceanica* studies (Mateo and Romero 1997; Serrano et al. 2012), but it appears conservative relative to the range of sediment carbon accumulation rates compiled by Mcleod et al. (2011), 0.45 to 1.90 t C ha^{-1} yr^{-1}. The IPCC (2014) number is also comparable to the sediment SOC accumulation rate observed in a *Zostera marina* restoration project, 0.37 t C ha^{-1} yr^{-1} (Greiner et al. 2013), which excludes biomass sequestration. Despite these allowances, we expect that most projects will need to make direct, stock-change measurements, because the project system exhibits different “geomorphic, hydrologic, and biological properties” and is, therefore, not “the same or similar” to these other systems (Emmer et al. 2015A section 8.1.4.1).

VM0033 also includes a VCS requirement that default factors undergo periodic re-assessment. If future work demonstrates that the current IPCC seagrass value is not conservative, the VCS will disallow its continued use (Emmer et al. 2015A section 8.1.4.1). We recommend that future amendments to the methodology include language instructing validators to specifically consider the concerns expressed by J&M,

especially in cases where projects use sedimentation rates to estimate SOC accumulation.

2.5. Other offset provisions safeguard against credit over-allocation

The VCS and other rigorous standards enforce additional safeguards against credit over-allocation, because credit oversupply already depresses the average credit price on the voluntary carbon market (Forest Trends 2016). Projects must meet the VCS ‘additionality’ requirement, which confirms that GHG benefits were a driver for the restoration effort (Emmer et al. 2015A section 7). Seagrass offset-credits will not be allocated for existing seagrass carbon pools, so concerns about seagrass global stock estimates are not relevant (J&M problem #2). Regarding export (J&M problem #5), projects only get credit for average, standing biomass, not leaf litter (Emmer et al. 2015A Table 5.1). VM0033 also requires that seagrass projects remove inorganic carbon from sediment cores prior to carbon content analysis (Emmer et al. 2015A section 9.3.7).

Finally, we note that concerns about allochthonous carbon (J&M problem #6) are addressed in VM0033 in considerable detail. J&M are correct to note that allochthonous carbon deposited in a seagrass bed could be buried and stored absent the meadow (i.e. in the baseline scenario). For this reason, VM0033 requires that projects deduct recalcitrant allochthonous carbon from project benefits, unless the project proponents can show that this fraction would have been returned to the atmosphere absent the project (Emmer et al. 2015A section 8.2.4.2.2). Seagrass meadows enhance accumulation and preservation rates for deposited allochthonous organic matter (Duarte et al. 2013A), which may account for more than half of the SOC sequestered in some seagrass beds (Kennedy et al. 2010; but also see chapter 4). VM0033 conservatively requires that seagrass projects identify and deduct all of this recalcitrant allochthonous carbon from project benefits—even in cases where a project cites the IPCC (2014) default value for total SOC enhancement.

2.6. Conclusions

J&M provide a timely, thought-provoking review of seagrass carbon burial considerations; however, they incorrectly suggest that VM0033 (and Emmer et al. 2015B) over-allocates carbon credits. We share J&M's general concern about potential offset-credit misallocation, which devalues legitimate offset-credits. For this reason, VM0033 and other rigorous methodologies require that offset projects account for a variety of factors, including future gain reversals, stock remineralization, biomass export, and allochthonous carbon, among others, that may render seagrass projects inoperable in practice. We acknowledge GHG accounting complexities in seagrass systems, including SOC accumulation and remineralization processes operating on different timescales, and, therefore, suggest that the blue carbon literature differentiate between SOC net 'sequestration' and 'burial' when discussing seagrass offset-credits. Literature values can be used in specific cases, provided these values represent conservative parameter estimates and validators approve their use. Validators must carefully review all cited literature values, emission factors, and models before approving project GHG calculations, given J&M's concerns. However, contrary to J&M's suggestion, VM0033 explicitly requires projects to either conservatively underestimate the GHG benefit or undertake sufficient monitoring to derive statistically accurate and scientifically defensible parameter estimates when calculating seagrass GHG stock changes.

Acknowledgements

I would like to thank my collaborators for their contributions: K.J. McGlathery, I.M. Emmer, B.A. Needelman, S. Emmett-Mattox, S. Crooks, J.P. Megonigal, and D. Myers, the *ERL* reviewer for helpful feedback, and the *ERL* editors for providing an opportunity to further an important dialogue on seagrass blue carbon science. Funding was provided by National Science Foundation VCR-LTER Grant DEB-1237733, the University of Virginia Jefferson Scholars Foundation, and Virginia Sea Grant. BAN's contribution was supported by the Maryland Department of Natural Resources Power Plant Research Program and the USDA National Institute of Food and Agriculture Hatch Project 1013805.

Chapter 3. Seagrass blue carbon spatial patterns at the meadow-scale

Oreska, M.P.J., K.J. McGlathery, J.H. Porter. 2017. Seagrass blue carbon spatial patterns at the meadow-scale. *PLoS ONE* 12(4):e0176630. DOI:10.1371/journal.pone.0176630.

Abstract

Most information on seagrass carbon burial derives from point measurements, which are sometimes scaled by meadow area to estimate carbon stocks; however, sediment organic carbon (C_{org}) concentrations may vary with distance from the meadow edge, resulting in spatial gradients that affect the accuracy of stock estimates. We mapped sediment C_{org} concentrations throughout a large (6 km^2) restored seagrass meadow to determine whether C_{org} distribution patterns exist at different spatial scales. The meadow originated from ≤1-acre plots seeded between 2001 and 2004, so we expected C_{org} to vary spatially according to the known meadow age at sample sites and with proximity to the meadow edge. Applying spatial autoregressive models allowed us to control for spatial autocorrelation and quantify the relative effects of edge proximity and age on C_{org} concentrations. We found that edge proximity, not age, significantly predicted the meadow-scale C_{org} distribution. We also evaluated relationships between C_{org} and a variety of specific explanatory variables, including site relative exposure, shoot density, sediment grain size, and bathymetry. Factors known to affect carbon burial at the plot-scale, such as meadow age and shoot density, were not significant controls on the meadow-scale C_{org} distribution. Strong correlations between C_{org}, grain size, and edge proximity suggest that current attenuation increases fine-sediment deposition and, therefore, carbon burial with distance into the meadow. By mapping the sediment C_{org} pool, we provide the first accurate quantification of an enhanced carbon stock attributable to seagrass restoration. The top 12 cm of the bed contain 3660 t C_{org}, approximately 1200 t more C_{org} than an equal area of bare sediment. Most

of that net increase is concentrated in a meadow area with low tidal current velocities. Managers should account for the effects of meadow configuration and current velocity when estimating seagrass blue carbon stocks. Our results suggest that a large, contiguous meadow should store more blue carbon than an equal area of small meadow patches.

3.1. Introduction

Seagrass meadows are highly productive ecosystems that bury organic carbon (Duarte and Chiscano 1999; Duarte et al. 2010; Greiner et al. 2013), making them sinks in the global carbon cycle (Smith 1981). Bed accretion from canopy particle trapping, seston burial, and sediment anoxia (de Boer 2007; Carr et al. 2010; Duarte et al. 2013A) facilitate high sediment carbon burial rates in seagrass meadows (Kennedy et al. 2010). However, the global disappearance of meadows (Waycott et al. 2009) causes bed erosion (Marbà et al. 2015) and the loss of accumulated sediment carbon (Macreadie et al. 2015), a significant carbon stock in many meadows (Fourqurean et al. 2012). Organic carbon (C_{org}) oxidation in degraded seagrass beds potentially releases 0.05 to 0.33 Pg CO_2 back to the atmosphere each year (Pendleton et al. 2012). Efforts to finance seagrass restoration through the sale of ‘blue carbon’ offset-credits aim to reverse this trend (Nellemann et al. 2009; Murray et al. 2011).

Despite significant work on seagrass sediment carbon dynamics (e.g. Moriarty et al. 1986; Duarte et al. 2005; Mateo et al. 2006), little is known about how sediment C_{org} accumulates spatially in seagrass beds (Mcleod et al. 2011). If the resulting stock is non-uniformly distributed throughout a meadow, multiplying an average cm^3-scale concentration obtained from individual plots by total meadow area (e.g. Duarte et al. 2010; Howard et al. 2014) would yield an inaccurate meadow-scale (ha or km^2) stock estimate. In a restored meadow that is expanding, C_{org} concentrations may vary spatially simply because younger meadow areas have had less time to accumulate C_{org}. However, other meadow and landscape-scale factors might also cause sediment C_{org} to exhibit spatial variability, including hydrodynamics (Fonseca and Bell 1998; Bell et al. 2006), canopy structure (Bell et al. 2006; Granata et al. 2001; Samper-Villarreal et al. 2016), and environmental gradients, such as bathymetry (Samper-Villarreal et al. 2016; Lavery et al. 2013; Serrano et al. 2015). Some of these factors may give rise to C_{org} spatial gradients, especially relative to the boundary between the meadow and bare subtidal areas, hereafter referred to as the ‘edge’ (Ricart et al. 2015).

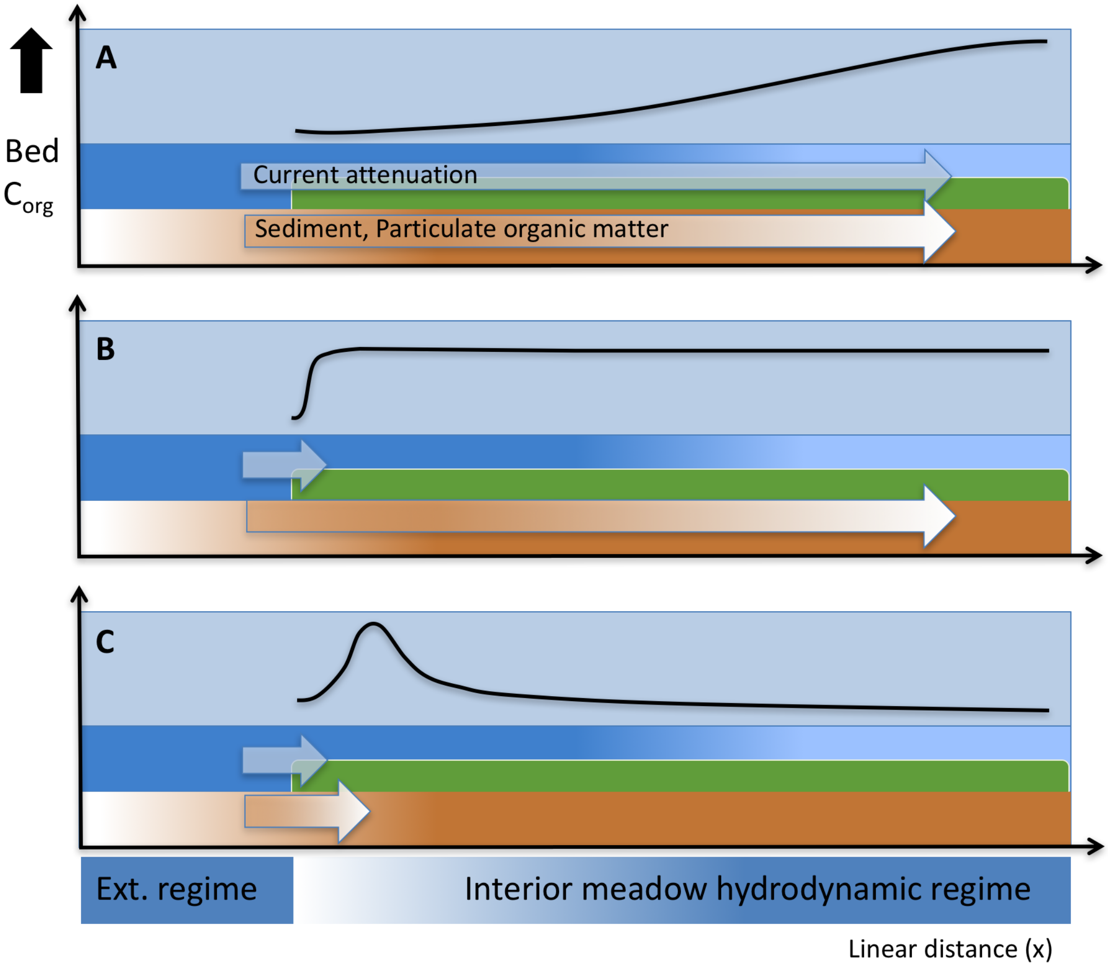

Figure 3.1. Hypothetical sediment C_{org} spatial distributions (black lines) relative to a seagrass meadow edge: these hypotheses assume (A) increasing current attenuation with distance into the meadow, (B) attenuation over a short distance and high suspended sediment availability, and (C) attenuation with low suspended sediment availability.

Several different C_{org} spatial gradients might result from current flow effects relative to the meadow edge (Figure 3.1). Seagrass canopies affect near-bed shear stress, which affects sediment accumulation (López and García 1998; Koch et al. 2006;

Hansen and Reidenbach 2012). Particle settling facilitates the burial of both seagrass detritus and external particulate organic matter (Duarte et al. 2013A). At the meadow edge, higher turbulence (Granata et al. 2001) and wave energy (Hansen and Reidenbach 2012) may cause erosion, potentially preventing C_{org} accumulation relative to interior sites. Progressive canopy attenuation of waves and tidal currents (Hansen and Reidenbach 2012; Mendez and Losada 1999; Chen et al. 2007) may result in increasing C_{org} burial with distance into the meadow (Figure 3.1A). If, however, canopies attenuate shear stress to a constant level over short distances (perhaps <0.5 m: cf. Lefebvre et al. 2010; Carr et al. 2015), the 'edge zone' may be narrow and have a negligible impact on the total C_{org} stock (Figure 3.1B). Alternatively, external sediment supply may decrease with distance as particles settle out (Chen et al. 2007), causing sediment accumulation to peak and then decrease towards the meadow center (Figure 3.1C). Canopy filtration of external particulate organic matter (Hendriks et al. 2008) and deflection of incoming wave energy (Bradley and Houser 2009; Gruber and Kemp 2010) may result in more C_{org} burial near the edge.

Some empirical evidence now exists for seagrass sediment C_{org} concentration variability at patch- and regional-scales (Ricart et al. 2015; Samper-Villarreal et al. 2016), but there is a lack of empirical support to link site and process-based studies with spatial patterns at the meadow-scale. Few seagrass studies sample over whole meadow areas and most do not account for spatial autocorrelation (e.g. Samper-Villarreal et al. 2016), thereby limiting their ability to identify statistically significant controls on C_{org} accumulation at spatial scales ≥1 km.

The existence of meadow-scale C_{org} spatial gradients would have implications for blue carbon finance for seagrass restoration. A framework now exists for allocating carbon dioxide equivalent (CO_2e) offset-credits to restoration projects. This framework, the Verified Carbon Standard methodology VM0033 (Emmer et al. 2015A), requires that managers stratify project areas to account for spatial variability when estimating blue carbon stocks (cf. VCS 2015 for information on stratification). If zones of higher and lower C_{org} accumulation exist within meadows, managers must identify these zones (i.e. strata) and scale average C_{org} concentrations within each zone separately to generate a whole-meadow stock estimate.

The restored *Zostera marina* (eelgrass) meadow in South Bay, Virginia, provides a unique opportunity to investigate sediment C_{org} spatial patterns at the meadow-scale. This mature meadow has a well-documented restoration and expansion history (Orth et al. 2006B; Orth et al. 2010; McGlathery et al. 2012; Orth et al. 2012), allowing us to consider C_{org} accumulation time (i.e. site meadow age) as an independent variable potentially affecting the C_{org} spatial distribution. Eelgrass seeds were broadcast in South Bay in 0.5 and 1-acre seed plots from 2001-2004 (Orth et al. 2006B), which later coalesced into a single, contiguous meadow encompassing >6 km^2 (Orth et al. 2012), making it the world's largest restored seagrass meadow. This meadow is accumulating C_{org} from both eelgrass and allochthonous sources relative to bare sites (McGlathery et al. 2012; Greiner et al. 2013; Greiner et al. 2016). Wind-generated shear stress is a dominant control on sediment suspension throughout this coastal bay system (Lawson et al. 2012; Fagherazzi and Wiberg 2009). The meadow attenuates both wave and tidal currents, thereby affecting suspended sediment concentrations and sediment accretion rates relative to bare areas (Greiner et al. 2013; Hansen and Reidenbach 2013). We expected to find sediment C_{org} spatial gradients related to edge proximity, in addition to a C_{org} distribution pattern related to meadow expansion. Spatial gradients related to differences in relative location and meadow age may be attributable to co-varying factors known to affect sediment accumulation at individual meadow sites, especially shoot density (Serrano et al. 2015; McGlathery et al. 2012).

3.2. Methods

3.2.1. Study area

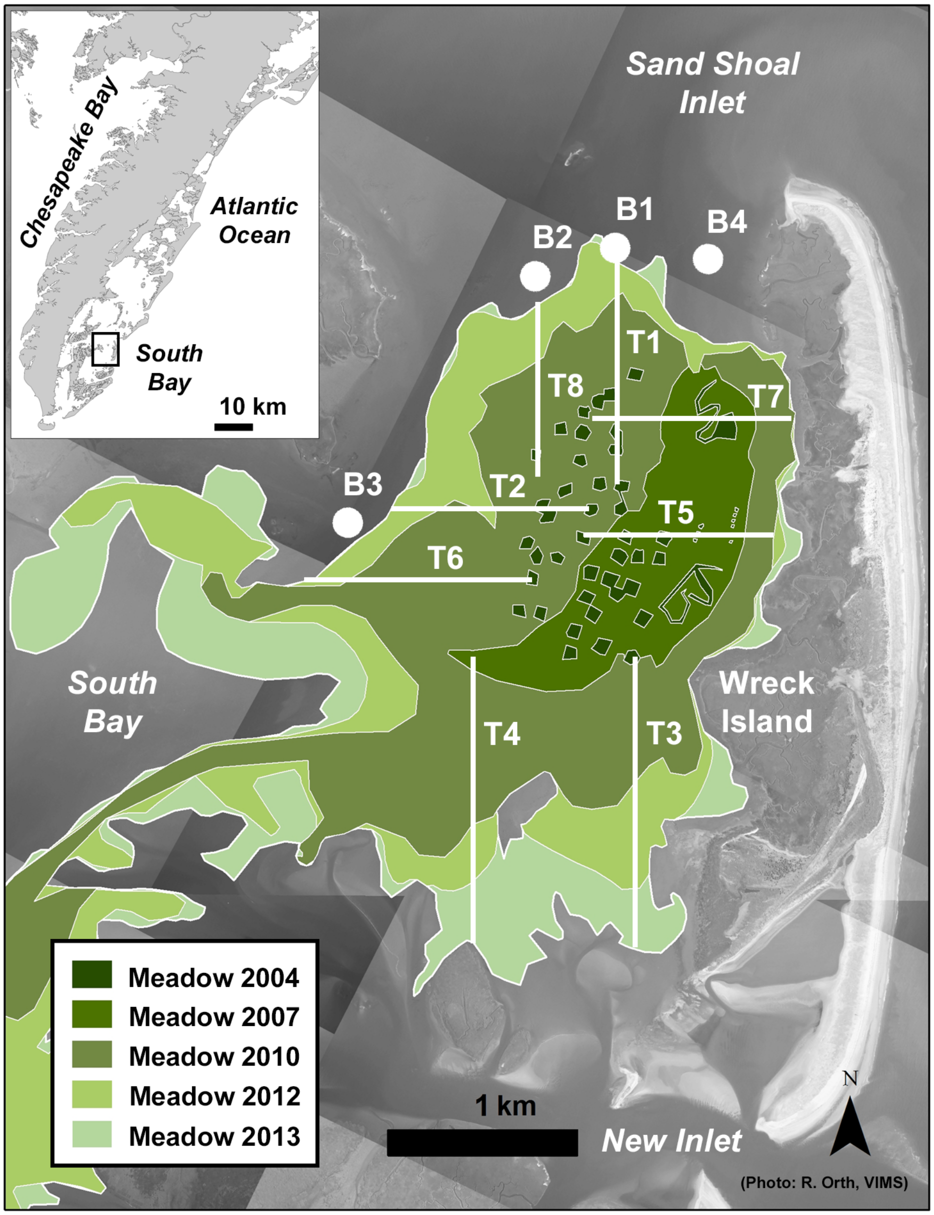

Figure 3.2. The restored South Bay eelgrass meadow, showing its expansion history and sampling transects; sites B1-4 provided bare control sites (background photo printed under a CC BY license, with permission from R. Orth, VIMS 2014).

The restored South Bay eelgrass meadow and surrounding area is part of the Virginia Coast Reserve, a Long-Term Ecological Research site (VCR-LTER). South Bay is separated from the Atlantic Ocean by Wreck Island to the east and bordered to the west by Man and Boy Channel. The meadow bathymetry is shallow, with an average depth at MSL of 0.76 m and a standard deviation of 0.28 m (Richardson et al. 2014). Tides enter and exit the area via inlets to the north and south of the meadow. The mean tidal range is 1.2 m (Figure 3.2; Fagherazzi and Wiberg 2009). The Virginia coastal bays are oligotrophic (McGlathery et al. 2007), resulting in a light environment conducive for plant growth (McGlathery et al. 2012; Moore et al. 2012). Shoot densities exceed 600 shoots m^{-2} at maximum biomass in the summer, and the canopy height ranges from 32-45 cm (McGlathery et al. 2012). The east half of the meadow adjoins Wreck Island; the west half of the meadow has a well-defined edge that separates the meadow from bare, subtidal areas (Figure 3.2). South Bay's large surface area, relatively constant bathymetry, and a water depth to canopy height ratio of approximately 2:1 at MSL make it an ideal location for assessing canopy-hydrodynamic effects. Restoration has resulted in increased sediment carbon concentrations in the meadow (McGlathery et al. 2012), such that a mid-meadow site exhibited significantly higher carbon content than an adjacent bare site in 2012, 0.52±0.010% versus 0.36±0.012% (Greiner et al. 2013). Hansen and Reidenbach (2012; 2013) measured bed shear stress and suspended sediment concentrations at locations both inside and outside of this meadow from 2010 to 2011. Average Reynolds stresses were lowest in the southwest part of the meadow, approximately 0.5 $cm^2\ s^{-2}$ ($z = 0.5$ m), compared with ~1 $cm^2\ s^{-2}$ at a mid-meadow site and 1.5 $cm^2\ s^{-2}$ outside of the meadow (Hansen and Reidenbach 2012). Suspended sediment concentrations averaged ~20 mg l^{-1} at a mid-meadow site and ~30 mg l^{-1} outside of the meadow (Hansen and Reidenbach 2013).

3.2.2. Data collection and sample preparation

Sediment samples were collected along eight subtidal transects in July 2013 to quantify C_{org} distribution patterns in the meadow (Figure 3.2). Parallel transects were laid out from meadow edge to interior in each cardinal direction to provide broad meadow coverage. The transect sites were arrayed systematically (note that permits were not required for sediment collection from public bottomlands). Each transect contained eight sites spaced 150 m apart with the exception of transect 1, which had ten sites. Eight sites fell within original restoration seed plots (Orth et al. 2006B) and the others represented meadow ages ranging from <1 to 12 years due to natural meadow expansion. Four sites near the meadow provided a bare control group (Figure 3.2). Four replicate 60 cc hand cores were collected at each site to a depth of 12 cm and divided into four 3-cm intervals to generate a sediment C_{org} profile for each site. The bed has aggraded ~3-4 cm due to restoration (Greiner et al. 2013). Each of the 264 cores collected during this study were visually inspected for compaction when collected, which was approximately 7%, given the predominantly sandy sediment in this study area (mean grain size = 71 μm: Lawson et al. 2012).

Macroscopic roots, rhizomes (i.e. belowground biomass), and shell fragments were removed from samples to isolate the sediment organic matter (OM) component from belowground biomass. Sediment bulk density, %OM, and percent carbon and nitrogen (%C and %N) were determined following standard methods used previously at this site (McGlathery et al. 2012; Greiner et al. 2013). Loss on ignition (LOI) in a muffle furnace at 500°C for six hours was used to determine %OM. A Carlo Erba NA 2500 Elemental Analyzer was used to determine %C and %N. Bulk C_{org} was determined using the element analyzer method described in Howard et al. (2014).

Meadow age at each site was established using aerial photographs taken annually beginning in 2001 (VIMS 2014; high resolution images provided by R. Orth, VIMS). Sample sites were georeferenced relative to each aerial photo in ArcGIS 10.2. By observing meadow presence/absence in each photo, we determined the length of time that seagrass has been present with one-year precision. The original seed plots coalesced over time into a single meadow, which continued to expand naturally, such that seagrass remained present at every meadow site after its first appearance (Figure 3.2).

The georeferenced aerial photographs also allowed us to determine site distance from the meadow perimeter. Site edge proximity was measured two different ways: linear distance along transects to the 2013 meadow perimeter and Euclidean distance to the 2013 edge (Near analysis in ArcGIS 10.2). The first measure allowed us to compare C_{org} concentration changes with distance along a given transect. The second measure established site location relative to the meadow boundary that intercepts incoming current and wave energy.

Several additional variables were also measured that could influence the C_{org} spatial distribution pattern, including site relative exposure, peak-summer (July) shoot density (shoots m^{-2}), sediment grain size distribution (top 3 cm of the bed), mean water depth (bathymetry), and sediment C:N ratio. A relative exposure index (REI) was calculated for every site according to methods in Fonseca and Bell (1998). Effective fetch was found by intersecting radiating lines at each site with surrounding land surfaces delineated using aerial imagery in ArcGIS 10.2. Wind vector and frequency data necessary for REI were obtained from a LTER monitoring station immediately south of the meadow on Godwin Island (Reidenbach and Timmerman 2014). Replicate shoot density counts and grain size samples were collected at a subset of sites that were randomly selected to provide broad spatial coverage (n = 16). Average density counts were also taken at six additional, mid-meadow sites during a VCR-LTER annual survey. Shell fragments were removed from grain size samples, which were oxidized using 30% H_20_2 and then acidified using a 5.0 pH acetic acid and NaOAc solution to remove OM and carbonates. Grain size distributions were determined using a Beckman-Coulter BLS 13 320 Laser Diffraction Particle Size Analyzer. Water depth at each site was determined by extracting bathymetric data (Richardson et al. 2014) by site in ArcGIS 10.2. REI and bathymetry provided measures of relative wave energy and tidal current strength, respectively (Mariotti and Fagherazzi 2012). Mean grain size provided a measure of time-integrated shear stress and water residence time (Lawson et al. 2007; Wiberg et al. 2015). The C:N ratio provided an indication of OM source.

3.2.3. Analyses

We identified meadow-scale spatial patterns by kriging sediment %OM, bulk C_{org}, bulk C:N, shoot density, and grain size (mean grain size and % sand fraction) in ArcGIS 10.2 Geostatistical Analyst. Kriging accounted for spatial autocorrelation and provided error estimates for interpolated values (cf. Zupo et al. 2006 and references therein), which allowed us to generate robust distribution maps. We fit multiple variogram models to each dataset (stable, circular, spherical, exponential, and Gaussian) and cross-validated the models using root mean square errors (Appendix I). Summing the kriged C_{org} distributions allowed us to quantify the gross C_{org} stock to a depth of 12 cm. We subtracted the average background concentration from each map cell by bed interval to assess the enhanced (i.e. net) stock attributable to the meadow.

We evaluated observed gradient relationships between C_{org}, meadow age, and edge proximity using regression analysis (lm, stats package) and Kendall correlation (rcor.test, ltm package) in R (R Project 2014) to determine whether the variables met multiple regression assumptions. Correlation analysis allowed us to check for possible multi-collinearity between age and edge proximity (Euclidean distance). Linear regression analyses allowed us to determine whether variable relationships exhibited linearity—a multiple regression assumption. Shapiro-Wilks tests were run on C_{org} concentrations by depth interval (shapiro.test, stats package) to verify that the response variables were normally distributed. In addition to age and edge proximity, our primary variables of interest, we also considered gradient relationships between C_{org} and several potential explanatory variables: REI, density, mean grain size, and bathymetry. The Kendall correlation analysis included kriged values for density and grain size, in addition to measured values, to obtain equal sample sizes for all six independent variables.

Spatial autocorrelation potentially confounds attempts to determine the relative importance of age and edge proximity in predicting sediment C_{org} concentrations at the meadow-scale. To address this, we compared meadow age and edge proximity (Euclidean distance) effects on sediment C_{org} using spatial autoregressive models (spded package version 0.6-4), which utilized a neighborhood weights matrix and Moran's *I* to account for autocorrelation (e.g. Genovesi et al. 2013). We evaluated the C_{org} data for both the 0-3 cm and 3-6 cm depth intervals. The top ~3 cm of the bed accumulated after the start of the restoration (Greiner et al. 2013). The 3-6 cm interval approximately corresponded with the rhizosphere in this system. Spatial lag and error dependencies were evaluated using Lagrange Multiplier tests (lm.LMtests, spdep package; cf. Zhang et al. 2010). The best models were determined by maximum likelihood estimation using Akaike's Information Criterion (AIC).

3.3. Results

3.3.1. Spatial distribution of sediment C_{org}

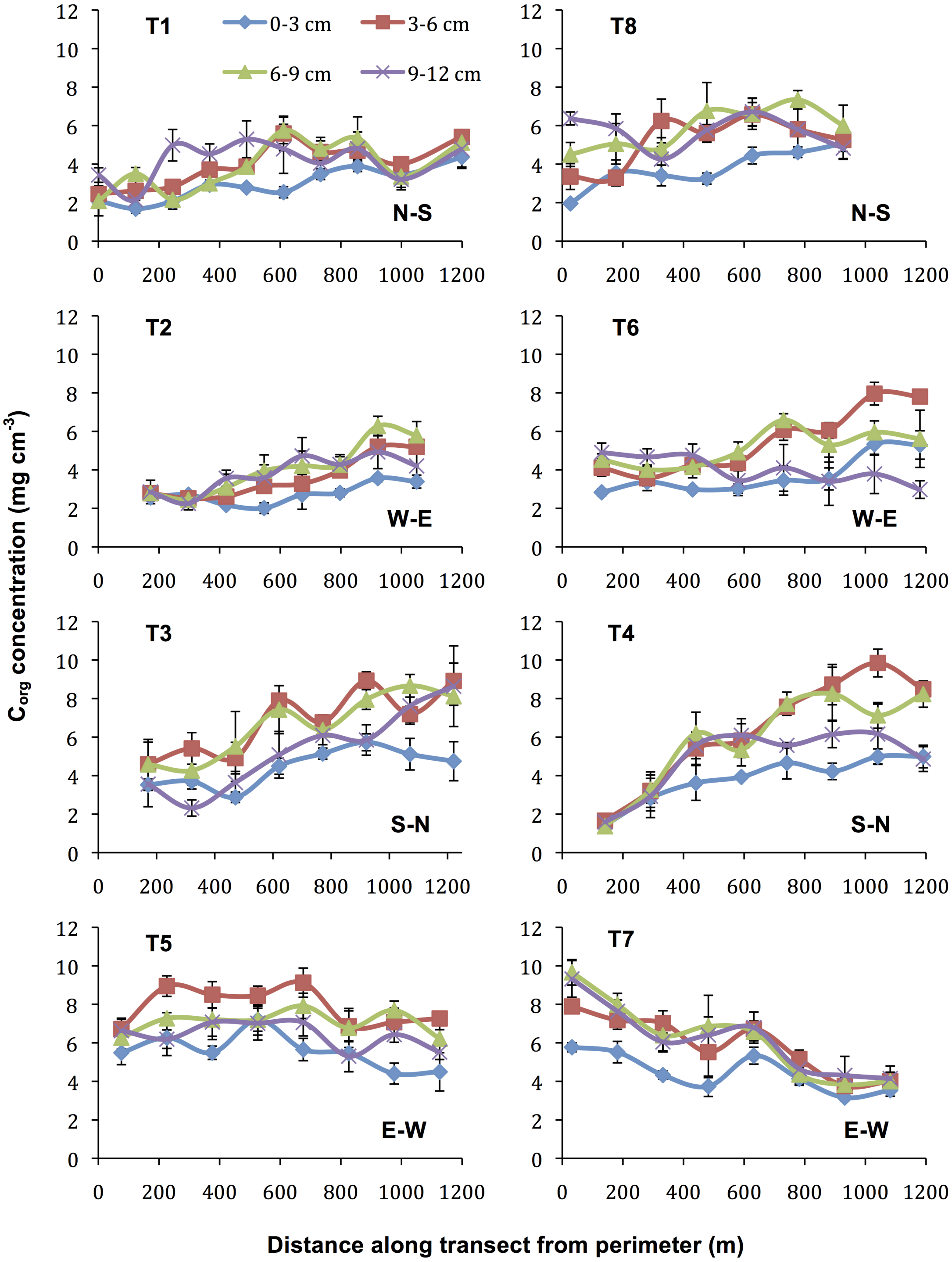

Figure 3.3. Sediment C_{org} concentrations along transects by bed depth interval; error = SE.

Table 3.1. Sediment C_{org} concentrations and blue carbon stocks within the seagrass meadow by bed depth interval (CO_2 estimated using molecular weight ratio).

		0-3 cm	**3-6 cm**	**6-9 cm**	**9-12 cm**
Bare concentration (mg cm^{-3})	Mean	2.53	3.53	4.09	4.87
	S	0.38	0.94	1.81	1.28
	SE	0.22	0.54	1.04	0.74
Meadow concentration (mg cm^{-3})	Mean	3.92	5.66	5.60	5.04
	S	1.23	2.03	1.80	1.57
	SE	0.15	0.25	0.22	0.20
Meadow stocks (t)	Gross C_{org}	706.50	1051.84	1007.63	896.01
	Net C_{org}	320.14	447.56	304.85	100.61
	Net CO_2	1173.85	1641.06	1117.79	368.92

Table 3.2. Linear relationships between sediment C_{org} and independent variables measured at sites by bed depth interval.

	n	Intercept±SE	M±SE	F (df)	*p*	adj-R^2
Transect Dist. (0-3 cm)	48	2.53±0.329	0.00217±4.64E-4	21.89 (1,46)	2.56E-05	0.308
Transect Dist. (3-6 cm)	48	3.30±0.548	0.00387±7.74E-4	25.03 (1,46)	8.72E-06	0.338
Transect Dist. (6-9 cm)	48	3.47±0.463	3.22E-3±6.54E-4	24.29 (1,46)	1.12E-05	0.331
Transect Dist. (9-12 cm)	48	3.36±0.415	2.26E-3±5.86E-4	14.86 (1,46)	3.57E-04	0.228
Euclid. Dist. (0-3 cm)	64	2.20±0.243	3.04E-3±3.84E-4	62.78 (1,62)	5.38E-11	0.495
Euclid. Dist. (3-6 cm)	64	2.81±0.401	5.02E-3±6.34E-4	62.88 (1,62)	5.24E-11	0.496
Euclid. Dist. (6-9 cm)	64	3.45±0.400	3.81E-3±6.32E-4	36.29 (1,62)	1.01E-07	0.359
Euclid. Dist. (9-12 cm)	64	3.74±0.398	2.31E-3±6.29E-4	13.42 (1,62)	5.18E-04	0.165
Age (0-3 cm)	66	2.84±0.192	0.192±4.68E-2	16.83 (1,64)	1.12E-04	0.196
Age (3-6 cm)	66	3.96±0.480	0.301±7.83E-2	14.81 (1,64)	2.77E-04	0.175
LogAge (0-3 cm)*	66	0.29±0.050	0.366±6.39E-2	32.91 (1,64)	2.84E-07	0.340
LogAge (3-6 cm)*	66	0.40±0.060	0.412±7.66E-2	28.95 (1,64)	1.13E-06	0.311
REI (0-3 cm)	66	8.68±1.30	-1.56E-6±4.19E-7	13.75 (1,64)	4.39E-04	0.164
REI (3-6 cm)	66	13.5±2.15	-2.58E-6±6.91E-7	13.92 (1,64)	4.08E-04	0.166
Density (0-3 cm)	16	2.37±0.835	3.64E-3±1.68E-3	4.687 (1,14)	4.82E-02	0.197
Density (3-6 cm)	16	4.43±1.29	3.60E-3±2.60E-3	1.919 (1,14)	1.88E-01	0.058
Grain size (0-3 cm)	16	9.72±0.939	-6.08E-2±9.93E-3	37.51 (1,14)	2.63E-05	0.709
Grain size (3-6 cm)	16	14.6±1.11	-9.17E-2±1.17E-2	61.1 (1,14)	1.79E-06	0.800

***Regressions were run on log-transformed C_{org} data**

Sediment C_{org} concentrations varied across the meadow and with sediment depth. The meadow-wide gross concentration for the top three cm of the bed averaged 3.92±0.15 (SE) mg C_{org} cm^{-3}; the 3-6 cm bed depth interval had the highest average concentration, 5.66±0.25 (SE) mg C_{org} cm^{-3} (Table 3.1). The gross concentration ranged from 1.42 to 7.19 mg C_{org} cm^{-3} in the top three cm and from 1.66 to 9.84 mg C_{org} cm^{-3} in the 3-6 cm interval. However, this variability was non-randomly distributed across the meadow. C_{org} concentrations showed significant spatial autocorrelation at all distances $\leq$ 1160 m for all bed depth intervals (Moran's $I > 0.04$, $p < 0.05$), resulting in strong spatial gradients. Sediment C_{org} decreased along each of the six transects extending from the meadow interior to the edge (Figure 3.3; Table 3.2). In contrast, C_{org} concentrations increased with distance from the meadow interior to the perimeter on the two transects adjacent to the barrier island (T5 and T7 in Figure 3.3).

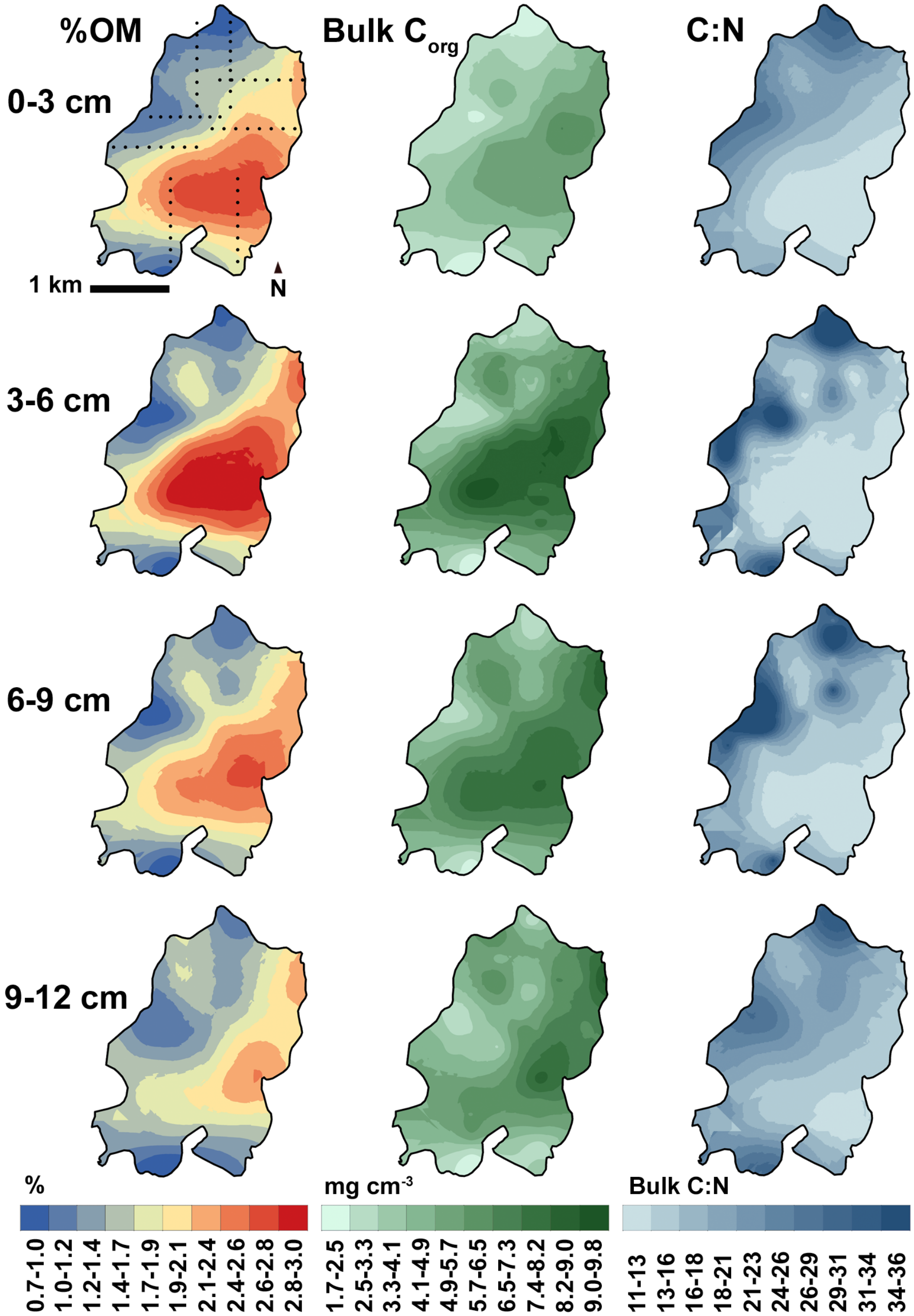

Figure 3.4. Organic matter, C_{org}, and bulk C:N distributions by bed depth interval within the meadow; transect sites are shown in the first figure; the maps were generated by kriging.

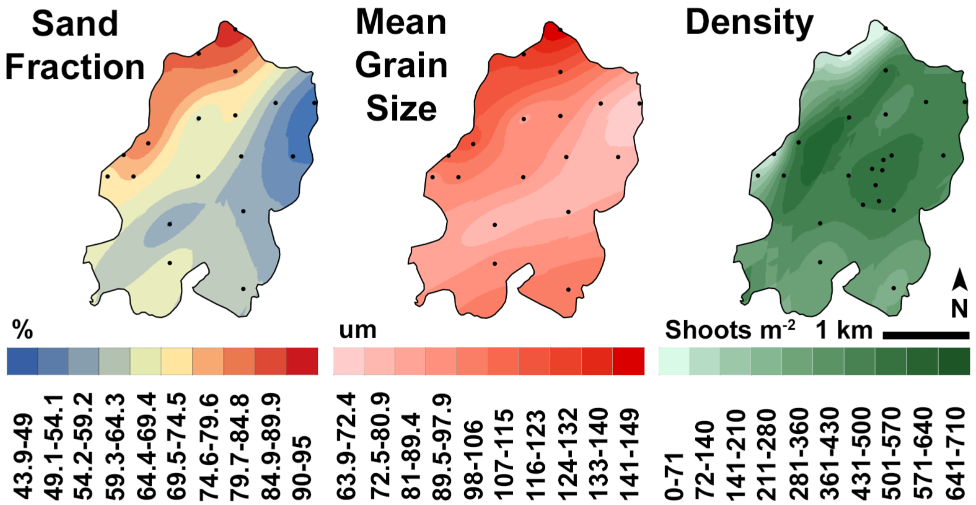

Figure 3.5. Meadow grain size (mean and sand fraction) and peak seagrass shoot density distributions; sample sites are shown in each figure; the maps were generated by kriging (note that the inverse of sand fraction represents < sand-size particles).

Interpolating the %OM, bulk C_{org}, and C:N data consistently yielded two discrete spatial regimes: a kriged zone of higher %OM and C_{org} encompassing most of the southeastern half of the meadow and another zone of decreasing %OM and C_{org} to the northwest (Figure 3.4). C:N ratios and grain size data yielded a similar kriged pattern, with higher C:N ratios and a higher percentage of larger grains to the northwest and lower values to the southeast, near Wreck Island (Figures 3.4; 3.5). Summing the interpolated sediment C_{org} within the meadow area to a bed depth of 12 cm gave a total meadow (gross) stock of 3662 t C_{org}. Subtracting average background concentrations measured at the bare sites from each meadow site by depth interval and interpolating the net increase gave a net stock of 1173 t C_{org}.

Table 3.3. Kendall correlation (Tau B) for sediment bulk C_{org} and possible explanatory variables (n = 66 sites; top number = τ, bottom number = *p*-value; significant correlations at Bonferroni adjusted α'<0.0018 highlighted in bold).

	0-3 C_{org}	**3-6 C_{org}**	**Euclid. Dist.**	**Age**	**REI**	**Density**	**Grain size**	**Bathymetry**
0-3 C_{org}	*****	0.692	0.534	0.396	-0.249	0.117	-0.605	0.322
3-6 C_{org}	**<0.001**	*****	0.517	0.376	-0.264	0.113	-0.56	0.294
Euclid. Dist.	**<0.001**	**<0.001**	*****	0.574	-0.186	0.289	-0.575	0.277
Age	**<0.001**	**<0.001**	**<0.001**	*****	-0.057	0.382	-0.45	0.121
REI	0.003	0.002	0.027	0.524	*****	0.067	0.29	-0.379
Density	0.165	0.179	**0.001**	**<0.001**	0.429	*****	-0.192	-0.037
Grain Size	**<0.001**	**<0.001**	**<0.001**	**<0.001**	**0.001**	0.023	*****	-0.339
Bathymetry	**<0.001**	**<0.001**	**0.001**	0.174	**<0.001**	0.662	**<0.001**	*****

3.3.2. Spatial variables

Several factors possibly account for the spatial distribution of sediment C_{org}. Edge proximity, meadow age, grain size and bathymetry were all significantly correlated with C_{org} at the meadow-scale. Edge proximity regression relationships (Euclidean distance) were highly significant at all four depth intervals. The highest adjusted-r^2 values were for the 0-3 and 3-6 cm intervals (Table 3.2). C_{org} and meadow age were highly correlated, but exhibited a relatively weak, positive linear regression relationship (Tables 3.2; 3.3). The strongest regression and correlation relationships were between the 0-3 cm C_{org} and sediment grain size (Tables 3.2; 3.3). C_{org} concentrations were not significantly correlated with shoot density or REI (Table 3.3). Unlike the kriged grain size distributions, the kriged density distribution did not match the C_{org} distribution (Figure 3.5).

Edge proximity, age, density, grain size, and bathymetry were also significantly correlated with one another, potentially indicative of landscape-scale interactions among the variables. Grain size was negatively correlated with edge proximity, age, and bathymetry, and positively correlated with REI (Table 3.3). The strongest correlation coefficient was between grain size and site distance from the open perimeter ($\tau = -0.575$). Site age and edge proximity (Euclidean distance) were also moderately correlated but not co-variates ($\tau = 0.574$), allowing us to compare their ability to predict C_{org} concentrations using multiple regression. The meadow has expanded outward over time, but it also coalesced in places and filled in behind Wreck Island relatively recently (Figure 3.2).

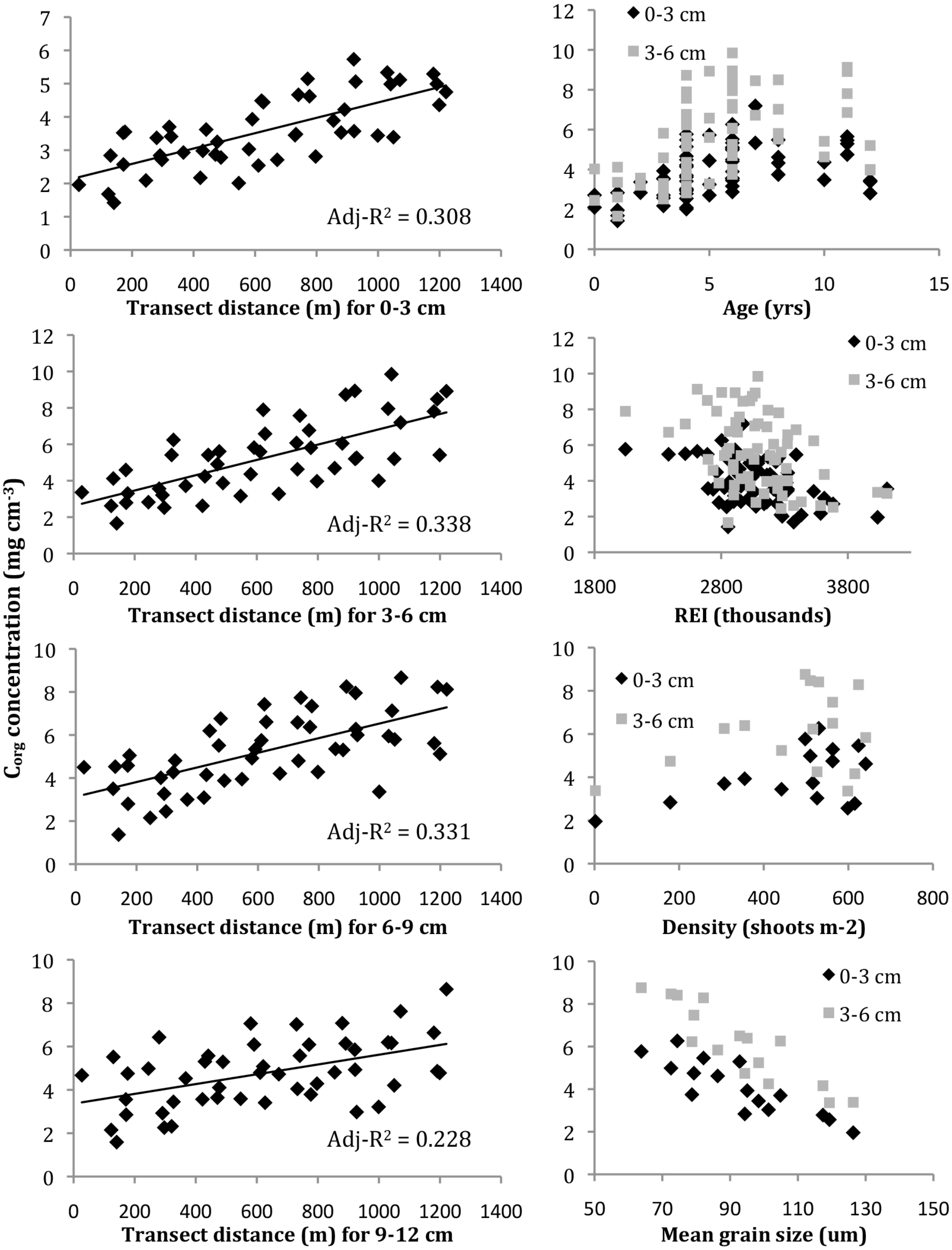

Figure 3.6. Sediment C_{org} concentration relationships with measured independent variables; comparisons are for the bed 0-3 cm depth interval (see Table 3.2 for individual regression statistics).

Table 3.4. Spatial autoregressive model results for 0-3 cm data.

LogC_{org} 0-3 cm Spatial Autoregressive Lag Model

	Coefficient	SE	Z	Probability
(Intercept)	2.26E-01	5.01E-02	4.52	6.27E-06
LogAge	4.76E-02	6.86E-02	0.693	0.488
Edge	1.91E-04	5.90E-05	3.24	1.21E-03
Z	4.40	0.081*		1.10E-05
rho	0.355			1.64E-04
AIC	-118			

LogC_{org} 0-3 cm Spatial Autoregressive Error Model

	Coefficient	SE	Z	Probability
(Intercept)	4.03E-01	4.75E-02	8.48	< 2.2e-16
LogAge	-5.95E-03	8.18E-02	-0.073	0.942
Edge	3.09E-04	7.42E-05	4.17	3.10E-05
Z	4.13	0.083*		3.57E-05
λ	0.345			9.53E-04
AIC	-114			

*Asymptotic standard error

Several factors complicated our ability to compare the effects of edge proximity and age on C_{org} concentrations directly through multiple regression. C_{org} varied non-linearly with age (Figure 3.6), so we applied a log-log transformation, which yielded linear relationships with adj-r^2 values >0.3 for both the 0-3 and 3-6 cm data (Table 3.2). The log-transformed C_{org} data for the 0-3 cm interval met the dependent variable normality assumption (W = 0.972, *p* = 0.143) and also varied linearly with the edge data. The log-transformed C_{org} data for the 3-6 cm interval was not normally distributed (W = 0.963, *p* = 0.044). Running a multiple regression analysis comparing edge and log-transformed age on C_{org} concentrations within the top three cm of the bed yielded spatially autocorrelated regression residuals (Moran's *I* = 0.535, *p*<1.10E-4). Lagrange Multiplier tests found strong spatial lag dependence (RLMlag = 6.1796, *p*<0.013). We accounted for this spatial autocorrelation using spatial lag and error analyses, both of which identified edge proximity—not age—as a significant predictor of C_{org} concentrations at the meadow-scale (Table 3.4).

3.4. Discussion

3.4.1. Meadow-scale controls on sediment C_{org} accumulation

Our results indicate that differences in relative location within the meadow affect the C_{org} stock distribution and overshadow other factors, including seagrass age and shoot density, that are known to affect C_{org} concentrations at the plot-scale. We show that edge proximity affects C_{org} concentrations over much larger spatial scales than previous studies have recognized, potentially resulting in seagrass meadow spatial gradients >1 km in length. Carbon stock estimates should take these potential meadow-scale spatial patterns into account.

Rather than reflecting the meadow's expansion history over the preceding 12-year period, the meadow-wide C_{org} distribution appears broadly consistent with the hypothesis that current attenuation promotes higher C_{org} concentrations with distance from the edge (Figure 3.1A). The meadow-wide grain size distribution (Figure 3.4) also supports this hypothesis. Previous studies have noted that suspended sediment is advected into this meadow (Hansen and Reidenbach 2012), increasing the percentage of silts and fine sands at meadow sites over time (McGlathery et al. 2012). This suspended sediment fractionates according to particle size as it is deposited across the meadow, with finer particles settling out in the southwestern meadow, where Hansen and

Reidenbach (2012) documented the lowest average Reynolds stress. This, in turn, facilitates more C_{org} storage, because smaller grains have more surface area for C_{org} adsorption (Wiberg et al. 2015). This process appears to be driven largely by tidal currents. Hansen and Reidenbach (2012) observed similar Reynolds stresses attributable to wave-dominated flows in different meadow locations, which may explain why we did not observe a significant correlation between C_{org} and REI. In addition to canopy current attenuation, basin geomorphology possibly accounts for some of the reduction in current velocity in the area of the meadow adjacent to Wreck Island and furthest from the two inlets. We note that a C_{org} spatial pattern is weakly present within the underlying 9-12 cm depth interval (Figure 3.4), which was deposited prior to the meadow restoration (Greiner et al. 2013). However, the meadow has clearly accentuated the observed pattern, as evidenced by the magnitude of the discrepancy in C_{org} concentrations between the two spatial regimes within the top 6 cm of the bed (Figure 3.4). Root and rhizome-derived carbon compounds may also contribute to sediment C_{org} accumulation below 6 cm.

These results confirm that large, sediment C_{org} spatial gradients are possible and should be considered when estimating blue carbon stocks. Similar studies are now needed to determine how varying current velocity, meadow configuration, and the water depth to canopy height ratio might give rise to particular sediment C_{org} gradients at this spatial scale. Other C_{org} distributions may be possible in other meadows. For example, an even larger meadow with a lower water depth to canopy height ratio might experience lower C_{org} concentrations further from the edge, because of reduced sediment delivery (Figure 3.1C). However, given that we observed increasing sediment C_{org} concentration gradients (Figure 3.1A) >1 km in length, and given that smaller, patchy meadows are relatively common, edge proximity possibly limits C_{org} accumulation in many systems. Other studies have speculated along these lines but lacked the ability to control for meadow expansion as a possible confounding variable (e.g. Ricart et al. 2015). Our results also highlight the importance of considering spatial autocorrelation and its potential effect on measured quantities at individual sites within a given seagrass meadow.

The potential importance of external sediment raises the possibility that much of the sediment C_{org} stored in this meadow is, in fact, allochthonous in origin. Greiner et al. (2016) found that only half of the sediment C_{org} at an interior site in the South Bay meadow derived from vascular plants. The C:N ratio in the C_{org} hotspot in the southeast part of the meadow (Figure 3.4) conforms more closely to the range observed for seston and macroalgae than for *Z. marina* in this system (Greiner 2013). The high C:N values in the northwest half of the meadow more closely resemble *Z. marina*. The grain size spatial distribution suggests that the southeastern meadow experiences lower current velocities and longer residence times, both of which possibly increase seston accumulation, which would increase the magnitude of observed C_{org} spatial gradients across the meadow. However, additional isotopic work is needed to conclusively identify C_{org} sources at this spatial scale.

The fact that edge proximity, not age, significantly predicts meadow-wide sediment C_{org} concentrations indicates that meadow- and regional-scale factors should be considered when estimating whole-meadow carbon stocks. Recent studies consider blue carbon accumulation as a function of plot-scale factors, including meadow age and plant density (e.g. Duarte et al. 2013B), without considering possible spatial scale effects. Age and C_{org} concentrations are positively correlated at individual sites in this study, but differences attributable to relative location overshadow differences due to age at this spatial scale. Shoot density also affects sediment C_{org} accumulation at the plot-scale (McGlathery et al. 2012; Widdows et al. 2008), but density alone is not a good proxy for site C_{org} concentrations at the meadow-scale. This is likely due to the fact that meadow canopy structure (i.e. shoot density and biomass) varies considerably over small spatial and short temporal scales (McGlathery et al. 2012; McGlathery 2013) and because density effects on sediment resuspension appear to be non-linear (Lawson et al. 2012). Consequently, a snapshot assessment of canopy structure would not necessarily correspond with the sediment C_{org} distribution, which reflects the balance of accumulation and resuspension over interannual timescales. Likewise, REI might correlate with C_{org} in isolated seagrass patches but does not account for current attenuation by the canopy.

3.4.2. Implications for financing seagrass restoration using blue carbon offset-credits

The distribution of sediment C_{org} in this meadow follows approximately linear C_{org} concentration gradients—not irregular zones of higher and lower C_{org} concentrations controlled by wind fetch, canopy complexity, age, or other factors. A representative C_{org} concentration for stock estimation might, therefore, be obtained by averaging samples collected from a relatively small number of sites distributed along the gradient. However, managers should avoid overestimating C_{org} stocks by relying on point-based literature values, models, or default values—all permissible approaches under VM0033 (Emmer et al. 2015A). Scaling the C_{org} measurement reported for this meadow by Greiner et al. (2013) by the total meadow area would overestimate the gross sediment C_{org} stock by almost 20%, because of the spatial gradients. Likewise, managers should not simply scale C_{org} accumulation model results calculated for small unit areas (e.g. Duarte et al. 2013B) or rely exclusively on near-surface ^{210}Pb accumulation rates that do not account for remineralization (Johannessen and Macdonald 2016), without understanding possible meadow-scale effects.

Regarding carbon offset-credit finance for seagrass restoration, the enhanced sediment C_{org} stock attributable to the meadow after more than a decade translates to approximately 4,300 t CO_2. Incorporating sequestered *Z. marina* biomass C_{org} would increase this total (Fourqurean et al. 2012). However, the aboveground biomass is sloughed off, and the fate of this exported C_{org} is uncertain, so the sequestered stock would correspond to the annual cycle average, not peak standing biomass.

Managers might be able to increase blue carbon storage by considering meadow configuration, basin geomorphology, and regional hydrodynamics when locating seagrass restoration sites. A large, contiguous meadow should store more blue carbon than an equal area of small meadow patches. If blue carbon storage is a management goal, restoration should be initiated at sites that are suitable for the accumulation of fine sediment. As the meadow expands, these locations should accumulate more blue carbon, due to scale-dependencies observed in this study, and adjacent areas should begin to bury blue carbon, thanks to the canopy particle-trapping feedback (Koch et al. 2006; Gruber and Kemp 2010). Additional studies that determine how current velocity, meadow configuration, and water depth interact to influence meadow-scale C_{org} gradients can aid blue carbon accumulation modeling efforts at spatial scales relevant to restoration managers.

3.5. Conclusions

This study indicates that edge proximity can better explain a seagrass meadow's sediment C_{org} distribution than spatial differences in accumulation time. Although meadow age and seagrass shoot density affect C_{org} accumulation at the plot-scale, these drivers can be overshadowed by differences in relative location at the meadow-scale. Progressive canopy attenuation of currents may explain the C_{org} distribution observed in this study. As currents move through the canopy, suspended sediment becomes stratified and is deposited according to particle size, which likely facilitates more C_{org} burial at more interior sites, irrespective of site meadow age. These findings highlight the potential importance of external sediment for seagrass blue carbon accumulation and the need to consider meadow-scale spatial gradients when quantifying whole-meadow carbon stocks.

Acknowledgements

I want to thank my collaborators: K.J. McGlathery and J.H. Porter. W. Clemo, P. Luckenbach, C. Buck, A. Schwarzschild, A. Al Haj, H. Parcells, M. Volaric, A. Lunstrum, E.

Murphy, and M. Kremer assisted with field sampling; M. Miller provided lab assistance; R. Orth and D. Wilcox provided access to aerial imagery; J. Carr, P. Wiberg, and M. Reidenbach provided advice. Funding was provided by National Science Foundation VCR-LTER Grant DEB-1237733, the University of Virginia Office of the Vice President and Department of Environmental Sciences, the University of Virginia Jefferson Scholars Foundation, and by Virginia Sea Grant. The authors also wish to thank the anonymous reviewers who helped improve the manuscript.

Data archiving

Data collected during this study can be obtained from the Long Term Ecological Research Network database (https://www.lternet.edu).

Chapter 4. Non-seagrass carbon contributions to seagrass sediment blue carbon

Oreska, M.P.J., G.M. Wilkinson, K.J. McGlathery, M. Bost, B.A. McKee. 2018. Non-seagrass carbon contributions to seagrass sediment blue carbon. *Limnology and Oceanography* 63(S1):S3-S18. DOI:10.1002/lno.10718.

Abstract

Non-seagrass sources account for ~50% of the sediment organic carbon (SOC) in many seagrass beds, a fraction that may derive from external organic matter advected into the meadow and trapped by the seagrass canopy. If allochthonous carbon fluxes are responsible for the non-seagrass SOC in a given seagrass bed, this fraction should decrease with distance from the meadow perimeter. Identifying the spatial origin of SOC is important for closing seagrass carbon budgets and 'blue carbon' offset-credit accounting, but studies have yet to quantify and map seagrass SOC stocks by carbon source. We measured sediment δ^{13}C, δ^{15}N, and δ^{34}S throughout a large (6 km^2), restored *Zostera marina* (eelgrass) meadow and applied Bayesian mixing models to quantify total SOC contributions from possible autotroph sources, *Z. marina*, *Spartina alterniflora*, and benthic microalgae (BMA). *Z. marina* accounted for <40% of total meadow SOC, but we did not find evidence for outwelling from the fringing *S. alterniflora* salt-marsh or organic matter advection from bare subtidal areas. *S. alterniflora* SOC contributions averaged 10% at sites both inside and outside of the meadow. The BMA fraction accounted for 51% of total meadow SOC and was highest at sites furthest from the bare subtidal-meadow edge, indicative of *in situ* production. ^{210}Pb profiles confirmed that meadow-enhanced sedimentation facilitates the burial of *in situ* BMA. Deducting this contribution from total SOC would underestimate total organic carbon fixation within the meadow. Seagrass meadows can enhance BMA burial, which likely accounts for most of the non-seagrass SOC stored in many seagrass beds.

4.1. Introduction

Seagrass meadows accumulate organic carbon (C_{org}) within their beds from seagrass and from the burial of non-seagrass organic matter (Gacia et al. 2002; Hendriks et al. 2008; Fourqurean et al. 2012). Seagrass bed sediment C_{org} (SOC) δ^{13}C ratios are typically depleted relative to associated seagrass tissue, irrespective of seagrass species and location (average depletion = 6.3 ‰), which suggests that non-seagrass sources contribute ~50% of the SOC in many meadows (Kennedy et al. 2010). Multiple studies point to the burial of particulate organic matter (POM) as the likely explanation for this non-seagrass fraction (e.g. Campbell et al. 2015; Huang et al. 2015) and, therefore, identify this SOC as allochthonous relative to the seagrass meadow (Howard et al. 2014; Greiner et al. 2016). Meadow canopies trap suspended particles through filtration and by attenuating currents, which contribute to bed accretion (Hendriks et al. 2008; Duarte et al. 2013A). However, studies that investigate seagrass SOC composition seldom consider C_{org} spatial origin. If advected POM contributes significantly to seagrass bed accretion, we should observe SOC isotope composition spatial gradients that change with distance from an external source or boundary.

Identifying the source of SOC remains a challenge in most subtidal habitats. Carbon fixed in one area is often exported to adjacent habitats (Duarte and Cebrián 1996; Cebrián et al. 1997), where it might be buried (Middleburg et al. 1997; Zonneveld et al. 2010), remobilized, or respired (Regnier et al. 2013; Hyndes et al. 2014). According to Duarte and Cebrián (1996), more seagrass and marsh production is exported than buried *in situ*. Particulate organic carbon (POC), dissolved organic carbon

(DOC), and dissolved inorganic carbon (DIC) fluxes often connect different habitats, especially over short distances (Cai 2011; Hyndes et al. 2014), which make tracking the generation, transport, and ultimate fate of autotrophic production difficult (Bouillon and Connolly 2009; Bauer et al. 2013; Hyndes et al. 2014). These linkages complicate efforts to assess net ecosystem metabolism in many coastal habitats (Gattuso et al. 1998; Borges et al. 2006; Cai 2011). Spatial gradients have, nevertheless, been used to successfully identify POC and DOC exchanges between adjacent mangrove and seagrass habitats (Heminga et al. 1994; Bouillon et al. 2007) and marsh DOC and DIC 'outwelling' (e.g. Tzortziou et al. 2011). In a coupled marsh-seagrass system, contributions from marsh POC outwelling should be discernable as a change in SOC isotope composition with distance into the seagrass bed.

Interest in financing seagrass restoration through the sale of blue carbon offset-credits (e.g. Nellemann et al. 2009; Murray et al. 2011; Hejnowicz et al. 2015) adds urgency to these questions about seagrass SOC source. A framework now exists for greenhouse gas benefit accounting in seagrass habitats, the Verified Carbon Standard Methodology VM0033 (Emmer et al. 2015A), which allocates offset-credits for net autotrophic production resulting from seagrass restoration activities within a specified project area. Offset-credits are not allocated under the framework for allochthonous C_{org} buried in the meadow, because carbon fixed outside the project area cannot necessarily be attributed to project activities (CEC 2014). Restoration projects must, therefore, quantify the autochthonous and allochthonous SOC fractions, presumably using unique isotope or biomarker signatures to identify different autotroph contributors (e.g. Volkman et al. 2008; Oakes and Eyre 2014). However, these chemical signatures often overlap, and isotope ratio measurement variability sometimes inhibits confident percent source estimation (Fry 2007). Howard et al. (2014) tentatively suggest an allochthonous carbon compensation factor (i.e. deduction) of 50% for seagrass meadows, based on the average non-seagrass SOC contribution of 50% found by Kennedy et al. (2010), but this percentage may not be accurate for carbon crediting purposes. The number might be an overestimate, because some non-seagrass C_{org} in the bed likely derives from *in situ* autotrophs, including epiphytes (Serrano et al. 2015). Alternatively, 50% may be an underestimate, because the average SOC $\delta^{13}C$ values used to generate this figure include a high number of mid-meadow sample sites, and we would expect allochthonous SOC percent contributions to be even higher near meadow edges.

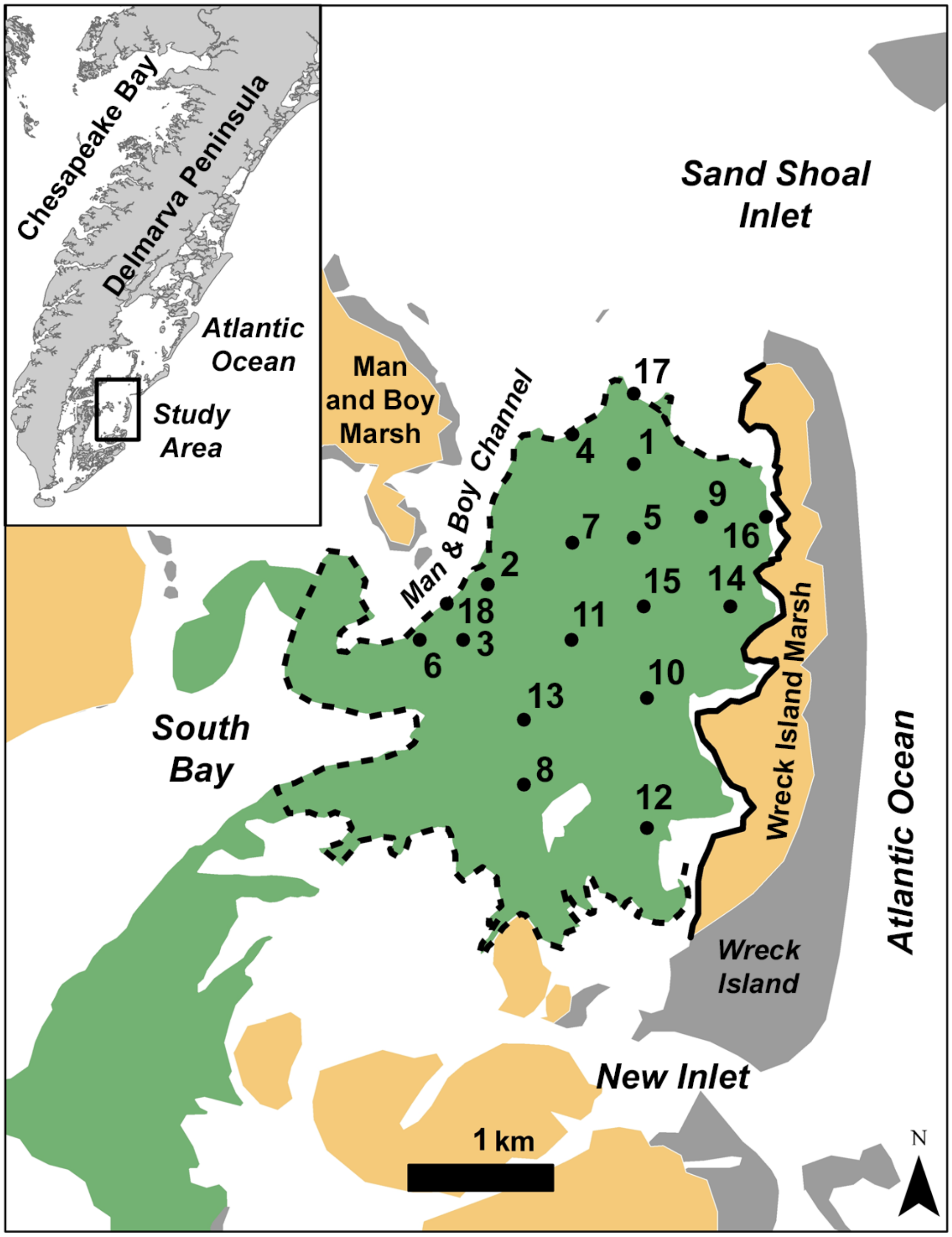

Figure 4.1. Study Area: The restored *Z. marina* meadow fills the area between Man & Boy Channel and Wreck Island; Two Euclidean distance measures were determined for each meadow site: site distance to Wreck Island Marsh (solid black line) and site distance to the meadow-bare subtidal edge (dashed line); two bare sites were also sampled immediately outside this meadow-bare subtidal boundary (sites 17 and 18).

This study investigates whether stable isotopes in seagrass sediment organic matter exhibit spatial variation that can be used to identify the geographic origin of non-seagrass SOC. The *Zostera marina* (eelgrass) meadow in South Bay, Virginia, U.S.A., is part of the Virginia Coast Reserve Long-Term Ecological Research (VCR-LTER) eelgrass restoration and represents the single largest, successfully restored seagrass meadow to date (Orth et al. 2006B; 2012; Orth and McGlathery 2012). SOC profile comparisons confirm that this meadow now stores significantly more SOC than adjacent bare sites (McGlathery et al. 2012; Greiner et al. 2013) and that much of this SOC is non-seagrass in origin (Greiner et al. 2016). However, the SOC is non-uniformly distributed. Percent organic matter (OM) and SOC concentrations decline with distance from the adjacent barrier island (chapter 3)—a spatial distribution that suggests 'outwelling' from the island's fringing marsh as a possible carbon source vector. The South Bay meadow is part of a coupled seagrass-marsh system, where marsh scarp erosion potentially supplies sediment to the seagrass bed (McGlathery et al. 2013; Figure 4.1). Greiner et al. (2016) quantified carbon sources at a single site within this seagrass bed but lacked an adequate tracer to distinguish between the two vascular plants in this system, the seagrass *Z. marina* and the salt marsh cordgrass *Spartina alterniflora*. The authors did, however, find that more than 50% of the C_{org} at their meadow sample site was apparently algal in origin. If allochthonous *S. alterniflora* and algae contribute significant amounts of carbon to the bed SOC pool, their percent contributions should increase with proximity to particular meadow boundaries. We hypothesized that 1) *S. alterniflora* POM inputs account for the SOC spatial gradient that increases with proximity to the fringing marsh on the east side of the meadow (Wreck Island Marsh in Figure 4.1), and that 2) the algal carbon percent contribution increases with proximity to the meadow-bare subtidal boundary (the meadow edge that does not adjoin Wreck Island Marsh in Figure 4.1), which would be indicative of canopy filtration of allochthonous, algal POM.

4.2. Methods

4.2.1. Site description

South Bay occurs on the Atlantic side of the southern Delmarva Peninsula, between Wreck Island and Mockhorn Island, VA. The central part of the restored meadow now covers an area approximately 6 km^2 in size. The Wreck Island fringing marsh adjoins the *Z. marina* meadow to the east, and the Man and Boy Marsh sits opposite Man and Boy Channel to the northwest (Figure 4.1). Tides enter and exit the meadow area via Sand Shoal Inlet to the north and New Inlet to the south. This system is oligotrophic—dissolved organic nitrogen averages 11.8±1.6 (SE) µM and dissolved inorganic phosphorous averages 0.5±0.1 (SE) µM over a year (McGlathery et al. 2001)—and experiences low total dissolved nitrogen loading relative to other shallow estuaries, 1 g N m^{-2} yr^{-1} (Tyler et al. 2001; McGlathery et al. 2007). Phytoplankton are present but not abundant in the outer coastal bays in this system on account of the low nutrient inputs (McGlathery et al. 2001; Tyler et al. 2001; Hondula 2012). Water column chlorophyll *a* peaks around 5 µg l^{-1} in the outer bays during the summer and declines to <1 µg l^{-1} during the fall; in comparison, benthic chlorophyll can exceed 80 mg m^{-2}

(McGlathery et al. 2001). Cultured bivalves in this system rely primarily on macroalgae and, to a lesser extent, benthic diatoms, the dominant primary producers in the coastal bays along with *Z. marina* (McGlathery et al. 2001; Hondula and Pace 2014). Likely SOC sources in this system are, therefore, *Z. marina*, the only seagrass species, macro- and benthic microalgae, and *S. alterniflora*, the dominant species in the surrounding salt marshes (Hondula and Pace 2014; Greiner et al. 2016). Dominant macroalgal species include *Ulva lactuca*, *Graciliaria vermiculophylla*, and *Codium fragile*, which are common on tidal flats but generally contribute <5% of SOC observed at bare and vegetated subtidal sites (McGlathery et al. 2007; Greiner et al. 2016).

4.2.2. Sample collection

Three replicate sediment samples were collected using 60 cc hand cores at each of 16 randomly selected sites within the South Bay meadow and at two bare sites immediately adjacent to the meadow during July 2014. The bare sites were located 3 meters (site #17) and 13 meters from the meadow edge (site #18 in Figure 4.1). Past studies have observed OM and SOC concentration peaks between 3 and 6 cm below the sediment-water interface in this meadow, the zone of maximum *Z. marina* root and rhizome biomass (Cole and McGlathery 2012; Greiner et al. 2013; chapter 3). The sediment samples collected in this study exactly captured this 3-6 cm bed depth interval. A ^{210}Pb dated core collected from this meadow indicated that the top ~5 cm of the bed accumulated following meadow re-establishment; in contrast, a nearby bare site showed no bed accretion (Greiner et al. 2013). The 3-6 cm interval within the seagrass bed, therefore, receives SOC inputs from multiple pathways: SOC buried due to particulate trapping by the meadow canopy—potentially including allochthonous POM—C_{org} accumulation from decomposing seagrass biomass, and C_{org} from seagrass root exudates. By omitting the top 3 cm on the bed, we excluded the zone of active sediment resuspension and mixing to obtain a relatively stable, time-averaged SOC sample. Compaction was approximately 7% in our cores, on account of their relatively small size and the fact that the sediment in this system is predominantly fine sand (chapter 3). Macroscopic root, rhizome, and shell fragments were removed from sediment samples prior to analysis to isolate SOC from belowground biomass, following methods used previously in this system (Greiner et al. 2013; 2016; chapter 3). Refractory roots and rhizomes did not occur in all of our core samples. Homogenizing individual roots or rhizomes would have biased particular sediment samples in favor of *Z. marina*, thereby affecting the meadow-wide sediment isotope distribution results. Sediment samples were dried for 48 hrs at 60°C and homogenized. We determined the inorganic carbon (IC) fraction by conducting element analysis using a Carlo Erba NA 2500 Element Analyzer on samples ashed in a muffle furnace at 500°C for 6 hrs, following Fourqurean et al. (2014).

We verified that the 3-6 cm depth interval included SOC burial due to bed accretion by collecting and dating additional sediment cores using the same ^{210}Pb methods employed by Greiner et al. (2013). Sediment cores were collected in July 2014 at two sites: a meadow site on an original restoration seed plot (site #5 in Figure 4.1) and a bare site adjacent to Man and Boy Channel (site #18 in Figure 4.1). The meadow site core analyzed in this study was collected from the northwest half of the meadow, which had lower SOC storage (chapter 3), for comparison with the Greiner et al. (2013) meadow core, which was collected in an original seed plot in the southeast half of the meadow (located between sites #10 and 15 in Figure 4.1). The Greiner et al. (2013) bare site was located northeast of site #17. Profiles were determined to a depth of 20 cm using ^{210}Pb (22.3 y half-life), which we compared with the two profiles obtained by Greiner et al. (2013). The cores were divided into 1-cm intervals, which were dated at the University of North Carolina Department of Marine Sciences. ^{210}Pb activities were determined via isotope-dilution alpha spectrometry for the ^{210}Pb granddaughter isotope ^{210}Po, which are in secular equilibrium with each other (Flynn 1968; Matthews et al. 2007). Supported ^{210}Pb was formed by *in situ* production of ^{210}Pb within sediment grains from the decay of ^{222}Rn. Unsupported ^{210}Pb was the activity supplied from the atmosphere that adsorbs to particles that then settle into the seagrass sediments, excess ^{210}Pb that was used to quantify sedimentation rates (Appleby and Oldfield 1983). We noted that excess ^{210}Pb activities decreased in a non-exponential manner, so a Constant Rate of Supply (CRS) model was applied to profiles within each core, which allows for variable sedimentation over time (Sanchez-Cabeza and Ruiz-Fernández 2012). Carbon accumulation rates were calculated by multiplying the sedimentation rate (cm y^{-1}) for each sediment interval by its bulk C_{org} value.

We considered potential SOC source contributions from three types of autotrophs: *Z. marina*, *S. alterniflora*, and benthic microalgae (BMA), represented in this system primarily by benthic diatoms (Hondula and Pace 2014). Phytoplankton were not considered as a possible source, both because of their low abundance relative to BMA

(McGlathery et al. 2001) and because phytoplankton appear isotopically similar to BMA in this system (Hondula and Pace 2014). *Z. marina* biomass (n = 4) and *S. alterniflora* biomass (n = 4) grab samples were collected from randomly located sites in the meadow and in Wreck Island Marsh in July 2014 to constrain the stable isotope ranges for these end-members. The *Z. marina* and *S. alterniflora* biomass samples were divided into above- (AGB) and belowground biomass (BGB) fractions, which were dried, ground, and analyzed separately to determine whether these fractions yielded different isotope values. The AGB and BGB values were then averaged to generate individual plant averages, which were subsequently averaged to generate end-member averages. Benthic diatom isotope values for this system were determined by Hondula and Pace (2011; 2014), using a vertical migration sampling approach (cf. Riera and Richard 1996). We limited the mixing model analysis to isotope ratios obtained from the VCR-LTER (Appendix II). Seston samples were collected on three separate occasions in July 2014 using an 80 μm tow net to determine whether *S. alterniflora* contributes to POM in this system. We evaluated seston as a possible vector connecting the marsh to the seagrass sediment carbon pool by comparing average seston isotope ratios with end-member isotope ratios, not as a separate end-member with a unique isotopic signature. Plant biomass and seston samples were dried for 48 hrs at 60°C and homogenized prior to stable isotope analysis.

All sediment, end-member biomass, and seston sample stable isotope compositions were measured at the Marine Biological Laboratory (MBL) Stable Isotope Laboratory in Woods Hole, MA, U.S.A. Sample carbon, nitrogen, and sulfur percentages and $\delta^{13}C$, $\delta^{15}N$, and $\delta^{34}S$ stable isotope ratios were determined using a Europa 20-20 continuous-flow isotope ratio mass spectrometer interfaced with a Europa ANCA-SL elemental analyzer. We considered $\delta^{34}S$ as a possible additional tracer, because *Z. marina* and *S. alterniflora* exhibit non-overlapping $\delta^{34}S$ ranges in this system (Harbeson 2010). All isotope ratios were related to their respective international standards and reported using per mil (‰) notation. The analytical precision based on replicate analyses of isotopically homogeneous international standards was +/- 0.1 ‰.

4.2.3. Bayesian mixing model

We used Bayesian mixing models to determine whether the observed isotopic spatial variation reflected different autotrophic source contributions to different locations within the meadow. Proportional contributions from the three major autotrophs in this system were calculated for each site. Discrete solutions can be obtained for mixing models, provided the number of sources exceeds the number of tracers used in analyses by n+1. Bayesian mixing models incorporate both observed data and uncertainty to quantify the likelihood of a given solution, which is obtained from the posterior distribution. We conducted 3-source (*Z. marina*, *S. alterniflora*, and BMA), 2-tracer ($\delta^{13}C$, $\delta^{15}N$) Bayesian mixing model analyses using Stable Isotope Analysis in R (siar package version 4.2), which employs isotope ratio means and standard deviations for each end-member (Inger et al. 2010). Previous studies conducted in the VCR-LTER have successfully used Bayesian mixing models to differentiate between these autotrophs in mixed isotope assemblages (Hondula and Pace 2014; Greiner et al. 2016). $\delta^{34}S$ values were ultimately excluded from this analysis, because of observed discrepancies between the δ^{34}S ranges of the sediment samples and potential end-members. The mixing model analysis did not require a separate IC term, because sediment sample IC was found to be <0.1%. Diagenetic factors can result in a 1.5 ‰ change in δ^{13}C and a 1.2 ‰ change in δ^{15}N in some systems (Jankowska et al. 2016). We did not include a specific diagenesis term in the model, because past work in this system suggests that diagenetic effects on end-member δ^{13}C and δ^{15}N isotope ratios are nominal (Greiner et al. 2016). Even if diagenetic effects are evident at particular sites, sample differences on the order of 1-2 ‰ should not substantially change mixing model results.

The following equations relate end-member contributions to the sediment at each site:

$$\begin{aligned}
&\delta^{13}C_{Sed} = \left(\phi_Z \times \delta^{13}C_Z\right) + \left(\phi_S \times \delta^{13}C_S\right) + \left(\phi_{BD} \times \delta^{13}C_{BD}\right) \\
&\delta^{15}N_{Sed} = \left(\phi_Z \times \delta^{15}N_Z\right) + \left(\phi_S \times \delta^{15}N_S\right) + \left(\phi_{BD} \times \delta^{15}N_{BD}\right) \\
&1 = \phi_Z + \phi_S + \phi_{BD}
\end{aligned}$$

Where δ^{13}C and δ^{15}N were isotope ratios measured in sediment and in the end-members (Z, S, and BMA).

We ultimately ran the 3-source, 2-tracer mixing model on both individual sites and on sites binned according to SOC concentration, because certain individual sites exhibited flattened distributions. We grouped meadow sites into four, spatially discrete categories based on their SOC concentrations relative to the meadow SOC mean (5.85±1.86 (SD) mg C_{org} cm^{-3}): 'lowest' sites with concentrations < the meadow mean-1 SD, 'low' sites with concentrations between the mean-1 SD and the mean, 'high' sites with concentrations between the mean and the mean+1 SD, and 'highest' sites with concentrations > the mean+1 SD. The bare sites provided a fifth SOC group, with concentrations <3.1 mg C_{org} cm^{-3}. Well-constrained posterior distribution results for these groups allowed us to calculate the bulk SOC contribution from each autotroph source within each meadow SOC zone. We multiplied the fractional contribution results by the average bulk SOC concentration measured in each zone.

4.2.4. Distribution analyses

We compared isotope spatial variability relative to the documented SOC spatial gradient within the seagrass bed (chapter 3) by mapping average site SOC concentrations and isotope ratios determined from the sediment samples collected during this study. Interpolated SOC, $\delta^{13}C$, $\delta^{15}N$, and $\delta^{34}S$ distributions were generated using kriging. We fit circular, exponential, spherical, stable, and Gaussian semivariogram models to each dataset in ArcGIS 10.2, Geostatistical Analyst. The most robust kriged map for each isotope distribution was selected by cross-validating root mean square errors (Appendix I).

We used the results of the mixing model analysis to address our specific spatial hypotheses: 1) the marsh SOC fraction should decrease with distance from Wreck Island Marsh and 2) the *Z. marina* fraction should increase with distance from the meadow-bare subtidal boundary (the 'edge') on account of allochthonous SOC contributions. Site isotope ratios and Bayesian mixing model source fraction posterior means were regressed against site distance from the Wreck Island Marsh and from the meadow-bare subtidal edge using the lm analysis (stats package) in R version 3.2.1. Euclidean distances from the two meadow boundaries were determined for each site using Near analysis in ArcGIS 10.2 (Figure 4.1). Data were normally distributed according to the Shapiro-Wilks test (shapiro.text, stats package). The homogeneity of variance assumption was met.

4.3. Results

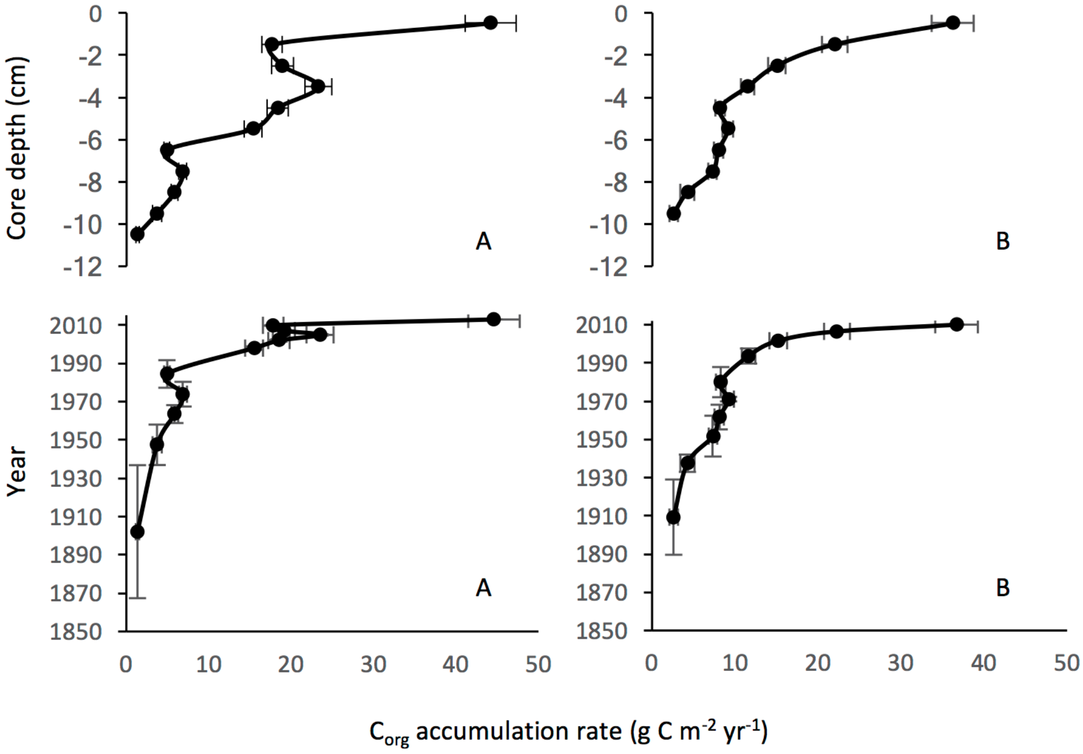

Figure 4.2. South Bay meadow sediment accumulation profiles: A) Bed depth- and age-calibrated C_{org} accumulation profiles for meadow site 5 and B) for a mid-meadow site analyzed in 2011 by Greiner et al. (2013) (adapted with permission). ^{210}Pb dating indicates that the top 5 cm of the bed at site #5 has accreted since the meadow restoration began in 2000. Bare control sites analyzed in this study (site 18) and by Greiner et al. (2013) were non-depositional.

Core dating using ^{210}Pb confirmed that the seagrass bed has accreted due to sediment accumulation, resulting in high, recent SOC accumulation rates. The meadow core obtained from site #5 indicated that the top 5+ cm of the bed at that site have accumulated since the restoration began. In comparison, the bare profile from site #18 had a ^{210}Pb profile with low (~0.6 dpm g^{-1}) activities, typical of non-depositional environments with supported activity only. The ^{210}Pb profile for site #5 was similar to that measured by Greiner et al. (2013) (Figure 4.2). Activities were higher in the top 11 cm (0.74 to 1.55 dpm g^{-1}), indicating the presence of excess ^{210}Pb. A CRS model applied to quantify sedimentation rates for the upper 11 cm of this core yielded a similar rate increase to the increase observed in the Greiner et al. (2013) meadow site core, from approximately 0.1 cm y^{-1} before restoration began in 2000 to 0.6 cm y^{-1} at the time of core collection. This sedimentation rate translated to a recent C burial rate >44 g C$_{org}$ m^{-2} yr^{-1} at site #5 (Figure 4.2).

Table 4.1. End-member stable isotope ratios used in the mixing model analysis.

		Mean δ^{13}C	SD δ^{13}C	Mean δ^{15}N	SD δ^{15}N	Mean δ^{34}S	SD δ^{34}S
Zostera	Whole plant	-9.37	0.55	6.79	0.34	-0.17	2.41
	AGB (n = 4)	-8.99	0.83	7.13	0.35	7.89	2.92
	BGB (n = 4)	-9.88	0.37	6.44	0.45	-8.24	2.99
Spartina	Whole plant	-13.67	0.15	8.96	0.15	-2.81	2.83
	AGB (n = 4)	-13.69	0.16	9.29	0.65	-3.07	2.87
	BGB (n = 4)	-13.37	0.35	8.01	1.33	-2.54	4.54
BMA	(n = 4)	-21.07	0.40	5.75	0.43	6.49	5.30

The different autotrophs in this system exhibited different ranges for the different stable isotopes, especially $\delta^{13}C$. The *Z. marina* samples collected during this study yielded $\delta^{13}C$ values from -8.79 to -9.92 ‰; whereas, the *S. alterniflora* values ranged from -13.36 to -13.72 ‰. Regarding $\delta^{15}N$, *Z. marina* values ranged from 6.48 to 7.26 ‰ and *S. alterniflora* values ranged from 7.20 to 9.86 ‰. In comparison, $\delta^{34}S$ provided less of a basis for differentiating *Z. marina* and *S. alterniflora*, due to notable $\delta^{34}S$ enrichment in *Z. marina* AGB and depletion in *Z. marina* BGB. The *Z. marina* AGB $\delta^{34}S$ ranged from 3.89 to 10.22 ‰; whereas, the BGB ranged from -12.52 to -5.77 ‰. *S. alterniflora* showed less $\delta^{34}S$ enrichment, yielding a range for AGB and BGB samples of -8.59 to 0.25 ‰. BMA showed greater average $\delta^{13}C$ depletion and greater average $\delta^{15}N$ and $\delta^{34}S$ enrichment than *Z. marina* or *S. alterniflora* (Table 4.1). In comparison, seston $\delta^{13}C$ and $\delta^{15}N$ averaged -14.62±0.55 (SE) ‰ and 9.41±0.31 (SE) ‰, respectively, a similar isotopic composition to *S. alterniflora*. Seston $\delta^{34}S$ values averaged 5.36±1.76 (SE) ‰.

Table 4.2. Sample site variables: Site numbers correspond to the map in Figure 4.1; C_{org}, isotope ratio, and source fractions (posterior means) represent site averages based on 3 replicates; Net C_{org} is the difference between the C_{org} measured at meadow sites and the average bare site concentration; the distance measures relate site Euclidean distance from Wreck Island Marsh and the meadow-bare subtidal boundary (the Edge).

Site	SOC Group	C_{org} (mg cm^{-3})	Net C_{org} (mg cm^{-3})	δ^{13}C	δ^{15}N	δ^{34}S	*Zostera* fraction	*Spartina* fraction	BMA fraction	WI Marsh dist. (m)	Edge dist. (m)
1	Lowest	3.80	0.95	-13.91	7.56	-17.13	0.369	0.377	0.254	800	345
2	Lowest	3.03	0.17	-12.66	6.84	-11.86	0.562	0.182	0.256	1703	134
3	Lowest	3.82	0.97	-13.97	6.27	-13.86	0.505	0.103	0.392	1699	284
4	Lowest	3.12	0.26	-14.05	6.89	-17.82	0.431	0.244	0.325	1171	25
5	Low	5.06	2.21	-15.82	6.79	-18.22	0.314	0.258	0.428	879	732
6	Low	4.28	1.43	-14.56	7.26	-16.39	0.338	0.343	0.318	1987	85
7	Low	5.54	2.69	-15.07	6.27	-15.17	0.447	0.098	0.455	1287	575
8	High	6.19	3.34	-15.49	6.29	-18.02	0.395	0.125	0.480	1270	610
9	High	6.01	3.15	-15.59	6.44	-17.07	0.390	0.127	0.483	522	412
10	High	7.23	4.37	-16.45	4.96	-19.12	0.225	0.272	0.503	364	1174
11	High	6.40	3.55	-16.10	6.06	-15.37	0.355	0.107	0.538	1009	803
12	High	6.26	3.40	-16.97	5.83	-14.98	0.245	0.184	0.571	451	362
13	Highest	8.37	5.51	-16.21	5.90	-17.57	0.234	0.289	0.476	1201	743
14	Highest	8.10	5.25	-17.03	5.96	-16.87	0.207	0.222	0.571	259	983
15	Highest	7.85	4.99	-15.93	6.35	-16.58	0.340	0.161	0.499	751	1121
16	Highest	8.51	5.66	-17.02	6.05	-18.60	0.285	0.095	0.619	92	364
17	Bare	2.58	NA	-14.03	6.90	-17.95	0.394	0.267	0.339	761	-3
18	Bare	3.06	NA	-13.07	6.63	-14.40	0.529	0.163	0.309	1894	-13

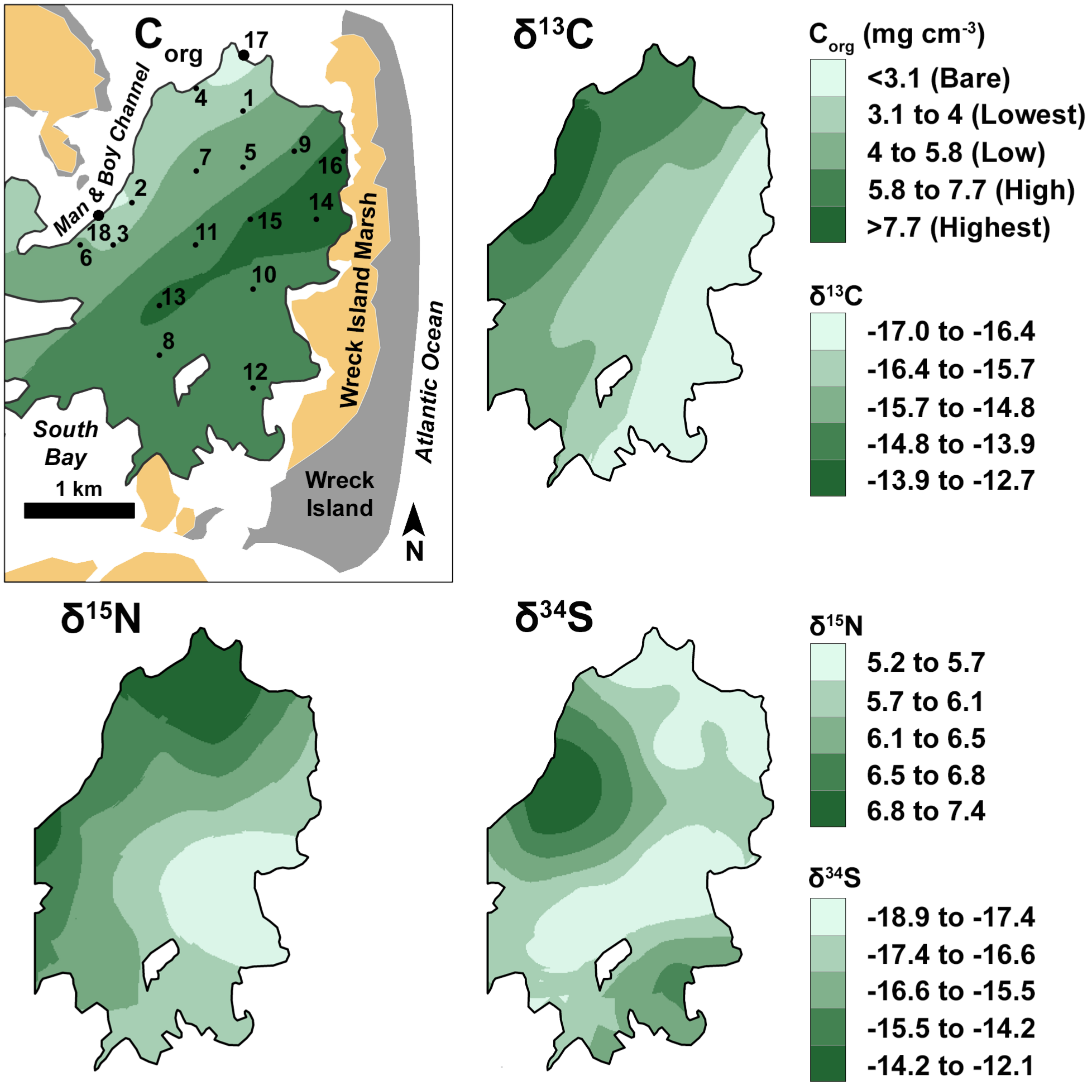

Figure 4.3. Kriged average sediment C_{org} and stable isotope ratios measured at sample sites (see Table 4.2 for site details); the C_{org} distribution is shown relative to the surrounding meadow (outlined), land areas (dark gray), and marshes (orange). Note that the sites are mapped according to the five SOC categories used in the group mixing model analysis; the group concentrations are defined in the corresponding C_{org} key.

The meadow SOC concentration averaged 5.85±0.46 (SE) mg C_{org} cm^{-3} across all 16 meadow sites, but average concentrations at individual sites varied depending on relative location within the meadow. The meadow-wide SOC distribution was kriged using a spherical semivariogram and exhibited anisotropy, with concentrations varying along a predominantly northwest to southeast axis. Kriging the SOC distribution confirmed that the aforementioned SOC site groups were spatially discrete and distributed along a discernable spatial gradient (Figure 4.3). SOC concentrations were generally highest near Wreck Island and decreased with proximity to the meadow edge. Four sites in the northwest meadow yielded concentrations < 1 SD below the meadow average, averaging 3.44±0.21 (SE) mg C_{org} cm^{-3}. Three sites yielded concentrations between the meadow average and -1 SD, averaging 4.96±0.37 (SE) mg C_{org} cm^{-3}. Five sites yielded ‘high’ concentrations, between the meadow average and +1 SD, averaging 6.42±0.21 (SE) mg C_{org} cm^{-3}. And four sites in the mid-meadow yielded the ‘highest’ concentrations, > 1 SD above the meadow average and averaging 8.21±0.15 (SE) mg C_{org} cm^{-3}. The two bare sites adjacent to the meadow yielded an average concentration of 2.82±0.24 (SE) mg C_{org} cm^{-3}, which was similar to the background SOC concentration measured at a third bare site in nearby Hog Island Bay, 2.93±0.16 (SE) mg C_{org} cm^{-3}.

The $\delta^{13}C$ and $\delta^{15}N$ data also exhibited spatial gradients. The $\delta^{13}C$ distribution was best fit by an exponential semivariogram, and like the SOC distribution, exhibited anisotropy. Average $\delta^{13}C$ values at sites showed increasing enrichment with distance from Wreck Island, ranging from -17.03 up to -12.66 ‰ (Table 4.2). The $\delta^{15}N$ distribution was best fit by a circular semivariogram and also showed isotope enrichment with distance from the island, with values ranging from 4.96 to 7.56 ‰. In comparison, the kriged $\delta^{34}S$ distribution was best fit by a spherical semivariogram but did not provide evidence for a single spatial gradient. Instead the kriged $\delta^{34}S$ distribution suggested local enrichment zones to the northwest and to the southeast (Figure 4.3). All of the $\delta^{34}S$ values showed significant depletion relative to seawater, with site values ranging from -19.12 to -11.86 ‰ (Table 4.2).

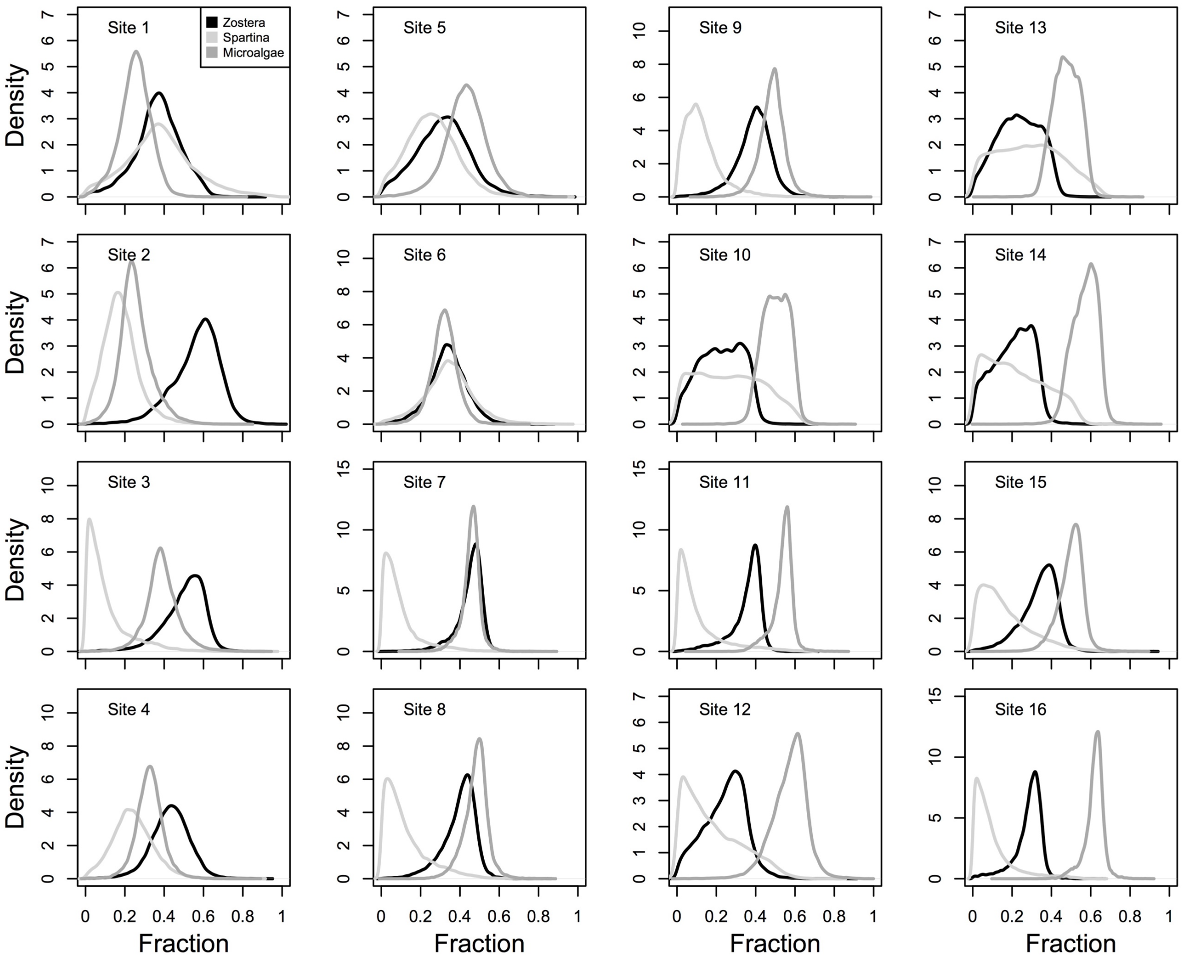

Figure 4.4. Modeled posterior distributions for potential autotroph sources (*Z. marina*, *S. alterniflora*, and BMA) at each meadow site (see Figure 4.1 for site locations).

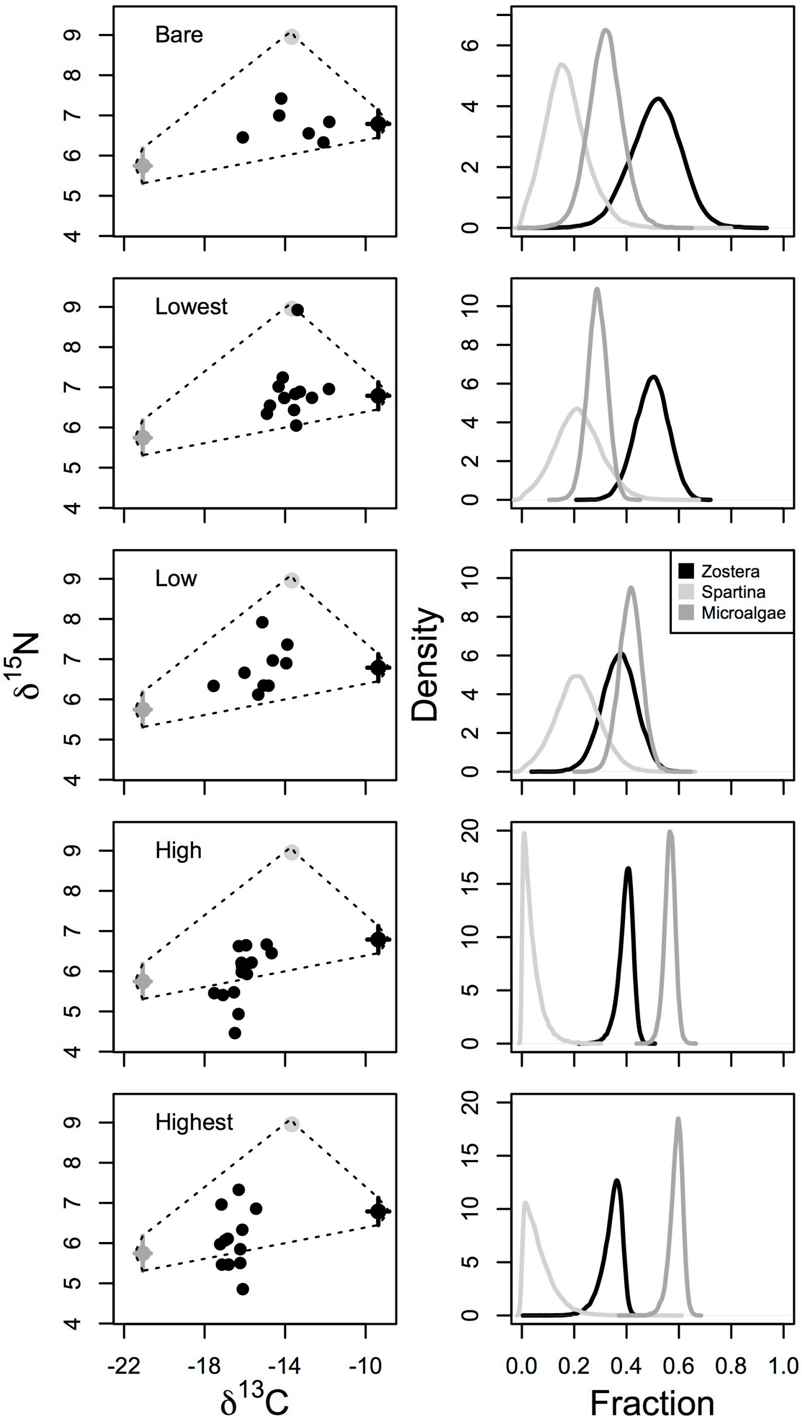

Figure 4.5. δ^{13}C and δ^{15}N biplots, showing individual sediment samples plotted relative to the autotroph end-members ranges by SOC Group, and corresponding mixing model posterior plots.

According to the mixing model results, different sites exhibited different autotroph source fractions (Figure 4.4). Most of the individual sediment samples from the different meadow sites yielded δ^{13}C and δ^{15}N compositions intermediate between the *Z. marina*, *S. alterniflora*, and BMA end-member compositions, plotting within the δ^{13}C and δ^{15}N bi-plot mixing polygon (see Appendix II for individual site bi-plots). When viewed by SOC group, sediment samples representing each group generally clustered together, but the location of the cluster within the mixing polygon shifted from closer proximity to the *Z. marina* end-member at bare and low SOC sites to the BMA end-member at higher SOC sites (Figure 4.5). Samples from two ‘high’ SOC sites (10 and 12 in Figure 4.3) and two ‘highest’ SOC sites (13 and 14) plotted outside of the mixing polygon. Omitting these four sites did not significantly alter SOC group mixing model results (Appendix II). The remaining sites yielded well-constrained posterior distributions, but several sites (#1, 6, and 7) had posterior distribution overlap (Figure 4.4).

Table 4.3. Mixing model output for each SOC group (n = number of sites).

Category	n	C_{org} (mg cm^{-3})	C_{org} SD	Source	Mean	SD
Lowest	4	3.44	0.43	*Zostera*	0.50	0.06
				Spartina	0.21	0.09
				BMA	0.29	0.04
Low	3	4.96	0.63	*Zostera*	0.37	0.07
				Spartina	0.21	0.08
				BMA	0.41	0.08
High	5	6.42	0.48	*Zostera*	0.40	0.03
				Spartina	0.04	0.04
				BMA	0.56	0.02
Highest	4	8.21	0.29	*Zostera*	0.34	0.04
				Spartina	0.06	0.06
				BMA	0.59	0.02
Bare	2	2.85	0.25	*Zostera*	0.51	0.10
				Spartina	0.17	0.08
				BMA	0.32	0.07

The mixing model found good end-member posterior separation at the SOC group-level (Figure 4.5; Appendix II). The *S. alterniflora* distribution had the lowest mean value in each case; whereas, the BMA posterior mean value differed considerably among the different SOC groups (Figure 4.5; Table 4.3). The well-constrained posterior distribution mean values allowed us to characterize the fractional contribution of each autotroph by site group. According to the mixing model, the BMA fraction increased from 0.29±0.04 (SD) at the ‘lowest’ SOC sites to 0.59±0.02 (SD) at the ‘highest’ sites. BMA contributed a fairly low fraction of the SOC at the bare control sites adjacent to the meadow, 0.32±0.07 (SD). In comparison, the mean of the posterior distribution estimating the *Z. marina* fraction was relatively high at the bare sites, 0.51±0.10 (SD), and decreased in the ‘high’ and ‘highest’ SOC groups to 0.34±0.04 (SD) (Table 4.3).

However, this end-member comparison did not account for the fact that total SOC also varied among the groups.

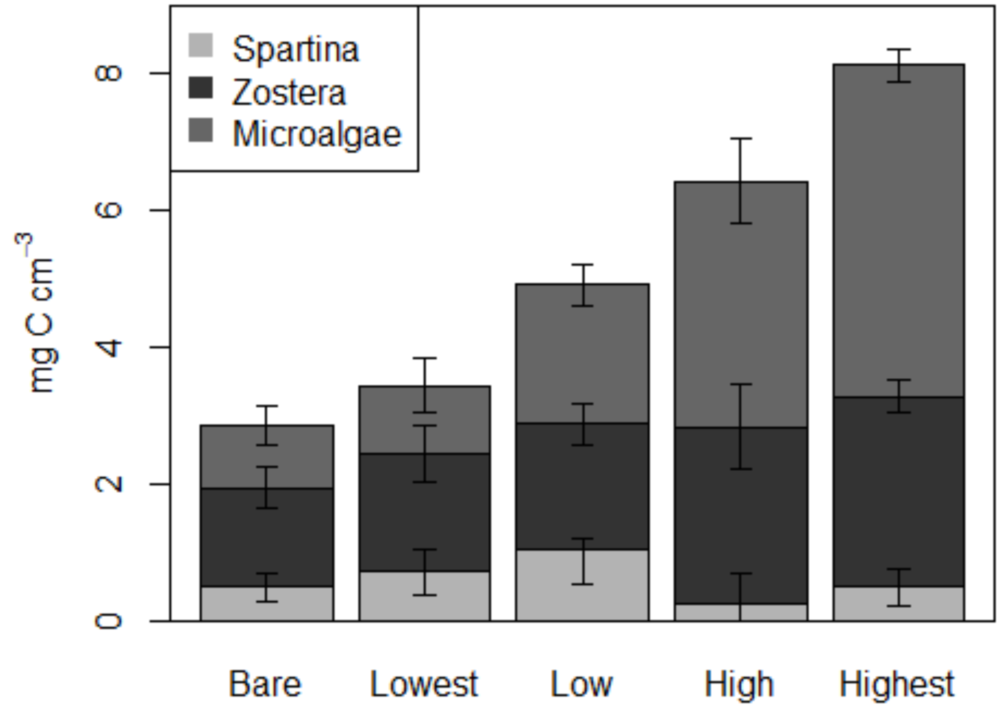

Figure 4.6. The change in end-member bulk C_{org} contributions within the restored meadow by site SOC group (see Figure 4.3 and Table 4.3 for information on each SOC group); error bars are the standard deviation of the source fraction posterior distribution applied to the calculation of the organic carbon from each source.

We determined *Z. marina*, *S. alterniflora*, and BMA bulk C_{org} contributions for each SOC group by multiplying the group average SOC concentration by end-member fraction, represented by the posterior distribution means. *Z. marina* and BMA bulk contributions were higher at sites with higher SOC concentrations, consistent with the spatial gradient (Figure 4.6). The SOC concentration attributable to *Z. marina* increased from 1.72 to 2.79 mg C_{org} cm^{-3}, a 62% increase. The *Z. marina* bulk contribution was lowest at the bare sites (Figure 4.6). The BMA SOC concentration increased even more substantially across the meadow gradient, from 1.00 to 4.84 mg C_{org} cm^{-3}, a 384% increase. The BMA contribution at the unvegetated sites was 0.91 mg C_{org} cm^{-3}. In comparison, the *S. alterniflora* concentration ranged from 0.26 to 1.04 mg C_{org} cm^{-3} but showed no consistent change across the meadow SOC spatial gradient. The estimated *S. alterniflora* concentration was approximately the same within the meadow 'highest' SOC area as at the bare sites, 0.49 mg C_{org} cm^{-3}. Despite exhibiting the highest *Z. marina* fractional contribution (Table 4.3), the bare sites yielded the lowest *Z. marina* bulk contribution, 1.45 mg C_{org} cm^{-3}.

By subtracting average SOC concentrations at the bare sites from the average concentrations within the 'highest' area by end-member, we identified the fraction of the net SOC increase within the 'highest' area attributable to each source. *Z. marina* contributed 25.3% of the net increase, *S. alterniflora* contributed <0.1%, and BMA contributed 74.5%. Averaging the end-member bulk contributions across all 16 meadow sites yielded an average *Z. marina* concentration of 2.27 mg C_{org} cm^{-3}, an average *S. alterniflora* concentration of 0.58 mg C_{org} cm^{-3}, and an average BMA concentration of 2.96 mg C_{org} cm^{-3}. At the meadow-scale, *Z. marina* contributes an estimated 39.09% of the total measured stock, *S. alterniflora* contributes 9.96%, and BMA contributes

50.95%. Non-seagrass C_{org}, therefore, accounts for >60% of total SOC within this bed interval, with BMA accounting for almost all (>83%) of that non-seagrass fraction.

Table 4.4. Meadow site (n = 16) isotope ratio and SOC source fraction relationships with distance from Wreck Island Marsh (Marsh) and from the meadow-bare subtidal edge (Edge).

	Intercept	SE	M	SE	$F_{(1,14)}$	*p*	adj-R^2
δ^{13}C~Marsh	-15.450	0.862	3.27E-05	1.14E-03	0.001	0.978	-0.071
δ^{13}C~Edge	-15.240	0.621	-3.48E-04	9.61E-04	0.131	0.723	-0.062
δ^{15}N~Marsh	6.422	0.415	-9.39E-05	5.49E-04	0.029	0.867	-0.069
δ^{15}N~Edge	6.454	0.299	-1.77E-04	4.63E-04	0.146	0.708	-0.060
δ^{34}S~Marsh	-17.030	1.263	7.01E-04	1.67E-03	0.176	0.681	-0.058
δ^{34}S~Edge	-15.603	0.873	-1.71E-03	1.35E-03	1.605	0.226	0.039
Zostera~Marsh	0.277	0.064	1.08E-04	8.52E-05	1.607	0.226	0.039
Zostera~Edge	0.442	0.040	-1.64E-04	6.24E-05	6.874	0.020	0.281
Spartina~Marsh	0.182	0.060	2.47E-05	8.00E-05	0.095	0.763	-0.064
Spartina~Edge	0.208	0.044	-1.61E-05	6.78E-05	0.056	0.816	-0.067
BMA~Marsh	0.541	0.070	-1.33E-04	9.22E-05	2.073	0.172	0.067
BMA~Edge	0.350	0.044	1.80E-04	6.84E-05	6.891	0.020	0.282

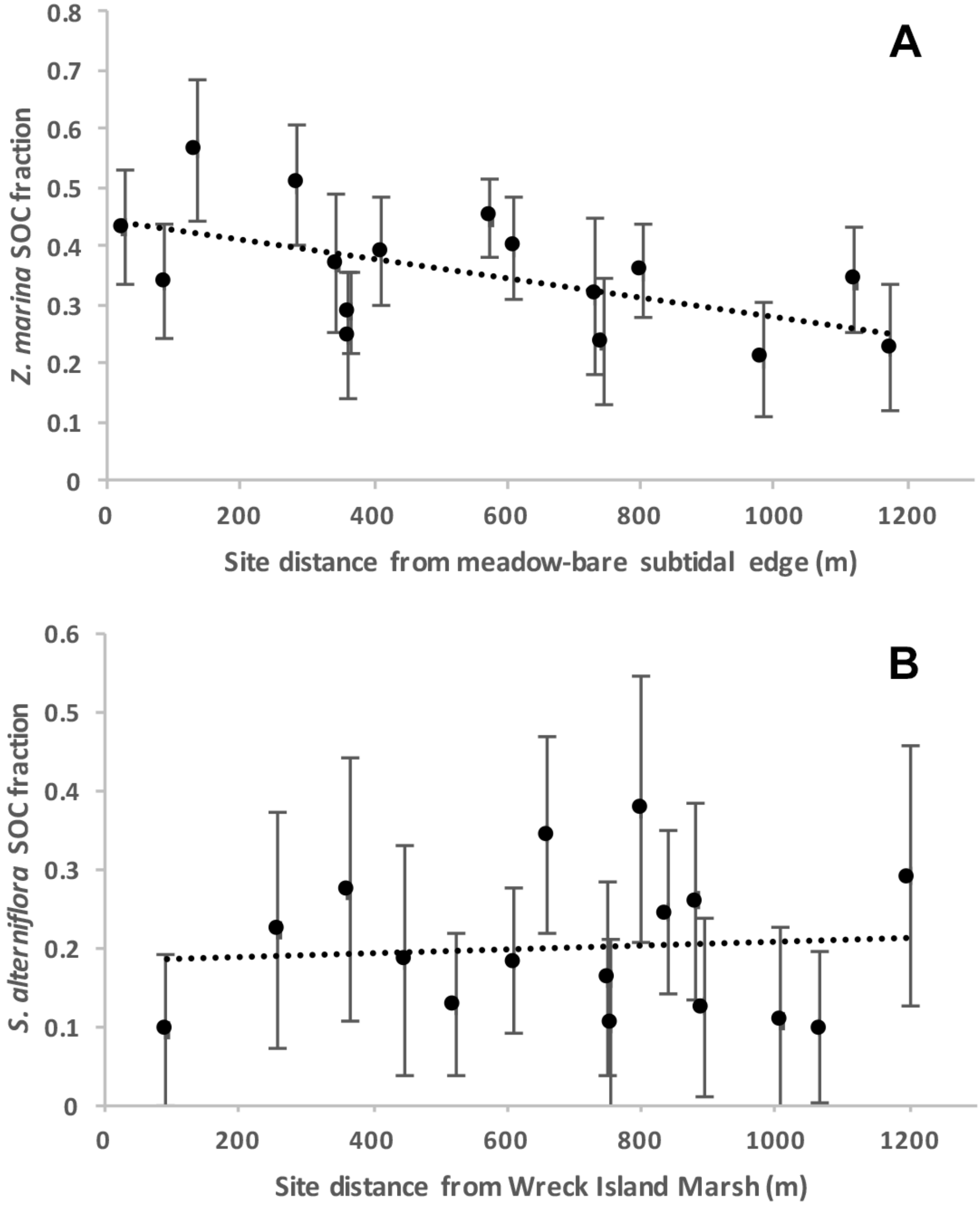

Figure 4.7. The spatial origin of seagrass SOC: A) *Z. marina* source fraction at each site compared with site distance from the bare subtidal edge (see Figure 4.1); B) *S. alterniflora* source fraction at each site compared with site distance from Wreck Island Marsh (source fractions equal posterior means; error bars represent posterior SD; regression statistics given in Table 4.4).

Measured isotope ratios and autotroph source fractions (represented by the mixing model posterior means) did not show strong regression relationships with site distance from either Wreck Island Marsh or the meadow-bare subtidal edge (Table 4.4). The *S. alterniflora* fraction did not show a significant relationship with site distance to Wreck Island Marsh (Table 4.4: $p > 0.7$; Figure 4.7). Relationships between the *Z. marina* and BMA fractions and distance to the meadow edge yielded *p*-values < 0.020. However, the *Z. marina* fraction showed an increase with proximity to this edge (Figure 4.7); whereas, the BMA fraction showed an increase with distance from the edge. Omitting sites with problematic posterior distribution results (sites 10, 12, 13, and 14) did not significantly change these regression results (Appendix II).

4.4. Discussion

4.4.1. The geographic sources of seagrass SOC

Sediment organic carbon stable isotope compositions varied at different sites within this seagrass bed according to location, consistent with spatial variation in relative contributions from different carbon sources. However, the observed spatial patterns did not match the hypothesized patterns that we would expect to find if the non-seagrass SOC fraction resulted primarily from meadow burial of allochthonous POM advected into the meadow. We did not observe a *S. alterniflora* concentration gradient in the seagrass bed that decreased with distance from the nearest marsh. *S. alterniflora* POM ‘outwelling’ did not account for the high SOC concentration in the eastern half of this meadow (hypothesis 1). Nor did we observe higher non-seagrass SOC concentrations at sites closer to bare subtidal areas, which would have supported the hypothesis that the non-seagrass fraction resulted primarily from allochthonous POM trapped by the meadow canopy (hypothesis 2). Seston trapping by the canopy may account for the *S. alterniflora* C_{org} in the bed—our seston and *S. alterniflora* biomass samples showed similar $\delta^{15}N$ enrichment—but this SOC fraction was nominal (<10%) and fairly evenly distributed both inside and outside of the meadow. Marsh POM 'outwelling' was not an important source of total seagrass SOC, despite the proximity of the adjoining marsh to the seagrass bed.

The $\delta^{13}C$ and $\delta^{15}N$ spatial gradients we observed instead provided evidence for autochthonous, not allochthonous, C_{org} burial. The *Z. marina* percent contribution was highest closer to the meadow-bare subtidal boundary, and the BMA percent contribution was highest in the meadow interior. We would expect to observe the opposite pattern if the microalgal SOC fraction resulted from BMA advection into the meadow. After accounting for the bulk SOC increase across the spatial gradient, we determined that the *Z. marina* SOC concentration was actually higher in the 'highest' SOC area than in the 'low' and 'lowest' areas (Figure 4.6). The *Z. marina* percent contribution appeared to decrease with distance from the bare-subtidal edge (Figure 4.7), because the BMA fraction exhibited an even larger increase at sites further from the edge (Table 4.4). The BMA bulk contribution was also highest at the 'highest' SOC sites (Figure 4.6). BMA contributed most of the C_{org} to this seagrass SOC pool.

Additional sources also contribute marginally to this SOC pool, but we were ultimately unable to consider another end-member, because we were not able to include δ^{34}S as a third tracer. The observed discrepancy between sediment and end-member δ^{34}S ranges likely resulted from sulfate reduction within the bed, which causes similar δ^{34}S depletion (Canfield 2001). Future studies may be able quantify this process and adjust measured δ^{34}S values accordingly. However, we noted that the magnitude of this process varied spatially (Figure 4.3), possibly due to both carbon source and bed sediment factors (cf. Oakes and Connolly 2004). We considered using the C:N ratio as a third tracer but ultimately excluded it due to possible preferential loss of N in different bed locations (chapter 3). Absent a third tracer, we were not able to simultaneously quantify the macroalgal contribution, which Greiner et al. (2016) found to be negligible (~3%), or include phytoplankton, which was likely a minor SOC contributor due to very low concentrations and productivity in the water column (McGlathery et al. 2001). Including macroalgae would not explain why samples representing four sites fell outside the bi-plot mixing polygon due to low δ^{15}N values. The macroalgae δ^{15}N range is similar to that for *S. alterniflora*, which was not a major contributor at these sites. These four sites hint at another SOC source, possibly N-fixers in the microphytobenthos or epiphyte communities (Cole and McGlathery 2012), which would explain why the site δ^{15}N values were biased towards atmospheric δ^{15}N. The δ^{15}N ratios at these sites could also be attributable to buried phytoplankton; however, the phytoplankton collected from this system by Hondula and Pace (2014) yielded lower δ^{13}C ratios (<-25 ‰).

Some of the BMA SOC we identified may be allochthonous, but the spatial pattern (highest contribution farthest from the meadow edge) indicates that the majority was likely fixed *in situ*. Hardison et al. (2013) and Timmerman (2014) documented high BMA activity within this system in bare areas, which they attributed to increased light availability at the sediment-water interface absent shading by macrophytes. Some BMA from outside the meadow might pass into the meadow in suspension before being deposited at interior meadow sites, along with other fine particulates (Hansen and Reidenbach 2012; 2013; chapter 3). However, there is also significant BMA activity within the meadow itself. BMA produce mats of extracellular polymeric substances (EPS) that bind sediment within this meadow and help protect the bed from erosion during winter months, when seagrass shoot density is lowest (Timmerman 2014). The 'high' and 'highest' SOC spatial regimes correspond with areas within the meadow where diatomaceous mats are sometimes visible in aerial photographs taken by the VIMS SAV monitoring program (VIMS SAV, http://web.vims.edu/bio/sav/, accessed 12 Dec 2016). The 2011 photo shows this spatial correspondence distinctly, suggesting that *in situ* BMA production contributes to the observed SOC spatial gradient. Timmerman (2014) also measured sediment chlorophyll and carbohydrate concentrations—proxies for BMA activity—concurrent with this study at a site inside the meadow and at a bare control site. Both measures were generally higher at the meadow site. The meadow chlorophyll concentration ranged as high as 220 mg m^{-2} at the seagrass site, compared with 71 mg m^{-2} at the bare site; meadow carbohydrate concentrations averaged 90.2 µg g^{-1} at the seagrass site, compared with 49.9 µg g^{-1} at the bare site over the same period (Timmerman 2014). Consequently, most—if not all—of the BMA SOC measured in this study was likely autochthonous.

The importance of BMA as a contributor to SOC within this meadow may be due, in part, to OM recycling within the seagrass microbial community, resulting from nutrient limitation (McGlathery et al. 2004; McGlathery et al. 2007; Hardison et al. 2011). BMA turnover occurs every few days, but immediate BMA OM uptake by bacteria, and subsequent re-uptake by BMA, results in tight BMA-bacterial nutrient coupling in this system, which likely facilitates organic matter retention in bed sediments (Hardison et al. 2013). It is, therefore, conceivable that *Z. marina* initially fixed a higher percentage of the SOC now stored within the bed, but that some of this C_{org} entered the bacteria-BMA uptake cycle and now exhibits a BMA isotopic signature. However, we do not see excessive isotope depletion consistent with multiple fractionation steps resulting from SOC recycling.

The BMA results, nevertheless, underscore the importance of considering the benthic microalgal community when constructing seagrass carbon budgets or calculating seagrass SOC burial fluxes. Studies should not assume that all—or even most—of the SOC beneath a seagrass meadow derives from seagrass. We note that BMA-derived C_{org} represents a dominant SOC constituent in both vegetated and unvegetated coastal habitats (e.g. Hardison et al. 2013; Oakes and Eyre 2014), due in part to long turnover times for EPS (McKew et al. 2013; Oakes and Eyre 2014). The percentage of total seagrass production that enters the sediment carbon pool may, therefore, be significantly lower than expected based on a site's SOC profile, with the remainder of the seagrass production decomposed at the sediment surface, exported, or consumed by herbivores (Duarte and Cebrián 1996).

4.4.2. Implications for blue carbon accounting

This study is the first to document BMA contributions augmenting SOC storage in a blue carbon system. Similar studies in marsh and mangrove habitats are still lacking. Oakes and Eyre (2014) speculated that BMA may contribute significantly to the blue carbon stored in marsh, mangrove, and seagrass sediments. However, in their recent blue carbon review, Macreadie et al. (2017A) only discuss microalgal carbon in the context of a regime shift from marsh or seagrass to microalgal production that results in less blue carbon storage—not coupling between these macrophytes and BMA that may increase BMA productivity and, therefore, SOC accumulation. By analyzing SOC at the meadow-scale, our results confirm initial suggestions by Greiner et al. (2016) that BMA represents the dominant contributor to the SOC stock in this particular seagrass meadow. BMA production—not allochthonous POM trapping—likely accounts for much of the non-seagrass SOC observed in seagrass meadows (Kennedy et al. 2010). We note that BMA are fairly ubiquitous in coastal habitats, even where macroalgal shading reduces light availability for photosynthesis (Hardison et al. 2011; Oakes and Eyre 2014). Seagrass canopies allow more incident light to reach the sediment surface and may, therefore, enhance BMA productivity relative to macroalgal-dominated habitats (Hardison et al. 2011; 2013).

The BMA SOC documented in this seagrass bed should be considered a carbon offset benefit of restoration provided the restored meadow either facilitates BMA presence or the burial of this material relative to bare sites. As previously noted, BMA occur at sites with and without seagrass and contribute to SOC accumulation at bare sites (e.g. Volkman et al. 2008; Hardison et al. 2013; Timmerman 2014). However, significantly higher chlorophyll and carbohydrate concentrations inside this meadow suggest BMA production is higher in the meadow than at bare control sites (Timmerman 2014). We also note that the seagrass plants facilitate bed accretion, thereby increasing the likelihood that within-meadow BMA C_{org} becomes buried. According to the ^{210}Pb profiles, nearby bare sites are not accreting. C_{org} fixed by BMA in bare areas, therefore, has a higher likelihood of being remineralized. The lower BMA SOC concentrations at the bare sites likely reflect both lower BMA production outside the meadow and lower preservation rates for that production. However, more work is needed to quantify these seagrass effects on BMA SOC burial rates.

Regarding the application of these results for seagrass offset-credit accounting (CEC 2014; Emmer et al. 2015A), we note that seagrass restoration projects will not likely be able to differentiate between allochthonous and autochthonous fractions in the seagrass SOC pool with complete certainty. Our effort to differentiate these fractions in the South Bay meadow benefitted from relatively few potential end-members (Hondula and Pace 2014), low potential for diagenesis (Greiner et al. 2013), significant past work on seagrass SOC accumulation and the biotic community within the VCR-LTER system (Hardison et al. 2011; 2013; McGlathery et al. 2012) and in South Bay in particular (Greiner et al. 2013; 2016; Timmerman 2014), and a known meadow restoration history that did not include any significant bed disturbances (Orth et al. 2006B; 2012; McGlathery et al. 2012). From an isotope-source modelling perspective, our results confirm that autotroph source differentiation is possible at the meadow-scale but by no means straightforward. Although we were able to constrain potential source isotope ranges and conduct a mixing model analysis, several of the posterior distributions exhibited significant spread about their means. These posterior distributions limited our ability to quantify source fractions at particular sites and, therefore, our ability to confidently quantify whole meadow stocks by source. We, consequently, refrained from kriging posterior means determined for individual sites to generate meadow-scale source maps. Some of this variability may be due to slight differences in diagenesis at individual sites or to additional sources that we were not able to include in our models. The problematic sites occur near Wreck Island (Figure 4.1: sites #10, 12, 13, and 14), where macroalgae sometimes accumulates. Diagenesis is possibly a factor at sites closer to Man & Boy Channel, which yield much higher C:N ratios (chapter 3).

Given the difficulties associated with conducting SOC source analysis, an allochthonous carbon compensation factor probably remains the best option for individual seagrass restoration projects trying to meet the CEC (2014) allochthonous carbon deduction requirement for seagrass blue carbon accounting. This study broadly supports using the Kennedy et al. (2010) 50% non-seagrass SOC compensation factor at the meadow-scale but casts doubt on whether most of that SOC is actually allochthonous. If the CEC (2014) goal is to conservatively exclude any SOC that was not fixed by the restored seagrass plants, then a 50% compensation factor applied to this meadow stock represents a reasonable deduction. However, an accurate allochthonous SOC deduction based on this system would be closer to 10%—not 50%. Additional work may confirm that *in situ* BMA contribute most of the non-seagrass SOC in most seagrass meadows. Provided the storage of this production can be attributed to meadow presence, projects should be able to count this SOC as a seagrass blue carbon benefit when requesting offset-credits under the VCS accounting guidelines (Emmer et al. 2015A).

4.5. Conclusions

This study identifies spatial variability in seagrass and BMA source contributions to a seagrass SOC pool, discernable from stable isotope spatial variability evident at the seagrass meadow-scale. *Z. marina* accounts for less than half of the total SOC stock (40%); however, canopy-trapping of allochthonous POM—represented in this system primarily by *S. alterniflora*-derived seston—only accounts for another 10% of the total. Most of the SOC within this seagrass bed apparently derives from BMA that occur within the meadow. The burial and long-term storage of this SOC is at least partly attributable to seagrass presence, because the seagrass canopy facilitates bed accretion. Enhanced burial of *in situ* BMA C_{org} should, therefore, be considered a possible blue carbon benefit of seagrass restoration. However, even with the aid of discernable stable isotope spatial gradients and isotope mixing models, quantifying the allochthonous and autochthonous SOC fractions within a seagrass bed remains somewhat speculative, because the geographic origin of SOC cannot be established with complete certainty. An allochthonous carbon compensation factor represents, perhaps, the best option for seagrass blue carbon offset-credit accounting, but the proposed 50% compensation factor would underestimate the autotrophic production fixed within this particular meadow and attributable to meadow presence. More work is needed to identify an appropriate allochthonous carbon percentage that can be generally applied to seagrass restoration projects.

Acknowledgements

I want to thank my collaborators: G.M. Wilkinson, K.J. McGlathery, M. Bost, and B.A. McKee. I also wish to thank M. Otter at MBL and P. Luckenbach, C. Buck, A. Schwarzschild, M. Miller, A. Lunstrum, L. Aoki, and M.-L. Delgard for field and/or lab assistance. We thank J. Greiner for allowing us to re-analyze ^{210}Pb data. R. Orth and D. Wilcox provided access to aerial imagery, and J. Porter, P. Wiberg, and R. Timmerman provided additional advice. This study was supported by National Science Foundation Virginia Coast Reserve Long Term Ecological Research Grant DEB-1237733, the University of Virginia Department of Environmental Sciences, the University of Virginia Jefferson Scholars Foundation, and by Virginia Sea Grant.

Data archiving

Data collected during this study can be obtained from the Long Term Ecological Research Network database (https://www.lternet.edu).

Chapter 5. The net greenhouse gas benefit from seagrass restoration

Abstract

In recent years, observers have noted CO_2-sequestration by seagrass meadows and suggested financing seagrass restoration through the sale of carbon offset-credits. A new greenhouse gas (GHG) accounting framework allows the Verified Carbon Standard (VCS) to allocate credits to seagrass projects. However, the net GHG offset benefit from seagrass restoration remains uncertain. Seagrass 'blue carbon' studies to date exclude possible meadow effects on CH_4 and N_2O fluxes, which may limit the benefit from CO_2-sequestration in plant biomass and bed sediment. We measured carbon pool stock changes and GHG fluxes to quantify the net GHG benefit from the most cost-effective seagrass project, the *Zostera marina* (eelgrass) restoration in the Virginia Coast Reserve, using the VCS framework. Repeated measurements in the 7 km^2 South Bay meadow confirmed both an increase in the enhanced, sequestered CO_2 stock, from 6,060 t in 2013 to 9,590 t in 2016, and meadow-enhanced CH_4 and N_2O fluxes, which have released an additional 950 t CO_2e since the restoration start. The net CO_2 sequestration rate has increased from 0.21 t C ha^{-1} yr^{-1} between 2001-2013 to 0.42 t C ha^{-1} yr^{-1} from 2013-2016, which approximately equals the IPCC seagrass sequestration rate for national GHG inventory accounting. This meadow sequesters approximately one quarter of GPP. However, the blue carbon financial benefit after 15 years, approximately $28.5K at the current offset price, only defrays 3.5% of the incurred restoration cost. Offset-credits provide a marginal incentive for seagrass restoration but are unlikely to completely finance additional restoration absent a dramatic increase in offset-credit demand.

5.1. Introduction

Seagrass meadows represent an important sink in the global carbon cycle, because many systems are net autotrophic and bury organic carbon (C_{org}) (Duarte et al. 2005; Champenois and Borges 2012; Tokoro et al. 2014). Fourqurean et al. (2012) recently estimated that seagrass meadows contain 4.2-8.4 Pg C_{org} in bed sediments and an additional 151 Tg C_{org} in above- and belowground biomass—a significant global carbon stock threatened by accelerating seagrass habitat conversion from coastal development, eutrophication, and other anthropogenic impacts (Orth et al. 2006A; Waycott et al. 2009). Bed erosion following seagrass meadow collapse results in the rapid remineralization of seagrass sediment C_{org} (SOC) (Macreadie et al. 2015; Marbà et al. 2015), which potentially releases 50-330 Tg CO_2 yr^{-1} back to the atmosphere (Pendleton et al. 2012). Seagrass restoration can reverse these losses by transferring C_{org} back to the sediment (Greiner et al. 2013; Marbà et al. 2015; Thorhaug et al. 2017).

Calls for certifying 'blue carbon' offset-credits to incentivize seagrass restoration efforts (Nellemann et al. 2009; Murray et al. 2011) prompted the development of *VM0033: Methodology for Tidal Wetland and Seagrass Restoration* (Emmer et al. 2015A) for the Verified Carbon Standard (VCS), so it can issue voluntary credits to applicant restoration projects. The VCS will award credits to seagrass restoration projects in proportion to their net greenhouse gas (GHG) benefit, the amount of CO_2 (or CO_2 equivalent GHG: CO_2e) removed from the atmosphere by project activities and permanently sequestered in a recognized carbon pool (Emmer et al. 2015B). Projects must document enhanced CO_2 sequestration relative to a business-as-usual (i.e.

without-project) baseline. The net GHG benefit for seagrass projects corresponds to enhanced CO_2 sequestration in bed SOC and seagrass above- (AGB) and belowground biomass (BGB), minus any enhanced GHG release (Emmer et al. 2015A). Despite considerable interest in seagrass ‘blue carbon,’ the net GHG benefit that will likely result from seagrass restoration remains uncertain (Belshe et al. 2017). A seagrass project has yet to apply for VCS credits (http://vcsprojectdatabase.org/, accessed 1 March 2018), and existing seagrass studies do not report a net benefit, because they do not consider baseline carbon stocks or possible restoration effects on CH_4 and N_2O production (e.g. Russell and Greening 2015; Reynolds et al. 2016; Thorhaug et al. 2017).

The ‘blue carbon’ literature typically quantifies the seagrass GHG benefit by measuring and reporting metabolic fluxes and/or SOC burial rates (e.g. Duarte et al. 2010; Champenois and Borges 2012; Johnson et al. 2017), but these measures do not equate directly with a 1:1 GHG removal from the atmosphere (Belshe et al. 2017; chapter 2). GPP fluxes likely overestimate enhanced CO_2 sequestration, because they do not account for remineralization and out-gassing of biomass exported to adjacent habitats (e.g. Cai 2011). GPP exported from the project area must be conservatively excluded under the VCS framework (Emmer et al. 2015A). Seagrass SOC burial rates may increase over time, due to positive meadow-hydrodynamic-sedimentation feedbacks (de Boer 2007; Duarte et al. 2013A); however, initial burial rate estimates likely overestimate enhanced SOC sequestration by failing to account for remineralization within the bed over long timescales and including allochthonous SOC (Johannessen and Macdonald 2016; chapter 2). Meadow canopy particle-trapping increases allochthonous C_{org} burial, which may account for half of the SOC pool in many meadows (Mateo et al. 2006; Kennedy et al. 2010; Mcleod et al. 2011), but the fate of this SOC absent the meadow is typically uncertain (CEC 2014; Johannessen and Macdonald 2016). The VCS *Methodology* requires that projects conservatively exclude non-reactive SOC that could be sequestered in the baseline scenario (Emmer et al. 2015A). Studies also frequently extrapolate carbon burial rates from individual sediment cores (Duarte et al. 2010 Data Set S1), but repeated measurements over decadal timescales are needed to verify seagrass SOC pool increases for carbon offset-credit accounting (chapter 2).

Table 5.1. Reported CH_4 flux data for seagrass systems.

Location	Seagrass	Method	CH_4 Flux (µmol m^{-2} hr^{-1})	Notes	Reference
Ria Formosa Lagoon, Portugal	*Zostera noltii*	Benthic chambers	4.4	Aerial exposure at night	Bahlmann et al. 2014
Ria Formosa Lagoon, Portugal	*Zostera noltii*	Benthic chambers	6.9	Aerial exposure during day	Bahlmann et al. 2014
Ria Formosa Lagoon, Portugal	*Zostera noltii*	Benthic chambers	9.0-30	During tidal flooding	Bahlmann et al. 2014
Ria Formosa Lagoon, Portugal	*Zostera noltii*	Benthic chambers	4.4-71 (mean = 12.8)		Bahlmann et al. 2014
Florida Bay, FL, USA	*Thalassia testudinum*	Benthic chambers and porewater samples	0.567	Dead seagrass areas in winter	Barber and Carlson 1993
Florida Bay, FL, USA	*Thalassia testudinum*	Benthic chambers and porewater samples	14.21	Live seagrass areas in fall	Barber and Carlson 1993
Celestun Lagoon, Mexico	(Seagrasses cover up to 65% of lagoon)	Benthic chambers	<0.41	Data represent sed-water flux	Chuang et al. 2017
Cape Lookout Bight, NC, USA	*Zostera marina and Halodule sp.*	Core extraction, centrifuging, porewater sampling	20-2000	Seagrass not specifically studied but occurs in the general study area	Crill and Martens 1983
Arcachon Bay, France	*Zostera noltii*	Benthic chambers	1.6-4.1		Deborde et al. 2010

Red Sea	Multispecies: *Thalassodendron ciliatum*, *Cymodocea serrulata*, *Halodule uninervis*, etc.	Core incubations	0.09-565.27	Salinity range = 37.98-42.29	Gacias-Bonet and Duarte 2017
Moreton Bay, Australia	*Zostera capricorni*	*In vitro* incubations	0.233		Moriarty et al. 1985
Florida Keys, FL, USA	*Thalassia testudinum*	Benthic chambers and inclubations	1.81-1.86		Oremland 1975
Bimini, Bahama Island	*Syringodium* sp.	Benthic chambers and inclubations	0.14-0.47		Oremland 1975
Tomales Bay, CA, USA	(*Zostera marina*)	Benthic chambers	2.08	Summer	Sansone et al. 1998
Tomales Bay, CA, USA	(*Zostera marina*)	Benthic chambers	0.896	Winter	Sansone et al. 1998
South Bay, VA, USA	***Zostera marina***	**Benthic chambers**	**5.697**	**Seagrass annual average**	**This study**
South Bay, VA, USA	***Zostera marina***	**Benthic chambers**	**0.739**	**Bare annual average**	**This study**

Table 5.2. Reported N_2O flux data for seagrass systems.

Location	**Seagrass**	**Method**	**N_2O Flux (µmol m^{-2} hr^{-1})**	**Notes**	**Reference**
Nanwan Bay, Taiwan	*Thalassia hemprichii, Halodule uninervis*	Sediment incubations	0.3-2.2*	12-hr incubations	Shieh and Yang 1997
South Bay, Virginia, USA	***Zostera marina***	**Benthic chambers**	**0.153**	**Seagrass annual average**	**This study**
South Bay, Virginia, USA	***Zostera marina***	**Benthic chambers**	**0.057**	**Bare annual average**	**This study**

*** µmol g wet wt^{-1} hr^{-1}**

Seagrass restoration effects on CH_4 and N_2O production are also uncertain. Marginal increases in the flux of these trace gases could be problematic, given their high global warming potentials (Neubauer and Megonigal 2015; UNFCCC 2017). Observers have long dismissed potential CH_4 and N_2O emissions from seagrass systems (Pollard and Moriarty 1991; Murray et al. 2011; Welsh et al. 2000), because sulfate reduction oxidizes CH_4 in marine sediments (Holmer et al. 2001; Poffenbarger et al. 2011) and seagrass nitrogen demand limits N_2O efflux (Shieh and Yang 1997; Welsh et al. 2000). Several available CH_4 release rates suggest that the seagrass-enhanced flux may be negligible (Oremland 1975; Moriarty et al. 1985), which the VCS defines as <5% of the GHG benefit from enhanced sequestration (i.e. *de minimis*). Sulfate reduction has been documented in seagrass beds and pore-water (Moriarty et al. 1985; Isaksen and Finster 1996; Lee and Dunton 2000). However, methanogenesis can vary considerably on diel and seasonal timescales within a system (Bahlmann et al. 2014), and recent data indicate that seagrass Ch_4 release rates may range has high as 565.27 µmol CH_4 m^{-2} d^{-1} (Table 5.1), compared with an open ocean flux of 1.2-4.4 µmol CH_4 m^{-2} d^{-1} (Garcias-Bonet and Duarte 2017). Benthic N_2O flux data from a seagrass system are still lacking (Table 5.2).

Absent a net GHG benefit case study, prospective seagrass restoration projects seeking offset-credits face uncertainty about likely project returns and the extent to which offset-credits will finance a restoration effort. Default factors used to estimate *ex ante* benefits may or may not be conservative, including the net benefit default factor for seagrass reestablishment that the IPCC (2014) allows countries to use for national

GHG inventory accounting, -0.43 t C ha^{-1} yr^{-1}. Individual projects seeking VCS credits may also cite this number to estimate particular stock change parameters (Emmer et al. 2015A), for example, gross SOC enhancement in the project scenario (Emmer et al. 2015B; chapter 2), but a seagrass restoration case study needs to determine whether this value is conservative for this purpose. If the IPCC (2014) is not conservative, projects will discover that they have overestimated the net project benefit when they conduct VCS-required monitoring in future time periods. Seagrass restoration projects have already been undertaken throughout the world, but many are either unsuccessful or small-scale efforts to augment natural recoveries (Paling et al. 2009). In cases where large-scale restoration has been successful, *in situ* measurements that could provide insight into the IPCC (2014) default factor are often lacking (e.g. Russell and Greening 2015; ESA 2016).

The *Zostera marina* (eelgrass) restoration in the Virginia Coast Reserve (VCR) represents, perhaps, the best case-study for quantifying the net GHG benefit from seagrass restoration and the likely financial benefit from awarding seagrass offset-credits. The restoration history (Orth et al. 2012), SOC stock enhancement (McGlathery et al. 2012; Greiner et al. 2013; chapter 3), and net ecosystem metabolism (Hume et al. 2011; Rheuban et al. 2014) of the restored meadow in South Bay, VA, are particularly well documented and permit a stock-change assessment, allowing us to assess GHG emission reductions from sequestration enhancement. This meadow contained an enhanced SOC stock of approximately 1,200 t C_{org} in 2013 and accumulates an estimated 37-44 g SOC m^{-2} yr^{-1} (Greiner et al. 2013; chapters 3 and 4). We compared average, annual, GHG fluxes from this meadow with measured SOC and biomass stock changes to quantify the net GHG benefit from this restoration project using the VCS GHG accounting framework (Emmer et al. 2015A). The results provide a benchmark for expectations about 'blue carbon' finance for seagrass restoration, generally, and allow us to address urgent GHG accounting questions: 1.) do seagrass GHG fluxes significantly affect the net benefit, and 2.) is the IPCC (2014) seagrass restoration default factor conservative for GHG accounting?

5.2. Methods

5.2.1. Project area

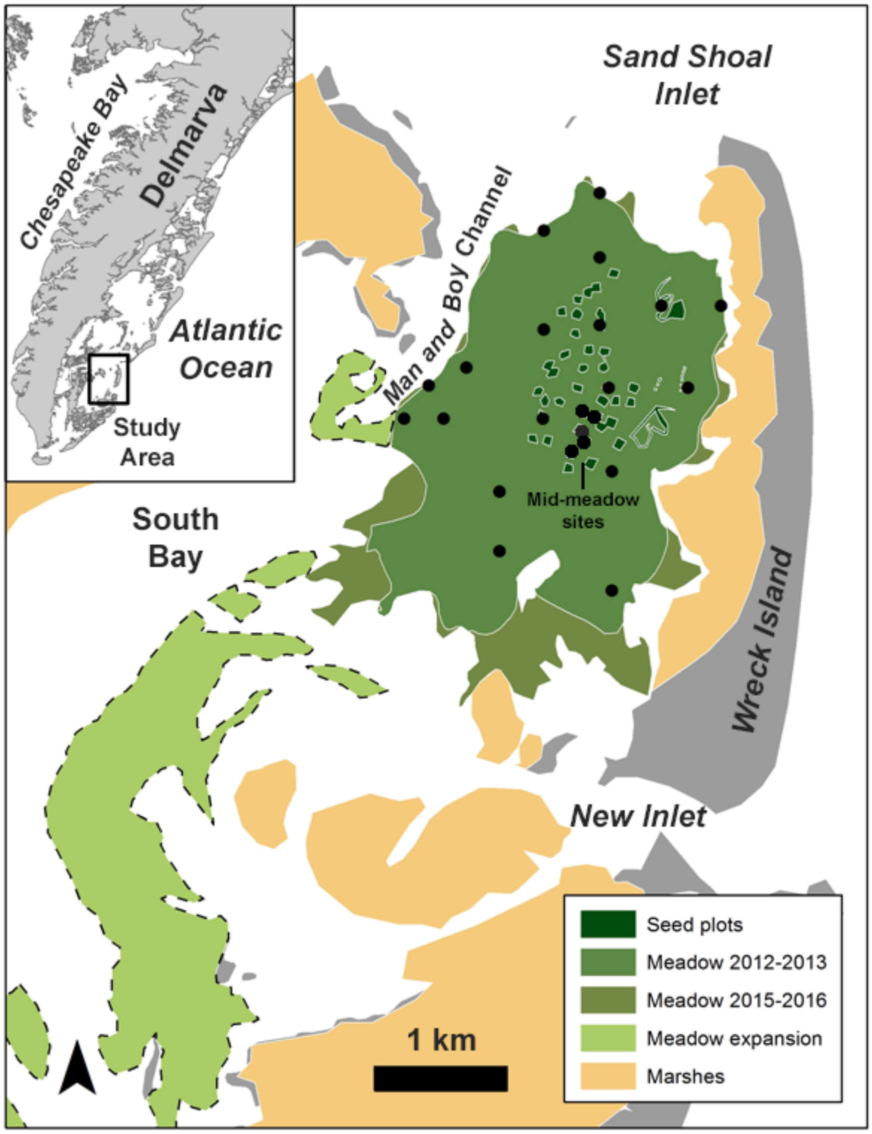

Figure 5.1. The South Bay, VA, study area, showing the locations of biomass and SOC sample sites (black circles), original restoration seed plots (established in 2000-2001: Orth et al. 2012), the central meadow extent prior to sampling in 2013, and the expanded meadow extent prior to sampling in 2016. Meadow expansion areas to the west and south (dashed lines) were excluded from the net GHG benefit calculations in this study.

Z. marina disappeared from the Delmarva coastal bays during the 1930s North Atlantic Eelgrass Pandemic (Oreska et al. 2017) and failed to recover naturally (Orth and McGlathery 2012). The system remained predominantly bare or algal dominated until restoration began in 1999. Between 2000-2002, 6.6M seeds were broadcast in 24 0.004 to 0.02 km^2 restoration seed plots in South Bay (Orth et al. 2006B), which expanded and coalesced naturally after active restoration ended in 2005 (Orth et al. 2012). By 2013, the restored meadow had filled the upper South Bay project area from Sand Shoal Inlet to the shoals around New Inlet, a contiguous meadow area ~6 km^2 in size (chapter 3). The meadow also expanded west around the south end of Man and Boy Channel and south along the west side of the marshes near Godwin Island (Figure 5.1). We focused on upper South Bay in the following analyses—the original restoration project area—and excluded the dynamic meadow expansions, because they periodically shift location.

The coastal bays are oligotrophic, with a light environment favorable to seagrass growth (McGlathery et al. 2001; Orth et al. 2010). Phytoplankton do not significantly affect *Z. marina* photosynthesis or SOC burial in the VCR coastal bays, which experience low nutrient loading, 1 g N m^{-2} yr^{-1} (Tyler et al. 2001; McGlathery et al. 2007). Water column chlorophyll α ranges from <1-5 $\mu g\ L^{-1}$ over the course of a year (McGlathery et al. 2001). South Bay has relatively shallow bathymetry, with a water depth at MSL of 0.76 ± 0.28 (SD) m (Richardson et al. 2014). Tidal exchange occurs through Sand Shoal and New Inlets (mean tidal range = 1.2 m: Fagherazzi and Wiberg 2009). The VA coastal bays exhibit negligible sediment inorganic carbon (Greiner et al. 2013). CO_2 evasion from $CaCO_3$ production, which may limit the net GHG benefit from other seagrass systems (Howard et al. 2017B), was not a concern in the VCR.

Past work confirms that there is net SOC enhancement by the meadow relative to bare control sites (McGlathery et al. 2012; Greiner et al. 2013; chapter 3), due in part to increased silt deposition attributable to tidal current attenuation by the canopy (Hansen and Reidenbach 2012; chapter 3). The SOC distribution may, therefore, reflect advection of allochthonous OM from non-seagrass sources. Recent isotopic work confirms that several different autotrophs contribute SOC. *Z. marina* contributes approximately 40% of the total SOC stock; whereas, *Spartina alterniflora* and macroalgae contribute <10% (Greiner et al. 2016; chapter 4). The remainder (51-56%) derives from benthic microalgae (BMA: Greiner et al. 2016; chapter 4), which occur *in situ* (Timmerman 2014). BMA extra-polymeric substances include labile constituents that turn-over every 2-3 months in unvegetated, intertidal sediment (McKew et al. 2013; Oakes and Eyre 2014). Canopy-mediated sedimentation within the South Bay meadow apparently facilitates BMA SOC stock enhancement relative to bare sites (chapters 3 and 4).

5.2.2. SOC stock enhancement

Only SOC stock enhancement above the background stock can be counted as a restoration benefit (Emmer et al. 2015A). SOC concentrations at unvegetated (i.e. bare) sites vary with sediment depth and site location. Bare site cores collected in 2013 yielded concentrations from 2.53 ± 0.22 (SE) mg C_{org} cm^{-3} in the top 3 cm to 4.87 ± 0.74 (SE) mg C_{org} cm^{-3} in the interval 9-12 cm below the sediment water interface (chapter 3).

Bare SOC profiles remain relatively constant over time (chapters 3 and 4), so we averaged available data (site n = 4) to generate a representative bare site profile for comparison with meadow site profiles (Greiner et al. 2013; chapters 3 and 4).

We used sedimentation rates calculated from ^{210}Pb profiles to identify a bed reference plane to stratigraphically calibrate cores and account for meadow accretion (Greiner et al. 2013; chapters 2, 3, and 4). We verified this depth calibration by comparing SOC profiles and identifying the bed depth where meadow and bare SOC concentrations became indistinguishable (Emmer et al. 2015A section 9.3.7). The seagrass bed accreted ~5 cm between meadow reestablishment in 2000 and 2011 and another 1+ cm by 2013; bare sites were non-depositional (Greiner et al. 2013; chapter 4). The reference plane was, therefore, approximately 6 cm below the sediment-water interface at bare sites outside the meadow, 12 cm below the interface inside the meadow in 2013, and 14 cm below the interface in the meadow in 2016, based on measured 0.6 cm yr^{-1} accretion rates for the years 2013-2016 (Greiner et al. 2017; chapter 4).

We randomly selected 16 of the 64 meadow sites sampled in 2013 and presented in chapter 3 for resampling to quantify SOC stock changes. We also resampled two bare sites to verify that background SOC concentrations remained relatively constant over time. Replicate, 12-cm cores were subdivided into 3-cm intervals. We measured %C on a Thermo Scientific Flash 2000 Organic Element Analyzer and calculated %C_{org} using element analysis of samples ashed at 500°C for six hours (cf. Fourqurean et al. 2014). We determined whether SOC concentrations increased between 2013 and 2016 by applying a paired, one-tailed *t*-test to average concentrations measured in the top 6-cm of the bed in R (R stats package version 3.4.2; R Core Team 2017).

We quantified meadow SOC stock change between 2013 and 2016 by mapping the meadow SOC pool in 2013 and 2016 in ArcGIS 10.2. Meadow-scale SOC stocks were quantified by interpolating the average 2013 and 2016 SOC enhancement at each site using the Kriging method in ArcGIS Geostatistical Analyst. We fit stable, circular, spherical, Gaussian, and exponential semivariogram models to each dataset and selected the SOC distribution maps with the lowest root mean square errors (Appendix I). We accounted for 2013-2016 meadow accretion by separately mapping the SOC distribution in the upper 2-cm of the 2016 bed and in the interval above the reference plane that corresponded with the 2013 bed (Greiner et al. 2013; chapter 3). The 2013 net SOC distribution was best modeled using a circular semivariogram. The net SOC distribution for the accreted 2-cm interval was best fit by an exponential semivariogram; the remainder of the 2016 bed above the reference plane was best fit by a Gaussian semivariogram.

5.2.3. Biomass CO_2 sequestration

Peak summer density averages approximately 616.7 shoots m^{-2} in South Bay, and biomass ranges from 0.26 to 0.781 g shoot^{-1} (McGlathery et al. 2012); however, canopy structure varies spatially and on seasonal timescales. Density is generally higher at older meadow sites (McGlathery et al. 2012), during the summer growing season (Thomas 2014), and in the meadow interior, away from the meadow edge (chapter 3).

Quantifying meadow-scale biomass stocks required information on this variability, which we acquired from previous studies (McGlathery et al. 2012; Thomas 2014; chapter 3) and by collecting additional biomass cores at sites in different locations relative to the meadow edge. We compared average AGB and BGB (g shoot^{-1}) at nine sites: five central-meadow sites, one north-central site (see chapter 4: #5 in Figure 4.1), one west-central site (#11 in Figure 4.1), and two sites near the edge (#3 and #6 in Figure 4.1). We also measured seasonal changes in live and dead BGB at the central meadow sites from June 2014-June 2016. BGB was collected using 15.2-cm diameter cores to a depth of 15 cm. Samples were sieved using a 1-mm mesh, separated the same day into live and dead fractions, and then dried to a constant weight at 60°C. The seasonal biomass data was averaged by site and then by month to generate seasonal averages, which were used to calculate average, annual standing stocks.

The VCS allows blue carbon projects to claim credit for average, annual, standing biomass but requires that projects conservatively exclude leaf litter and C_{org} exported from the project area (Emmer et al. 2015A). Seagrass AGB is sloughed off periodically during the spring and summer and at the end of the growing season (Thomas 2014). Shoot density also varies spatially (chapter 3). Estimating the average, annual AGB stock, therefore, requires accounting for spatial and temporal variability in canopy structure. We calculated the AGB stock by scaling the peak-summer shoot densities (shoots m^{-2}) measured at sites throughout the meadow in 2014 (presented in chapter 3) by the average, annual coverage as a fraction of the summer peak, 0.48 (Thomas 2014). Average, annual densities were multiplied by average biomass shoot^{-1} (n= 9 sites, this study) and by 37.1% C g^{-1} biomass (VCR-LTER 2012 Synoptic 5-site averages, sample n = 26: McGlathery 2017A). The resulting AGB values (C_{org} m^{-2}) were kriged in ArcGIS 10.2 Geostatistical Analyst. Interpolated values were summed to generate average, annual AGB stocks for the 2013 and 2016 meadow extents. Average live and dead BGB values (g m^{-2}) were multiplied by 33.8% C g^{-1} biomass (2012 Synoptic 5-site averages, sample n = 14: McGlathery 2017B) and scaled by the 2013 and 2016 meadow areas to generate C_{org} stocks.

5.2.4. GHG fluxes

We deployed transparent benthic chambers over vegetated and experimentally cleared bare plots located at the five central meadow sites (VCR-LTER Synoptic sites SB105, SB106, SB128, SB148, and SB152) to quantify the change in benthic CH_4 and N_2O fluxes attributable to *Z. marina* presence. Comparing trace gas fluxes from cleared, mid-meadow plots allowed us to control for differences in sediment composition and hydrodynamic regime at bare sites outside of the meadow, which could confound determination of a seagrass flux effect (Hansen and Reidenbach 2012; chapter 3). We cleared the 2m x 2m bare plots during spring 2015, installed plastic lawn edging to a depth of 8 cm to prevent seagrass rhizome re-colonization, and allowed plots to equilibrate for six months. Eight chambers were deployed at each site during each observation, four replicates over seagrass and four over bare sediment. Each chamber sat on the sediment surface, covering a 0.046 m^2 area and enclosing a 10.5 L volume. Replicate results were averaged to generate plot averages. Every deployment exactly bracketed low tide, such that gas accumulation time captured equal parts falling- and rising-tide. Deployment durations ranged from 1 to 5 hours. Trace gases were collected on multiple days per month in October 2015, April 2016, June 2016, July 2016, August 2016, and October 2016.

The gas that collected in each chamber was extracted with a syringe and injected into an exetainer filled with 12 ml N_2 and 0.2 ml 0.01M $ZnC_4H_6O_4$ to prevent microbial activity resulting from the syringe transfer. The total gas volume that collected within each chamber was noted and used to calculate the gas flux as a function of time and bed surface area. We also measured CH_4 and N_2O concentrations in replicate porewater samples collected at bare and vegetated sites in August (site n = 6) and October (site n = 4) 2016 by extracting 7 ml of porewater through piezometers at 3-cm intervals, from 1.5 cm down to 13.5 cm. The water samples were syringe injected into exetainers filled with 12 ml N_2 and fixed with 0.2 ml ZnCl. Exetainer samples were analyzed on a Varian 450-Gas Chromatograph with a Bruker GC/MS workstation at the Smithsonian Environmental Research Center. We determined sample CH_4 and N_2O concentrations using onsite standards and corrected for differences in atmospheric temperature and pressure during each GC analysis.

We tested for an effect of seagrass presence on CH_4 and N_2O fluxes using linear mixed effects analyses in R (Bates et al. 2015; R Core Team 2017). Replicates were averaged by site; site averages were grouped by season. Seagrass presence/absence and month were treated as fixed effects; individual sites were randomly selected. Tests were run on each GHG dataset using the lmer function (lme4 package version 1.1-14). We expected to find increased GHG fluxes attributable to seagrass presence, as well as a seagrass*month interaction effect. Data transformations were required for both the CH_4 and N_2O datasets, because they exhibited heteroscedasticity. We identified the best data transformation using the optim.boxcox function in R (boxcoxmix package version 0.14). The optimal transformation for the averaged CH_4 and N_2O data was λ = 0.133 (maximum log-likelihood = -77.608). Model *p*-values were obtained from likelihood ratio tests on the full model and a reduced model without the fixed effects. Average, annual seagrass and bare CH_4 and N_2O fluxes were determined by averaging seasonal fluxes. The difference represented the net fluxes attributable to seagrass presence.

5.2.5. Net GHG benefit accounting

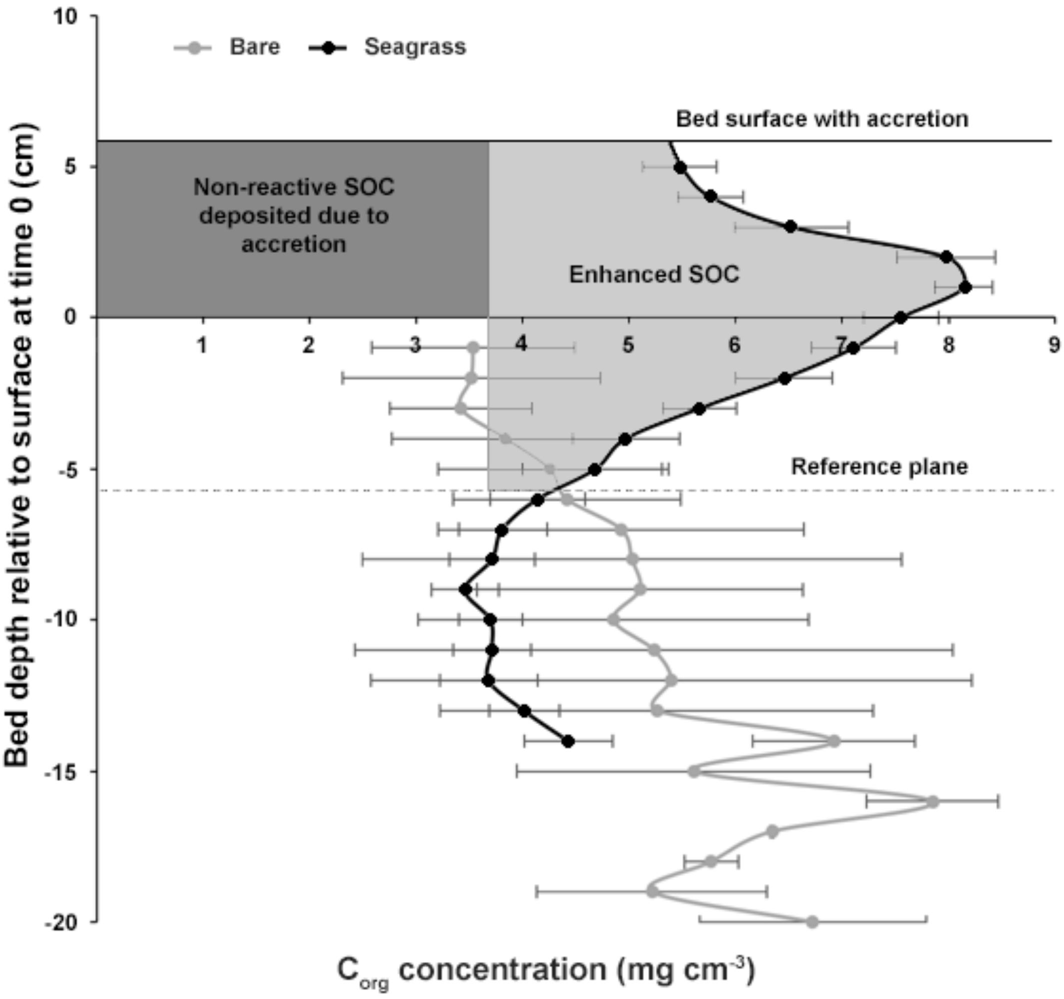

Figure 5.2. Seagrass meadow and background (i.e. bare site) SOC concentration comparison: SOC profiles were calibrated to account for meadow bed accretion, determined using ^{210}Pb (Greiner et al. 2013; adapted with permission). Error bars = standard error. The reference plane was 6 cm below the bed surface at bare sites and 12 cm in the meadow ca. 2012. We conservatively deducted the dark gray fraction (equivalent to the average bare SOC fraction above the reference plane) when calculating the seagrass-enhanced SOC stock, because this fraction may be allochthonous.

We applied the VCS accounting framework to calculate the net seagrass GHG benefit in 2013 and in 2016 (Emmer et al. 2015A), which required establishing the GHG benefit increase attributable to the project, relative to a baseline (i.e. without project) scenario. We calculated an average SOC concentration for the bed at the four bare sites, 3.67 ± 0.55 (SE) mg C_{org} cm^{-3}, and deducted this average from depth-equivalent SOC concentrations observed within the meadow in 2013 and in 2016 (6-12 cm below the sediment-water interface in 2013) to determine the net SOC increase above the reference plane—the meadow-enhanced SOC pool. The seagrass bed above the depth-calibrated bare site surface accumulated due to accretion (Figure 5.2), so the SOC within this interval (0-6 cm in 2013; 0-8 cm in 2016) may derive in part from allochthonous C_{org} deposition. Rather than deducting the proposed 50% 'allochthonous compensation factor' from the meadow SOC stock (Howard et al. 2014), we accounted for possibly-allochthonous, non-reactive C_{org} that could have been deposited in the baseline scenario by deducting the 0-6 cm bare site SOC average from this interval (Figure 5.2).

Total meadow CO_2-sequestration was calculated by summing the enhanced SOC, AGB and BGB (live and dead) stocks. We calculated this total GHG benefit for the meadow in 2013 and in 2016. Cumulative, enhanced CH_4 and N_2O emissions attributable to the South Bay meadow were estimated by multiplying the average enhanced (i.e. net) fluxes (g m^{-2} yr^{-1}) by meadow area over time. Cumulative, net GHG emissions in 2013 and 2016 were subtracted from the total GHG benefit in these years to determine the net benefit in each time period. Average, annual GPP was also scaled by meadow area over time to generate cumulative totals for 2013 and 2016, which we compared with the total and net GHG benefits in each year.

5.3. Results

Average SOC concentrations within the top 6-cm of the bed were significantly higher in 2016 than in 2013 ($p < 0.001$, df = 15, $t = -3.78$), confirming SOC accumulation. The meadow-wide, average SOC concentration increased to 6.1 mg C_{org} cm^{-3} in 2016 from 5.0 mg C_{org} cm^{-3} in 2013. We mapped the interpolated, enhanced SOC stock above the reference plane in both 2013 and in 2016 to compare stocks after accounting for bed accretion. Net SOC increased from 1,130 t C_{org} in 2013 to 2,010 t C_{org} in 2016. Approximately 280 t C_{org} of this increase accumulated due to sediment accretion: the top 2 cm of the 2016 bed. The remainder, 600 t C_{org}, accumulated within the bed. Dividing the 2013 and 2016 SOC stocks by accumulation time confirmed that the SOC sequestration rate has also increased. Meadow SOC sequestration averaged 346 t CO_2 yr^{-1} from 2001-2013; the 2013-2016 rate was 1070 t CO_2 yr^{-1}.

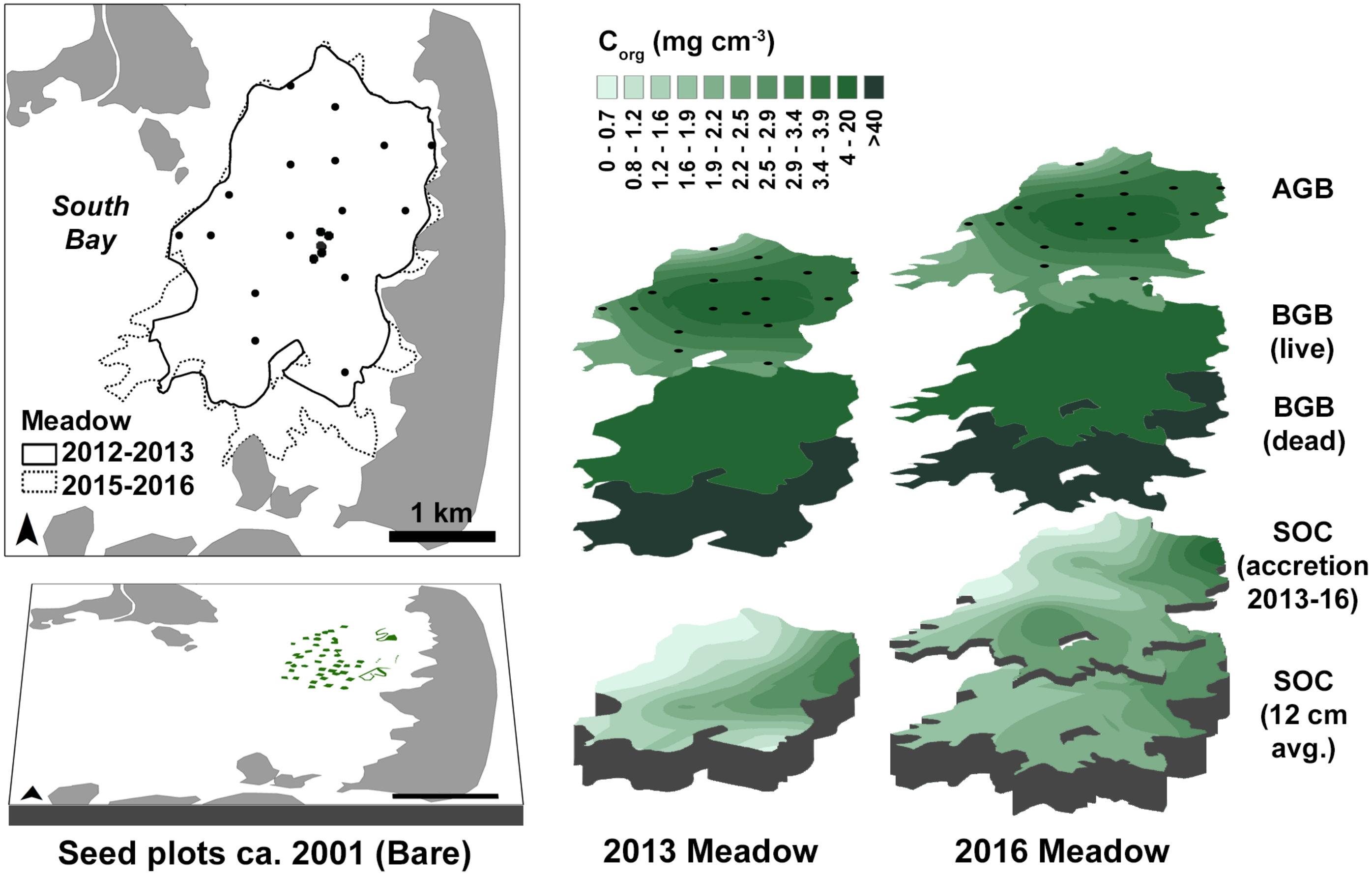

Figure 5.3. Sequestered GHG pools (AGB, BGB, and net SOC) in 2013 and in 2016: maps generated by kriging data measured at sample sites (n = 21: circles in inset map); Note that the SOC reference plane is 6 cm below the sediment-water interface in the original seed plots at the project start, 12 cm inside the 2013 meadow, and 14 cm inside the 2016 meadow.

AGB fluctuated seasonally from 331.1 g m^{-2} in August 2014 to 38.5 g m^{-2} in March 2015. The average annual value was 136.3 g m^{-2}, equivalent to approximately 50.4 g C_{org} m^{-2}. The average biomass $shoot^{-1}$ was 0.4 g. We modeled the total ABG stock as a function of the summer shoot density at sites (n = 16) using a Gaussian semivariogram (Figure 5.3). The resulting average, annual standing stock in 2013 sequestered an estimated 710 t CO_2; the 2016 stock increased to 810 t CO_2 due to meadow expansion. Live BGB increased from 35.5 g m^{-2} in the winter to 63.8 g m^{-2} in the summer. The annual average was 47.1 g m^{-2}. Dead BGB fluctuated from 110.013 in the summer to 128 g m^{-2} in the winter, resulting in an average, annual dead BGB quantity of 119 g m^{-2}. The unit area estimate for live BGB was 16.0 g C_{org} m^{-2}; the estimate for dead BGB was 40.4 g C_{org} m^{-2}. Multiplied by the respective meadow areas, the combined BGB stock sequestered 1,200 t CO_2 in 2013 and 1,520 t CO_2 in 2016.

Table 5.3. Sequestered CO_2 stocks (negative values), cumulative GHG emissions, and the net GHG benefit from the South Bay meadow in 2013 and in 2016; all values are Mt CO_2e.

	2001 Start (Bare)	2013 Gross	2013 Net	2016 Gross	2016 Net
Meadow area (km2)	0.096[a]	5.79	5.79	6.86	6.86
RH depth (cm)	6	12	12	14	14
AGB	0	-710	-710	-810	-810
Live BGB	0	-339	-339	-401	-401
Dead BGB	0	-857	-857	-1020	-1020
SOC	-78[b]	-13500	-4150	-20400	-7360
Total GHG Benefit	-78	-15400	-6060	-22600	-9590
CH4	0	385	335	611	532
N2O	1	420	264	667	420
Total Emissions		804	599	1160	952
Net GHG benefit			-5460		-8630

[a] area from Orth et al. (2006B)

[b] background (i.e. baseline) stock within seed plots

Meadow enhanced SOC, therefore, represented the single largest sequestered carbon pool in both 2013 and 2016, accounting for 68.5% of the total GHG benefit in 2013 and more than three-quarters of the total GHG benefit in 2016. Combined BGB (live + dead BGB) accounted for 14.7% of the total 2016 sequestered stock; average, annual AGB represented 8.4%. Enhanced SOC, AGB, and BGB sequestered a combined 6,060 t CO_2 in 2013 and 9,590 t CO_2 in 2016 (Table 5.3).

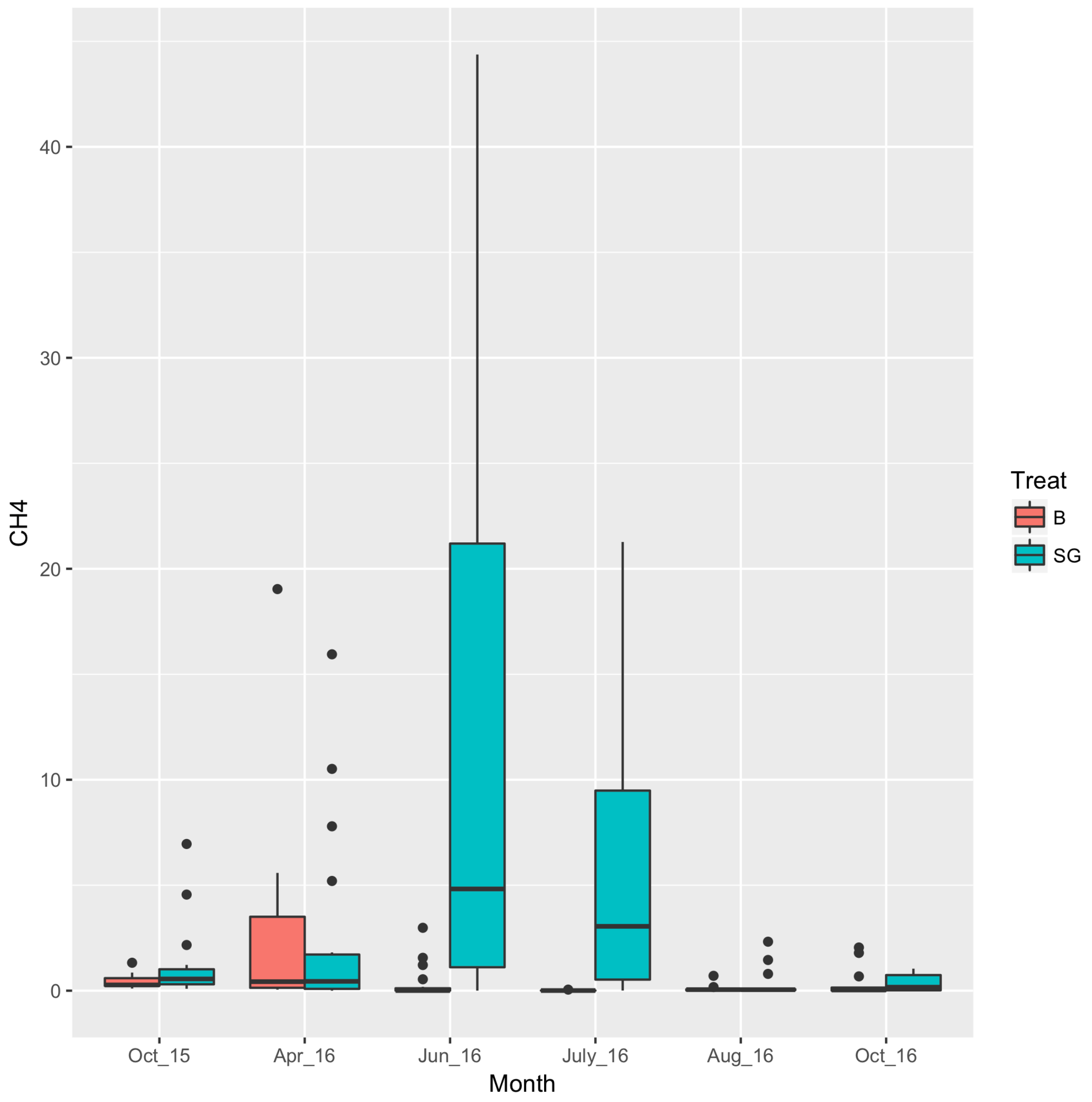

Figure 5.4A. CH_4 flux (μmol m^{-2} hr^{-1}) at sites by treatment (B: bare, SG: seagrass) over time (Oct. 2015-Oct. 2016; site n = 10).

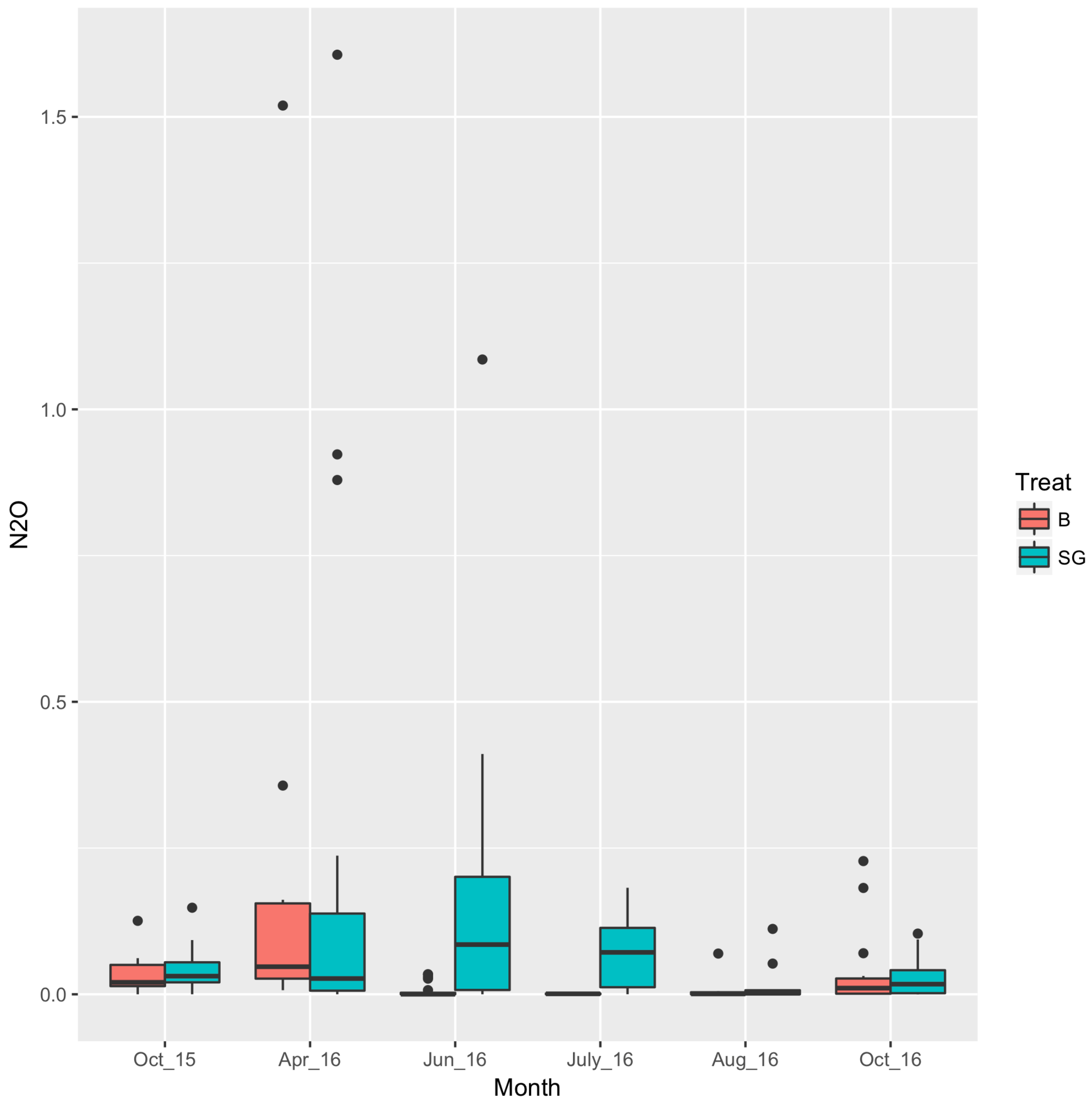

Figure 5.4B. N_2O flux (µmol m^{-2} hr^{-1}) at sites by treatment (B: bare, SG: seagrass) over time (Oct. 2015-Oct. 2016; site n = 10).

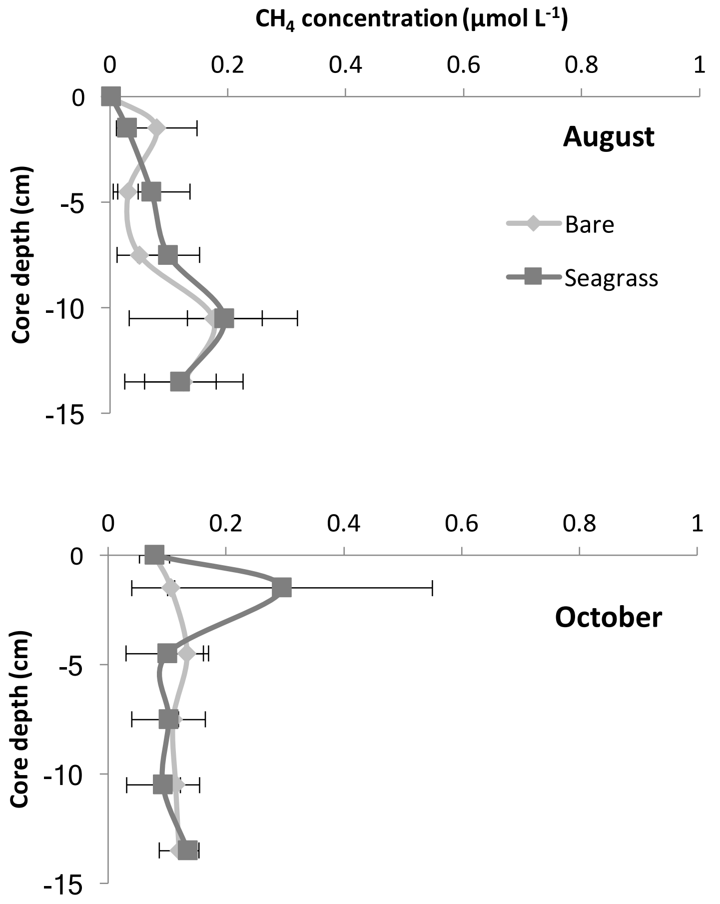

Figure 5.5. Porewater profile CH_4 concentrations, measured at bare and seagrass sites in August (site n = 6) and in October (site n = 4).

Seagrass presence significantly increased the flux of CH_4 ($\chi^2(1) = 13.1$, $p < 0.0003$) and N_2O ($\chi^2(1) = 8.46$, $p < 0.004$) (Figures 5.4A and 5.4B). The seagrass presence*month interaction effect was also significant ($\chi^2(10) = 36.4$, $p < 7.08e-5$), as was The N_2O interaction effect ($\chi^2(10) = 35.8$, $p < 9.09e-5$). The seagrass CH_4 flux was highest in June, 15.853 ± 6.949 (SE) µmol CH_4 m^{-2} hr^{-1} and lowest in August, 0.319 ± 0.220 (SE) µmol CH_4 m^{-2} hr^{-1}. The October 2016 flux was also low, 0.377 ± 0.062 (SE) µmol CH_4 m^{-2} hr^{-1}. The average bare site CH_4 flux ranged from 3.367 ± 1.594 (SE) µmol

CH_4 m^{-2} hr^{-1} in April to 0.012 ± 0.007 (SE) µmol CH_4 m^{-2} hr^{-1} in July. The average, annual enhanced CH_4 flux was 0.695 ± 0.459 (SE) g CH_4 m^{-2} yr^{-1}, given average, annual fluxes of 0.799 ± 0.528(SE) g CH_4 m^{-2} yr^{-1} from vegetated sites and 0.104 ± 0.074 (SE) g CH_4 m^{-2} yr^{-1} from bare sites (Figure 5.4A). However, porewater CH_4 concentrations were fairly similar at seagrass and bare sites in both August and October (Figure 5.5). The average seagrass site N_2O fluxes ranged from 0.664 ± 0.419 (SE) in April to 0.012 ± 0.010 (SE) µmol N_2O m^{-2} hr^{-1} in August. N_2O fluxes were lower at bare sites, ranging from 0.208 ± 0.137 (SE) in April to 0.001 ± 0.0004 (SE) µmol N_2O m^{-2} hr^{-1} in July (Figure 5.4B). The average, annual vegetated flux was 0.059 ± 0.043 (SE) g N_2O m^{-2} yr^{-1}; the average, annual bare flux was 0.022 ± 0.013 (SE) g N_2O m^{-2} yr^{-1}. The enhanced N_2O flux was, therefore, 0.037 ± 0.031 (SE) g N_2O m^{-2} yr^{-1}.

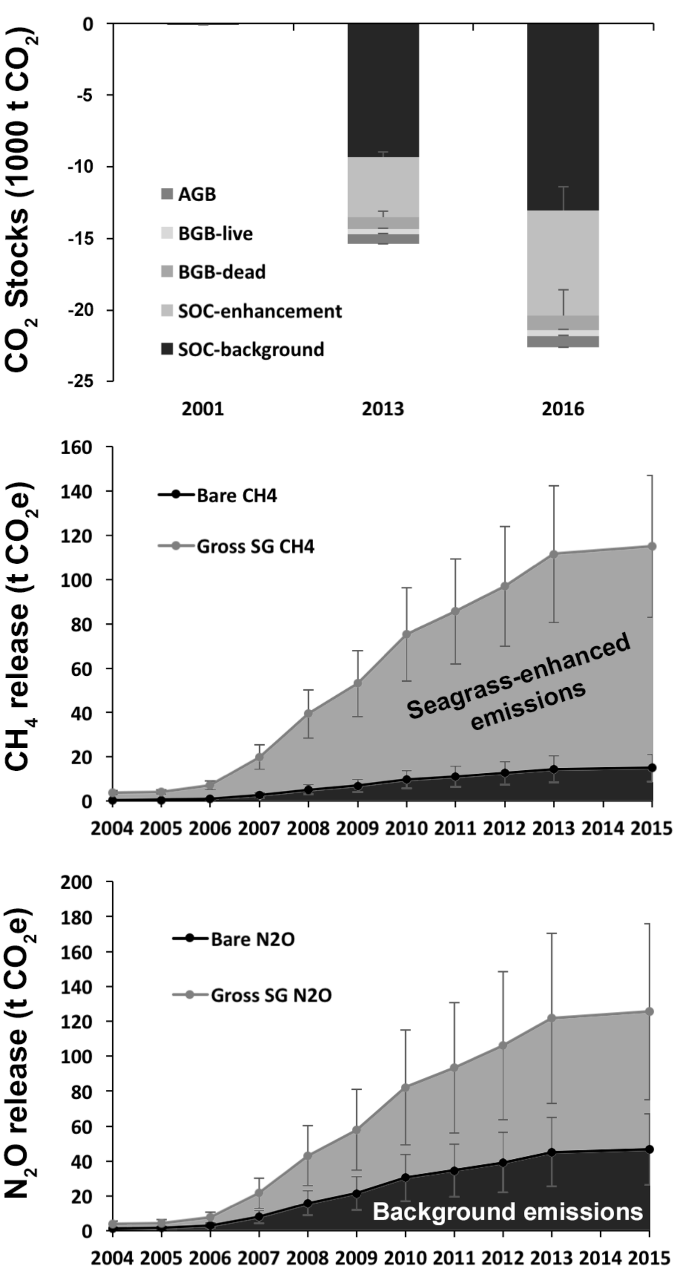

Figure 5.6. Cumulative GHG stocks and fluxes (MtCO$_2$e) as a function of restored meadow area over time (sequestration is negative); background (i.e. bare) quantities shown in dark gray; Error bars relate SE after accounting for error propagation; 100-yr global warming potential conversion factors from UNFCCC (2017): CH$_4$ = 21x, N$_2$O = 310x.

Scaling the trace GHG fluxes by meadow area over time and by their 100-year GWPs (UNFCCC 2017), meadow-enhanced CH_4 and N_2O fluxes released 532 and 420 t CO_2e between 2004-2016, respectively (Table 5.3; Figure 5.6). Seagrass meadow restoration, nevertheless, generates a net GHG benefit, which increased in the restored South Bay *Z. marina* meadow from 0.21 t C ha^{-1} yr^{-1} between 2001-2013 to 0.42 t C ha^{-1} yr^{-1} from 2013-2016.

5.4. Discussion

5.4.1. Seagrass-effects on trace GHG release

Seagrass presence increases CH_4 and N_2O production, but this increased trace GHG release had a relatively small effect on the net GHG benefit. The cumulative CH_4 flux was not, technically, *de minimis*, because the enhanced CH_4 emissions reduced the total GHG benefit by 5.5% in 2013 and 5.6% in 2016. In comparison, the enhanced N_2O flux was below the *de minimis* threshold in both years (4.7% in 2013 and 4.4% in 2016), so N_2O could be excluded from the net benefit calculation under the VCS accounting guidelines (Emmer et al. 2015A; 2015B). However, both trace gas fluxes exceeded the conservative general default factors that Emmer et al. (2015A) allow for net benefit accounting: 0.56 g CH_4 m^{-2} yr^{-1} in salinities >20 ppt and 0.016 g N_2O m^{-2} yr^{-1} (Section 8.1.4.3.4). These general default factors should, therefore, be revised upward. We advise other seagrass blue carbon studies to measure both trace gases directly, until a sufficient number of additional studies suggest conservative, generally-applicable release rates for seagrass GHG accounting.

5.4.2. Identifying the net GHG benefit from seagrass restoration

The net CO_2 sequestration rate that we observed in this study, 0.42 t C ha^{-1} yr^{-1} supports widespread use of the IPCC (2014) default factor for seagrass restoration, 0.43 t C ha^{-1} yr^{-1}. The similarity in the rates is noteworthy, given that our rate derives from observed stock changes in a *Z. marina* system in Virginia; whereas, the IPCC (2014) value was based on two *Posidonia oceanica* systems in the Mediterranean Sea (Mateo and Romero 1997; Serrano et al. 2012). However, the IPCC value is not, technically, conservative for estimating the restoration benefit in our system, especially over the first decade. We also possibly overestimated the seagrass benefit in both 2013 and 2016 by assuming uniform sediment accretion throughout the meadow and scaling average SOC concentrations by the resulting sediment volumes. Actual bed accretion was likely lower near the meadow-bare subtidal edge, as evidenced by the meadow grain size distribution and reported Reynolds stress (Hansen and Reidenbach 2012; chapter 3). In addition, we excluded possible carbonate cycling effects on the net GHG benefit in our system. Recent studies point out that CO_2 evasion associated with $CaCO_3$ buried in seagrass sediment should also be deducted from the seagrass GHG benefit (Howard et al. 2017B; Macreadie et al. 2017B). We observed negligible sediment inorganic carbon. However, direct plant uptake of bicarbonate would also increase pCO_2, potentially resulting in a CO_2 flux back to the atmosphere. The seagrass plants in the VCS likely rely on dissolved CO_2 uptake, given that the meadow occurs in a shallow waterbody with a large surface area to water volume ratio. We, nevertheless, agree that carbonate cycle effects need further study.

Our results indicate that the restored *Z. marina* meadow in South Bay, VA, sequesters approximately one quarter to one third of GPP. The total, sequestered, CO_2 stock in 2013 in the South Bay meadow represented 26.5% of total GPP within the meadow produced between 2001-2013, estimated by averaging available GPP data from bare, 5-, and 11-year old sites within this system (Hume et al. 2011; Rheuban 2013; Rheuban et al. 2014). The 2016 stock accounted for 26.4% of total GPP by 2016. If we use bare site GPP as the system baseline and instead calculate cumulative, meadow-enhanced GPP, the 2013 and 2016 SOC stocks accounted for 30.8% and 30.7% of meadow GPP, respectively. These results may be generally applicable for estimating the net GHG benefit in other systems from published GPP data. However, we recognize that *Zostera* spp. systems appear to be metabolically balanced (Rheuban et al. 2014; Ferguson et al. 2017); whereas, other meadows appear net autotrophic (Duarte et al. 2010 Data Set S1). Researchers should investigate whether other seagrass systems and/or species sequester a similar percentage of GPP.

More work is also necessary before we can determine whether our net GHG benefit result is generally applicable to seagrass systems, because we have insufficient data from other systems for a net GHG benefit comparison. Most seagrass studies reporting seagrass carbon burial rates do not report burial rates at bare control sites for a baseline assessment or differentiate between autochthonous and allochthonous SOC fractions (e.g. Röhr et al. 2016; Rozaimi et al. 2017). The net benefit presented in Table 5.3 conservatively excludes allochthonous SOC in the accreted part of the bed, as required by the VCS (CEC 2014; Emmer et al. 2015A). Had we included this SOC as a project benefit, the apparent net benefit would have been 10.1K t CO_2e in 2013 and 17.2K t CO_2e in 2016. We agree that the allochthonous SOC fraction should be conservatively excluded as a general rule (CEC 2014; Johannessen and Macdonald 2016), but this approach halves the net benefit result in our study system.

We recommend that studies employ the SOC stock change method for calculating the seagrass net GHG benefit (Figure 5.2), both because of issues with long-term SOC remineralization that affect burial rates and to account for BGB biomass accumulation (Johannessen and Macdonald 2016; chapter 2). The 2013-2016 SOC stock increase exceeded our expectation based on a scaled, surface burial flux calculated for this system (Greiner et al. 2013), 874 t C_{org} versus 755 t C_{org}, because of SOC accumulation below the accreted surface interval. However, we also observed SOC loss within the bed at particular sites, which affected the 2016 SOC spatial distribution (Figure 5.3). Disturbance events will likely affect long-term (i.e. decadal) SOC accumulation rates by periodically diminishing SOC stock accumulation.

5.4.3. Offset-credit finance as an incentive for seagrass restoration:

Had the VCS framework existed in 2001, and had the VCR eelgrass restoration applied for offset-credits, the current offset-credit benefit from the 6.9 km^2 meadow project area after 15 years would equal approximately 8,630 credits (1 credit = 1 tCO_2e; note that Emmer et al. 2015A does not allocate credits to existing meadows). This amount is currently below the standard viability threshold for offset projects. According to Kollmuss et al. (2010), investors do not typically consider offset projects viable unless they sequester at least 50K tCO_2e. The VCS offset allocation for this project would actually be slightly lower than 8.6K credits, because the VCS also requires projects to deduct CO_2 emissions from project activities (i.e. fossil fuel use to travel to and from the restoration site, etc.) and set aside credits in a 'buffer pool' proportional to the benefit non-permanence risk (Emmer et al. 2015A). The meadow sequestration rate may continue to increase, absent significant bed disturbance. However, at this current sequestration rate, it will take the current meadow area another 140 years to reach the viability threshold. VCS offset projects typically operate over a 30-year window (chapter 2). Smaller restoration efforts, transient meadow patches, and meadows subject to periodic disturbance are unlikely to generate more VCS-certified offset-credits on an equal area basis.

Voluntary offset-credits are, therefore, unlikely to completely finance additional seagrass restoration at the average offset-credit price on the voluntary market in 2016, \$3.02 per tCO_2e (Forest Trends 2017). Compared with the *Z. marina* restoration in the VCR, other seagrass restoration projects cost more but achieve less. Between 1999-2010, 1,714 ha were restored in the VCR at a cost of \$2M (Reynolds et al. 2016). The VCR unit cost, \$1.2K/ha, is lower than the range for other projects: \$1.9K to \$4M/ha (Paling et al. 2009). The South Bay meadow component of the VCR restoration cost was approximately \$823K. At the average 2016 voluntary offset price, offset-credits awarded for the benefit realized to date would finance approximately 3% of the South Bay restoration cost (note that the cost was incurred between 2001-2005 and this calculation ignores both net present value discounting and cost adjustment for inflation). This result is partly attributable to the recent fall in the average, voluntary offset price, down from approximately \$5.9 per tCO_2e in 2012 (Forest Trends 2013). A voluntary offset price closer to \$36, the EPA's 2015 social cost of carbon (EPA 2017: 2007 USD at a 3% average discount rate), would reimburse project managers for 37.8% of the restoration expense. Financing a seagrass restoration project with a unit cost equivalent to this South Bay *Z. marina* restoration would require a voluntary offset price greater than \$95. Note, however, that credits are awarded *ex post*, so projects would need to discount the expected benefit over the latency period.

5.5. Conclusions

Seagrass restoration increases annual CH_4 and N_2O production, but these trace gas fluxes do not substantially diminish the net GHG benefit provided by seagrass CO_2 sequestration in SOC and standing biomass. The large, mature, restored *Z. marina* meadow in South Bay, VA, is now sequestering CO_2 at an accelerating rate, far surpassing CO_2e-adjusted trace GHG emissions over time. However, the net GHG benefit from this system suggests that the financial benefit from monetizing offset-credits awarded to seagrass restoration projects will likely be small relative to restoration expenses. This result from the world's largest, most successful seagrass restoration effort is due in part to annual export of aboveground biomass, and to the current SOC burial rate, but also to the depressed value of voluntary offset-credits. A significant increase in demand for voluntary offset-credits would be necessary to finance seagrass restoration projects through the sale of offset-credits. We also note that individual seagrass restoration efforts are unlikely to generate the offset economies of scale necessary to attract investors used to financing large, terrestrial reforestation projects, because many seagrass meadows have a limited spatial extent. Managers will likely need to bundle seagrass restoration projects before applying for credits. Offset-credits can, however, provide a marginal incentive for seagrass restoration, assuming enhanced carbon stocks remain sequestered over decadal timescales. Additional, long-term stock change studies are needed to verify anticipated SOC stock increases. Seagrass meadows remain critically-important ecosystems that provide a variety of ecosystem services. Rather than relying primarily on seagrass carbon sequestration to motivate meadow conservation and restoration efforts, coastal managers should think holistically about the values that seagrass systems provide, including co-benefits associated with fishery habitat provisioning, water clarity, sediment stabilization, nutrient cycling, ocean acidification buffering, and other beneficial services.

Acknowledgements

I would like to thank my collaborators: Lillian R. Aoki, Karen J. McGlathery, Amélie Berger, Peter Berg, Marie-Lise Delgard, and Lindsay L. Edwards. Abby Lunstrum, Amy Bartenfelder, Pat Megonigal, Drew Peresta, Kyle Derby, Aaron Mills, and Max Castorani also contributed to this study. Funding for this study was provided by VA Sea Grant, the University of Virginia Dept. of Environmental Sciences, and by the Jefferson Scholars Foundation.

Chapter 6. Sustained restoration effort is necessary to maximize restored seagrass extent

Abstract

Multiple anthropogenic threats are driving seagrass meadow collapse on a global scale. Seagrass restoration can restore seagrass meadows and lost ecosystem services, including habitat for commercial fish and shellfish stocks; however, restoration projects are generally expensive and many are unsuccessful. Site selection remains a key challenge, even for *Zostera marina* (eelgrass) and other common restoration species. Species distribution models and information on established eelgrass occurrences can be used to identify suitable areas for additional restoration. The eelgrass restoration in the Virginia Coast Reserve provides a unique opportunity to improve our understanding of the eelgrass environmental niche and evaluate whether sustained restoration effort is required to maximize restored meadow area. We analyzed survival and failure data from restoration plots and from natural recruitment sites, which helped us constrain the *Z. marina* niche with respect to several environmental predictors: water residence time, fetch length, water temperature, bathymetry, and sediment grain size. We applied machine learning methods to model the total eelgrass habitable area within the Virginia coastal bays. The total habitable area identified using recruitment site data is smaller than that determined using the restoration plot data, approximately 34 km^2 compared with 107 km^2. This result indicates that the restored meadows will continue to expand naturally, beyond their current, 25 km^2 extent, but that additional restoration effort will be necessary to maximize eelgrass coverage within this system. Coastal managers can, therefore, select the appropriate level of restoration effort, depending on management objectives, and calibrate restoration extent for subtidal spatial planning.

6.1. Introduction

Many seagrass species are ecosystem engineers that provide a range of ecosystem services by establishing dense, submerged meadows (Schmidt et al. 2011). In addition to providing habitat for fish and shellfish (Mizerek et al. 2011; Oreska et al. 2017), seagrasses stabilize coastal sediment (de Boer 2007), sequester carbon (Fourqurean et al. 2012; Greiner et al. 2013; Howard et al. 2017A), and filter nutrients (McGlathery et al. 2007). However, global meadow area is rapidly declining (Waycott et al. 2009), because of development pressures, direct disturbance, eutrophication, and other anthropogenic impacts (Orth et al. 2006A; Grech et al. 2012). Many seagrass systems are bistable, and, therefore, susceptible to sudden meadow collapse following disturbance (Carr et al. 2010). Meadow disappearance results in increased CO_2 emissions, due to the remineralization of buried organic carbon (Marbà et al. 2015), and the loss of economically important fish and shellfish species that depend on seagrass habitats, such as the bay scallop (*Argopecten irradians*) (Oreska et al. 2017).

Seagrass restoration efforts seek to reverse meadow declines and restore lost ecosystem services (Suding 2011; van Katwijk et al. 2016). These projects are often expensive, time-consuming, and, in many cases, unsuccessful (Paling et al. 2009; Fonseca 2011). Restoration activities range from sediment loading abatement for improved water quality to broadcast seeding and manual planting (Paling et al. 2009; ESA 2016). Manual restoration efforts, particularly transplanting, can be labor intensive and expensive, with restoration costs >> \$200K km^{-2} (Paling et al. 2009). High restoration costs can be a barrier to prospective habitat restoration projects, particularly in coastal areas with limited resources and/or competing management objectives. Coastal managers interested in return on investment must minimize the risk of restoration project failure. Restoration site selection is, therefore, an important consideration for prospective restoration project managers (van Katwijk et al. 2009; Fonseca 2011).

In the past, efforts to inform restoration site selection have been qualitative or semi-quantitative (e.g. Short et al. 2002). Species distribution models (SDMs) can help predict seagrass habitable areas to guide restoration site selection (Adams et al. 2015). Ecologists have used geographical data and a variety of SDMs to predict species distributions in diverse terrestrial and aquatic settings (Guisan and Zimmerman 2000; Elith and Leathwick 2009). Common SDM techniques range from regression-based approaches (i.e. generalized linear models, GLM) to Bayesian and machine-learning models (Valle et al. 2013). Despite long-standing interest, proponents have noted challenges with species distribution modeling, some of which stem from relying primarily on observed occurrences to model potential distributions (Vaughan and Ormerod 2005). SDM approaches have, nevertheless, been applied to forecast potential seagrass distributions (e.g. Grech and Coles 2010; Valle et al. 2013; Chefaoui et al. 2016). Valle et al. (2013) note that machine learning methods appear to outperform regression-based techniques for this purpose (e.g. Downie et al. 2013). However, environmental preference data derived from existing populations may be too limited to predict the entire habitable area that may be conducive for restoration (e.g. Downie et al. 2013; Valle et al. 2013). Accurate modeling requires information on the full ranges of a species' environmental tolerances (Adams et al. 2015), which is not always available.

Several recent studies use SDMs to map potential eelgrass (*Zostera* spp.) distributions at both regional and continental scales; however, these studies rely primarily on eelgrass presence data from long-established populations to make distribution predictions (Valle et al. 2011; 2013; 2014) or define the niche for a geographically disparate part of the eelgrass range (Downie et al. 2013). The *Zostera marina* (eelgrass) restoration along the Atlantic side of the southern Delmarva Peninsula provides a unique opportunity for describing the eelgrass environmental niche and assessing the utility of SDMs for seagrass distribution prediction. This case constitutes the most successful seagrass restoration project on record (cf. Orth and McGlathery 2012 and other studies in the *Marine Ecology Progress Series* v448 theme section). The successful reestablishment of *Z. marina* in restoration plots created a seed source for additional, natural meadow expansion, which contributed significantly to the project's overall success. In addition to survival data from the restoration plots, the observed pattern of eelgrass dispersal within this system allows us to define the eelgrass environmental niche with respect to recruitment sites. The realized niche for natural recruits may be different from the niche indicated by the restoration plots, which benefitted from an intensive broadcast seeding effort. Data on eelgrass restoration and recruitment failure within the Virginia coastal bays potentially allows us to better define the limits of the eelgrass niche with respect to multiple environmental parameters that may prove useful for guiding eelgrass restoration in temperate regions.

This study identifies the environmental parameters that best predict eelgrass survival in restoration seed plots and investigates whether the same parameters also explain the distribution and survival of naturally-dispersing recruits. We hypothesize that the environmental niche for natural recruits is more restricted than the niche observed at restoration plots. In which case, additional, restoration effort will be necessary to significantly expand eelgrass coverage within the Virginia coastal bays and similar systems. If survival data from both actively restored and natural-dispersing plants instead indicate the same eelgrass niche, eelgrass will likely recolonize all potentially habitable areas within this system over time without additional restoration effort. High natural dispersal capacity would ultimately reduce restoration cost over time as a function of total restored area. However, additional natural dispersal within this system may also lead to increased conflict with shellfish aquaculture. Spatial competition between expanding habitat restoration areas and private shellfish leases is one of the region's defining spatial management issues (Luckenbach and Ross 2011). We, therefore, consider whether the model-predicted eelgrass habitable area includes areas reserved for other uses.

6.2. Methods

6.2.1. Study area

The southern coastal bays along the Delmarva Peninsula are studied by a Long-Term Ecological Research site, the Virginia Coast Reserve (VCR-LTER). These bays occur within a marsh-lagoon-barrier islands system, where inlets between the barrier islands allow ocean water exchange (McGlathery et al. 2013). This system has two broadly distinct, subtidal steady states: eelgrass meadow coverage and bare and/or macroalgae dominated flats (Carr et al. 2010). Most of the bays are relatively shallow (1-2 m MSL) and oligotrophic, with broad subtidal flats drained by channels (McGlathery et al. 2001; 2013). Low nutrient loading and high water quality distinguishes the Virginia coastal bays from the Chesapeake Bay, where *Z. marina* restoration efforts have not been as successful (Orth et al. 2010). The mean tidal range is approximately 1.2 m; tides enter and exit the bays on a twice daily cycle (Fagherazzi and Wiberg 2009). Bay depth is relatively constant within individual bays (Richardson et al. 2014), and the salinity in the outer bays approaches full marine salinity.

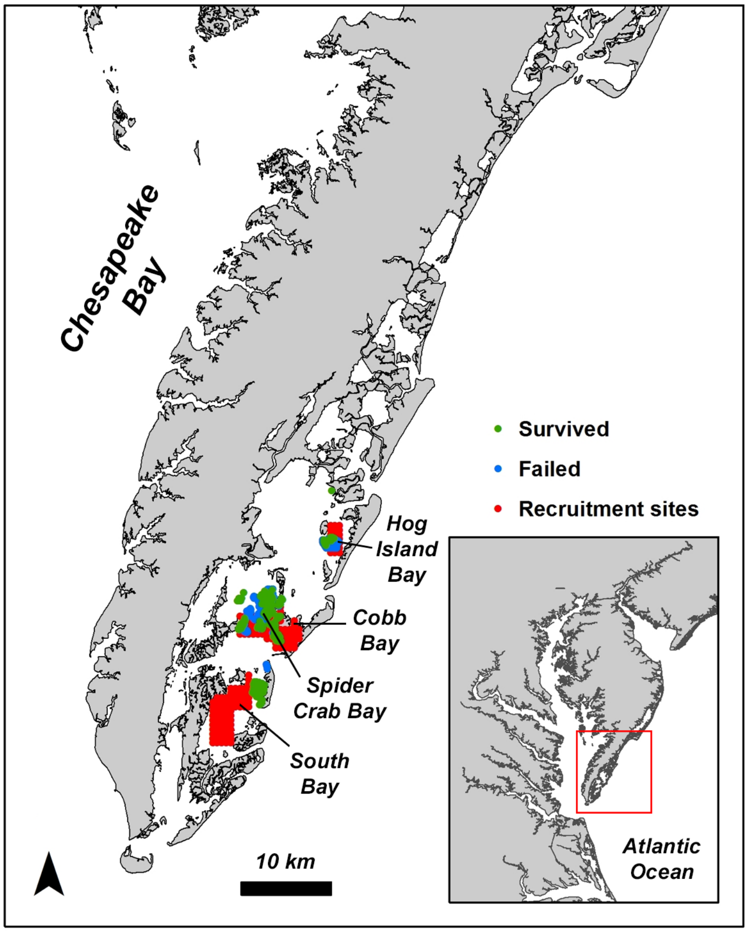

Figure 6.1. Study area location relative to the Chesapeake Bay region; Restored sites coded by survival status; Recruitment sites shown in red.

The VCR-LTER hosted *Z. marina* meadows prior to the 1932 North Atlantic Eelgrass Pandemic, although the historical extent and distribution of these meadows remains uncertain (Cottam 1935; Oreska et al. 2017). Area watermen began harvesting hard clams (*Mercenaria mercenaria*) in large numbers after the 1932 meadow collapse resulted in the disappearance of the local bay scallop (*Argopecten irradians*) industry (Oreska et al. 2017). *M. mercenaria* are now cultured in clam beds located within subtidal areas originally leased by the Commonwealth of Virginia to watermen for oyster (*Crassostrea virginica*) planting. New shellfish leases can only be obtained in unclaimed bottom areas outside of the 'Baylor Grounds,' extensive set-aside areas designated in the 1890s to conserve the remaining natural oyster reefs (Baylor 1893). The eelgrass restoration effort began in the late 1990s in South Bay and Magothy Bay, and restoration plot coalescence and expansion has since resulted in large meadows in four bays: South, Cobb, Spider Crab and Hog Island Bays (Figure 6.1; Orth et al. 2006B; Orth et al. 2012). The restoration effort entailed broadcasting almost 40M seeds in those four bays between 1999-2010 (Orth et al. 2012). However, most of the restored meadow area is due to natural seed dispersal. Restoration plots covered < 0.5 km^2 in 2005 (Orth et al. 2012). By 2012, restored meadows covered more than 17 km^2 (Orth and McGlathery 2012; Orth et al. 2016), and this area now exceeds 25 km^2. The Virginia Marine Resource Commission recently allocated new restoration set-asides to avoid use conflicts related to this natural eelgrass expansion (Orth et al. 2016). Virginia regulations prevent clearing existing submerged aquatic vegetation, except in cases where plants invade existing leases (Commonwealth of Virginia 2000). The hard clam aquaculture industry, therefore, equates continued eelgrass expansion with lost option value from forgone lease opportunities (Luckenbach and Ross 2011).

6.2.2. Environmental data

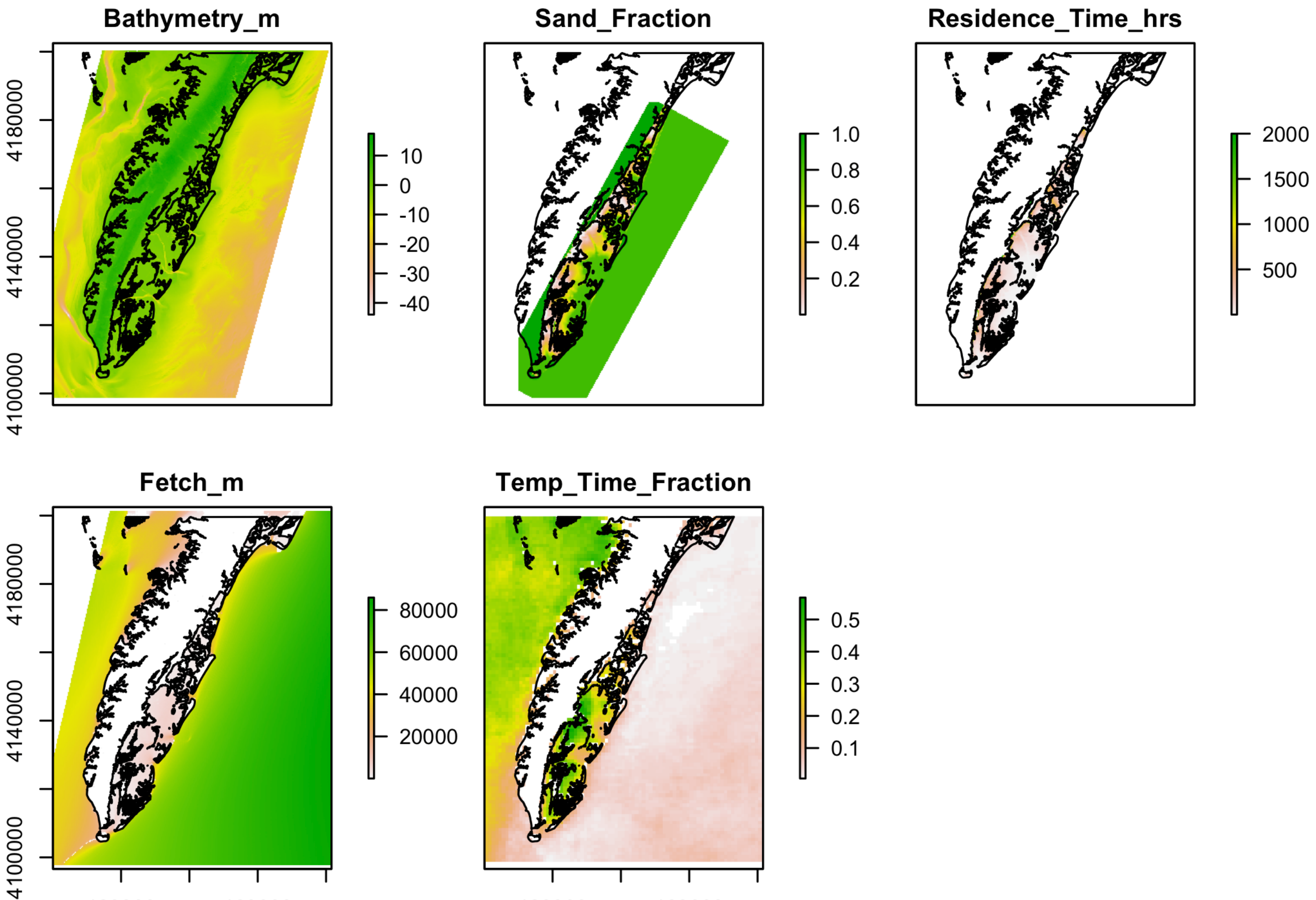

Figure 6.2. Environmental parameters used to define the *Z. marina* niche.

We evaluated the influence of five environmental parameters on the eelgrass distribution in the VCR (Figure 6.2): bathymetry (m), grain size (sand fraction), residence time (hrs), fetch length (m), and temperature (% time in JJA above 28°C). According to Fonseca and Uhrin (2009), these factors generally define the eelgrass niche. Water depth reduces light availability, a factor that affects regional eelgrass persistence (Moore and Jarvis 2008; York et al. 2013). According to Carr et al. (2012A), the habitable depth range for eelgrass in this system extends to at least 1.6 m and potentially 1.8 m, depending on meadow-suspended sediment feedbacks (Carr et al. 2010). Bathymetric data were obtained from Richardson et al. (2014). VCR-wide grain size and residence time distributions were obtained from Safak et al. (2015) and Wiberg et al. (2015). Wiberg et al. (2015) modeled the grain size distribution throughout the system using empirical observations along transects. This sediment distribution allowed Wiberg et al. (2015) to calculate VCR-wide root-mean-square velocities. Safak et al. (2015) calculated VCR-wide residence times as a function of these root-mean-square velocities and site distance from the nearest inlet. Reported residence times relate the time required for a particle to exit the VCR bay system from a given point (Lagrangian particle tracking: Safak et al. 2015).

Fetch length affects the light environment in the VCR coastal bays by driving sediment resuspension (Lawson et al. 2007). Wave exposure may, therefore, represent an important control on regional seagrass distributions (Fonseca and Bell 1998; Grech and Coles 2000). Fetch length (m) was calculated for locations throughout the VCR system using the USGS Fetch Model in the ArcGIS 10.2 Waves Toolbox (available from:

http://www.umesc.usgs.gov/management/dss/wind_fetch_wave_models.html, downloaded 11 Jan 2016). This model employed the SPM method for calculating average fetch length (Rohweder et al. 2008). The model intersected radiating lines for each cell within the study area with a shapefile of observed 2015 land surface areas, digitized in ArcGIS 10.2 from aerial imagery compiled by the VIMS SAV Monitoring Program (VIMS 2016).

The eelgrass distribution at this southern end of its North Atlantic range is also controlled by warm water exposure during summer months, especially prolonged exposure to temperatures in excess of approximately 28°C (Moore and Jarvis 2008; Carr et al. 2012B; Lefcheck et al. 2017). Regional sea surface temperature (SST) data was obtained for the Delmarva region from the Rutgers University Coastal Ocean Observation Laboratory database, a compilation of Advanced Very High Resolution Radiometer data collected by the NOAA-15, 17, and 18 satellites (https://marine.rutgers.edu/cool/sat_data/, accessed 8 September 2015). We compiled SST data observed during summer months (JJA) in recent years (2010-2013) to assess spatial variability in temperature. The spatial temperature data used in the SDM analyses represented percent time above 28°C during JJA in 2010, which revealed considerable spatial variability in high temperature exposure within and among the VCR coastal bays.

Valle et al. (2013) determined that spatial differences in salinity and sea floor slope have marginal importance for predicting *Z. marina* occurrence, especially compared with current velocity, wave exposure, and bathymetry. The former variables were not modeled directly in this study, in part, because the coastal bay system is characterized by broad, subtidal flats and high salinities.

6.2.3. Success/failure data

We evaluated eelgrass presence/absence in restoration plots that were actively seeded by the Virginia Institute of Marine Science (VIMS) (plot n = 490). Restoration locations within the four VCR bays were chosen systematically and included both areas deemed favorable for eelgrass growth and marginal locations for restoration trials. Individual plots were located haphazardly within these areas. Eelgrass survival was assessed by VIMS and by coding presence/absence in all plots for all years since the restoration start (2001-2015) using an annual aerial photograph database (VIMS 2016). Aerial images had a spatial resolution of 24 cm, which permitted identification of individual plants (Orth et al. 2016). At most sites where *Z. marina* became established, eelgrass was continually present after the first observation. In the following analyses, eelgrass survival refers to presence in 2015, the most recent year for which we had system-wide observation data.

In addition to these restoration plots, possible recruitment sites were arranged systematically within the four VCR bays (n = 173), and eelgrass presence/absence was evaluated at these sites over time using the aerial images. These sites were spaced 500 m apart in a grid fashion to provide broad coverage in areas subject to natural seed dispersal (recruitment sites were not located over land areas). Hydrodynamics within the VCR potentially disperse eelgrass seeds throughout the system. We, therefore, assumed that all of the recruitment sites receive seed propagules (e.g. Robinson et al.

2011). However, seed densities are highest within approximately 300-400 m of their source in this system (Manley et al. 2015). All of the recruitment sites were located within bays containing restoration plots and within the observed extent of recruitment patches.

6.2.4. Analyses

The environmental parameter layers were combined into a raster stack using the R raster package (version 2.6-7); environmental values were subsequently extracted by site. Test and training data were randomly selected from eelgrass presence and absence datasets (restoration plots and recruitment sites) using the kfold function in the dismo package (version 1.1-12). Analyses were run on the restoration plot and recruitment datasets separately and on the combined dataset (n = 663 sites). The SDM analysis spatial resolution was 30 m (note, however, that the SST data resolution = 1 km^2).

We employed boosted-regression tree (BRT) and random forest (RF) machine learning methods to generate eelgrass occurrence prediction maps (Hijmans and Elith 2017). BRT and RF machine learning techniques generate more robust SDMs than other methods, including GLM and other regression-based approaches (Valle et al. 2013). We ran a Gaussian GLM on the data for comparison. All SDM techniques were run in R (version 3.4.2, R Core Team). BRT models were run using the gbm.step function in the dismo package (version 1.1-4). Elith and Leathwick (2017) provide an overview of BRT modeling for SDM purposes. We ran RF models using the randomForest function in the randomForest package (version 4.6-12). See Ciss (2015) for more information on applying RF models.

The probability of eelgrass presence was mapped by fitting BRT and RF model object outputs to the VCR environmental parameter dataset. BRT model objects were generated using a tree complexity = 5, a learning rate of 0.01, and a bag function of 0.5. Model interactions were evaluated using the gbm.interactions function and plotted using the gbm.precspec function (dismo package). Model cross-validation was performed by applying the evaluate function (dismo package) to the test data (both presence and absence). Predicted presence/absence was then determined for the RF output using the threshold function (dismo package), according to Hijmans and Elith (2017). This threshold was calculated using the specificity-sensitivity sum maximization approach (Liu et al. 2005), which sums the confusion matrix true positive rate (TPR) and true negative rate (TNR) for the test data. Separate analyses were run on the VIMS restoration site data (restored dataset) and on the natural recruitment sites (recruit dataset) to determine whether the modeled habitable area differs due to restoration effort. We also ran the models on the combined data (all dataset). We assessed model accuracy by comparing calculated Area Under the Receiver Operator Curve values (AUC: cf. Valle et al. 2013). BRT and RF model results were averaged to generate a single predicted output for the restored, recruit, and all data analyses.

6.2.5. Comparisons with shellfish grounds

We compared the predicted eelgrass habitable area output with the distribution of modern shellfish leases within the VCR (obtained from N. Meade, VA DEQ CZM, 12

November 2014) and with other management areas. Shapefiles for the Baylor Grounds were obtained from the VIMS Center for Coastal Resource Management (http://ccrm.vims.edu/gis_data_maps/interactive_maps/blueinfrastructure/disclaimer_bi.html, accessed 22 May 2014). The locations of the former Public Scallop Grounds were obtained from Oreska et al. (2017). These areas were established for scallop harvesting between 1926-1927, prior to the original meadow disappearance, and removed in 1986 (Oreska et al. 2017).

6.3. Results

6.3.1. Observed environmental parameter ranges at restored plots and recruitment sites

Table 6.1. Environmental parameter values at sites: restoration plot and recruitment sites grouped by eelgrass success or failure in 2015 (Average values ± SE).

			Bathymetry (m)	**Grain size** (sand fraction)	**Residence time** (hrs)	**Fetch** (m)	**Temperature** (% time >28° C)
Restored	Survived (n = 284)	Min	-2.38	0.42	0.86	2948.02	0.17
		Avg	-0.89±0.02	0.74±0.01	13.46±1.1	4921.77±83	0.29±0.0
		Max	-0.14	0.81	76.69	9859.41	0.52
	Failed (n = 206)	Min	-2.67	0.42	0.00	3358.72	0.20
		Avg	-1.24±0.03	0.63±0.01	36.80±1.4	6391.75±230	0.32±0.0
		Max	-0.68	0.80	90.68	21105.98	0.45
Recruit	Survived (n = 58)	Min	-1.44	0.29	1.53	2003.20	0.16
		Avg	-0.84±0.03	0.69±0.02	26.83±4.7	3916.54±130	0.32±0.01
		Max	-0.23	0.81	141.25	7501.54	0.43
	Failed (n = 115)	Min	-3.28	0.24	0.83	0.00	0.00
		Avg	-0.99±0.04	0.63±0.01	40.77±3.3	4224.85±180	0.30±0.01
		Max	-0.30	0.89	161.00	9166.99	0.50

Table 6.2. Model fit: AUC and max TPR+TNR threshold for RF presence/absence.

	BRT AUC	**SE**	**RF AUC**	**max TPR+TNR**	**GLM AUC**
Restored	0.89	0.02	0.94	0.54	0.89
Recruit	0.9	0.04	0.72	0.54	0.43
All	0.89	0.02	0.86	0.6	0.78

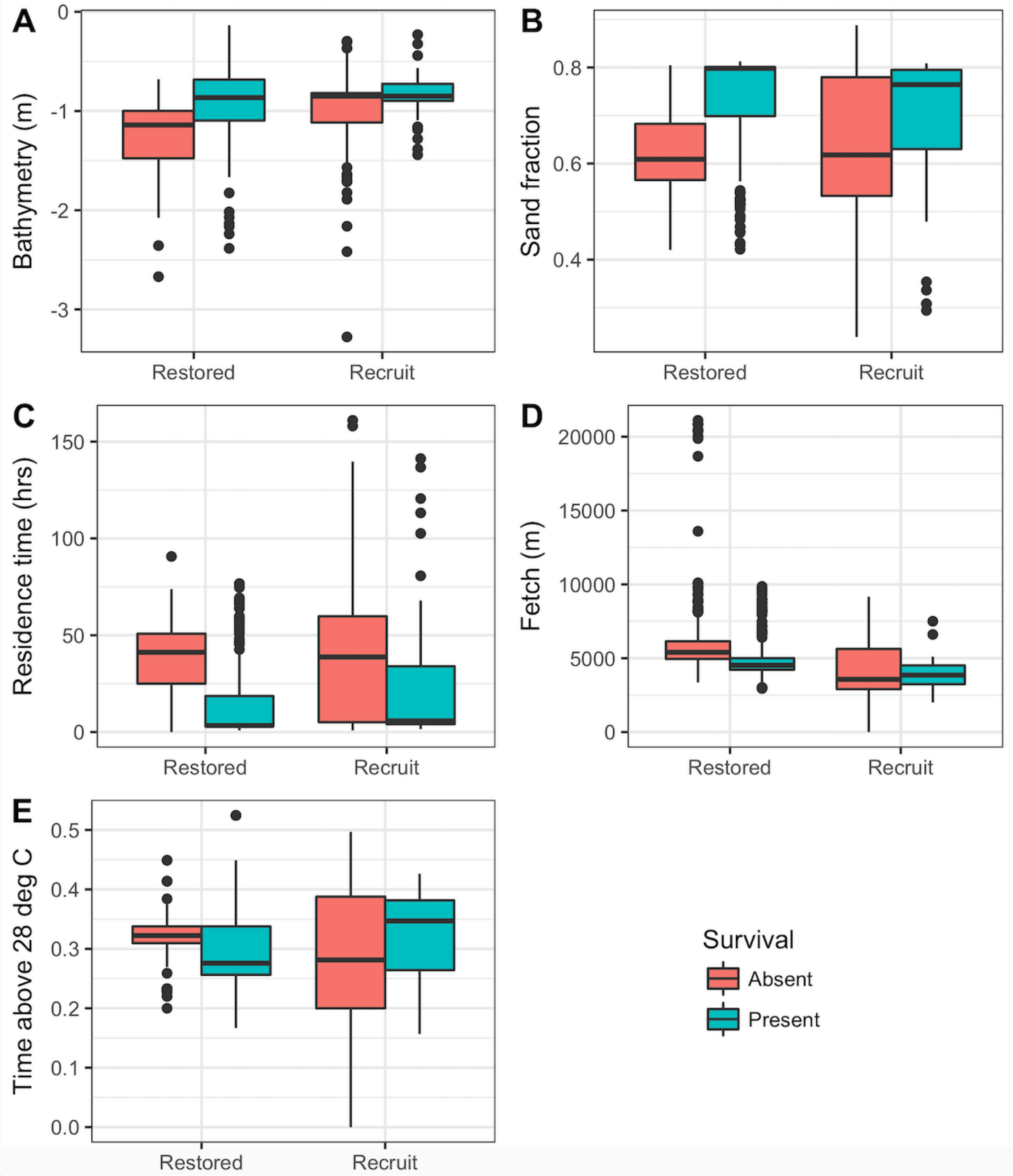

Figure 6.3. Boxplots showing environmental parameter ranges for restored plots (n = 518) and possible recruitment sites (n = 175) by eelgrass survival (presence/absence). Data were extracted by site from the environmental parameter raster stack (Note: comparison E shows differences in temperature: the fraction of summer months, JJA, when SST exceeded 28°C).

Eelgrass survived in 284 of the 490 restoration plots (Figure 6.1). We observed successful eelgrass recruitment at 58 of the 173 systematically arrayed recruitment sites. Eelgrass generally survived in restoration plots with shallower average (± SE) water depth (-0.89±0.02 m), lower water residence times (13.5±1.1 hrs), fetch (4921±83 m), and temperature exposure (0.29±0.0 summertime above 28°C), and higher average sand fractions (0.74±0.01 sand). Parameter ranges are given in Table 6.1. The recruitment sites where eelgrass established and survived show broadly similar environmental parameter ranges (Figure 6.3), although the average fetch at these sites was lower, 3920±130 (SE) m, and the average high water temperature exposure time was marginally higher 0.32±0.01 (SE) (Table 6.1).

6.3.2. Species Distribution Model fit

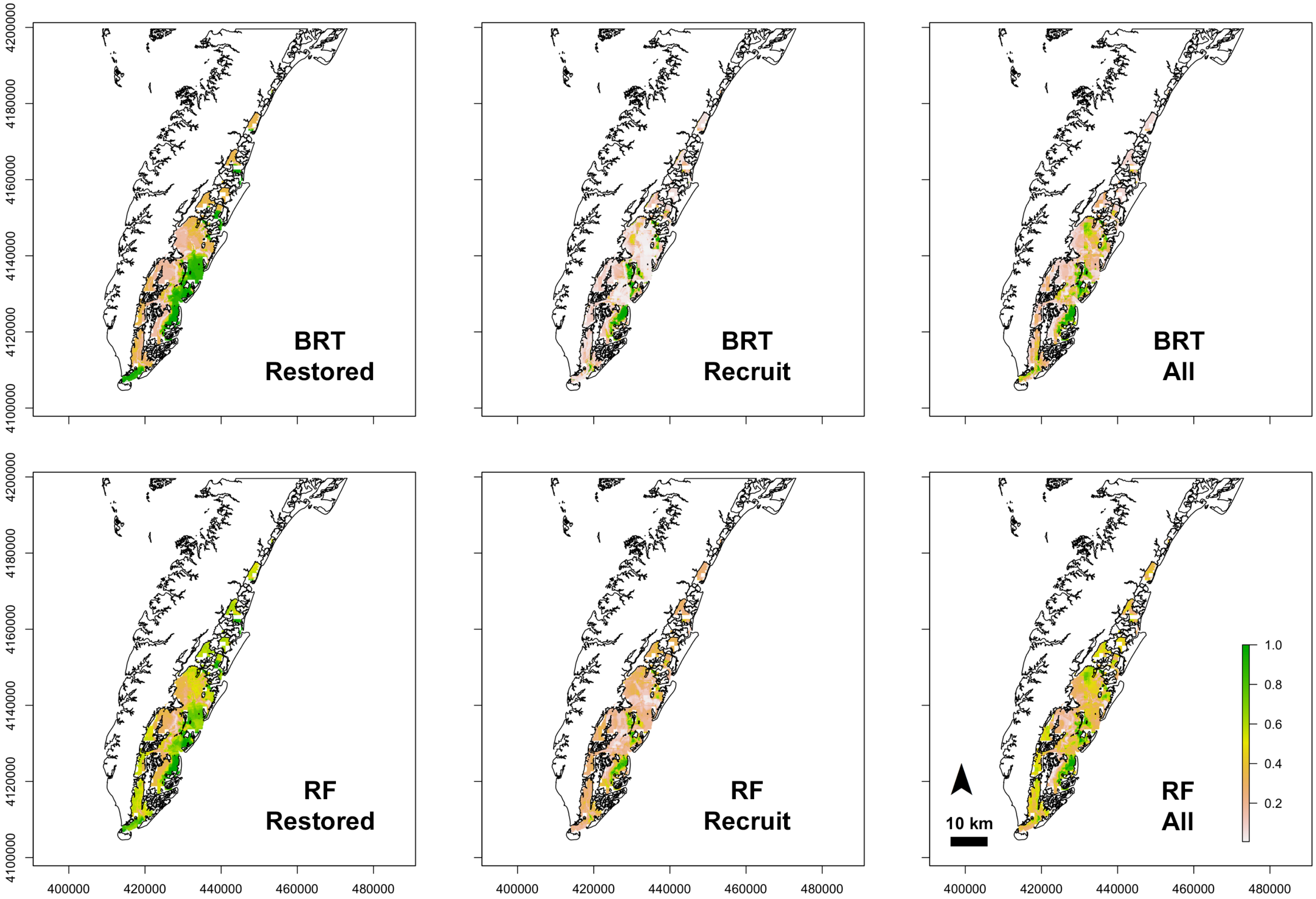

Figure 6.4. BRT and RF model results by data set (NAD83 UTM Zone 18N); scale = probability of presence.

Applying the BRT and RF models to three datasets (restored, recruit, and all data) yielded predictive models that allowed us to quantify the probability of *Z. marina* presence throughout the VCR (Figure 6.4). All of the individual BRT and RF models exhibited relatively high AUC values. The restored plot RF model had the highest AUC, 0.94. The RF model applied to the recruitment sites had the lowest AUC, 0.72 (Table 6.2). AUC values for the other models were approximately 0.9. The GLM and BRT models applied to the restored plot data yielded similar AUCs, 0.89, but the other GLM model AUCs were lower than those for the respective machine learning models (Table 6.2).

Table 6.3. Variable relative importance for boosted regression tree (BRT) and random forest (RF) models on combinations of site data; rel.inf = relative influence; %IncMSE = mean decrease in model accuracy from permuting variable.

Variable	**BRT (Restored)** rel.inf	**BRT (Recruit)** rel.inf	**BRT (All)** rel.inf	**RF (Restored)** %IncMSE	**RF (Recruit)** %IncMSE	**RF (All)** %IncMSE
Res. Time	**66.2**	13.7	**41.9**	**28.0**	13.7	30.8
Fetch	11.8	**39.7**	24.1	20.1	**19.5**	28.8
Temperature	9.5	16.2	13.7	26.7	13.4	**35.9**
Grain Size	6.7	19.1	10.0	25.0	15.7	33.0
Bathymetry	5.7	11.3	10.3	19.8	10.9	26.5

Water residence time proved to be the most influential variable in three of the six models: the BRT and RF models applied to the restored dataset and the BRT model applied to the combined dataset. Residence time accounted for 66.2 and 41.9 percent of the variable influence in the BRT restored and combined model runs, respectively

(Table 6.3). Fetch was the most important predictor for the BRT and RF models applied to the recruitment site dataset, accounting for 39.7% of the variable influence in the BRT model. Water temperature marginally exceeded grain size as the most influential variable for the RF model applied to the combined dataset (Table 6.3).

6.3.3. The predicted eelgrass distribution in the VCR

We categorized individual sites as predicting *Z. marina* presence using the specificity-sensitivity threshold results for the RF models. The restored and recruit RF models both had probability threshold cut-offs of 0.54. The combined model had a threshold of 0.6 (Table 6.2). We averaged the model outputs for the restored plot and recruitment site datasets and applied the RF specificity-sensitivity thresholds, 0.54 for both datasets, to generate eelgrass presence maps. The habitable area predicted by the restored dataset yielded a 107 km^2 habitable area. The recruitment site dataset yielded a habitable area approximately one-third that size, 34 km^2. This more restricted area encompassed areas behind barrier islands but not the tidal flats surrounding the major inlets. Averaging the BRT and RF all data models and applying the probability threshold for that dataset, 0.6, yielded a VCR-wide eelgrass habitable area of approximately 42.9 km^2. This total habitable area may be conservative. The model only predicted eelgrass presence in 13.6 km^2 of the 18.8 km^2 *Z. marina* area observed in 2012, a 27% omission.

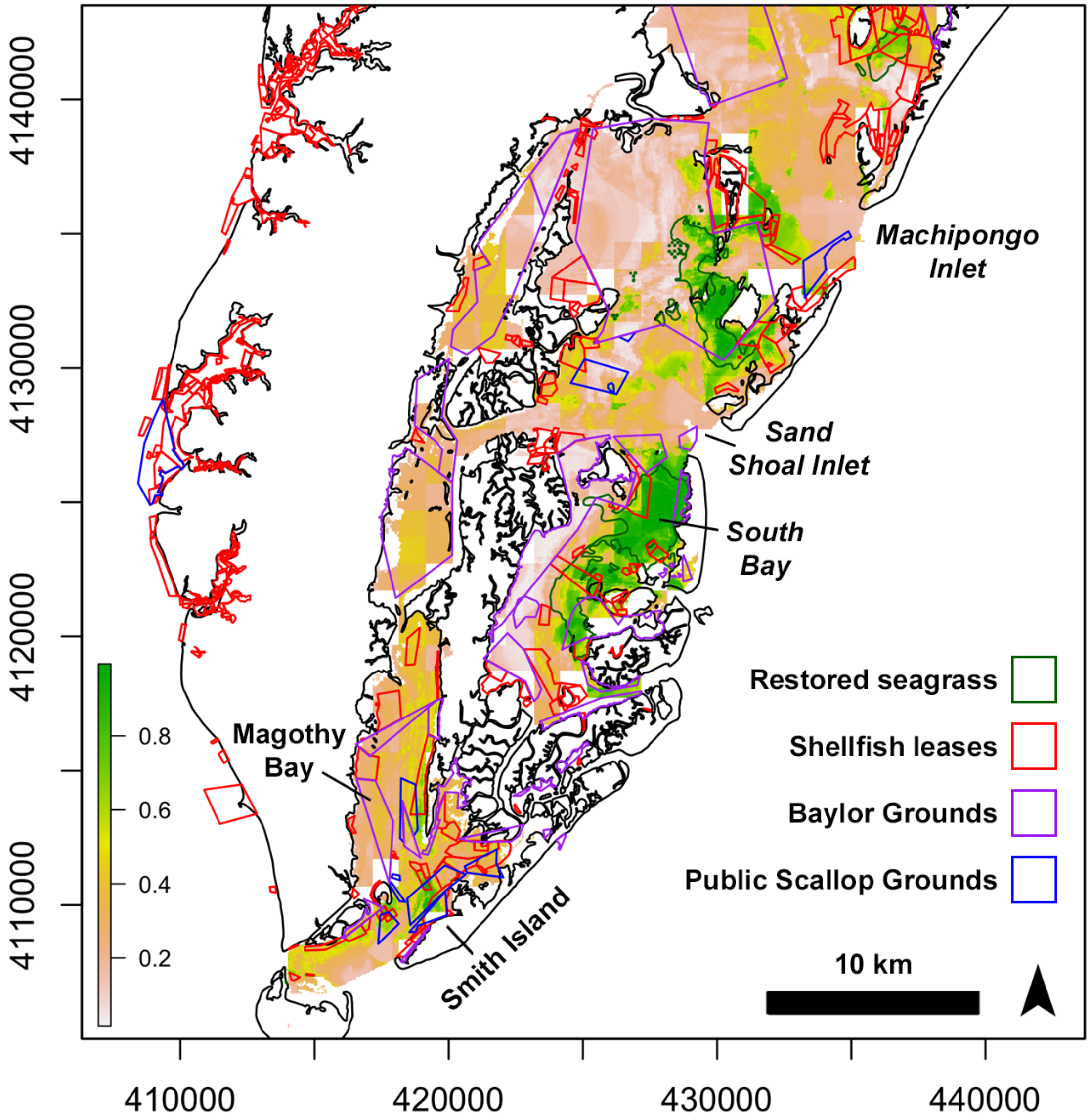

Figure 6.5. Bottom use competition within the VCR: modeled VCR *Z. marina* habitable area (average BRT and RF All models) relative to observed restored meadows (green), extant shellfish leases, the Baylor Grounds, and the former Public Scallop Grounds (NAD83 UTM Zone 18N); scale = probability of presence.

The model-predicted habitable area output overlaps several of the managed areas within the VCR system. Approximately 13.7 km^2 of this predicted habitable area occurs within the Baylor Grounds, 8.76 km^2 occurs within existing shellfish leases, and 1.1 km^2 occurs within the former Public Scallop Grounds (Figure 6.5). This model-predicted shellfish lease overlap represents a 3 to 4-fold increase relative to the current eelgrass coverage within leased plots, approximately 2.3 km^2.

6.4. Discussion

6.4.1. The eelgrass environmental niche and historical distribution

Low water residence time provides the single best predictor of eelgrass presence at the regional, VCR-wide scale, especially when only the restoration plot data is considered. This result supports Fonseca and Uhrin's (2009) observation that *Z. marina* prefers areas with moderate to high current velocities. The apparent importance of residence time likely reflects the fact that both grain size and water temperature also define the eelgrass niche. The residence time data was derived, in part, from the grain size data and incorporates distance from the inlets, where warm bay water exchanges with cooler ocean water. A higher sand fraction facilitates pore-water exchange and prevents the build-up of anaerobic metabolites and phytotoxins, especially sulfides, at the expense of sediment nutrient retention (Moore and Jarvis 2008). Areas characterized by rapid water exchange are also generally cooler (Figure 6.2). The variable influence results for the combined dataset indicate that temperature also controls the regional spatial distribution of eelgrass (Table 6.3). This supports past indications that warm water exposure adversely impacts *Z. marina* at this southern end of its range (Lefcheck et al. 2017), because prolonged heat stress leads to photo-inhibition (Koch et al. 2013).

When only the natural-recruitment site data is considered, the eelgrass habitable area is more constrained, and fetch length represents the best predictor of the overall distribution. Areas with lower fetch length tend to be more quiescent, because they experience less wave energy. Regional hydrodynamic patterns likely concentrate seed propagules produced in meadow patches in these areas, where they have a better chance of germinating and establishing new, viable meadows. The areas behind the barrier islands are generally more sheltered from fetch-induced wave exposure. Fetch represents one of the dominant controls on bed shear stress in this system (Fagherazzi and Wiberg 2009). Long fetches result in increased sediment resuspension, which reduces light availability for eelgrass (Lawson et al. 2007). These observations allow us to explain both the observed, restored eelgrass distribution pattern and the total, predicted, habitable area, which show considerable overlap (Figures 6.4 and 6.5). Although currents potentially disperse seed propagules throughout the VCR system, new meadow patches are more likely to initiate in quiescent, protected areas. Patches that become established in cool, sandy, well-flushed areas are likely to survive and expand into larger meadows.

The model-predicted habitable area provides an indication of the historic eelgrass extent within this system. Anecdotal historical information about the distribution of seagrass in the VCR system prior to the 1932 eelgrass pandemic supports these findings. According to one account, eelgrass occurred in sandy areas behind the barrier islands in about two feet of water at low tide (Truitt and Barnes 1997; Oreska et al. 2017), which conforms with the habitable area predictions (Figures 6.4 and 6.5). The predicted habitable area output includes part of seven of the 10 former Public Scallop Grounds in the VCR, suggesting that these bay scallop harvesting areas were purposely located in or near former eelgrass meadows. Most of the predicted areal overlap is concentrated in three scallop grounds located near Smith Island, an area with low water residence times (Figure 6.5). These scallop grounds at the intersection of Magothy and Smith Island Bays were among the first scallop grounds designated in 1926 (Oreska et al. 2017). Restored eelgrass has not yet become established in this area, despite restoration attempts (Orth et al. 2006B), which cast doubt on whether any of the 11 Public Scallop Grounds originally hosted eelgrass meadows (Oreska et al. 2017). However, the SDM results suggest that eelgrass meadows were formerly widespread in this area. The former scallop grounds are, therefore, candidate locations for additional restoration effort; however, that there are some spatial discrepancies. The SDM model results suggest that eelgrass may become widespread on flats inside Sand Shoal and Machipongo Inlets near, but not specifically in, three of the other former Public Scallop Grounds (Figure 6.5). Aerial photographs taken by the VIMS SAV monitoring program in 2017 indicate that eelgrass is now present in one of these areas, just north of the Sand Shoal Inlet Channel behind Cobb Island.

6.4.2. Active restoration versus natural dispersal: Implications for regional spatial management

Applying the BRT and RF models to only the recruitment site data confirmed our hypothesis that the eelgrass niche for natural recruits is more restricted than the niche realized at the restoration plots (Figure 6.4). Restoration effort resulted in eelgrass presence in marginal, bistable areas (cf. Carr et al. 2010) where eelgrass was not predicted to reestablish naturally. This result suggests that it may be possible to actively expand eelgrass coverage beyond the limits of its historical distribution. Such an effort would constitute 'additional' eelgrass restoration for voluntary carbon-offset crediting purposes (Emmer et al. 2015A; 2015B) and may facilitate further restoration of the bay scallop population (Orth et al. 2016). However, the total habitable area suggested by the restoration plot data includes both large, contiguous areas and small meadow patches (Figure 6.5). The latter may prove transient (cf. Valle et al. 2013), especially given that this system is dynamic over decadal timescales, and local environmental conditions are likely to change (McGlathery et al. 2013). This would have implications for seagrass restoration for CO_2 sequestration, given that accumulated sediment organic carbon stocks will be lost if meadow patches move (Marbà et al. 2015).

The predicted habitable area does not directly overlap many of the existing shellfish leases for hard clam culture within the VCR; however, additional restoration effort would likely increase meadow coverage within existing leases. Even absent additional effort, current lease holders can expect to see roughly 6 km^2 of additional eelgrass expansion within leased areas. We note that the current subtidal use conflict is driven primarily by clam industry concern about lost option value from eelgrass expanding into currently unclaimed bottom areas (Luckenbach and Ross 2011). Given model results suggesting that the restored eelgrass area may double without additional restoration effort, managers should consider addressing this option value concern. One possible solution would be to allow limited removal of additional eelgrass in future leases, provided this removal does not reduce VCR-wide eelgrass coverage below the current baseline. The Commonwealth of Virginia should also consider incentivizing toleration of eelgrass expansion in existing leased areas, perhaps by applying for VCS-certified offset-credits for the carbon sequestration resulting from additional restoration effort and extending the financial benefit to subtidal leasees who commit to maintaining a particular amount of eelgrass cover. Individual leasees cannot apply for seagrass carbon offset-credits, because leasees do not have legal title to the subtidal bottom.

6.5. Conclusions

Species distribution models applied to *Z. marina* presence/absence data from the VCR eelgrass restoration indicate that restored eelgrass area will continue to increase naturally in the VCR. Eelgrass will expand into shallow, sandy areas with low water residence time and generally cooler water temperatures. This expansion will marginally increase bottom use conflict with the hard clam industry. Managers can use the habitable area distribution maps generated by this study to minimize that spatial conflict. Water residence time represents the single best predictor of the eelgrass habitable area at this regional scale and can be used as a spatial management guide. These results can also guide site selection for additional eelgrass restoration in this and similar coastal systems.

Acknowledgements

I would like to thank my collaborators: K.J. McGlathery, P.L. Wiberg, R.J. Orth, D.J. Wilcox.

Chapter 7. Conclusions

7.1. Seagrass blue carbon challenges

Voluntary carbon offset-credits will incentivize seagrass restoration efforts at the margin, but selling awarded offset-credits is unlikely to finance seagrass restoration absent a dramatic increase in the average voluntary offset market price. The difficulties are two-fold: the average offset price is too low relative to high seagrass restoration costs (Paling et al. 2009), and seagrass meadows do not permanently sequester enough carbon on the timescales necessary to meet the offset project viability threshold of 50K tCO2e (Kollmuss et al. 2010).

The first difficulty relates to exogenous socioeconomic factors, both credit oversupply and insufficient demand, and may change in the future. The average offset price has fallen by half between 2012 and 2016, from approximately \$6 to \$3 tCO_2e^{-1} (Forest Trends 2013; 2017). This recent price decline is due primarily to an oversupply of REDD+ credits from tropical forestry projects (Forest Trends 2017). A sudden influx of VCS blue carbon offsets under Emmer et al. (2015A) would increase downward pressure on the average voluntary offset price. The average offset price may go back up if demand increases for some reason. For example, universities may opt to meet their pending GHG reduction pledges through voluntary offset purchases, rather than default on their stated goals (cf. Robinson and Kemp 2015). Even if universities only offset part of their pledged emissions reductions, this dramatic increase in demand would put upward pressure on the voluntary offset price.

The second difficulty is due to ecological factors that complicate prospects for seagrass blue carbon finance in ways that generally increase uncertainty about the expected financial benefit from restoration. As shown in chapter 5, the carbon offset benefit from seagrass restoration derives primarily from enhanced SOC accumulation, not standing biomass. Seagrass meadows and other blue carbon habitats can generate much larger SOC stocks than terrestrial forests (Mcleod et al. 2011); however, these stocks may be remineralized if meadows are subject to disturbance (Marbà et al. 2015). The restored *Z. marina* meadow in South Bay, VA, is contiguous and relatively stable, but many meadows are patchy and transient. Even within the VCR, the SDM results presented in chapter 6 suggest that meadows may recolonize a total of 40 km^2, but this total area includes multiple, small meadow patches that may collapse or move due to regional dynamics (e.g. McGlathery et al. 2013). As chapter 3 suggests, the smaller patches are unlikely to accumulate as much SOC as the larger meadows in South, Cobb, and Spider Crab Bays. The large meadows may also be subject to collapse over the 100-year credit permanence timescale required by the VCS (chapter 2), due to increasing water temperatures and sea-level rise (Carr et al. 2012A). From a project perspective, these uncertainties will require more stringent carbon pool monitoring and necessitate a larger credit withholding in the VCS risk 'buffer pool' (Emmer et al. 2015A section 8.5.3), which will increase compliance costs and reduce anticipated financial benefits.

In comparison, many terrestrial offset projects are financially viable, despite the low offset credit price, because most of the offset benefit is represented by standing tree biomass on discrete forest plots. Forest carbon pools are also subject to periodic disturbance risk. Emmer et al. (2015A) incorporates the VCS procedures for quantifying fire risk for marsh and mangrove projects. However, this disturbance risk for forest projects is mitigated by active forest management. Periodic harvesting diminishes the offset benefit but generates financial co-benefits that increase project viability. Forest tracts are also generally easier to manage from a spatial perspective, with clear land ownership and less uncertainty about restored plant survival.

7.2. Seagrass blue carbon opportunities

Despite challenges associated with seagrass blue carbon, coastal managers have ample reason to be optimistic about seagrass restoration for climate mitigation purposes. Seagrass meadows are extremely productive ecosystems (Duarte and Chiscano 1999), but most of this productivity is not currently counted towards the seagrass offset benefit. In chapter 5, we conservatively excluded exported aboveground biomass, because of uncertainty about where it goes and whether this carbon is returned to the atmosphere. However, the C_{org} in this material tends to be refractory, and it may return to the atmosphere very slowly if the exported seagrass wrack accumulates in adjacent habitats and becomes buried (Duarte and Krause-Jensen 2017). Some of the wrack exported from the restored *Z. marina* meadow in South Bay, VA, appears to accumulate on the adjacent barrier islands and may contribute to dune formation (cf. Truitt and Wesson 1997). Some wrack may also accumulate in the adjacent salt marshes, an ecological linkage that warrants further study. Defining the restored meadow project boundary to include these depositional sites and quantifying wrack accumulation could substantially increase the creditable GHG benefit. Coupled seagrass-marsh or seagrass-mangrove blue carbon projects will likely be more attractive to managers and offset-investors than stand-alone seagrass projects. Project bundling may, therefore, represent an option for advancing seagrass blue carbon initiatives, despite the current state of the voluntary offset market.

The chapter 4 result that most of the non-seagrass carbon in many seagrass beds may, in fact, derive from *in situ* benthic microalgae means that this carbon can, potentially, be counted as an offset credit benefit. The VCS guidelines that require excluding allochthonous carbon currently appear to disadvantage seagrass projects (Emmer et al. 2015A), given the recent assumption that non-seagrass carbon derives primarily from allochthonous seston trapping (Hendriks et al. 2008; Kennedy et al. 2010; Howard et al. 2014). However, the hydrodynamic processes identified in chapter 3, coupled with the SOC source results from chapter 4, strongly suggest that meadow presence increases the burial of benthic microalgae and, therefore, increases the preservation of this non-seagrass carbon relative to bare control sites. The causal mechanism appears to be seagrass-enhanced deposition of fine sediment at interior meadow sites. However, more work on seagrass-microalgal ecology is needed to ascertain the extent to which seagrass presence increases the productivity of associated microalgal communities and the sequestration of this increased production.

The chapter 3 results confirm a strong correlation between seagrass SOC and sediment grain size, which may facilitate both more accurate estimation of regional seagrass SOC stocks and regional spatial planning to maximize seagrass CO_2 sequestration. Estimating meadow-scale SOC stocks by scaling SOC concentrations measured at individual sites by meadow area is tenuous, because of canopy-hydrodynamic-sedimentation effects. However, these same effects may also facilitate comprehensive, landscape-scale, seagrass blue carbon accounting by mapping changes in sediment grain size distributions attributable to seagrass restoration. Managers can map the regional grain size distribution prior to restoration using methods outlined by Wiberg et al. (2015) and initiate restoration in areas deemed favorable for seagrass establishment using SMDs, as outlined in chapter 6. In many cases, these will likely be areas with low residence times and higher sand factions. Over time, however, the sand faction in successfully restored meadows will decline, due to the meadow-mediated increase in fine sediment deposition (McGlathery et al. 2012). This change in grain size can be used to estimate SOC enhancement relative to the pre-restoration baseline, given the strong seagrass SOC-grain size correlation confirmed in chapter 3. If this change in grain size can be accurately modeled as a function of seagrass distribution at the regional-scale, managers can accurately quantify seagrass blue carbon stock changes at meadow- and regional-scales and manage restored seagrass systems for climate mitigation.

Literature cited

Adams, M.P., M.I. Saunders, P.S. Maxwell, D. Tuazon, C.M. Roelfsema, D.P. Callaghan, J. Leon, A.R. Grinham, K.R. O'Brien. 2015. Prioritizing localized management actions for seagrass conservation and restoration using a species distribution model. *Aquatic Conservation: Marine and Freshwater Ecosystems*. DOI:10.1002/aqc.2573.

Appleby, P.G., F. Oldfield. 1983. The assessment of ^{210}Pb data from sites with varying sediment accumulation rates. *Hydrobiologia* 103:29-35.

Bahlmann, E., I. Weinberg, J. V. Lavric, T. Eckhard, W. Michaelis, R. Santos, R. Siefert. 2014. Tidal controls on trace gas dynamics in a seagrass meadow of the Ria Formosa lagoon (southern Portugal). *Biogeosciences Discussions* 11:10571-10603.

Barber, T.R., P.R. Carlson. 1993. Effects of seagrass die-off on benthic fluxes and porewater concentrations of $\sum CO_2$, $\sum H_2S$, and CH_4 in Florida Bay sediments. *In:* R.S. Oremland (ed.). *Biogeochemistry of Global Change: Radiatively Active Trace Gases.* New York: Chapman & Hall, 530-550.

Bates, D., M. Mächler, B. Bolker, S. Walker. 2015. Fitting linear mixed-effects models using lme4. *Journal of Statistical Software* 67(1): 51p. DOI:10.18637/jss.v067.i01

Bauer, J.E., W.-J. Cai, P.A. Raymond, T.S. Bianchi, C.S. Hopkinson, P.A.G. Regnier. 2013. The changing carbon cycle of the coastal ocean. *Nature* 504: 61-70.

Baylor, J. 1893. Report to the Governor of VA of J.B. Baylor, in reference to the survey of the oyster grounds. Senate Doc. No. 11. Richmond, VA: Commonwealth of Virginia, Available at Small Special Collections Library, University of VA. 11p.

Bell, S.S., M.S. Fonseca, N.B. Stafford. 2006. Seagrass ecology: New contributions from a landscape perspective. *In:* A.W.D. Larkum, R.J. Orth, C.M. Duarte (eds.). *Seagrasses: Biology, Ecology and Conservation*. Netherlands: Springer, pp. 625-645.

Belshe, E.F., M.A. Mateo, L. Gillis, M. Zimmer, M. Teichberg. 2017. Muddy waters: unintentional consequences of blue carbon research obscure our understanding of organic carbon dynamics in seagrass ecosystems. *Frontiers in Marine Science* 4:125.

Borges, A.V., L.-S. Schiettecatte, G. Abril, B. Delille, F. Gazeau. 2006. Carbon dioxide in European coastal waters. *Estuarine, Coastal and Shelf Science* 70(3): 375-387.

Bos, A.R., T.J. Bouma, G.L.J. de Kort, M.M. van Katwijk. 2007. Ecosystem engineering by annual intertidal seagrass beds: sediment accretion and modification. *Estuarine, Coastal and Shelf Science* 74:344-348.

Bouillon, S. R.M. Connolly. 2009. Carbon exchange among tropical coastal ecosystems. *In:* I. Nagelkerken (ed.). *Ecological Connectivity among Tropical Coastal Ecosystems.* Dordrecht, Germany: Springer, pp. 45-70.

Bouillon, S., F. Dehairs, B. Velimirov, G. Abril, A. Vieira Borges. 2007. Dynamics of organic and inorganic carbon across contiguous mangrove and seagrass systems (Gazi Bay, Kenya). *Journal of Geophysical Research* 112: G02018.

Bradley, K., C. Houser. 2009. Relative velocity of seagrass blades: Implications for wave attenuation in low-energy environments. *Journal of Geophysical Research* 114:F01004.

Cai, W.-J. 2011. Estuarine and coastal ocean carbon paradox: CO_2 sinks or sites of terrestrial carbon incineration? *Annual Review of Marine Science* 3:123-145.

Campbell, J.E., E.A. Lacey, R.A. Decker, S. Crooks, J.W. Fourqurean. 2015. Carbon storage in seagrass beds of Abu Dhabi, United Arab Emirates. *Estuaries and Coasts* 38:242-251.

Canfield, D.E. 2001. Isotope fractionation by natural populations of sulfate-reducing bacteria. *Geochimica et Cosmochimica Acta* 65(7): 1117-1124.

Carr, J.A., P. D'Odorico, K. McGlathery, P. Wiberg. 2010. Stability and bistability of seagrass ecosystems in shallow coastal lagoons: Role of feedbacks with sediment resuspension and light attenuation. *Journal of Geophysical Research* 115:G03011.

Carr, J.A., P. D'Odorico, K.J. McGlathery, P.L. Wiberg. 2012A. Modeling the effects of climate change on eelgrass stability and resilience: future scenarios and leading indicators of collapse. *Marine Ecology Progress Series* 448:289-301.

Carr, J.A., P. D'Odorico, K.J. McGlathery, P.L. Wiberg. 2012B. Stability and resilience of seagrass meadows to seasonal and interannual dynamics and environmental stress. *Journal of Geophysical Research* 117:G01007.

Carr, J.A., P. D'Odorico, K.J. McGlathery, P.L. Wiberg. 2015. Spatially explicit feedbacks between seagrass meadow structure, sediment and light: Habitat suitability for seagrass growth. *Advances in Water Resources* 000:1-11.

Cebrián, J., C.M. Duarte, N. Marbà, S. Enríquez. 1997. Magnitude and fate of the production of four co-occurring Western Mediterranean seagrass species. *Marine Ecology Progress Series* 155:29-44.

Champenois, W., A.V. Borges. 2012. Seasonal and interannual variations of community metabolism rates of a *Posidonia oceanica* seagrass meadow. *Limnology and Oceanography* 57(1): 347-361.

Chefaoui, R.M., J. Assis, C.M. Duarte, E.A. Serrão. 2016. Large-scale prediction of seagrass distribution integrating landscape metrics and environmental factors: The case of *Cymodocea nodosa* (Mediterranean-Atlantic). *Estuaries and Coasts* 39(1):123-137.

Chen, S.-N., L.P. Sanford, E.W. Koch, F. Shi, E.W. North. 2007. A nearshore model to investigate the effects of seagrass bed geometry on wave attenuation and suspended sediment transport. *Estuaries and Coasts* 30(2):296-310.

Chuang, P.-C., M.B. Young, A.W. Dale, L.G. Miller, J.A. Herrara-Silveira, A. Paytan. 2017. Methane fluxes from tropical coastal lagoons surrounded by mangroves, Yucatán, Mexico. *Journal of Geophysical Research: Biogeosciences* 122. DOI:10.1002/2017JG003761.

Ciss, S. 2015. Variable importance in random uniform forests. Available at: https://cran.r-project.org/web/packages/randomUniformForest/vignettes/VariableImportanceInRandomUniformForests.pdf (accessed 25 March 2018).

Cole, L.W., K.J. McGlathery. 2012. Nitrogen fixation in restored eelgrass meadows. *Marine Ecology Progress Series* 448:235-246.

Commission for Environmental Cooperation (CEC). 2014. Greenhouse gas offset methodology criteria for tidal wetland conservation. Montreal, Canada: Commission for Environmental Cooperation.

Commission of Fisheries of Virginia (CF). 1932. Report of the Commission of Fisheries of Virginia. Richmond, VA: Public Printing, p. 7.

Commonwealth of Virginia. 2000. Submerged Aquatic Vegetation (SAV) Transplantation Guidelines. Virginia Register of Regulations 17(5):4 VAC 20-337-10.

Cottam, C. 1935. Further notes on past periods of eelgrass scarcity. *Rhodora* 37(440):269-271.

Crill, P. M., C. S. Martens. 1983. Spatial and temporal fluctuations of methane production in anoxic coastal marine sediments. *Limnology and Oceanography* 28(6):1117-1130.

de Boer, W.F. 2007. Seagrass–sediment interactions, positive feedbacks and critical thresholds for occurrence: a review. *Hydrobiologia* 591:5−24.

Deborde, J., P. Anschutz, I. Auby, F. Guérin, D. Poirier, D. Marty, G. Boucher, G. Thouzeau, M. Canton, G. Abrril. 2010. Methane sources, sinks, and fluxes in a temperate tidal lagoon: the Archachon lagoon (SW France). *Estuarine, Coastal and Shelf Science* 89(4):256-266.

Downie, A.-L., M. von Numers, C. Boström. 2013. Influence of model selection on the predicted distribution of the seagrass *Zostera marina*. *Estuarine, Coastal and Shelf Science* 121-122:8-19.

Duarte, C.M. 2017. Reviews and syntheses: Hidden forests, the role of vegetated coastal habitats in the ocean carbon budget. *Biogeosciences* 14:301-310.

Duarte, C.M., J. Cebrián. 1996. The fate of marine autotrophic production. *Limnology and Oceanography* 41(8):1758-1766.

Duarte, C.M., C.L. Chiscano. 1999. Seagrass biomass and production: a reassessment. *Aquatic Botany* 65:159-174.

Duarte, C.M., D. Krause-Jensen. 2017. Export from seagrass meadows contributes to marine carbon sequestration. *Frontiers in Marine Science* 4:13

Duarte, C.M., J.J. Middelburg, N. Caraco. 2005. Major role of marine vegetation on the oceanic carbon cycle. *Biogeosciences* 2:1-8.

Duarte, C.M, N. Marbà, E. Gacia, J.W. Fourqurean, J. Beggins, C. Barron, E.T. Apostolaki. 2010. Seagrass community metabolism: assessing the carbon sink capacity of seagrass meadows. *Global Biogeochemical Cycles* 24:GB4032.

Duarte, C.M., H. Kennedy, N. Marbà, I. Hendricks. 2013A. Assessing the capacity of seagrass meadows for carbon burial: Current limitations and future strategies. *Ocean & Coastal Management* 83:32-38.

Duarte, C.M., T. Sintes, N. Marbà. 2013B. Assessing the CO_2 capture potential of seagrass restoration projects. *Journal of Applied Ecology* 50(6):1341-1349.

Elith, J., J.R. Leathwick. 2009. Species distribution models: Ecological explanation and prediction across space and time. *Annual Review of Ecology, Evolution, and Systematics* 40:677-697.

Elith, J., J.R. Leathwick. 2017. Boosted Regression Trees for ecological modeling. Available at: https://cran.r-project.org/web/packages/dismo/vignettes/brt.pdf (accessed 25 March 2018).

Emmer, I., B. Needelman, S., Emmett-Mattox, S. Crooks, P. Megonigal, D. Myers, M. Oreska, K. McGlathery, and others. 2015A. Methodology for Tidal Wetland and Seagrass Restoration. Verified Carbon Standard, VM0033 Version 1.0.

Emmer, I., M. von Unger, B.A. Needelman, S. Crooks, S. Emmett-Mattox. 2015B. Coastal Blue Carbon in Practice: A Manual for Using the VCS Methodology for Tidal Wetland and Seagrass Restoration, V 1.0. Arlington, VA: Restore America's Estuaries, 82p.

Environmental Science Associates (ESA). 2016. Tampa Bay Blue Carbon Assessment: Summary of Findings. Tampa: Environmental Science Associates, 331p.

Fagherazzi, S., P.L. Wiberg. 2009. Importance of wind conditions, fetch, and water levels on wave-generated shear stresses in shallow intertidal basins. *Journal of Geophysical Research* 114:F03022.

Ferguson, A.J.P., R. Gruber, J. Potts, A. Wright, D.T. Welsh, P. Scanes. 2017. Oxygen and carbon metabolism of *Zostera muelleri* across a depth gradient – Implications for resilience and blue carbon. *Estuarine, Coastal and Shelf Science* 187(5):216-230.

Flynn W. 1968. The determination of low levels of polonium-210 in environmental materials. *Analytica Chimica Acta* 43:221-227.

Fonseca, M.S. 2011. Addy revisited: What has changed with seagrass restoration in 64 years? *Ecological Restoration* 29(1-2):73-81.

Fonseca, M.S., S.S. Bell. 1998. Influence of physical setting on seagrass landscapes near Beaufort, North Carolina, USA. *Marine Ecology Progress Series* 171:109-121.

Fonseca, M.S., A.V. Uhrin. 2009. The status of eelgrass, *Zostera marina*, as bay scallop habitat: consequences for the fishery in the western Atlantic. *Marine Fisheries Review* 71(3):20-33.

Forest Trends. 2013. Maneuvering the Mosaic: State of the Voluntary Carbon Markets 2013. M. Peters-Stanley, D. Yin (eds.). Washington, D.C.: Forest Trends' Ecosystem Marketplace. 20p.

Forest Trends. 2016. Rising Ambition: State of the Voluntary Carbon Markets 2016. Available at: http://www.forest-trends.org/documents/files/doc_5242.pdf (accessed 5 April 2017).

Forest Trends. 2017. Unlocking Potential: State of the Voluntary Carbon Markets 2017. Washington, D.C.: Forest Trends' Ecosystem Marketplace, 52p.

Fourqurean, J.W., C.M. Duarte, H. Kennedy, N. Marbà, M. Holmer, M.A. Mateo, E.T. Apostolaki, G.A. Kendrick, D. Krause-Jensen, K.J. McGlathery, O. Serrano. 2012. Seagrass ecosystems as a globally significant carbon stock. *Nature Geoscience* 5:505-509.

Fourqurean, J., B. Johnson, J.B. Kauffman, H. Kennedy, C. Lovelock, D.M. Alongi, M. Cifuentes, M. Copertino, S. Crooks, C.M. Duarte, M. Fortes, J. Howard, A. Hutahaean, J. Kairo, N. Marbà, J. Morris, D. Murdiyarso, E. Pidgeon, P. Ralph, N.

Saintilan, O. Serrano. 2014. Field sampling of soil carbon pools in coastal ecosystems, p. 39-66. In J. Howard, S. Hoyt, K. Isensee, E. Pidgeon, M. Telszewski [eds.], Coastal blue carbon: methods for assessing carbon stocks and emissions factors in mangroves, tidal salt marshes, and seagrass meadows. Conservation International, Intergovernmental Oceanographic Commission of UNESCO, International Union for Conservation of Nature.

Fry, B. 2007. *Stable Isotope Ecology*. New York: Springer. 308p.

Gacia, E., C.M. Duarte, J.J. Middelburg. 2002. Carbon and nutrient deposition in a Mediterranean seagrass (*Posidonia oceanica*) meadow. *Limnology and Oceanography* 47(1):23-32.

Garcias-Bonet, N., C.M. Duarte. 2017. Methane production by seagrass ecosystems in the Red Sea. *Frontiers in Marine Science* 4:340. DOI:10.3389/fmars.2017.00340

Gattuso, J.-P., M. Frankignoulle, R. Wollast. 1998. Carbon and carbonate metabolism in coastal aquatic ecosystems. *Annual Review of Ecology, Evolution, and Systematics* 29:405-434.

Genovesi, B., D. Mouillot, T. Laugier, A. Fiandrino, M. Laabir, A. Vaquer, D. Grzebyk. 2013. Influences of sedimentation and hydrodynamics on the spatial distribution of *Alexandrium catenella*/*tamarense* resting cysts in a shellfish farming lagoon impacted by toxic blooms. *Harmful Algae* 25:15-25.

Granata, T.C., T. Serra, J. Colomer, X. Casamitjana, C.M. Duarte, E. Gacia. 2001. Flow and particle distributions in a nearshore seagrass meadow before and after a storm. *Marine Ecology Progress Series* 218: 95-106.

Grech, A., R.G. Coles. 2010. An ecosystem-scale predictive model of coastal seagrass distribution. *Aquatic Conservation: Marine and Freshwater Ecosystems* 20:437-444.

Grech, A., K. Chartrand-Miller, P. Erftemeijer, M. Fonseca, L. McKenzie, M. Rasheed, H. Taylor, and R. Coles. 2012. A comparison of threats, vulnerabilities and management approaches in global seagrass bioregions. *Environmental Research Letters* 7:024006.

Greiner, J.T. 2013. Assessing the importance of seagrass habitat restoration to "blue carbon" sequestration in shallow coastal waters. Ms Thesis, University of Virginia. Available from: http://search.lib.virginia.edu/catalog/u6124019.

Greiner, J.T., K.J. McGlathery, J. Gunnell, B.A. McKee. 2013. Seagrass restoration enhances "blue carbon" sequestration in coastal waters. *PLoS ONE* 8(8):e72469.

Greiner, J.T., G.M. Wilkinson, K.J. McGlathery, K.A. Emery. 2016. Sources of sediment carbon sequestered in restored seagrass meadows. *Marine Ecology Progress Series* 551: 95-105.

Gruber, R.K., W.M. Kemp. 2010. Feedback effects in a coastal canopy-forming submersed plant bed. *Limnology and Oceanography* 55(6):2285-2298.

Guisan, A., N.E. Zimmerman. 2000. Predictive habitat distribution models in ecology. *Ecological Modeling* 135:147-186.

Hansen, J.C.R., M.A. Reidenbach. 2012. Wave and tidally driven flows in eelgrass beds and their effect on sediment suspension. *Marine Ecology Progress Series* 448:271-287.

Hansen, J.C.R., M.A. Reidenbach. 2013. Seasonal growth and senescence of a *Zostera marina* seagrass meadow alters wave-dominated flow and sediment suspension within a coastal bay. *Estuaries and Coasts* 36:1099-1114.

Harbeson, S.A. 2010. An investigation of nutrient transfer in a restored eelgrass, *Zostera marina*, meadow. Ph.D. dissertation submitted to the University of Virginia.

Hardison, A.K., I.C. Anderson, E.A. Canuel, C.R. Tobias, B. Vueger. 2011. Carbon and nitrogen dynamics in shallow photic systems: Interactions between macroalgae, microalgae, and bacteria. *Limnology and Oceanography* 56(4):1489-1503.

Hardison, A.K., E.A. Canuel, I.C. Anderson, C.R. Tobias, B. Veuger, M.N. Waters. 2013. Microphytobenthos and benthic macroalgae determine sediment organic matter composition in shallow photic sediments. *Biogeosciences* 10:5571-5588.

Hejnowicz, A.P., H. Kennedy, M.A. Rudd, M.R. Huxham. 2015. Harnessing the climate mitigation, conservation and poverty alleviation potential of seagrasses: prospects for developing blue carbon initiatives and payment for ecosystem service programmes. *Frontiers in Marine Science* 2:32.

Heminga, M.A., F.J. Slim, J. Kazungu, G.M. Ganssen, J. Nieuwenhuize, N.M. Kruyt. 1994. Carbon outwelling from a mangrove forest with adjacent seagrass beds and coral reefs (Gazi Bay, Kenya). *Marine Ecology Progress Series* 106:291-301.

Hendriks, I.E., T. Sintes, T.J. Bouma, C.M. Duarte. 2008. Experimental assessment and modeling evaluation of the effects of the seagrass *Posidonia oceanica* on flow and particle trapping. *Marine Ecology Progress Series* 356:163-173.

Hijmans, R.J., J. Elith. 2017. Species distribution modeling in R. Available at: https://cran.r-project.org/web/packages/dismo/vignettes/sdm.pdf (accessed 25 March 2018).

Holloway, V., E. Giandomenico. 2009. The History of REDD Policy. Adelaide, SA: Carbon Planet Limited. Available at: http://redd.unfccc.int/uploads/2_164_redd_20091216_carbon_planet_the_history_of_redd_carbon_planet.pdf (accessed 11 March 2018).

Holmer, M., F.Ø. Anderson, S.L. Nielsen, H.T.S. Boschker. 2001. The importance of mineralization based on sulfate reduction for nutrient regeneration in tropical seagrass sediments. *Aquatic Botany* 71:1-17.

Hondula, K.L. 2012. Using multiple stable isotopes including deuterium (δ^2H) to trace organic matter in a complex near-shore lagoon. M.S. thesis submitted to the University of Virginia.

Hondula, K., M. Pace. 2011. Stable isotopes of M. mercenaria and plant sources on the Virginia Coast. Data publication knb-lter-vcr.200.9. Available at: https://portal.lternet.edu/nis/mapbrowse?packageid=knb-lter-vcr.200.9 (accessed 30 September 2016).

Hondula, K.L., M.L. Pace. 2014. Macroalgal support of cultured hard clams in a low nitrogen coastal lagoon. *Marine Ecology Progress Series* 498:187-201.

Howard, J., S. Hoyt, K. Isensee, E. Pidgeon, M. Telszewski (eds). 2014. *Coastal blue* *carbon: methods for assessing carbon stocks and emissions factors in mangroves, tidal salt marshes, and seagrass meadows.* Conservation International, Intergovernmental Oceanographic Commission of UNESCO. Arlington, Virginia: IUCN.

Howard, J., A. Sutton-Grier, D. Herr, J. Kleypas, E. Landis, E. Mcleod, E. Pidgeon, S. Simpson. 2017A. Clarifying the role of coastal and marine systems in climate mitigation. *Frontiers in Ecology and the Environment* 15(1):42-50.

Howard, J.L., J.C. Creed, M.V.P. Aguiar, J.W. Fourqurean. 2017B. CO_2 released by carbonate sediment production in some coastal areas may offset the benefits of seagrass “Blue Carbon” storage. *Limnology and Oceanography* DOI:10.1002/lno.10621

Huang, Y.-H., C.-L. Lee, C.-Y. Chung, S.-C. Hsiao, H.-J. Lin. 2015. Carbon budgets of multispecies seagrass beds at Dongsha Island in the South China Sea. *Marine Environmental Research* 106:92-102.

Hume, A.C., P. Berg, K.J. McGlathery. 2011. Dissolved oxygen fluxes and ecosystem metabolism in an eelgrass (*Zostera marina*) meadow measured with the eddy correlation technique. *Limnology and Oceanography* 56(1):86-96.

Hyndes, G.A., I. Nagelkerken, R.J. McLeod, R.M. Connolly, P.S. Lavery, M.A. Vanderklift. 2014. Mechanisms and ecological role of carbon transfer within coastal seascapes. *Biological Reviews* 89(1):232-254.

Inger, R., A. Jackson, A. Parnell, S. Bearhop. 2010. SIAR V4 (Stable Isotope Analysis in R):

An Ecologists's Guide. Available at https://www.tcd.ie/Zoology/research/research/theoretical/siar/SIAR_For_Ecologists.pdf (accessed 30 September 2016).

Isaksen, M.F., K. Finster. 1996. Sulphate reduction in the root zone of the seagrass *Zostera noltii* on the intertidal flats of a coastal lagoon (Arcachon, France). *Marine Ecology Progress Series* 137:187-194.

Intergovernmental Panel on Climate Change (IPCC). 2001. The Carbon Cycle and Atmospheric Carbon Dioxide. *In:* IPCC. 2001. Climate Change 2001: The Scientific Basis. Contributions of Working Group I to the Third Assessment Report of the Intergovernmental Panel on Climate Change. Cambridge: Cambridge University Press, 183-238.

Intergovernmental Panel on Climate Change (IPCC). 2006. 2006 IPCC Guidelines for National Greenhouse Gas Inventories, Prepared by the National Greenhouse Gas Inventories Programme. H.S. Eggleston, L. Buendia, K. Miwa, T. Ngara, K. Tanabe (eds.). Japan: Institute for Global Environmental Strategies.

Intergovernmental Panel on Climate Change (IPCC). 2014. 2013 Supplement to the 2006 IPCC Guidelines for National Greenhouse Gas Inventories: Wetlands. T. Hirashi et al (eds.). Switzerland: IPCC Press, 354 p.

Jankowska, E., L.N. Michel, A. Zaborska, and M. Włodarska-Kowalczuk. 2016. Sediment carbon sink in low-density temperate eelgrass meadows (Baltic Sea). *Journal of Geophysical Research: Biogeosciences* 121:10.1001/2016JG003424.

Johannessen, S.C., R.W. Macdonald. 2016. Geoengineering with seagrasses: is credit due where credit is given? *Environmental Research Letters* 11:113001.

Johnson, R.A., A.G. Gulick, A.B. Bolten, K.A. Bjorndal. 2017. Blue carbon stores in tropical seagrass meadows maintained under green turtle grazing. *Scientific Reports* 7:13545.

Kennedy, H., J. Beggins, C.M. Duarte, J.W. Fourqurean, M. Holmer, N. Marbà, J.J. Middelburg. 2010. Seagrass sediments as a global carbon sink: Isotopic constraints. *Global Biogeochemical Cycles.* 24:GB4026.

Koch, E.W., J.D. Ackerman, J. Verduin, M. van Keulen. 2006. Fluid dynamics in seagrass ecology—from molecules to ecosystems. *In:* A.W.D. Larkum, R.J. Orth, C.M. Duarte (eds.). *Seagrasses: Biology, Ecology and Conservation*. Netherlands: Springer, pp. 193-225.

Koch, M., G. Bowes, C. Ross, X.-H. Zhang. 2013. Climate change and ocean acidification effects on seagrasses and marine macroalgae. *Global Change Biology* 19:103-132.

Kollmuss, A., M. Lazarus, C. Lee, M. LeFranc, C. Polycarp. 2010. Handbook of Carbon Offset Programs: Trading Systems, Funds, Protocols and Standards. London.: Earthscan, p. 210.

Lavery, P.S., M.- Á. Mateo, O. Serrano, M. Rozaimi. 2013. Variability in the carbon storage of seagrass habitats and its implications for global estimates of blue carbon ecosystem service. *PLoS ONE* 8(9):e73748.

Lawson, S.E., P.L. Wiberg, K.J. McGlathery, D.C. Fugate. 2007. Wind-driven sediment suspension controls light availability in a shallow coastal lagoon. *Estuaries and Coasts* 30:102−112.

Lawson, S.E., K.J. McGlathery, P.L. Wiberg. 2012. Enhancement of sediment suspension and nutrient flux by benthic macrophytes at low biomass. *Marine Ecology Progress Series* 448:259-270.

Lefcheck, J.S., D.J. Wilcox, R.R. Murphy, S.R. Marion, R.J. Orth. 2017. Multiple stressors threaten the imperiled coastal foundation species eelgrass (*Zostera marina*) in Chesapeake Bay, USA. *Global Change Biology* 23(9):3474-3483.

Lefebvre, A., C.E.L. Thompson, C.L. Amos. 2010. Influence of *Zostera marina* canopies on unidirectional flow, hydraulic roughenss and sediment movement. *Continental and Shelf Research* 30:1783-1794.

Lee, K.-S., K.H. Dunton. 2000. Diurnal changes in pore water sulfide concentrations in the seagrass *Thalassia testudinum* beds: the effects of seagrasses on sulfide dynamics. *Journal of Experimental Marine Biology and Ecology* 255:201-214.

Liu, C., P.M. Berry, T.P. Dawson, R.G. Pearson. 2005. Selecting thresholds of occurrence in the prediction of species distributions. *Ecography* 28(3):385-393.

López, F., M. García. 1998. Open-channel flow through simulated vegetation: Suspended sediment transport modeling. *Water Resources Research* 34(9):2341-2352.

Luckenbach, M.W., P.G. Ross. 2011. Seaside special area management plan: spatial information analysis and interpretation for shellfish ground and SAV beds. Final Report to the Virginia Department of Environmental Quality, Task #96.02.

Macreadie, P.I., S.M. Trevathan-Tackett, C.G. Skilbeck, J. Sanderman, N. Curlevski, G. Jacobsen, J.R. Seymour. 2015. Losses and recovery of organic carbon from a seagrass ecosystem following disturbance. *Proceedings of the Royal Society B* 282:20151537.

Macreadie, P.I., D.A. Nielson, J.J. Kelleway, T.B. Atwood, J.R. Seymour, K. Petrou, R.M. Connolly, A.C.G. Thomson, S.M. Trevathan-Tackett, P.J. Ralph. 2017A. Can we manage coastal ecosystems to sequester more blue carbon? *Frontiers in Ecology and the Environment* 15(4):206-213.

Macreadie, P.I., O. Serrano, D.T. Maher, C.M. Duarte, J. Beardall. 2017B. Addressing calcium carbonate cycling in blue carbon accounting. *Limnology and Oceanography Letters* 2(6):195-201.

Manley, S.R., R.J. Orth, L. Ruiz-Montoya. 2015. Roles of dispersal and predation in determining seedling recruitment patterns in a foundational marine angiosperm. *Marine Ecology Progress Series* 533:109-120.

Marbà, N., A. Arias-Ortiz, P. Masqué, G.A. Kendrick, I. Mazarrasa, G.R. Bastyan, J. Garcia-Orellana, C.M. Duarte. 2015. Impact of seagrass loss and subsequent revegetation on carbon sequestration and stocks. *Journal of Ecology* 103:296-302.

Mariotti, G., S. Fagherazzi. 2012. Modeling the effect of tides and waves on benthic biofilms. *Journal of Geophysical Research* 117:G04010.

Mateo, M.A., J. Romero. 1997. Detritus dynamics in the seagrass *Posidonia oceanica*:

elements for an ecosystem carbon and nutrient budget. *Marine Ecology Progress Series* 151:43-53.

Mateo, M.A., J. Cebrián, K. Dunton, T. Mutchler. 2006. Carbon flux in seagrass ecosystems. *In:* A.W.D. Larkum, R.J. Orth, C.M. Duarte (eds.). *Seagrasses: Biology, Ecology and Conservation*. Netherlands: Springer, pp. 159-192.

Matthews, K.M., C. Kim, P. Martin. 2007. Determination of ^{210}Po in environmental materials: A review of analytical methodology. *Applied Radiation and Isotopes* 65(3):267-279.

McGlathery, K. 2013. Above- and below-ground biomass and canopy height of seagrass in Hog Island Bay, VA 2007-2013. Database: LTER Network [Internet]. Available from: https://portal.lternet.edu/nis/mapbrowse?packageid=knb-lter-vcr.183.13 (accessed 25 July 2016).

McGlathery, K.J. 2017A. *Above- and Below-Ground Biomass and Canopy Height of Seagrass in Hog Island Bay and South Bay, VA 2007-2017.* Environmental Data Initiative. http://dx.doi.org/10.6073/pasta/09a0ce35bb3fc72113b5a16ad5b0d6bd. Dataset accessed 3/03/2018.

McGlathery K.J. 2017B. *Carbon and Nitrogen in Seagrass Tissue from Virginia Coastal Bays, 2010-2017.* Environmental Data Initiative. http://dx.doi.org/10.6073/pasta/b4d1f74041d329386591a32e9ea202b2. Dataset accessed 3/03/2018.

McGlathery, K.J., I.C. Anderson, A.C. Tyler. 2001. Magnitude and variability of benthic and pelagic metabolism in a temperate coastal lagoon. *Marine Ecology Progress Series* 216:1-15.

McGlathery, K. J., K. Sundbäck, I.C. Anderson. 2004. The importance of primary producers for benthic nitrogen and phosphorus cycling. *In:* S.L. Nielsen, G.T. Banta, M.F. Pedersen (eds.). *Estuarine Nutrient Cycling: The Influence of Primary Producers*. Netherlands: Kluwer Academic Publishers, pp. 231-261.

McGlathery, K.J., K. Sundback, I.C. Anderson. 2007. Eutrophication in the shallow coastal bays and lagoons: the role of plants in the coastal filter. *Marine Ecology Progress Series* 348:1–18.

McGlathery, K.J., L.K. Reynolds, L.W. Cole, R.J. Orth, S.R. Marion, A. Schwarzschild. 2012. Recovery trajectories during state change from bare sediment to eelgrass dominance. *Marine Ecology Progress Series* 448:209-221.

McGlathery, K.J., M.A. Reidenbach, P. D'Odorico, S. Fagherazzi, M.L. Pace, J.H. Porter. 2013. Nonlinear dynamics and alternative stable states in shallow coastal systems. *Oceanography* 26(3):220-231.

McKew, B.A., A.J. Dumbrell, J.D. Taylor, T.J. McGenity, G.J.C. Underwood. 2013. Differences between aerobic and anaerobic degradation of microphytobenthic biofilm-derived organic matter within intertidal sediments. *FEMS Microbiology Ecology* 84:495-509.

Mcleod, E., G.L. Chmura, S. Bouillon, R. Salm, M. Björk, C.M. Duarte, C.E. Lovelock, W.H.

Schlesinger, B.R. Silliman. 2011. A blueprint for blue carbon: toward an improved understanding of the role of vegetated coastal habitats in sequestering CO_2. *Frontiers in Ecology and the Environment* 9(10):552-560.

Mendez, F.J., I.J. Losada. 1999. Hydrodynamics induced by wind waves in a vegetation field. *Journal of Geophysical Research* 104(C8):18383-18396.

Middelburg, J.J., J. Nieuwenhuize, R.K. Lubberts, O. van de Plassche. 1997. Organic carbon isotope systematics of coastal marshes. *Estuarine, Coastal and Shelf Science* 45:681-687.

Mizerek, T., H.M. Regan, K.A. Hovel. 2011. Seagrass habitat loss and fragmentation influence management strategies for a blue crab *Callinectes sapidus* fishery. *Marine Ecology Progress Series* 427:247-257.

Moore, K.A., J.C. Jarvis. 2008. Environmental factors affecting recent summertime eelgrass diebacks in the Lower Chesapeake Bay: Implications for long-term persistence. *Journal of Coastal Research* 55:135-147.

Moore, K.A., E.C. Shields, D.B. Parrish, R.J. Orth. 2012. Eelgrass survival in two contrasting systems: role of turbidity and summer water temperatures. *Marine Ecology Progress Series* 448:247-258.

Moriarty, D.J.W., P.I. Boon, J.A. Hansen, W.G. Hunt, I.R. Poiner, P.C. Pollard, G.W. Skyring, D.C. White. 1985. Microbial biomass and productivity in seagrass beds. *Geomicrobiology Journal* 4(1):21-51.

Moriarty, D.J.W., R.L. Iverson, P.C. Pollard. 1986. Exudation of organic carbon by the seagrass *Halodule wrightii Aschers* and its effect on bacterial growth in the sediment. *Journal of Experimental Marine Biology and Ecology* 96(2):115-126.

Muehlstein, L.K., D. Porter, F.T. Short. 1991. *Labyrinthula zosterae* sp. nov., the causative agent of wasting disease of eelgrass, *Zostera marina*. *Mycologia* 83(2):180-191.

Murray, B.C., L. Pendleton, W.A. Jenkins, S. Sifleet. 2011. *Green Payments for Blue Carbon: Economic Incentives for Protecting Threatened Coastal Habitats*. Nicholas Institute for Environmental Policy Solutions Report NI R 11-04. Durham, North Carolina: Duke University.

Needelman, B.A., I.M. Emmer, S. Emmett-Mattox, S. Crooks, J.P. Megonigal, D. Myers, M.P.J. Oreska, K.J. McGlathery. (*in review*). The science and policy of the Verified Carbon Standard Methodology for Tidal Wetland and Seagrass Restoration. *Estuaries and Coasts.*

Nellemann, C., E. Corcoran, C.M. Duarte, L. Valdés, C. De Young, L. Fonseca, G. Grimsditch (eds.). 2009. *Blue Carbon: A Rapid Response Assessment*. United Nations Environment Programme, GRID-Arendal.

Neubauer, S.C., J.P. Megonigal. 2015. Moving beyond global warming potentials to quantify the climatic role of ecosystems. *Ecosystems* 18:1000-1013.

Oakes, J.M., R.M. Connolly. 2004. Causes of sulfur isotope variability in the seagrass, *Zostera capricorni*. *Journal of Experimental Marine Biology and Ecology* 302:153-164.

Oakes, J.M., B.M.A. Eyre. 2014. Transformation and fate of microphytobenthos carbon in subtropical, intertidal sediments: potential for long-term carbon retention revealed by ^{13}C-labeling. *Biogeoscience* 11:1927-1940.

Oremland, R.S. 1975. Methane production in shallow-water, tropical marine sediments. *Applied and Environmental Microbiology* 30(4):602-608.

Oreska, M.P.J., B. Truitt, R.J. Orth, M.W. Luckenbach. 2017. The bay scallop (*Argopecten irradians*) industry collapse in Virginia and its implications for the successful management of scallop-seagrass habitats. *Marine Policy* 75:116-124.

Orth, R.J., K.J. McGlathery. 2012. Eelgrass recovery in the coastal bays of the Virginia Coast Reserve, USA. *Marine Ecology Progress Series* 448:173-176.

Orth, R.J., T.J.B. Carruthers, W.C. Dennison, C.M. Duarte, J.W. Fourqurean, K.L. Heck, A.R. Hughes, G.A. Kendrick, W.J. Kenworthy, S. Olyarnik, F.T. Short, M. Waycott, S.L. Williams. 2006A. A global crisis for seagrass ecosystems. *BioScience* 56(12):987-996.

Orth, R.J., M.L. Luckenbach, S.R. Marion, K.A. Moore, D.J. Wilcox. 2006B. Seagrass recovery in the Delmarva Coastal Bays, USA. *Aquatic Botany* 84:26–36.

Orth, R.J., S.R. Marion, K.A. Moore, D.J. Wilcox. 2010. Eelgrass (*Zostera marina* L.) in the Chesapeake Bay Region of Mid-Atlantic Coast of the USA: Challenges in Conservation and Restoration. *Estuaries and Coasts* 33:139-150.

Orth, R.J., K.A. Moore, S.R. Marion, D.J. Wilcox, D.B. Parrish. 2012. Seed addition facilitates eelgrass recovery in a coastal bay system. *Marine Ecology Progress Series* 448:177-195.

Orth, R.J., D.J. Wilcox, J.R. Whiting, A.K. Kenne, L. Nagey, E.R. Smith. 2016. 2015

Distribution of Submerged Aquatic Vegetation in the Chesapeake Bay and Coastal Bays. VIMS Special Scientific Report Number 159. Final report to EPA,Chesapeake Bay Program, Annapolis, MD. Grant No CB96321901-0, http://www.vims.edu/bio/sav/sav15 (accessed 25 March 2018).

Paling E.I., M. Fonseca, M.M. van Katwijk, M. van Keulen. 2009. Seagrass restoration. *In:* G.M.E. Perillo, E. Wolanski, D.R. Cahoon, M. Brinson (eds.). *Coastal Wetlands: An Integrated Ecosystems Approach*. Amsterdam: Elsevier, pp. 687–713.

Pendleton, L., D.C. Donato, B.C. Murray, S. Crooks, W.A. Jenkins, S. Sifleet, C. Craft, J.W. Fourqurean, J.B. Kauffman, N. Marbà, P. Megonigal, E. Pidgeon, D. Herr, D. Gordon, A. Baldera. 2012. Estimating global “blue carbon” emissions from conversion and degradation of vegetated coastal ecosystems. *PLoS ONE* 7(9):e43542.

Poffenbarger, H.J., B.A. Needelman, J.P. Megonigal. 2011. Salinity influence on methane emissions from tidal marshes. *Wetlands* 31:831-842.

Pollard, P.C., D.J.W. Moriarty. 1991. Organic carbon decomposition, primary and bacterial productivity, and sulphate reduction, in tropical seagrass beds of the Gulf of Carpentaria, Australia. *Marine Ecology Progress Series* 69:149-159.

R Core Team. 2017. R: The R Project for Statistical Computing. Available at: https://www.r-project.org (accessed 5 October 2017).

Regnier, P., P. Friedlingstein, P. Ciais, F.T. Mackenzie, N. Gruber, I.A. Janssens, G.G. Laruelle, R. Lauerwald, S. Luyssaert, A.J. Andersson, S. Arndt, C. Arnosti, A.V. Borges, A.W. Dale, A. Gallego-Sala, Y. Goddéris, N. Goossens, J. Hartmann, C.

Heinze, T. Ilyina, F. Joos, D.E. LaRowe, J. Leifeld, F.J.R. Meysman, G. Munhoven, P.A. Raymond, R. Spahni, P. Suntharalingam, M. Thullner. 2013. Anthropogenic perturbation of the carbon fluxes from land to ocean. *Nature Geoscience* 6:597-607.

Reidenbach, M., R. Timmerman. 2014. Wind speed and direction on Godwin Island, 2013-2014. Database: LTER Network [Internet]. Available from: http://dx.doi.org/10.6073/pasta/0d07604a03d09e327abbe2b81e44ac11 (accessed 24 February 2016).

Reynolds, L.K., M. Waycott, K.J. McGlathery, R.J. Orth. 2016. Ecosystem services returned through seagrass restoration. *Restoration Ecology* 24(5):583-588.

Rheuban, J.E. 2013. Oxygen metabolism in restored eelgrass (*Zostera marina L.*) meadows measured by eddy correlation. Thesis submitted to the University of Virginia. 143p.

Rheuban, J.E., P. Berg, K.J. McGlathery. 2014. Ecosystem metabolism along a colonization gradient of eelgrass (*Zostera marina*) measured by eddy correlation. *Limnology and Oceanography* 59(4):1376-1387.

Ricart, A.M., P.H. York, M.A. Rasheed, M. Pérez, J. Romero, C.V. Bryant, P.I. Macreadie. 2015. Variability of sedimentary organic carbon in patch seagrass landscapes. *Marine Pollution Bulletin* 100(1):476-482.

Richardson, D., J. Porter, G. Oertel, R. Zimmerman, C. Carlson, K. Overman. 2014. Integrated topography and bathymetry for the Eastern Shore of Virginia. Database: LTER Network [Internet]. Available from:

http://dx.doi.org/10.6073/pasta/0d07604a03d09e327abbe2b81e44ac11 (accessed 12 January 2016).

Riera, P., P. Richard. 1996. Temporal variation of δ^{13}C in particulate organic matter and oyster *Crassostrea gigas* in Marennes-Oléron Bay (France): effect of freshwater inflow. *Marine Ecology Progress Series* 147:105-115.

Robinson, O., S. Kemp, I. Williams. 2015. Carbon management at universities: a reality check. *Journal of Cleaner Production* 106:109-118.

Robinson, L.M., J. Elith, A.J. Hobday, R.G. Pearson, B.E. Kendall, H.P. Possingham, A.J. Richardson. 2011. Pushing the limits in marine species distribution modelling: lessons from the land present challenges and opportunities. *Global Ecology and Biogeography* 20:789-802.

Röhr, M.E., C. Boström, P. Canal-Vergés, M. Holmer. 2016. Blue carbon stocks in Baltic Sea eelgrass (*Zostera marina*) meadows. *Biogeosciences* 13:6139-6153.

Rohweder, J., J.T. Rogala, B.L. Johnson, D. Anderson, S. Clark, F. Chamberlin, K. Runyon. 2008. Application of wind fetch and wave models for habitat rehabilitation and enhancement projects: U.S. Geological Survey Open-File Report 2008-1200. 43p.

Rozaimi, M., M. Fairoz, T. M. Hakimi, N. H. Hamdan, R. Omar, M. M. Ali, S. A. Tahirin. 2017. Carbon stores from a tropical seagrass meadow in the midst of anthropogenic disturbance. *Marine Pollution Bulletin* 119:253-260.

Russell, M., H. Greening. 2015. Estimating benefits in a recovering estuary: Tampa Bay, Florida. *Estuaries and Coasts* 38(Suppl 1):S9-S18.

Safak, I., P.L. Wiberg, D.L. Richardson, M.O. Kurum. 2015. Controls on residence time and exchange in a system of shallow coastal bays. *Continental Shelf Research* 97:7-20.

Samper-Villarreal, J., C.E. Lovelock, M.I. Saunders, C. Roelfsema, P.J. Mumby. 2016. Organic carbon in seagrass sediments is influenced by seagrass canopy complexity, turbidity, wave height, and water depth. *Limnology and Oceanography* 61:938-952.

Sanchez-Cabeza, J.A., A.C. Ruiz-Fernández. 2012. ^{210}Pb sediment radiochronology: An integrated formulation and classification of dating models. *Geochimica et Cosmochimica Acta* 82:183-200.

Sansone, F.J., T.M. Rust, S.V. Smith. 1998. Methane distribution and cycling in Tomales Bay, California. *Estuaries* 21(1):66-77.

Schmidt, A.L., M. Coll, T.N. Romanuk, H.K. Lotze. 2011. Ecosystem structure and services in eelgrass *Zostera marina* and rockweed *Ascophyllum nodosum* habitats. *Marine Ecology Progress Series* 437:51-68.

Serrano, O., M.A. Mateo, P. Renom, R. Julià. 2012. Characterization of soils beneath a *Posidonia oceanica* meadow. *Geoderma* 185-186:26-36.

Serrano, O., A.M. Ricart, P.S. Lavery, M.A. Mateo, A. Arias-Ortiz, P. Masque, A. Steven, C.M. Duarte. 2015. Key biogeochemical factors affecting soil carbon storage in *Posidonia* meadows. *Biogeosciences Discussions* 12:18913-18944.

Shieh, W.Y., J.T. Yang. 1997. Denitrification in the rhizosphere of the two seagrasses *Thalassia hemprichii* (Ehrenb.) Aschers and *Halodule uninervis* (Forsk.) Aschers. *Journal of Experimental Marine Biology and Ecology* 218:229-241.

Short, F.T., R.C. Davis, B.S. Kopp, C.A. Short, D.M. Burdick. 2002. Site-selection model for optimal transplantation of eelgrass *Zostera marina* in the northeastern US. *Marine Ecology Progress Series* 227:253-267.

Smith, S.V. 1981. Marine macrophytes as a global carbon sink. *Science* 211(4484):838-840.

State of California. 2016. California Ocean Protection Act. Public Resources Code § 35500.

Suding, K.N. 2011. Toward an era of restoration in ecology: Successes, failures, and opportunities ahead. *Annual Review of Ecology, Evolution, and Systematics* 42:465-487.

Thomas, E. 2014. Influence of *Zostera marina* on wave dynamics, sediment suspension, and bottom boundary layer development within a shallow coastal bay. Thesis submitted to the University of Virginia. 146p.

Thorhaug, A., H.M. Poulos, L. López-Portillo, T.C.W. Ku, G.P. Berlyn. 2017. Seagrass blue carbon dynamics in the Gulf of Mexico: Stocks, losses from anthropogenic disturbance, and gains through seagrass restoration. *Science of the Total Environment* 605-6:626-636.

Timmerman, R. 2014. Biophysical controls on sediment suspension in a shallow coastal bay. Thesis submitted to the University of Virginia. 90p.

Tokoro, T., S. Hosokawa, E. Miyoshi, K. Tada, K. Watanabe, S. Montain, H. Kayanne, T. Kuwae. 2014. Net uptake of atmospheric CO2 by coastal submerged aquatic vegetation. *Global Change Biology* 20(6):1873-1884.

Truitt, B., J. Wesson (comps.). 1997. Captain B. L. Berlie Bell interview transcript. Available at the Barrier Island Center, Machipongo, VA.

Tyler, A.C., K.J. McGlathery, I.C. Anderson. 2001. Macroalgae mediation of dissolved organic nitrogen fluxes in a temperate coastal lagoon. *Estuarine, Coastal and Shelf Science* 53:155-168.

Tzortziou, M., P.J. Neale, J.P. Megonigal, C.L. Pow, M. Butterworth. 2011. Spatial gradients in dissolved carbon due to tidal marsh outwelling into a Chesapeake Bay estuary. *Marine Ecology Progress Series* 426:41-56.

United Nations Environment Programme (UNEP). 2018. Coastal zone management. Available at: https://www.unenvironment.org/explore-topics/oceans-seas/what-we-do/working-regional-seas/coastal-zone-management (accessed 11 March 2018).

United Nations Framework Convention on Climate Change (UNFCCC). 2007. Agenda item 4: Report of the co-facilitators of the dialogue on long-term cooperative action to address climate change by enhancing implementation of the Convention. FCCC/CP/2007/L.7/Rev.1. Available at: http://unfccc.int/files/meetings/cop_13/application/pdf/cp_bali_act_p.pdf (accessed 11 March 2018).

United Nations Framework Convention on Climate Change (UNFCCC). 2017. Global Warming Potentials. Available at: http://unfccc.int/ghg_data/items/3825.php (accessed 3 March 2018).

United Nations Reducing Emissions from Deforestation and forest Degradation (UN-

REDD). 2017. UN-REDD Programme. Available at: http://www.unredd.net/about/un-redd-programme.html (accessed 11 March 2018).

United States Department of Energy (DOE). 2015. How much CO2 does each country from COP21 produce? Available at: https://www.energy.gov/articles/interactive-how-much-carbon-do-countries-emit (accessed 11 March 2018).

United States Environmental Protection Agency (EPA). 2017. The social cost of carbon: Estimating the benefits of reducing greenhouse gas emissions. Available at: http://19january2017snapshot.epa.gov/climatechange/social-cost-carbon_.html (accessed 20 Feb 2018).

Valle, M., Á. Borja, G. Chust, I. Galparsoro, J.M. Garmendia. 2011. Modelling suitable estuarine habitats for *Zostera noltii*, using Ecological Niche Factor Analysis and Bathymetric LiDAR. *Estuarine, Coastal and Shelf Science* 94:144-154.

Valle, M., M.M. van Katwijk, D.J. de Jong, T.J. Bouma, A.M. Schipper, G. Chust, B.M. Benito, J.M. Garmendia, Á. Borja. 2013. Comparing the performance of species distribution models of *Zostera marina*: Implications for conservation. *Journal of Sea Research* 83:56-64.

Valle, M., G. Chust, A. del Campo, M.S. Wisz, S.M. Olsen, J.M. Garmendia, Á. Borja. 2014. Projecting future distribution of the seagrass *Zostera noltii* under global warming and sea level rise. *Biological Conservation* 170:74-85.

van Katwijk, M.M., A.R. Bos, V.N. de Jonge, L.S.A.M. Hanssen, D.C.R. Hermus, D.J. de

Jong. 2009. Guidelines for seagrass restoration: Importance of habitat selection and donor population, spreading of risks, and ecosystem engineering effects. *Marine Pollution Bulletin* 58:179-188.

van Katwijk, M.M., A. Thorhaug, N. Marbà, R.J. Orth, C.M. Duarte, G.A. Kendrick, I.H.J. Althuizen, E. Balestri, G. Bernard, M.L. Cambridge, A. Cunha, C. Durance, W. Giesen, Q. Han, S. Hosokawa, W. Kiswara, T. Komatsu, C. Lardicci, K.-S. Lee, A. Meinesz, M. Nakaoka, K.R. O'Brien, E.I. Paling, C. Pickerell, A.M.A. Ransijn, J.J. Verduin. 2016. Global analysis of seagrass restoration: the importance of large-scale planting. *Journal of Applied Ecology* 53:567-578.

Vaughan, I.P., S.J. Ormerod. 2005. The continuing challenges of testing species distribution models. *Journal of Applied Ecology* 42:720-732.

Verified Carbon Standard (VCS). 2012. AFOLU Non-Permanence Risk Tool VCS Version 3 Procedural Document v3.3 Available at http://database.v-c-s.org/program-documents/afolu-non-permanence-risk-tool-v33 (accessed 5 Dec 2017).

Verified Carbon Standard (VCS). 2015. Mangrove restoration and coastal greenbelt protection in the East coast of Aceh and North Sumatra Province, Indonesia. VCS Project ID 1493. Available at: http://www.vcsprojectdatabase.org/#/project_details/1493 (accessed 11 March 2018).

Verified Carbon Standard (VCS). 2015. Methods for stratification of the project area (X-

STR). VMD0016. 2015. Available from: http://database.v-c-s.org/sites/vcs.benfredaconsulting.com/files/VMD0016%20X-STR,%20v1.0%20(valid%20until%209%20September%202015).pdf

Verified Carbon Standard (VCS). 2017. *Agriculture, Forestry, and Other Land Use (AFOLU) Requirements. VCS Version 3 Requirements Document*. Verified Carbon Standard, Washington, D.C.

Verified Carbon Standard (VCS). 2018. VCS Project Database. Available at: http://vcsprojectdatabase.org/ (accessed 1 March 2018).

Virginia Institute of Marine Science (VIMS). 2014. SAV in Chesapeake Bay and Coastal Bays. Database: Maps and Data [Internet]. Available from: http://web.vims.edu/bio/sav/ (accessed 19 November 2014).

Virginia Institute of Marine Science (VIMS). 2016. SAV in Chesapeake Bay and Coastal Bays. Available at: http://web.vims.edu/ bio/sav/ (accessed 12 December 2016).

Volkman, J.K., A.T. Revill, D.G. Holdsworth, D. Fredericks. 2008. Organic matter sources in an enclosed coastal inlet assessed using lipid biomarkers and stable isotopes. *Organic Geochemistry* 39:689-710.

Waycott, M., C.M. Duarte, T.J.B. Carruthers, R.J. Orth, W.C. Dennison, S. Olyarnik, A. Calladine, J.W. Fourqurean, K.L. Heck, A.R. Hughes, G.A. Kendrick, W.J. Kenworthy, F.T. Short, S.L. Williams. 2009. Accelerating loss of seagrass across the globe threatens coastal ecosystems. *Proceedings of the National Academy of Sciences* 106(30):12377–12381.

Welsh, D., M. Bartoli, D. Nizzoli, G. Castaldelli, S.A. Riou, P. Viaroli. 2000.

Denitrification, nitrogen fixation, community primary productivity and inorganic-N and oxygen fluxes in an intertidal *Zostera noltii* meadow. *Marine Ecology Progress Series* 208:65-77.

Wiberg, P.L., J.A. Carr, I. Safak, A. Anutaliya. 2015. Quantifying the distribution and influence of non-uniform bed properties in shallow coastal bays. *Limnology and Oceanography: Methods* 13:746-762.

Widdows, J., N.D. Pope, M.D. Brinsley, H. Asmus, R.M. Asmus. 2008. Effects of seagrass beds (*Zostera noltii* and *Z. marina*) on near-bed hydrodynamics and sediment resuspension. *Marine Ecology Progress Series* 358:125-136.

York, P.H., R.K. Gruber, R. Hill, P.J. Ralph, D.J. Booth, P.I. Macreadie. 2013. Physiological and morphological responses of the temperate seagrass *Zostera muelleri* to multiple stressors: Investigating the interactive effects of light and temperature. *PLoS ONE* 8(10):e76377.

Zhang, X., D. Tang, Z. Li, Z. Yan, F. Zhang. 2010. Analysis of the spatio-temporal distribution of chlorophyll-α in the eastern Indian Ocean near the time of the 2004 South Asian tsunami. *International Journal of Remote Sensing* 31(17-18):4579-4593.

Zimmerman, R.C., V.J. Hill, C.L. Gallegos. 2015. Predicting effects of ocean warming, acidification, and water quality on Chesapeake region eelgrass. *Limnology and Oceanography* 60:1781-1804.

Zonneveld, K.A.F., G.J.M. Versteegh, S. Kasten, T.I. Eglinton, K.-C. Emeis, C. Huguet, B.P.

Koch, G. J. de Lange, J.W. de Leeuw, J.J. Middelburg, G. Mollenhauer, F.G. Prahl, J. Rethemeyer, S.G. Wakeham. 2010. Selective preservation of organic matter in marine environments; processes and impact on the sedimentary record. *Biogeosciences* 7:483-511.

Zupo, V., L. Mazzella, M.C. Buia, M.C. Gambi, M. Lorenti, M.B. Scipione, G. Cancemi. 2006. A Small-scale analysis of the spatial structure of a *Posidonia oceanic* meadow off the Island of Ischia (Gulf of Naples, Italy): Relationship with the seafloor morphology. *Aquatic Botany* 84:101-109.

Appendix I. Kriging methods

Supplemental spatial statistics for maps presented in chapters 3, 4, and 5

Data were interpolated using kriging in ArcGIS 10.2 Geostatistical Analyst (10 m cell size). Stable, circular, spherical, exponential, and Gaussian semivariogram models were fit to each data set and cross-validated by comparing root mean square errors (RMSE). Isotropy and anisotropy were also evaluated for each model fit. Minor differences in RMSEs were noted in select cases, but interpolated maps were broadly consistent for different model types. Data transformations were considered but not necessary to generate kriged distributions.

Variogram cross-validation:

Table A1.1. RMSE for 0-3 cm interval variogram models (chapter 3).

Model	Direction	Bulk C	Inorg. C	%OM	C:N
Stable	Isotropic	6.55E-04	1.24E-04	3.15E-01	3.94E+00
	Anisotropic	7.21E-04	1.16E-04	3.24E-01	4.38E+00
Circular	Isotropic	6.61E-04	1.13E-04	3.21E-01	3.91E+00
	Anisotropic	6.76E-04	1.12E-04	3.27E-01	4.05E+00
Spherical	Isotropic	6.58E-04	1.13E-04	3.20E-01	3.90E+00
	Anisotropic	6.68E-04	1.13E-04	3.24E-01	4.03E+00
Exponential	Isotropic	6.57E-04	1.24E-04	3.25E-01	3.93E+00
	Anisotropic	6.74E-04	1.18E-04	3.37E-01	4.04E+00
Gaussian	Isotropic	6.95E-04	1.12E-04	3.19E-01	4.33E+00
	Anisotropic	7.21E-04	1.14E-04	3.24E-01	4.38E+00

Table A1.2. RMSE for 3-6 cm interval variogram models (chapter 3).

Model	Direction	Bulk C	Inorg. C	%OM	C:N
Stable	Isotropic	1.03E-03	1.82E-04	3.28E-01	6.07E+00
	Anisotropic	9.21E-04	1.89E-04	3.33E-01	6.15E+00
Circular	Isotropic	9.65E-04	1.82E-04	3.33E-01	5.81E+00
	Anisotropic	9.83E-04	1.90E-04	3.36E-01	5.67E+00
Spherical	Isotropic	9.70E-04	1.83E-04	3.30E-01	5.70E+00
	Anisotropic	9.82E-04	1.90E-04	3.33E-01	5.64E+00
Exponential	Isotropic	9.75E-04	1.83E-04	3.39E-01	5.63E+00
	Anisotropic	9.85E-04	1.90E-04	3.48E-01	5.69E+00
Gaussian	Isotropic	8.86E-04	1.82E-04	3.23E-01	6.11E+00
	Anisotropic	9.16E-04	1.89E-04	3.33E-01	6.17E+00

Table A1.3. RMSE for 6-9 cm interval variogram models (chapter 3).

Model	Direction	Bulk C	Inorg. C	%OM	C:N
Stable	Isotropic	9.88E-04	1.58E-04	3.06E-01	8.40E+00
	Anisotropic	1.12E-03	1.47E-04	3.20E-01	9.31E+00
Circular	Isotropic	9.92E-04	1.60E-04	3.09E-01	8.58E+00
	Anisotropic	1.11E-03	1.48E-04	3.28E-01	9.21E+00
Spherical	Isotropic	9.88E-04	1.61E-04	3.09E-01	8.55E+00
	Anisotropic	1.08E-03	1.48E-04	3.43E-01	9.15E+00
Exponential	Isotropic	1.00E-03	1.58E-04	3.33E-01	8.42E+00
	Anisotropic	1.06E-03	1.50E-04	3.40E-01	9.29E+00
Gaussian	Isotropic	9.95E-04	1.58E-04	3.08E-01	8.43E+00
	Anisotropic	1.20E-03	1.47E-04	3.20E-01	9.20E+00

Table A1.4. RMSE for 9-12 cm interval variogram models (chapter 3).

Model	Direction	Bulk C	Inorg. C	%OM	C:N
Stable	Isotropic	8.55E-04	1.69E-04	2.53E-01	9.57E+00
	Anisotropic	1.04E-03	1.69E-04	2.61E-01	1.04E+01
Circular	Isotropic	8.67E-04	1.69E-04	2.46E-01	9.58E+00
	Anisotropic	9.54E-04	1.69E-04	2.51E-01	1.03E+01
Spherical	Isotropic	8.64E-04	1.69E-04	2.47E-01	9.61E+00
	Anisotropic	9.20E-04	1.69E-04	2.50E-01	1.07E+01
Exponential	Isotropic	8.60E-04	1.69E-04	2.44E-01	9.62E+00
	Anisotropic	8.67E-04	1.69E-04	2.48E-01	1.02E+01
Gaussian	Isotropic	9.25E-04	1.69E-04	2.55E-01	9.57E+00
	Anisotropic	1.07E-03	1.69E-04	2.61E-01	1.03E+01

Table A1.5. RMSE for other variable variogram models (chapter 3).

Model	Direction	Density	Mean Grain Size	% Sand Fraction
Stable	Isotropic	1.93E+02	1.37E+01	9.18E+00
	Anisotropic	1.59E+02	1.38E+01	8.67E+00
Circular	Isotropic	1.94E+02	1.43E+01	8.37E+00
	Anisotropic	1.53E+02	1.35E+01	7.99E+00
Spherical	Isotropic	1.90E+02	1.43E+01	8.36E+00
	Anisotropic	1.59E+02	1.38E+01	8.01E+00
Exponential	Isotropic	1.87E+02	1.49E+01	8.68E+00
	Anisotropic	1.67E+02	1.42E+01	8.10E+00
Gaussian	Isotropic	1.94E+02	1.37E+01	1.03E+01
	Anisotropic	1.63E+02	1.38E+01	8.67E+00

Table A1.6. RMSE for 2014 C_{org} and stable isotope data (chapter 4).

Model	Direction	2014_Corg	δ13C	δ15N	δ34S
Stable	Isotropic	1.57E+00	7.17E-01	4.44E-01	1.51E+00
	Anisotropic	1.11E+00	7.28E-01	4.96E-01	1.65E+00
Circular	Isotropic	1.11E+00	6.97E-01	4.43E-01	1.52E+00
	Anisotropic	1.00E+00	6.52E-01	4.97E-01	1.67E+00
Spherical	Isotropic	1.11E+00	6.96E-01	4.45E-01	1.49E+00
	Anisotropic	9.92E-01	6.50E-01	4.95E-01	1.64E+00
Exponential	Isotropic	1.12E+00	6.99E-01	4.51E-01	1.50E+00
	Anisotropic	1.00E+00	6.28E-01	4.93E-01	1.62E+00
Gaussian	Isotropic	1.57E+00	6.74E-01	4.44E-01	1.51E+00
	Anisotropic	1.11E+00	7.28E-01	4.96E-01	1.64E+00

Table A1.7. RMSE for chapter 5 stock change distribution maps (Figure 5.3); AVG_half = the background SOC concentration was deducted from the meadow profile interval above the reference plane and below the accreted interval; AVG_net = the background SOC concentration was deducted from the entire meadow profile (including the accreted interval); CA = the accreted interval in 2016, relative to 2013; ABG = aboveground biomass.

Model	Direction	2013 AVG	2013 AVG_half	2013 AVG_net	CA 2016	CA 2016_net	2016 12cm_AVG	2016 AVG_half	2016 AVG_net	AGB
Stable	Isotropic	1.47E-03	1.47E-03	1.47E-03	1.95E-03	1.95E-03	1.74E-03	1.78E-03	1.76E-03	1.41E-03
	Anisotropic	1.55E-03	1.55E-03	1.55E-03	1.91E-03	1.91E-03	1.71E-03	1.78E-03	1.73E-03	1.43E-03
Circular	Isotropic	1.43E-03	1.43E-03	1.43E-03	2.00E-03	2.00E-03	1.74E-03	1.78E-03	1.76E-03	1.41E-03
	Anisotropic	1.50E-03	1.50E-03	1.50E-03	2.01E-03	2.01E-03	1.72E-03	1.77E-03	1.74E-03	1.39E-03
Spherical	Isotropic	1.44E-03	1.44E-03	1.44E-03	1.99E-03	1.99E-03	1.74E-03	1.78E-03	1.76E-03	1.41E-03
	Anisotropic	1.54E-03	1.54E-03	1.54E-03	2.01E-03	2.01E-03	1.71E-03	1.79E-03	1.73E-03	1.39E-03
Exp.ial	Isotropic	1.45E-03	1.45E-03	1.45E-03	1.92E-03	1.92E-03	1.75E-03	1.78E-03	1.76E-03	1.42E-03
	Anisotropic	1.41E-03	1.41E-03	1.41E-03	1.91E-03	1.91E-03	1.75E-03	1.79E-03	1.73E-03	1.35E-03
Gaussian	Isotropic	1.45E-03	1.45E-03	1.45E-03	1.99E-03	1.99E-03	1.74E-03	1.78E-03	1.76E-03	1.41E-03
	Anisotropic	1.55E-03	1.55E-03	1.55E-03	1.99E-03	1.99E-03	1.71E-03	1.78E-03	1.73E-03	1.43E-03

Variograms:

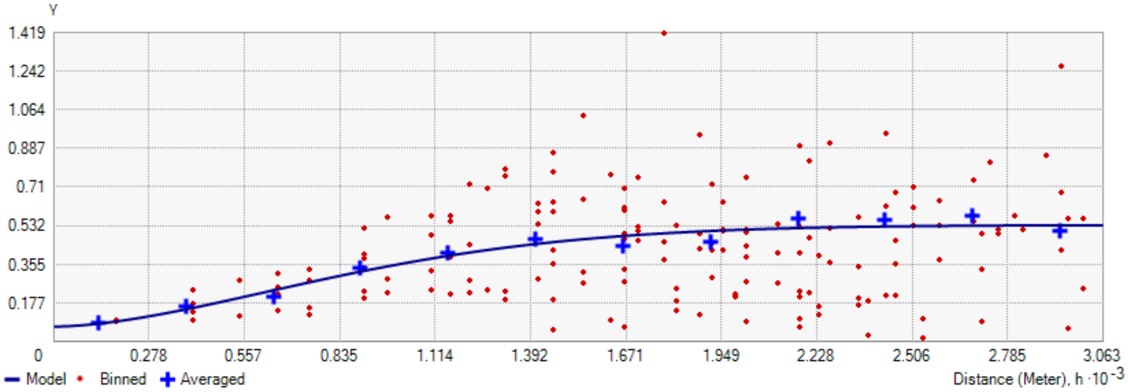

Figure A1.1A. % OM, A interval (Ordinary kriging, Stable model, Isotropic); Nugget = 0.0687; Major range = 1981.064; Partial sill = 0.467 (chapter 3).

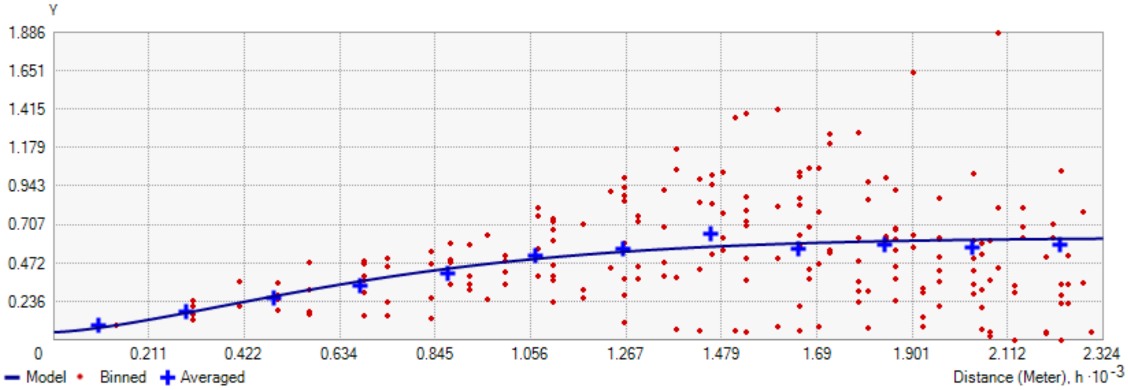

Figure A1.1B. % OM, B interval (Ordinary kriging, Stable model, Isotropic); Nugget = 0.0470; Major range = 1720.767; Partial sill = 0.579 [Note: Gaussian model gave a lower RMSE but a slightly larger 'nugget effect'] (chapter 3).

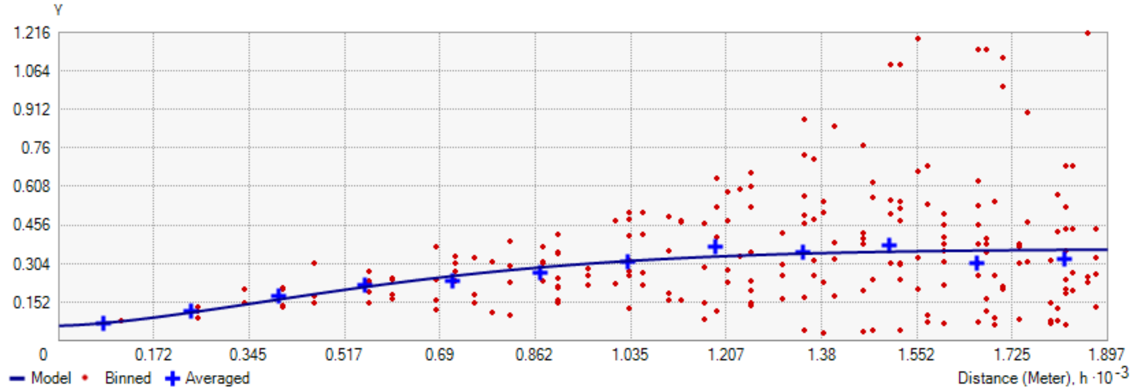

Figure A1.1C. % OM, C interval (Ordinary kriging, Stable model, Isotropic); Nugget = 0.0591; Major range = 1399.775; Partial sill = 0.302 (chapter 3).

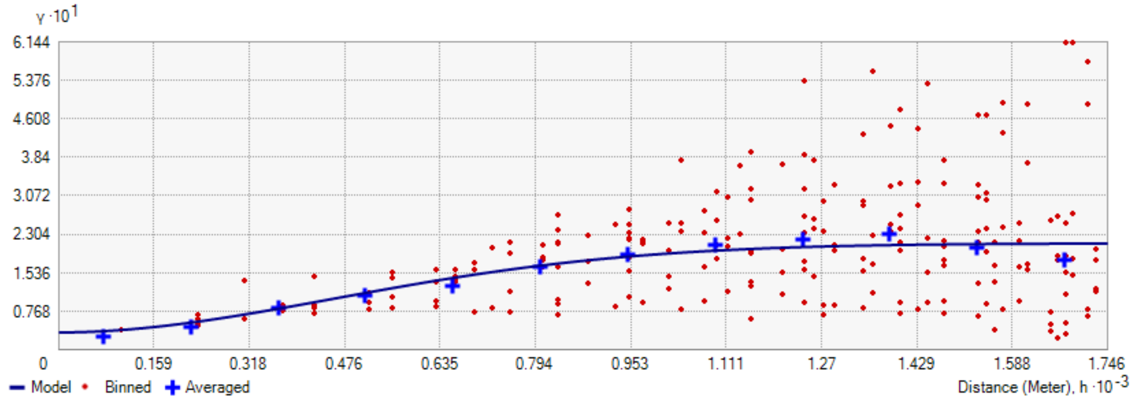

Figure A1.1D. % OM, D interval (Ordinary kriging, Stable model, Isotropic); Nugget = 0.0349; Major range = 1202.317; Partial sill = 0.179 [Note: Exponential model gave a lower RMSE and 'nugget effect'] (chapter 3).

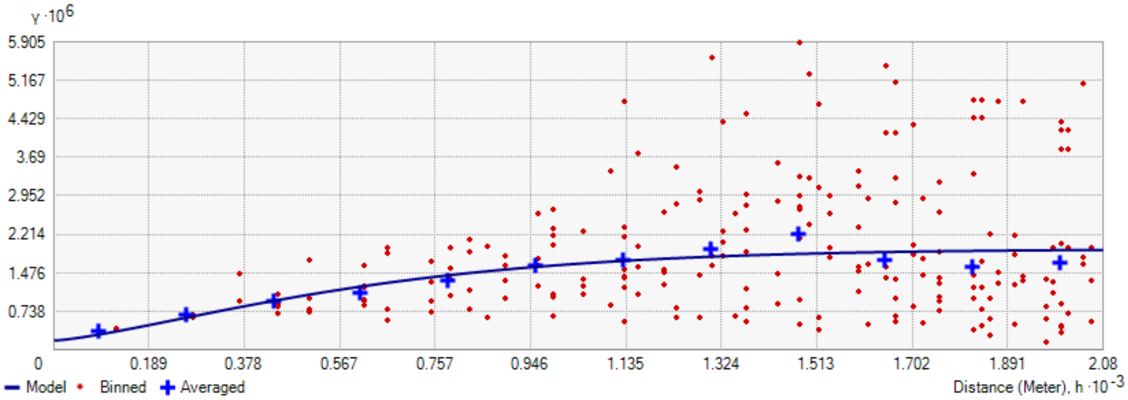

Figure A1.2A. Bulk C, A interval (Ordinary kriging, Stable model, Isotropic) Nugget = 1.772e-7; Major range = 1500.913; Partial sill = 1.755e-6 (chapter 3).

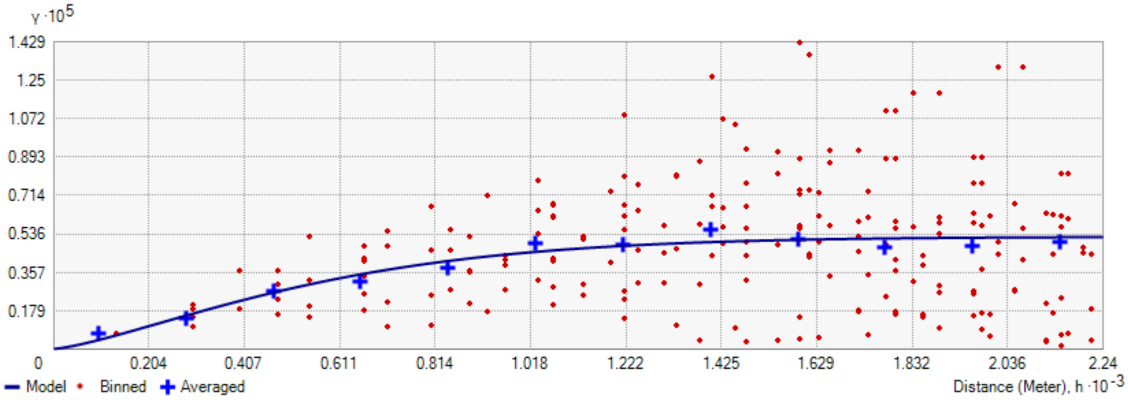

Figure A1.2B. Bulk C, B interval (Ordinary kriging, Stable model, Isotropic); Nugget = 2.294e-8; Major range = 1387.756; Partial sill = 5.209e-6 [Note: Gaussian model gave a lower RMSE but a slightly larger 'nugget effect'] (chapter 3).

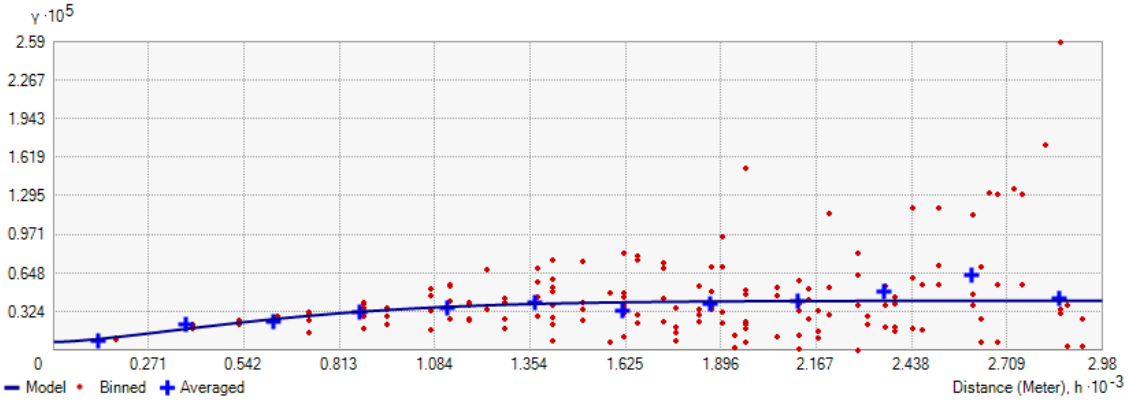

Figure A1.2C. Bulk C, C interval (Ordinary kriging, Stable model, Isotropic); Nugget = 6.637e-7; Major range = 1518.038; Partial sill = 3.467e-6 (chapter 3).

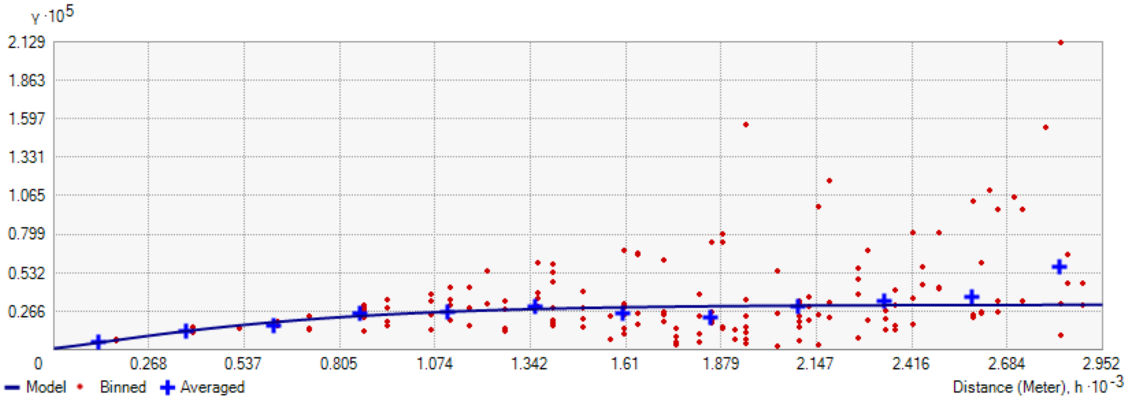

Figure A1.2D. Bulk C, D interval (Ordinary kriging, Stable model, Isotropic); Nugget = 1.052e-7; Major range = 1686.695; Partial sill = 3.007e-6 (chapter 3).

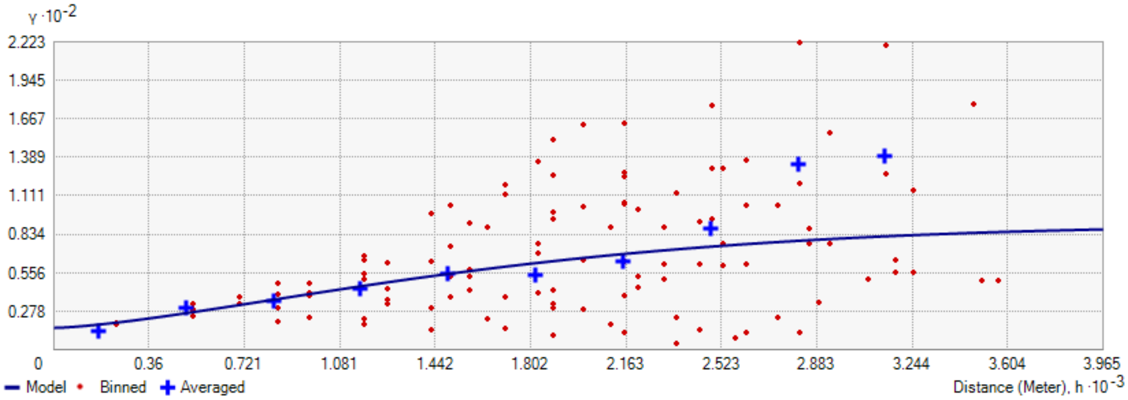

Figure A1.3A. Bulk C:N, A interval (Ordinary kriging, Stable model, Isotropic); Nugget = 15.798; Major range = 3964.666; Partial sill = 74.845 [Note: Spherical model gave a lower RMSE] (chapter 3).

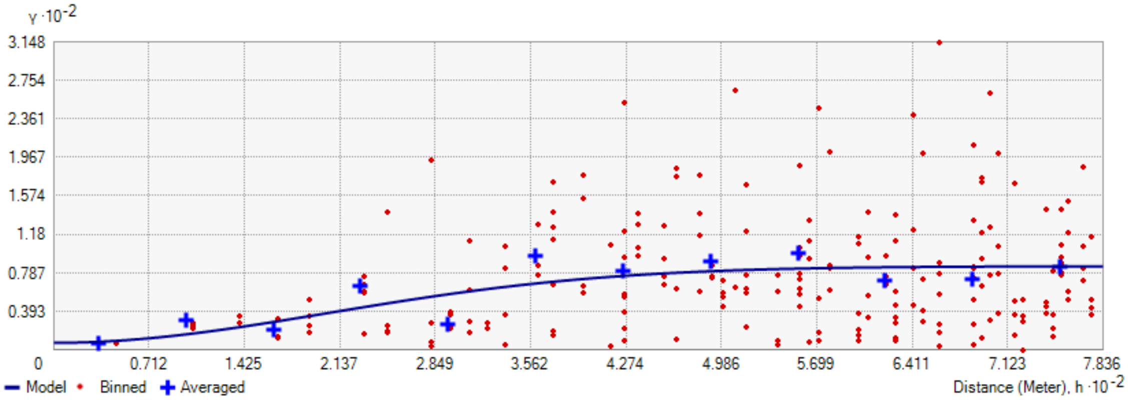

Figure A1.3B. Bulk C:N, B interval (Ordinary kriging, Stable model, Isotropic); Nugget = 7.044; Major range = 513.185; Partial sill = 78.283 [Note: Exponential model gave a lower RMSE] (chapter 3).

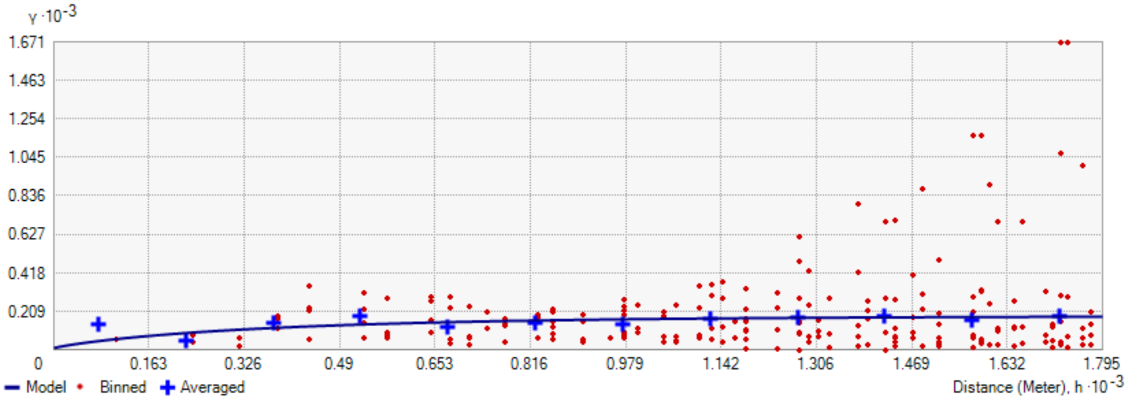

Figure A1.3C. Bulk C:N, C interval (Ordinary kriging, Stable model, Isotropic); Nugget = 9.045; Major range = 1336.166; Partial sill = 173.7842 (chapter 3).

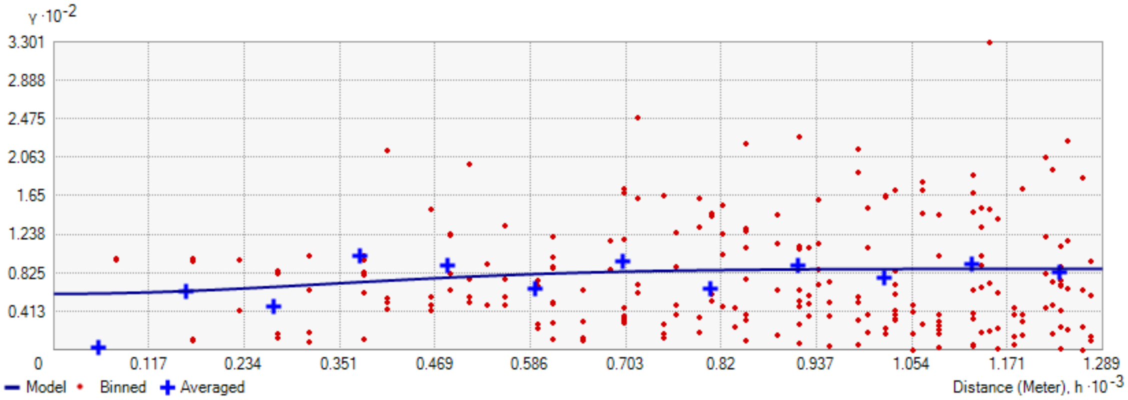

Figure A1.3D. Bulk C:N, D interval (Ordinary kriging, Stable model, Isotropic); Nugget = 59.937; Major range = 820.958; Partial sill = 26.822 (chapter 3).

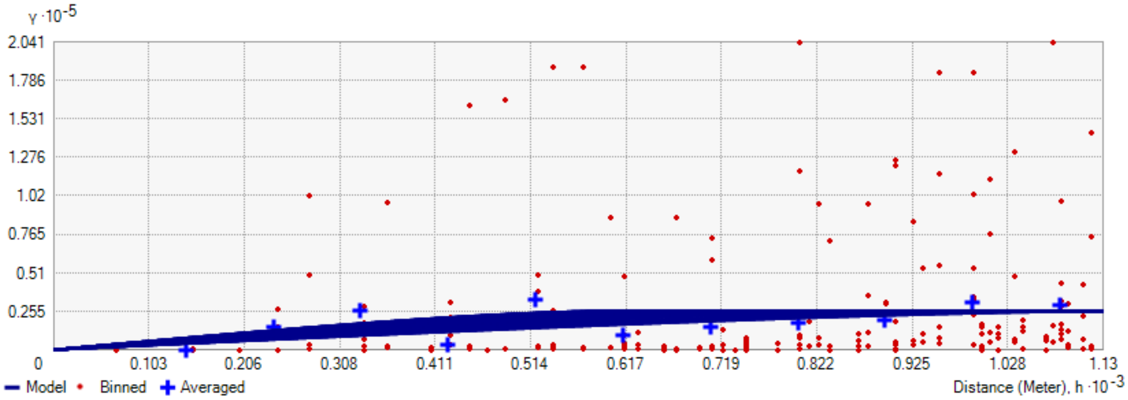

Figure A1.4. Shoot density (Ordinary kriging, Circular model, Anisotropic); Nugget = 0; Major range = 1130.374; Partial sill = 25511.45 (chapter 3).

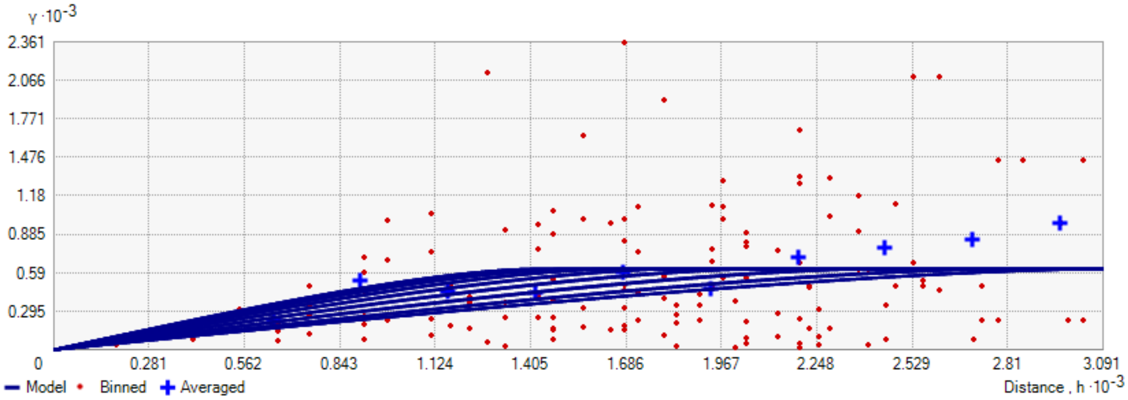

Figure A1.5. Mean GS (Ordinary kriging, Circular model, Anisotropic); Nugget = 0; Major range = 3090.847; Partial sill = 617.975 (chapter 3).

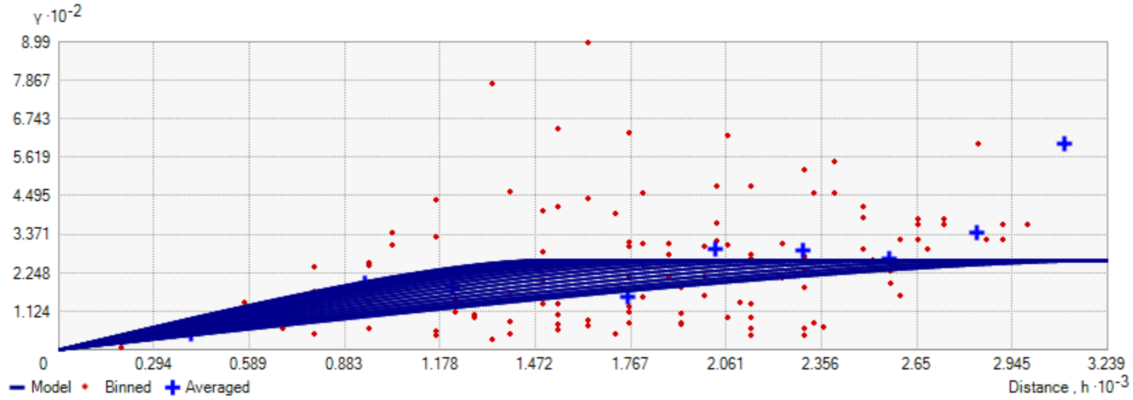

Figure A1.6. Sand fraction (Ordinary kriging, Circular model, Anisotropic); Nugget = 0; Major range = 3239.113; Partial sill = 260.635 (chapter 3).

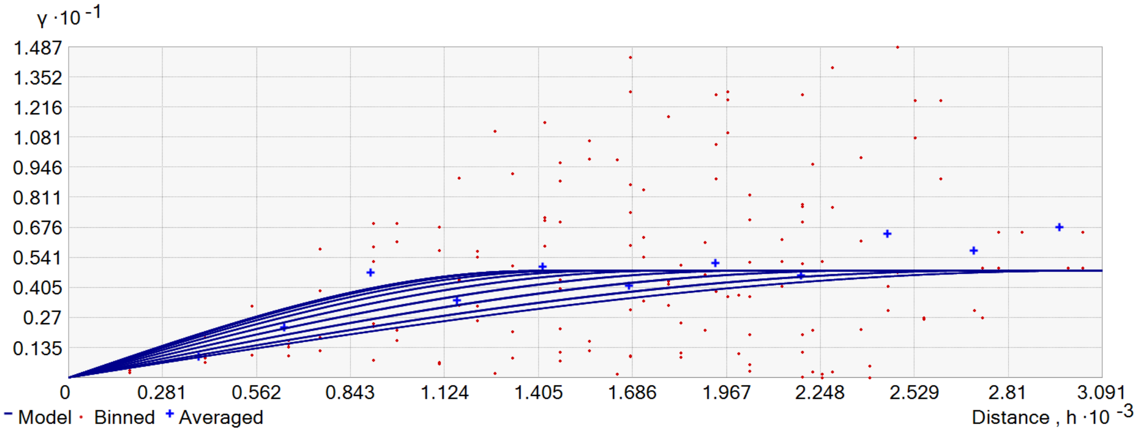

Figure A1.7. 2014 SOC distribution (Ordinary kriging, Spherical model, Anisotropic); Nugget = 0; Major range = 3090.847; Partial sill = 4.803 (chapter 4).

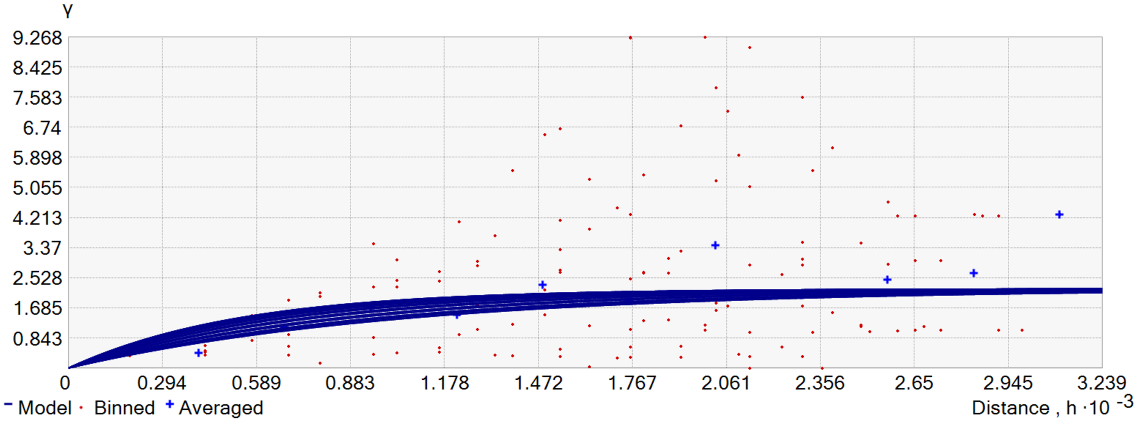

Figure A1.8. δ13C distribution (Ordinary kriging, Exponential model, Anisotropic); Nugget = 0; Major range = 3239.113; Partial sill = 2.219 (chapter 4).

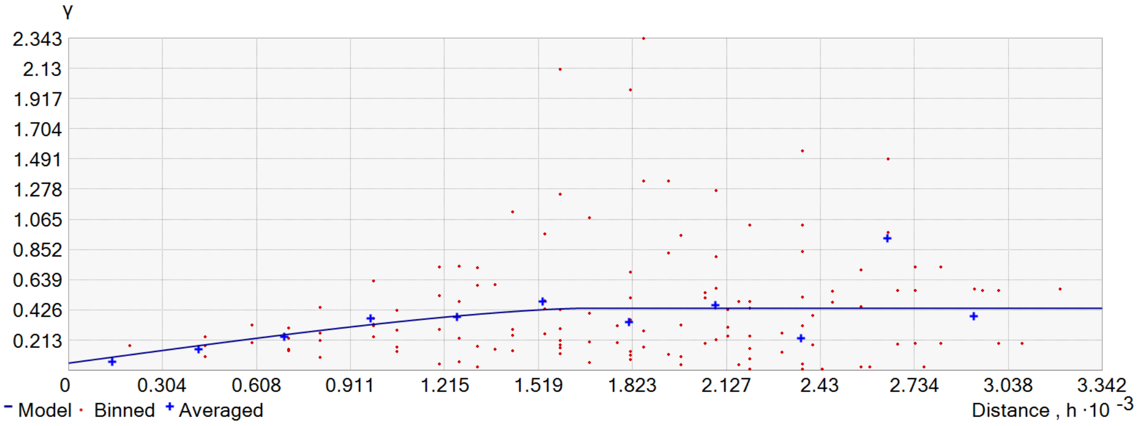

Figure A1.9. δ15N distribution (Ordinary kriging, Circular model, Isotropic); Nugget = 0.051; Major range = 1669.841; Partial sill = 0.387 (chapter 4).

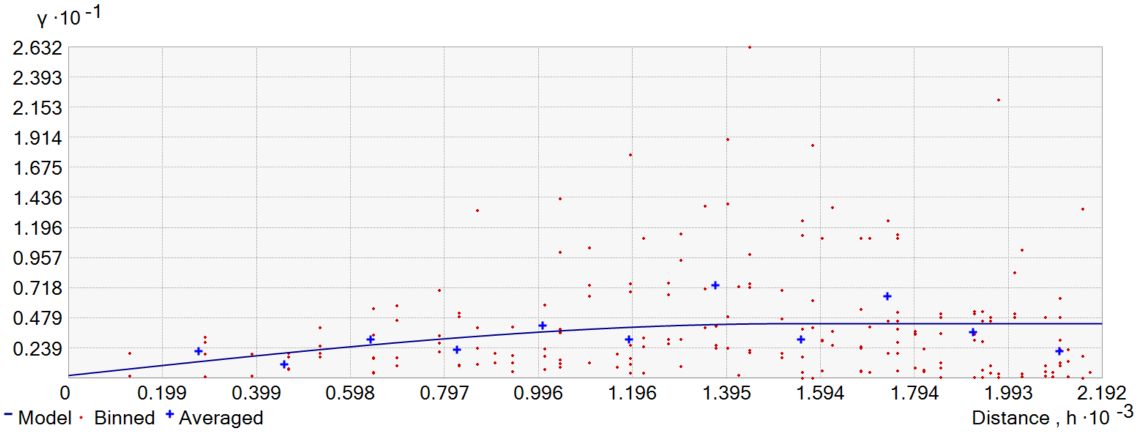

Figure A1.10. δ34S distribution (Ordinary kriging, Spherical model, Isotropic); Nugget = 0.199; Major range = 1537.359; Partial sill = 4.119 (chapter 4).

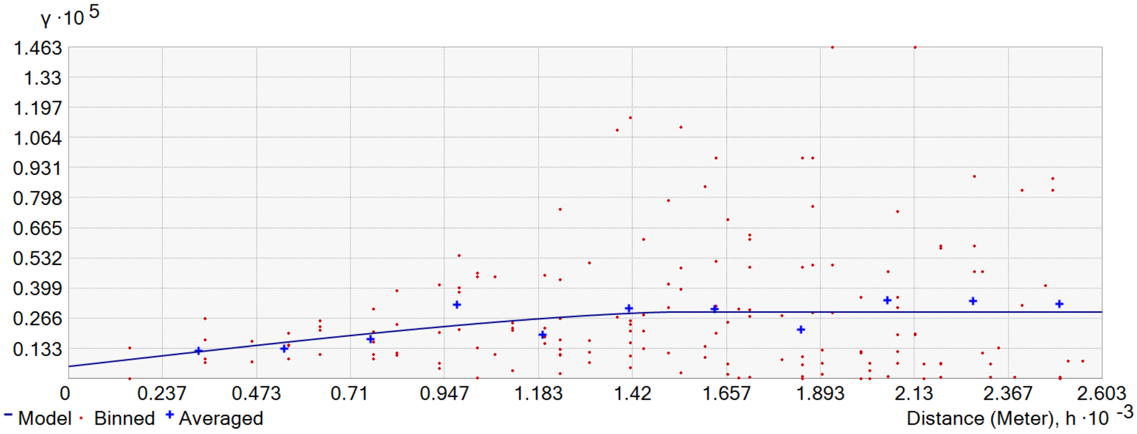

Figure A1.11. 12-cm net SOC accumulation in 2013 (Ordinary kriging, Circular model, Isotropic); Nugget = 5.29e-7; Major range = 1535.658; Partial sill = 2.407e-6 (chapter 5).

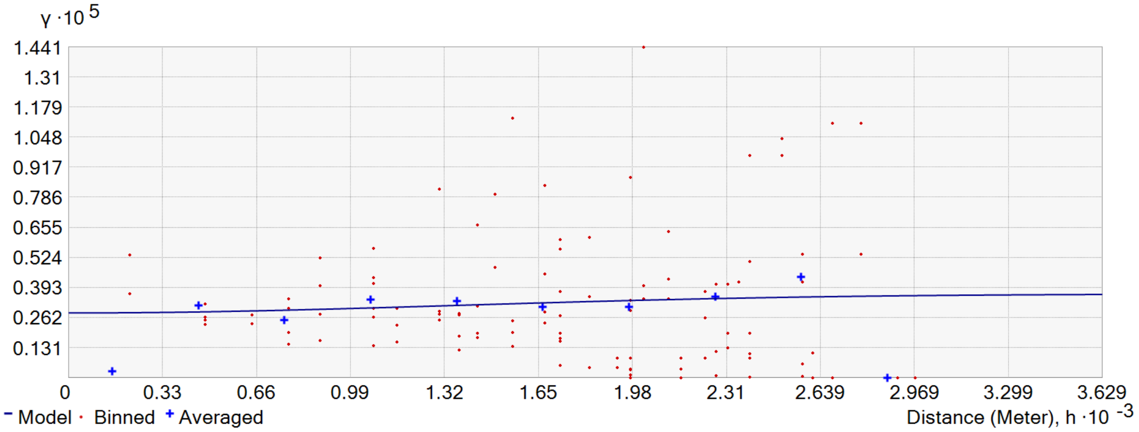

Figure A1.12. 12-cm net SOC accumulation in 2016 (Ordinary kriging, Gaussian model, Anisotropic); Nugget = 2.814e-6; Major range = 3310.331; Partial sill = 8.289e-7 (chapter 5).

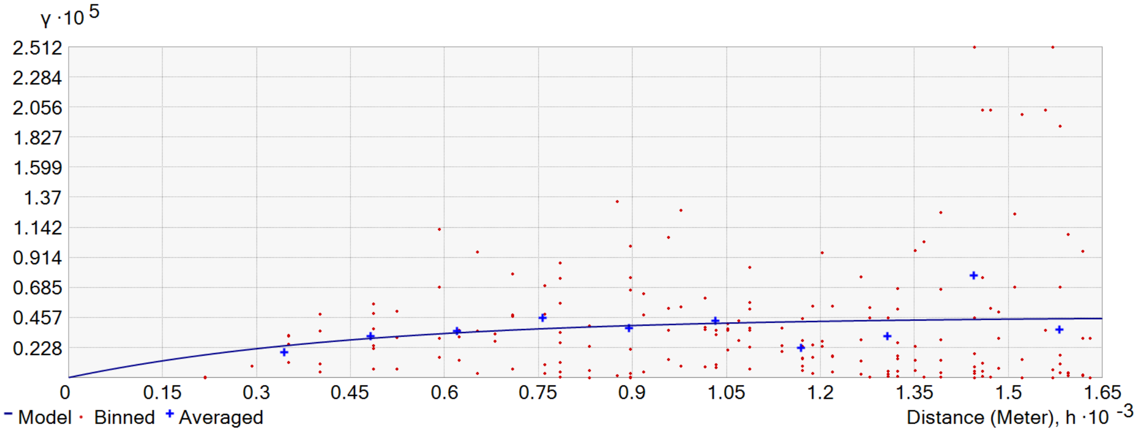

Figure A1.13. Net SOC accumulation 2-cm accreted interval in 2016 (Ordinary kriging, Exponential model, Isotropic); Nugget = 0; Major range = 1399.445; Partial sill = 4.623e-6 (chapter 5).

Appendix II. Carbon source supplement

End-member source data:

The BMA δ^{13}C and δ^{15}N values were obtained from Hondula and Pace (2011) in adjacent Cobb Island Bay. We used the April sample values to approximate annual averages (Table S1). We compiled end-member δ^{34}S isotope values from multiple studies (Table S2), but we ultimately limited the mixing model analysis to δ^{13}C and δ^{15}N isotope ratios obtained from the VCR-LTER.

Table A2.1. δ^{13}C and δ^{15}N values for BMA were obtained from Hondula and Pace (2011).

Sample ID	Date Collected	Field Site	δ^{13}C	δ^{15}N
KLH4 MPB1	4/25/11	Cobb Island Bay	-21.03	5.92
KLH4 MPB2	4/25/11	Cobb Island Bay	-20.62	5.71
KLH4 MPB3	4/25/11	Cobb Island Bay	-21.60	5.166
KLH4 MPB4	4/25/11	Cobb Island Bay	-21.04	6.19

Table A2.2. δ^{34}S values for BMA (benthic diatoms) and macroalgae from the literature.

Taxon	Location	δ^{34}S	SD or SE	Reference
Benthic diatoms	PIE, MA	18.5	1.5 (SD)	Baker et al. 2016
BMA-mudflat	Delaware Bay	8.66	0.91 (SE)	Currin et al. 2003
BMA-mudflat	Delaware Bay	7.35	0.77 (SE)	Currin et al. 2003
BMA-mudflat	Delaware Bay	8.2	0.74 (SE)	Currin et al. 2003
BMA-marsh surface	Delaware Bay	5.02	0.89 (SE)	Currin et al. 2003
BMA-marsh surface	Delaware Bay	11.58	(1 sample)	Currin et al. 2003
BMA	Newport River Estuary, NC	3.9		Currin et al. 1995
Benthic diatoms	SFB, CA	-1.18	3.06 (SD)	Howe and Simenstad 2007

Benthic diatoms	Columbia River Estuary	3.7		Maier et al. 2011
Benthic diatoms	Columbia River Estuary	2.8		Maier et al. 2011
Benthic diatoms	Columbia River Estuary	2.9		Maier et al. 2011
Ulva lactuca	Herring River Salt Marsh, MA	16.4	0.5 (SE)	Wozniak et al. 2006
Gracilaria tikviahae	Herring River Salt Marsh, MA	18.2	0.1 (SE)	Wozniak et al. 2006
Ulva lactuca	Apalachicola Bay, FL	17.9		Chanton and Lewis 2002
Ulva lactuca	Apalachicola Bay, FL	16.5		Chanton and Lewis 2002
Gracilaria sp.	Apalachicola Bay, FL	11.5		Chanton and Lewis 2002
Gracilaria sp.	Apalachicola Bay, FL	14.5		Chanton and Lewis 2002
Enteromorpha sp.	Horn Island, MS	20.4		Moncreiff and Sullivan 2001
Gracilaria verrucosa	Horn Island, MS	16.6		Moncreiff and Sullivan 2001
Benthic macroalgae	Columbia River Estuary	9.7		Maier et al. 2011
Benthic macroalgae	Columbia River Estuary	7.6		Maier et al. 2011

Fit-diagnostic plots:

The mixing model found good end-member posterior separation for each of the SOC groups.

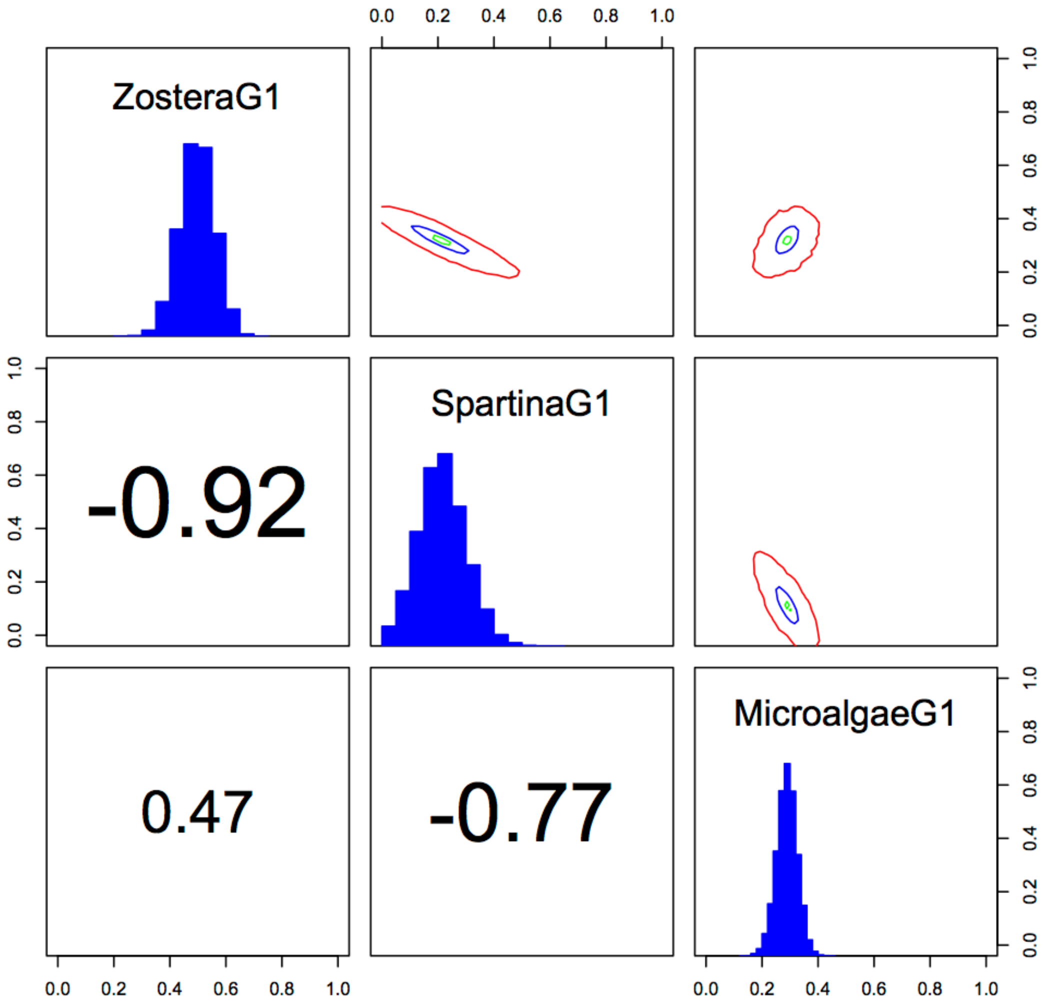

Figure A2.1. Matrix plot of proportions for group 1 ('lowest' OC) mixing model results.

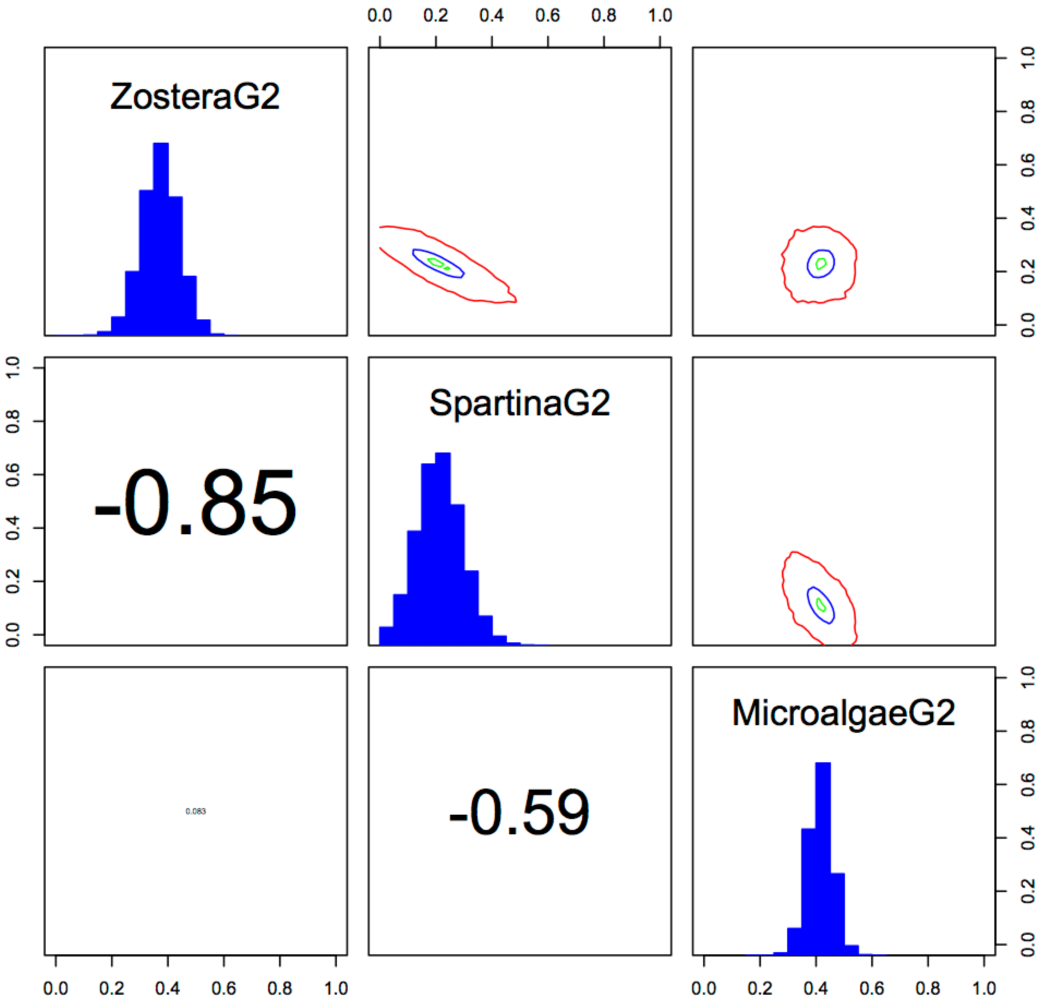

Figure A2.2. Matrix plot of proportions for group 2 (‘low’ OC) mixing model results.

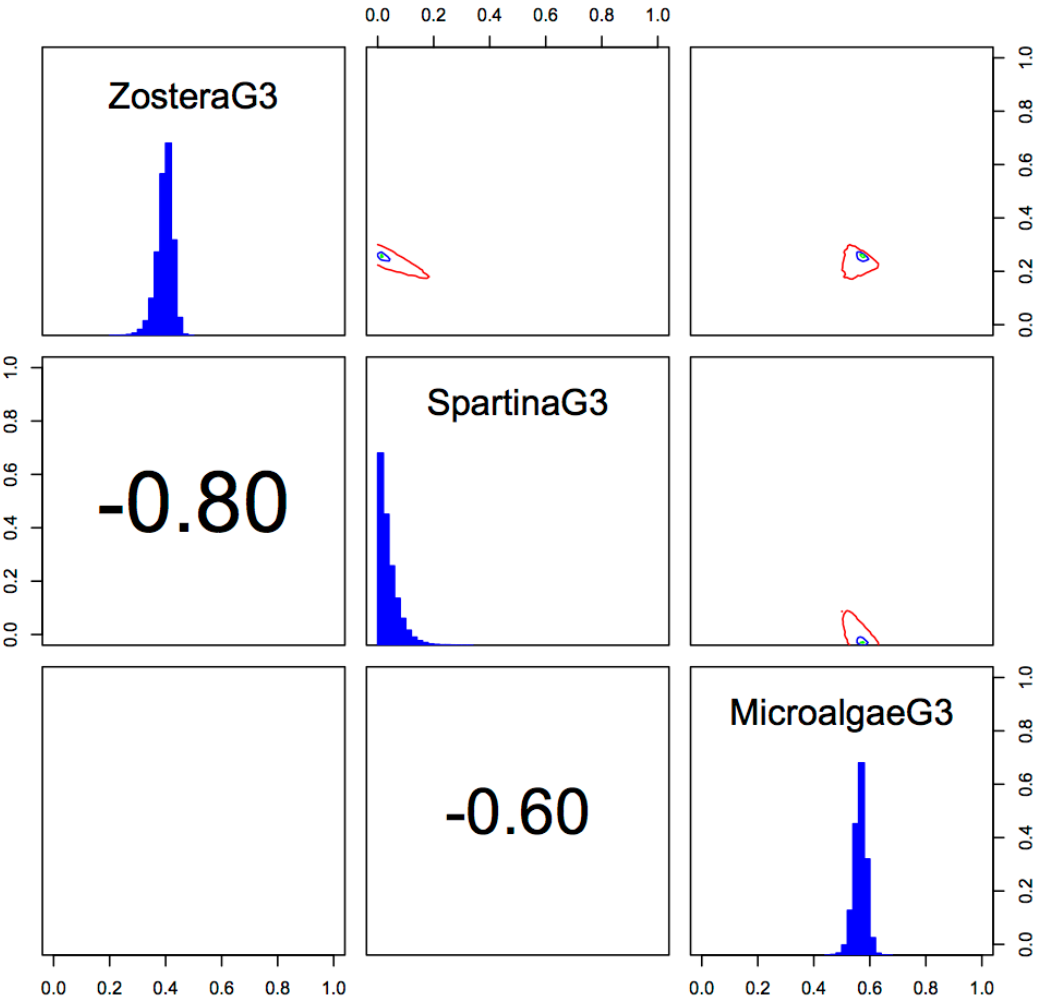

Figure A2.3. Matrix plot of proportions for group 3 ('high' OC) mixing model results.

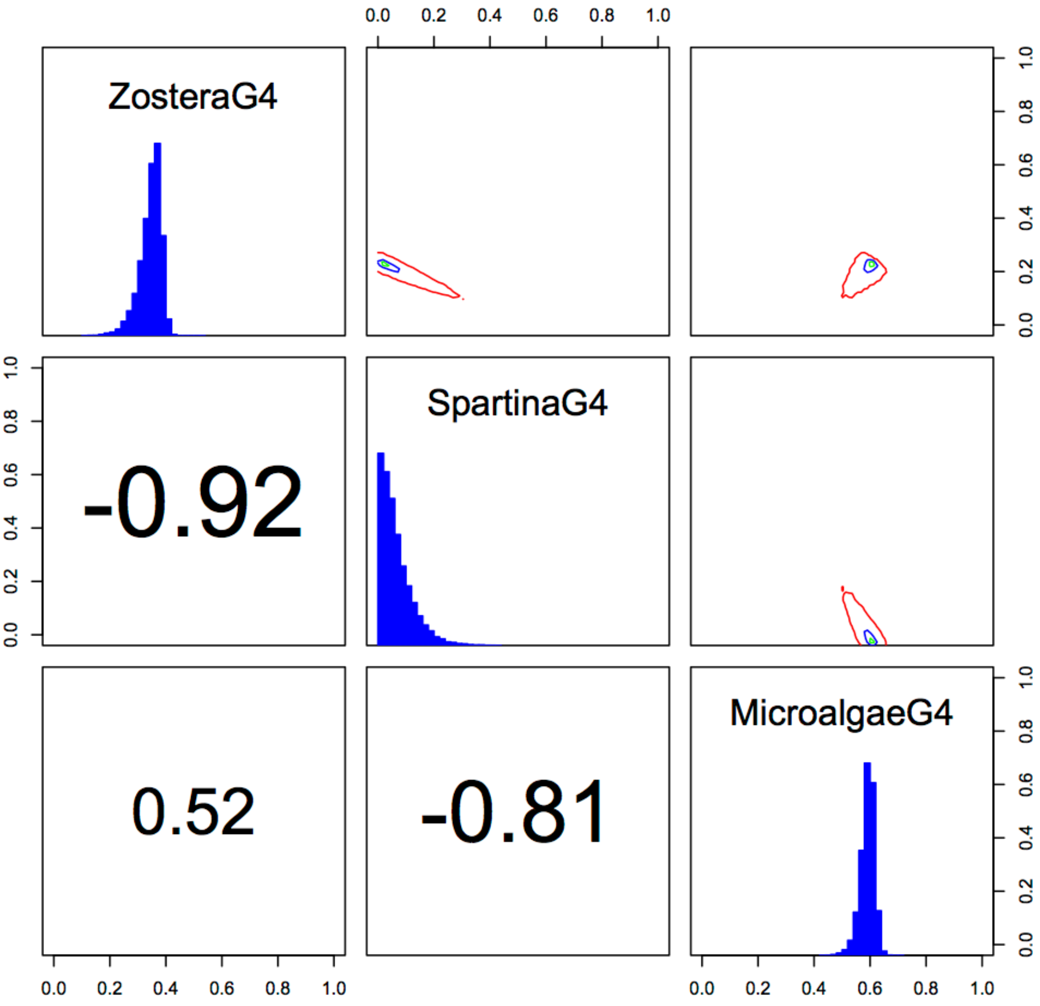

Figure A2.4. Matrix plot of proportions for group 4 ('highest' OC) mixing model results.

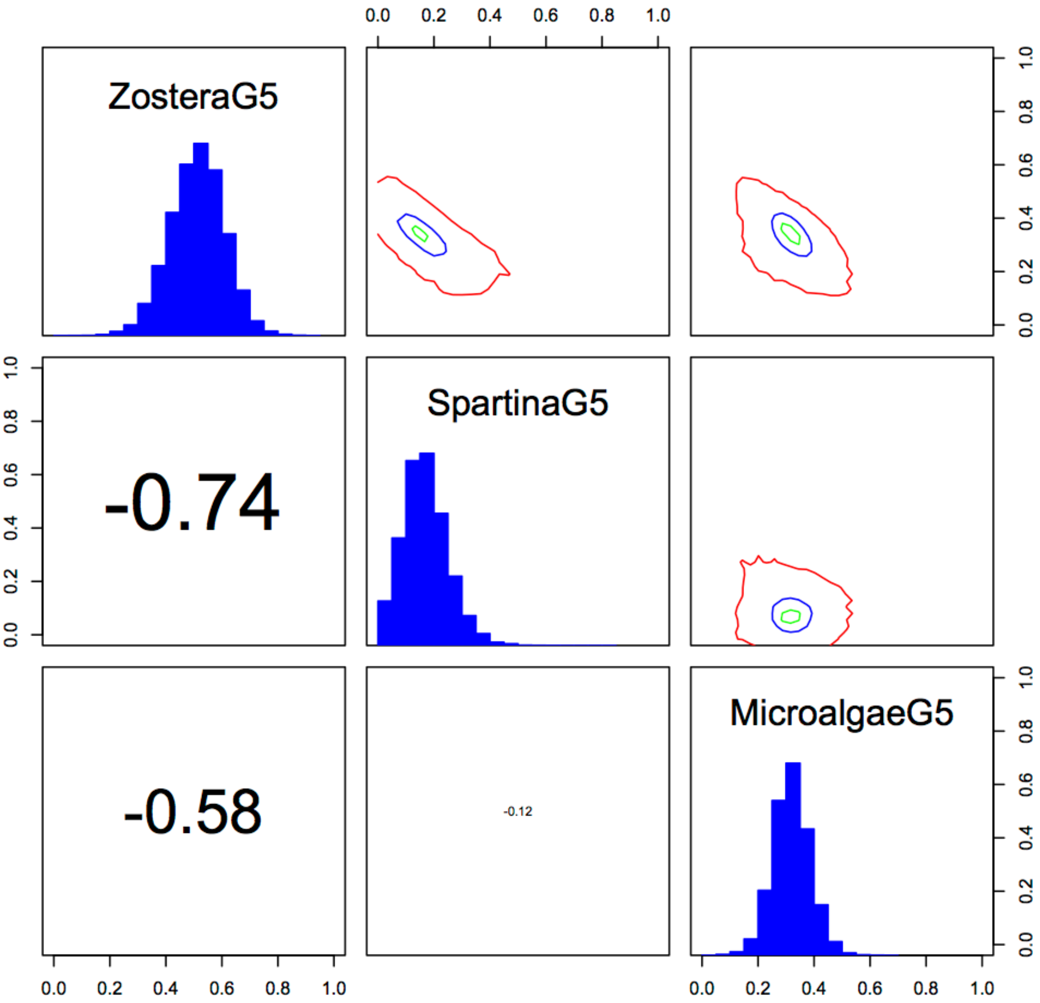

Figure A2.5. Matrix plot of proportions for group 5 (bare sites) mixing model results.

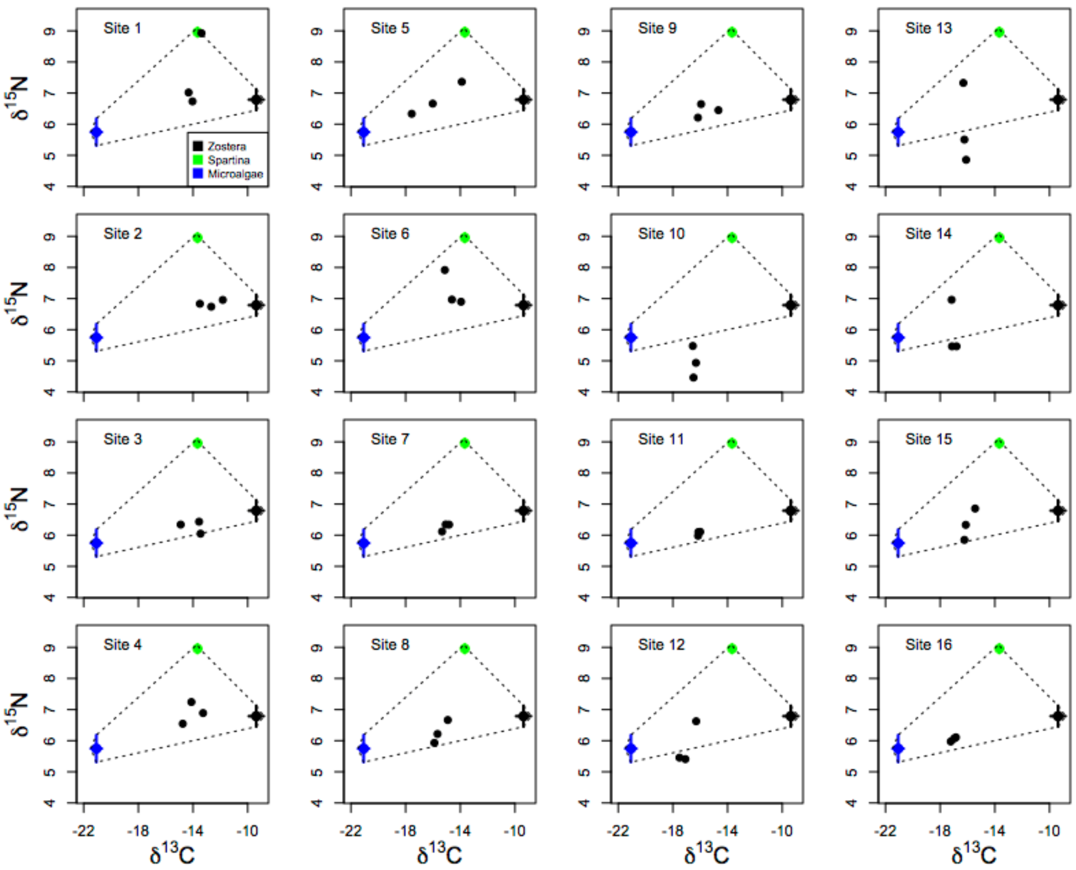

Figure A2.6. Bi-plots for each meadow site (n = 16). Note: samples for two ‘high’ SOC sites (10 and 12 in Figure 1) and two ‘highest’ SOC sites (13 and 14) plotted outside of the mixing polygon. Omitting these four sites did not significantly alter SOC group mixing model results or site-distance regression analyses (see Figure A2.7 and Table A2.3).

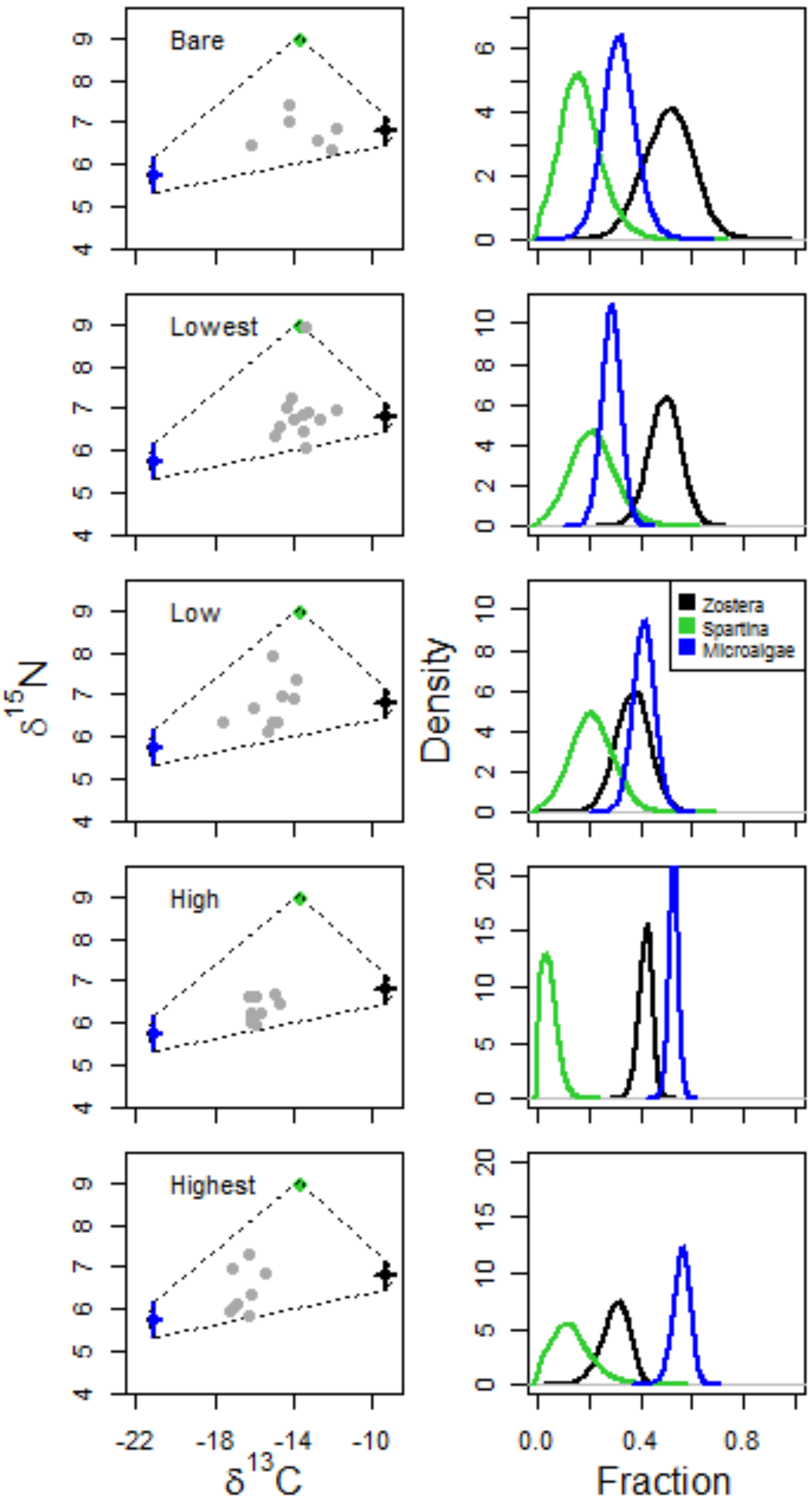

Figure A2.7. Mixing model results by OC group without samples that fell outside of the mixing polygon (samples for ‘high’ sites 10 and 12 and ‘highest’ sites 13 and 14).

Table A2.3. Meadow site (n = 12) isotope ratio and SOC source fraction relationships with distance from Wreck Island Marsh (Marsh) and from the meadow-bare subtidal edge (Edge); Note: sites 10, 12, 13, and 14 omitted.

	Intercept	SE	M	SE	$F_{(1,14)}$	*p*	adj-R^2
δ^{13}C~Marsh	-16.149	1.240	1.145E-03	1.590E-03	0.519	0.488	-0.046
δ^{13}C~Edge	-14.904	0.699	-8.700E-04	1.263E-03	0.474	0.507	-0.050
δ^{15}N~Marsh	6.269	0.653	1.563E-04	8.374E-04	0.035	0.856	-0.096
δ^{15}N~Edge	6.640	0.355	-5.594E-04	6.413E-04	0.761	0.404	-0.022
δ^{34}S~Marsh	-16.630	2.058	4.241E-04	2.639E-03	0.026	0.876	-0.097
δ^{34}S~Edge	-15.395	1.104	-2.012E-03	1.996E-03	1.016	0.337	0.001
Zostera~Marsh	0.341	0.075	7.244E-05	9.612E-05	0.568	0.468	-0.041
Zostera~Edge	0.442	0.039	-1.042E-04	7.110E-05	2.148	0.174	0.095
Spartina~Marsh	0.158	0.094	3.594E-05	1.206E-04	0.089	0.772	-0.090
Spartina~Edge	0.234	0.050	-1.058E-04	9.005E-05	1.381	0.267	0.033
BMA~Marsh	0.501	0.106	-1.084E-04	1.363E-04	0.632	0.445	-0.035
BMA~Edge	0.325	0.049	2.100E-04	8.951E-05	5.506	0.041	0.291

Appendix II References:

Baker, H.K., J.A. Nelson, H.M. Leslie. 2016. Quantifying striped bass (*Morone saxatilis*) dependence on saltmarsh-derived productivity using stable isotope analysis. *Estuaries and Coasts* 39:1537-1542.

Chanton, J., F.G. Lewis. 2002. Examiniation of coupling between primary and secondary production in a river-dominated estuary: Apalachicola Bay, Florida, U.S.A. *Limnology and Oceanography* 47(3):683-697.

Currin, C.A., S.Y. Newell, H.W. Paerl. 1995. The role of standing dead *Spartina alterniflora* and benthic microalgae in salt marsh food webs: considerations based on multiple stable isotope analysis. *Marine Ecology Progress Series* 121:99-116.

Currin, C.A., S.C. Wainright, K.W. Able, M.P. Weinstein, C.M. Fuller. 2003. Determination of food web support and trophic position of the mummichog, *Fundulus heteroclitus*, in New Jersey smooth cordgrass (*Spartina alterniflora*), common reed (*Phragmites australis*), and restored salt marshes. *Estuaries* 26(2B):495-510.

Hondula, K., M. Pace. 2011. Stable isotopes of M. mercenaria and plant sources on the Virginia Coast. Data publication knb-lter-vcr.200.9. Available at: https://portal.lternet.edu/nis/mapbrowse?packageid=knb-lter-vcr.200.9.

Howe, E.R., C.A. Simenstad. 2007. Restoration trajectories and food web linkages in San Francisco Bay's estuarine marshes: a manipulative translocation experiment. *Marine Ecology Progress Series* 351:61-76.

Maier, G.O., J.D. Toft, C.A. Simenstad. 2011. Variability in isotope (δ^{13}C, δ^{15}N, δ^{34}S) composition of organic matter contributing to detritus-based food webs of the Columbia River Estuary. *Northwest Science* 85(1):41-54.

Moncreiff, C.A., M.J. Sullivan. 2001. Trophic importance of epiphytic algae in subtropical seagrass beds: evidence from multiple stable isotope analyses. *Marine Ecology Progress Series* 215:93-106.

Wozniak, A.S., C.T. Roman, S.C. Wainright, R.A. McKinney, M.-J. James-Pirri. 2006. Monitoring food web changes in tide-restored salt marshes: A carbon stable isotope approach. *Estuaries and Coasts* 29(4):568-578.